Appendices

Appendix A A-1

A.1. Supplementary data for Chapter Two A-1

A.1.1. NMR spectra of synthesised compounds A-1

A.1.2. Crystallographic parameters A-36

A.1.3. Supplementary X-ray crystal structures A-42

A.1.4. NMR spectra of cationic complexes A-43

A.1.5. ssNMR spectra of solid catalysts A-48

A.2. Supplementary data for Chapter Three A-61

A.2.1. Homogeneous polymerisation data A-61

A.2.2. Heterogeneous polymerisation data A-62

A.2.3. Ethylene uptake profiles A-69

A.2.4. Gel-permeation chromatography A-69

A.2.5. Differential scanning calorimetry A-76

A.2.6. High-throughput (Xplore s.r.l.) A-79

A.2.7. UHMWPE Mechanical test report (Norner AS) A-92

A.2.8. Differential scanning calorimetry (annealing) A-93

A.2.9. ssNMR A-99

A.2.10. Thermogravimetric analysis A-99

A.2.11. Microcompounding/film extrusion report (Nanoforce Technology Ltd.) A-100

A.2.12. PE/UHMWPE characterisation A-102

A.3. Supplementary data for Chapter Four A-104

A.3.1. Polymerisation data A-104

A.3.2. Gel-permeation chromatography A-108

A.3.3. Thermogravimetric analysis A-111

A.3.4. Differential scanning calorimetry A-112

A.3.5. ^{13}C NMR spectroscopy A-115

A.3.6. Rheology A-121

A.3.7. Optical characterisation A-121

A.3.8. Mechanical characterisation (Norner AS) A-124

A.4. Supplementary data for Chapter Five A-126

A.4.1. Ethylene-propylene copolymerisation data A-126

A.4.2. Ethylene-propylene-diene terpolymerisation data A-127

A.4.3. Propylene-hexene copolymerisation data A-127

A.4.4. Ethylene-linear-α-olefin copolymerisation data A-128
A.4.5. Gel-permeation chromatography A-132
A.4.6. Differential scanning calorimetry A-137
A.4.7. NMR spectroscopy A-142
A.4.8. Designer LLDPE A-145
A.5. Mechanical testing report (Norner AS) A-147
Appendix B B-1
Analysis of variance (ANOVA) B-1
Appendix C C-1
Crystallographic information file ..... .cif
Appendix D D-1

Appendix A

A.1. Supplementary data for Chapter Two

A.1.1. NMR spectra of synthesised compounds

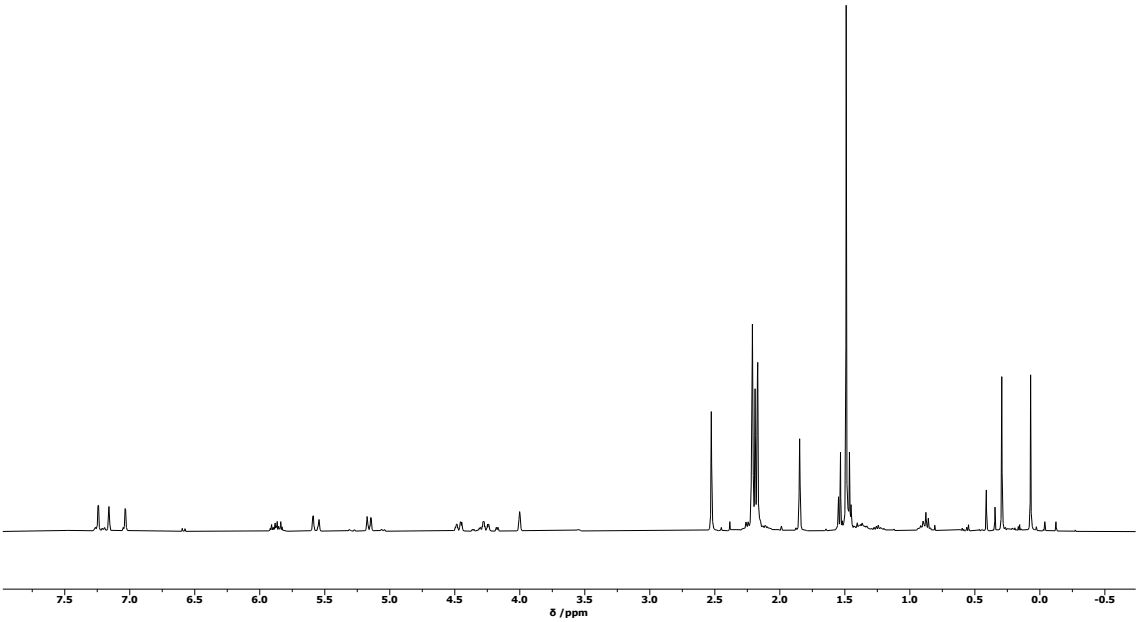

Figure A.1 ^{1}H NMR spectrum of ^{Me_2}SB($^{t\text{Bu,Me}}$ArOAllyl,I*)H (**1e**) (benzene-d_6, 400 MHz, 298 K).

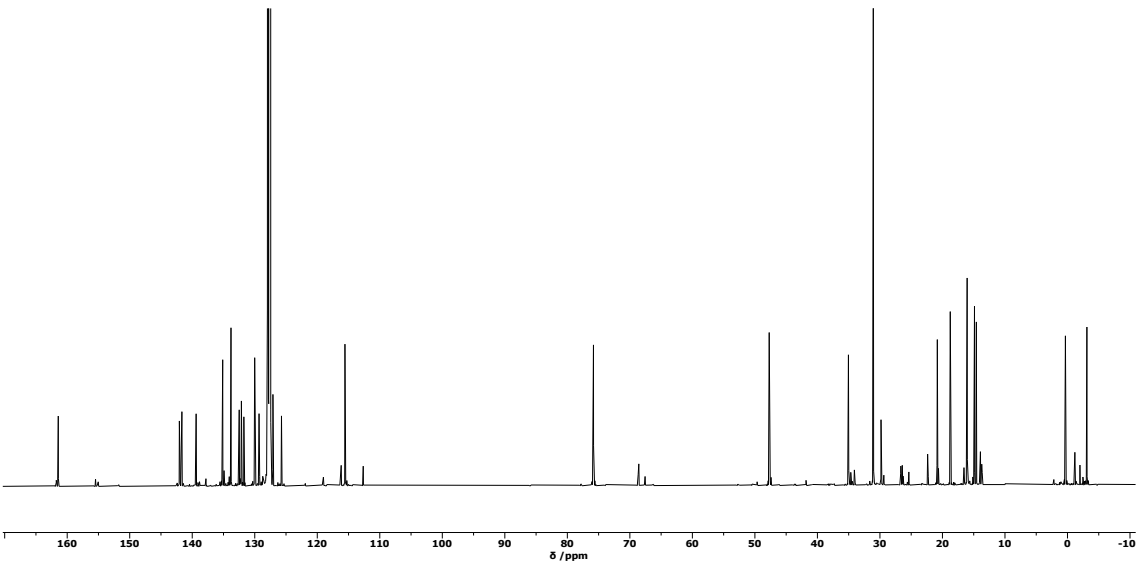

Figure A.2 ^{13}C{^{1}H} NMR spectrum of ^{Me_2}SB($^{t\text{Bu,Me}}$ArOAllyl,I*)H (**1e**) (benzene-d_6, 126 MHz, 298 K).

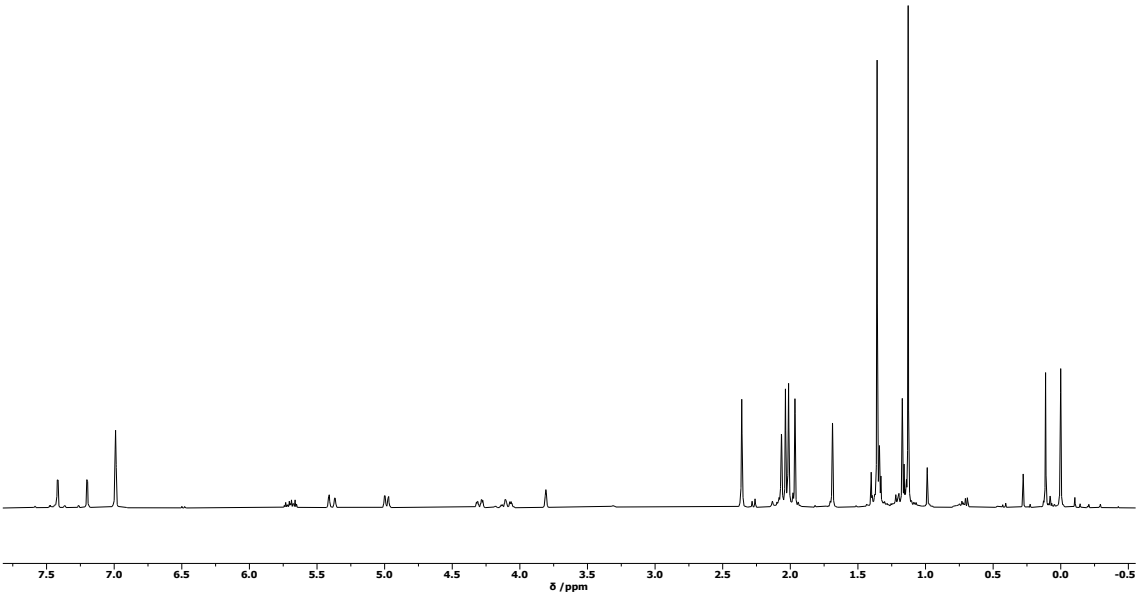

Figure A.3 ^{1}H NMR spectrum of ^{Me_2}SB($^{t Bu_2}$ArOAllyl,I*)H (**2e**) (benzene-d_6, 400 MHz, 298 K).

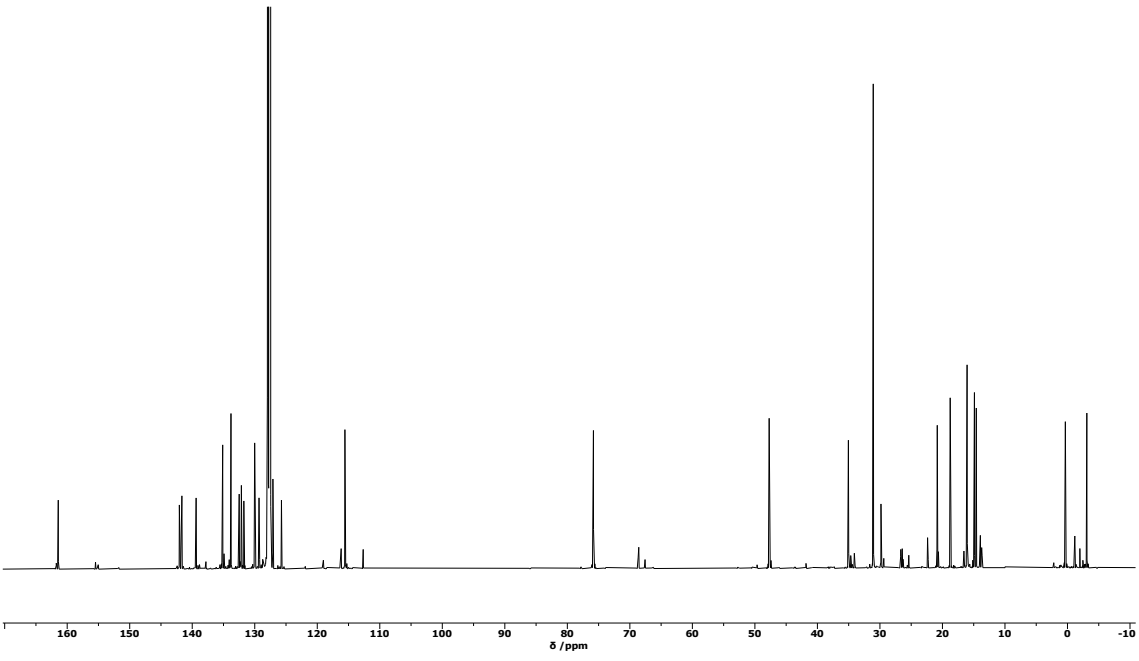

Figure A.4 ^{13}C{^{1}H} NMR spectrum of ^{Me_2}SB($^{t Bu_2}$ArOAllyl,I*)H (**2e**) (benzene-d_6, 126 MHz, 298 K).

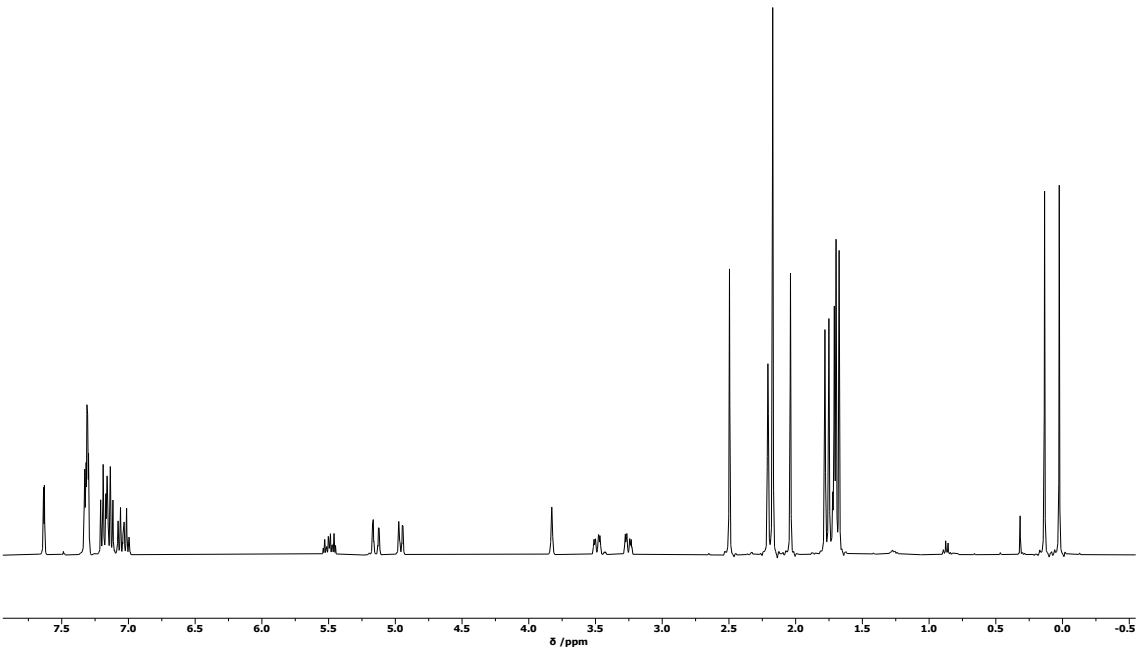

Figure A.5 ^{1}H NMR spectrum of ^{Me_2}SB(^{Cumyl_2}ArOAllyl,I*)H (**11e**) (benzene-d_6, 400 MHz, 298 K).

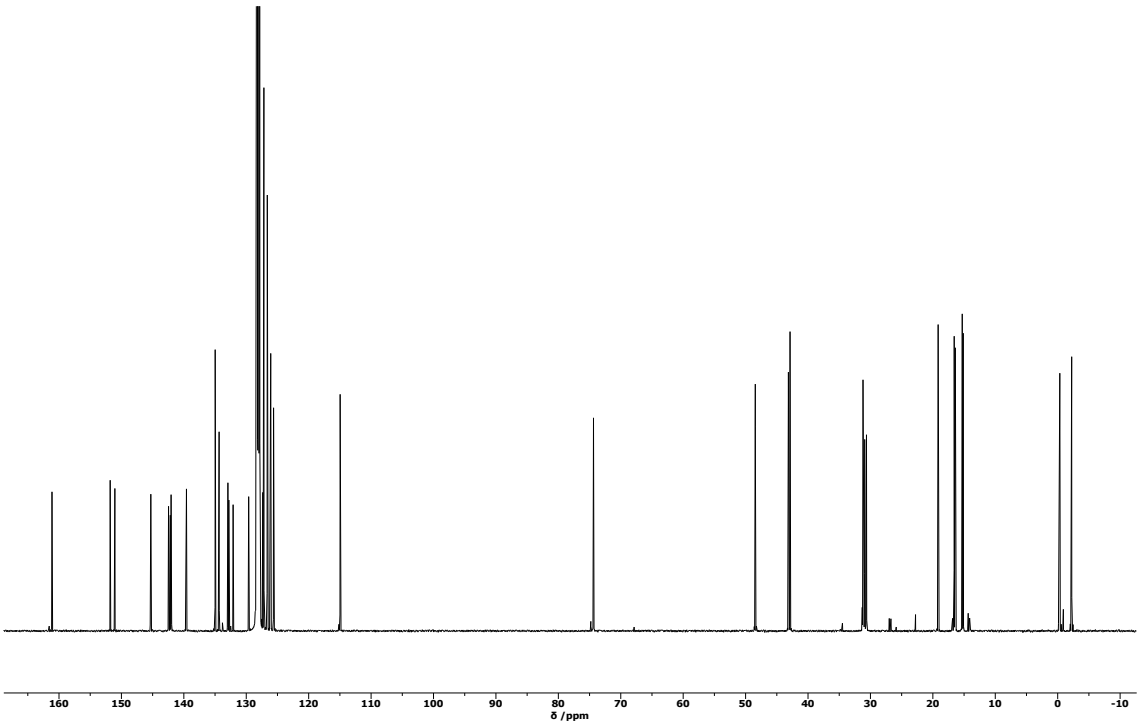

Figure A.6 ^{13}C{^{1}H} NMR spectrum of ^{Me_2}SB(^{Cumyl_2}ArOAllyl,I*)H (**11e**) (benzene-d_6, 126 MHz, 298 K).

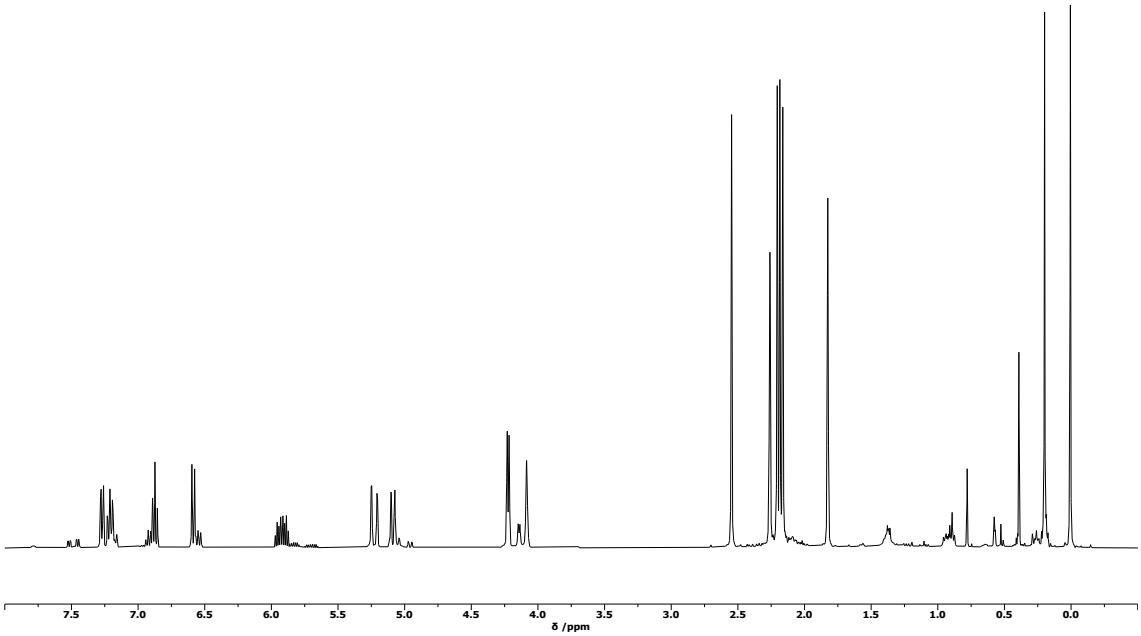

Figure A.7 ^{1}H NMR spectrum of ^{Me_2}SB(^{H_2}ArOAllyl,I*)H (**19e**) (benzene-d_6, 400 MHz, 306 K).

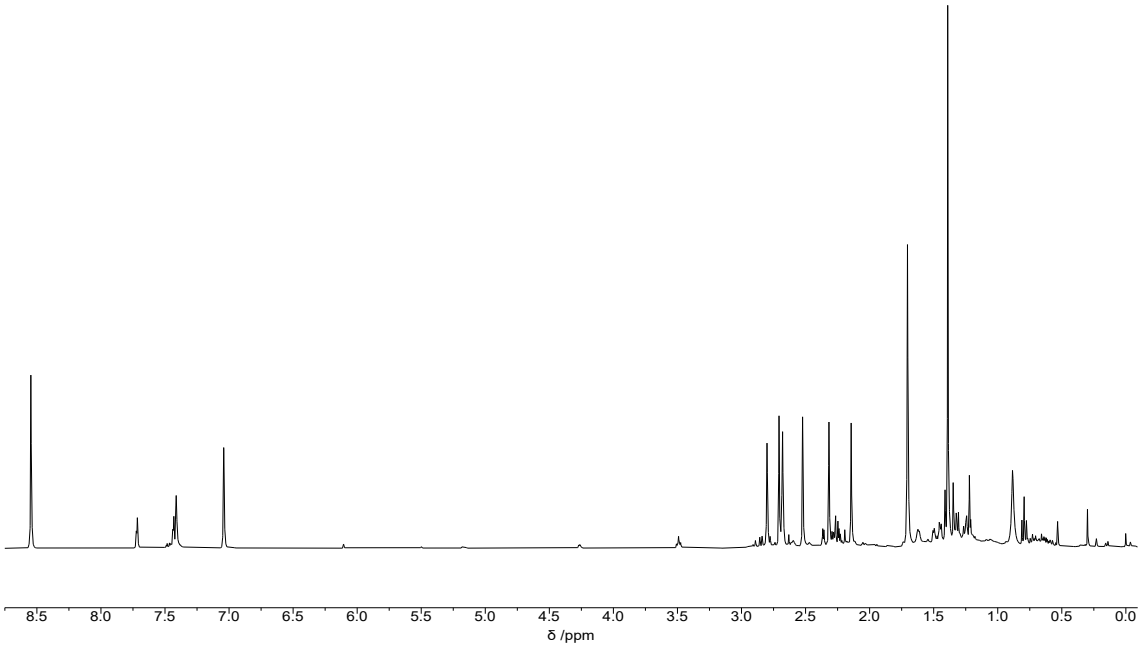

Figure A.8 ^{1}H NMR spectrum of ^{Me_2}SB($^{t Bu_2}$ArO,I*)Li_2 (**2f**) (pyridine-d_5, 400 MHz, 298 K).

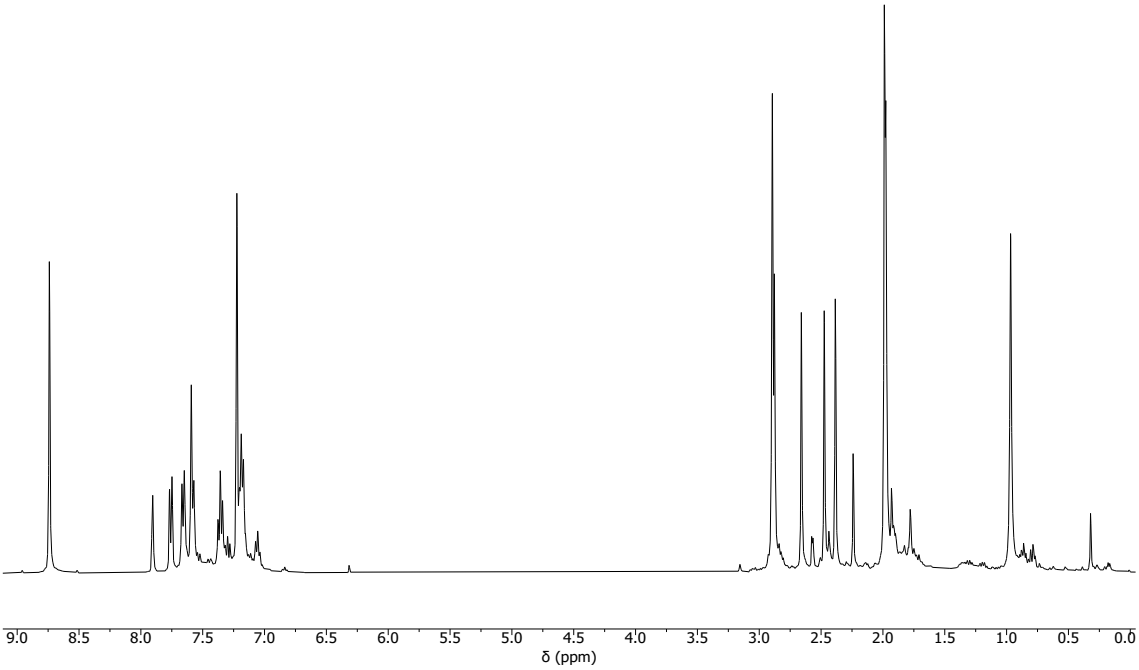

Figure A.9 ^{1}H NMR spectrum of ^{Me_2}SB(^{Cumyl_2}ArO,I*)Li$_2$ (**11f**) (pyridine-d_5, 400 MHz, 298 K).

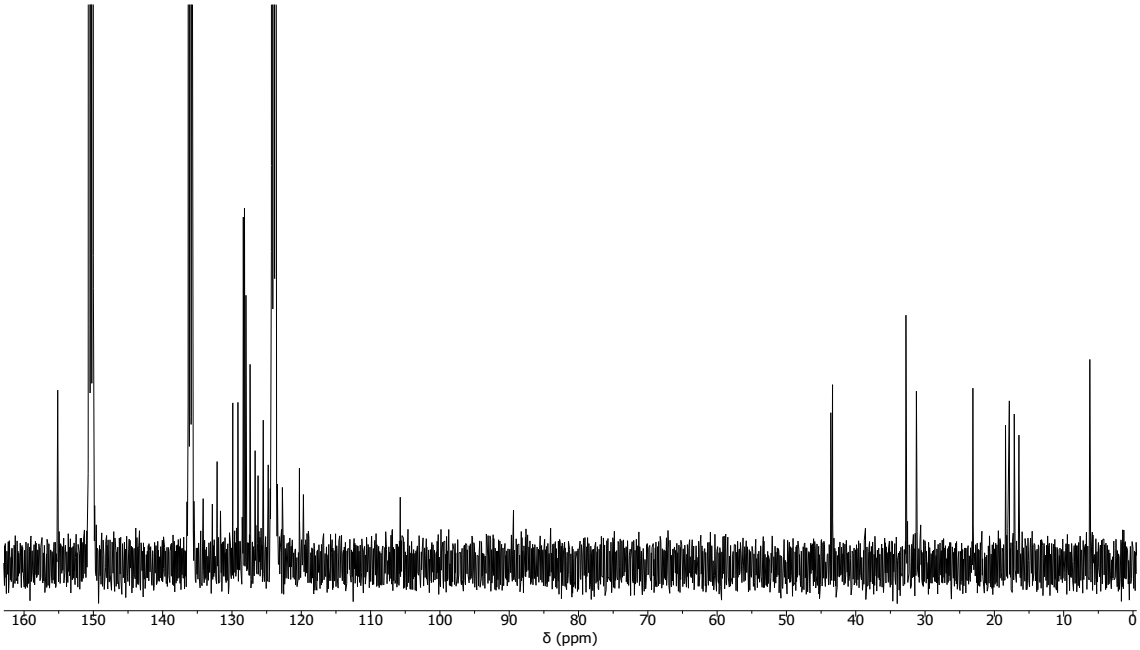

Figure A.10 ^{13}C{^{1}H} NMR spectrum of ^{Me_2}SB(^{Cumyl_2}ArO,I*)Li$_2$ (**11f**) (pyridine-d_5, 101 MHz, 298 K).

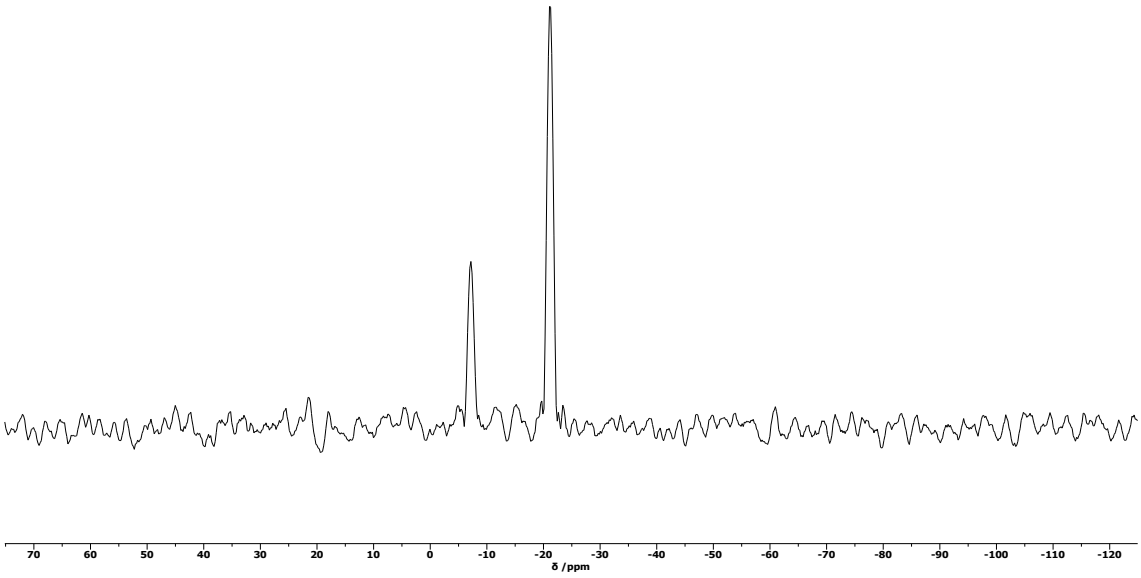

Figure A.11 ^{29}Si NMR spectrum of ^{Me_2}SB(^{Cumyl_2}ArO,I*)Li$_2$ (**11f**) (^{1}H-observed HMBC, pyridine-d_5, 80 MHz, 298 K).

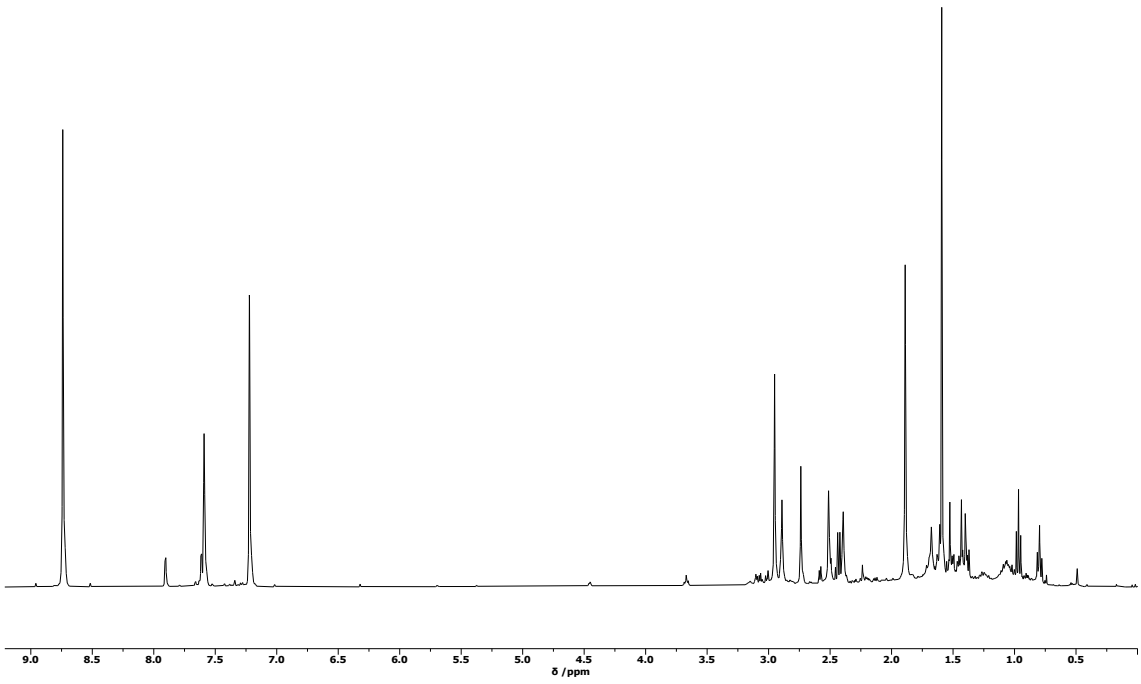

Figure A.12 ^{1}H NMR spectrum of *rac*-$^{Me,{}^n Pr}$SB($^{{}^t Bu_2}$ArO,I*)Li$_2$ (**12f**) (pyridine-d_5, 400 MHz, 298 K).

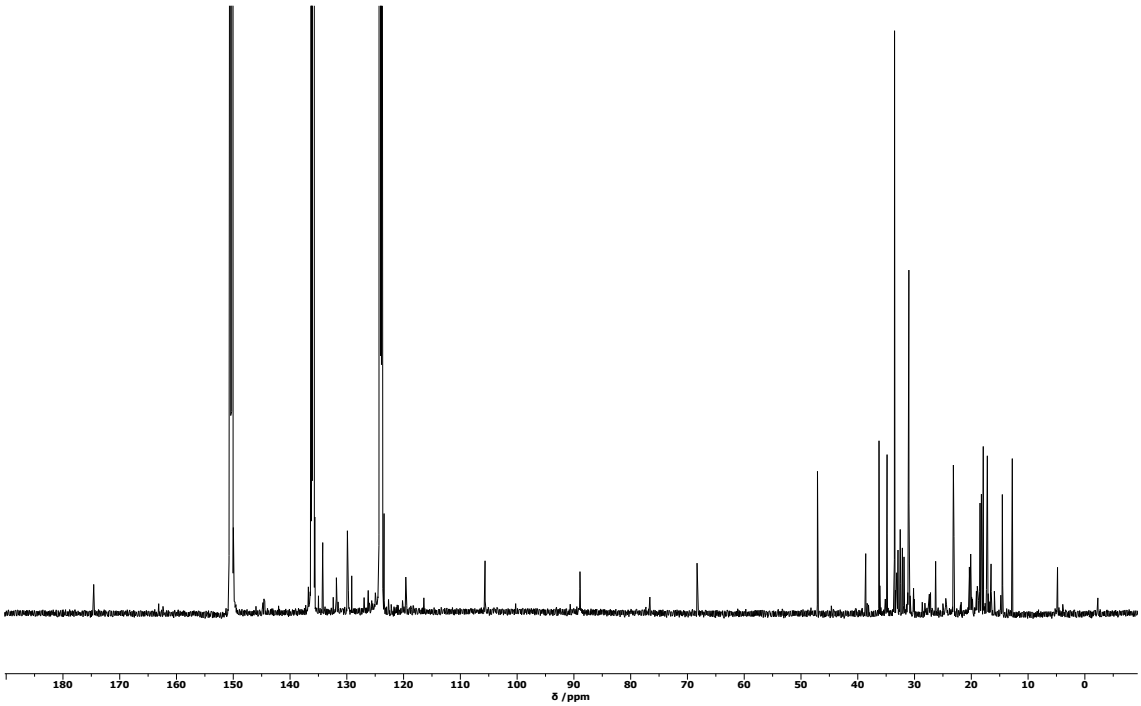

Figure A.13 $^{13}C\{^{1}H\}$ NMR spectrum of *rac*-^{Me,nPr}SB(^{tBu2}ArO,I*)Li_2 (**12f**) (pyridine-d_5, 151 MHz, 298 K).

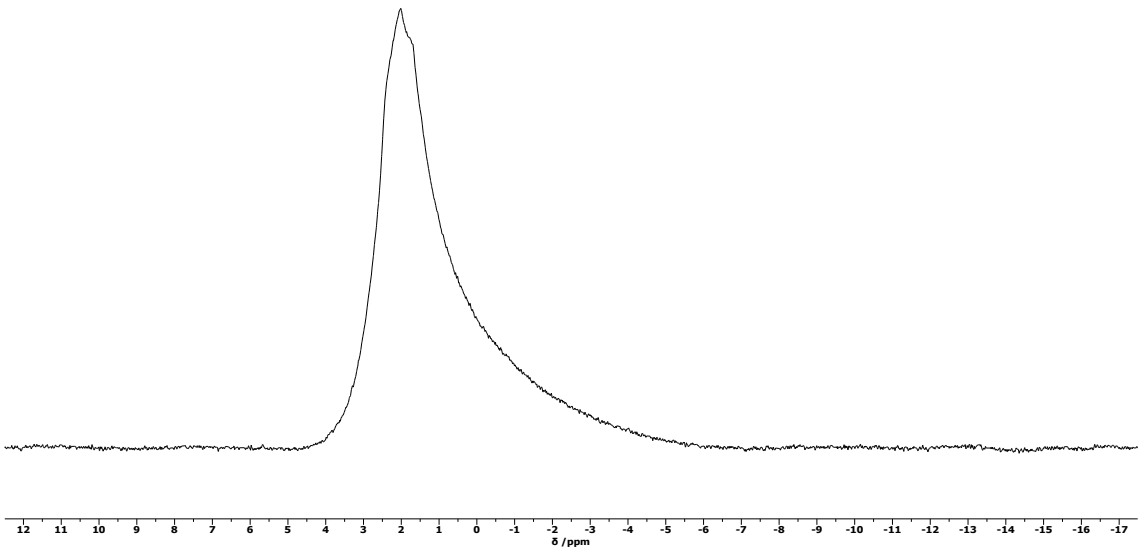

Figure A.14 ^{7}Li NMR spectrum of *rac*-^{Me,nPr}SB(^{tBu2}ArO,I*)Li_2 (**12f**) (pyridine-d_5, 156 MHz, 298 K).

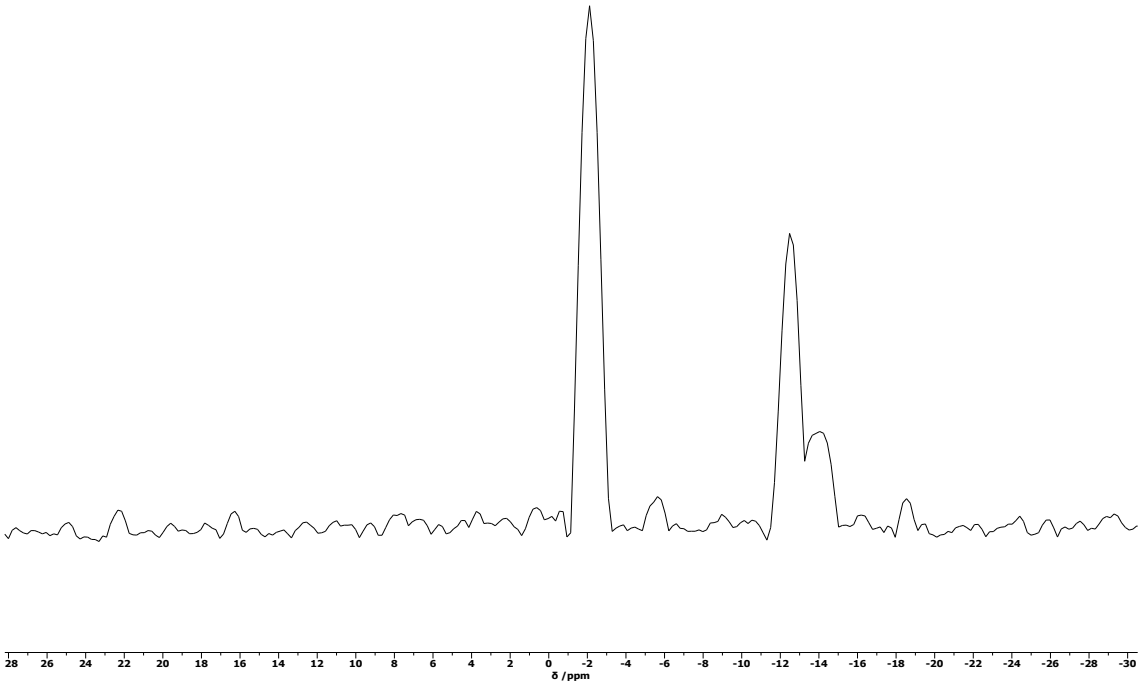

Figure A.15 ^{29}Si NMR spectrum of *rac*-$^{Me,{}^{n}Pr}$SB($^{t}Bu_2$ArO,I*)Li_2 (**12f**) (^{1}H-observed HMBC, pyridine-d_5, 80 MHz, 298 K).

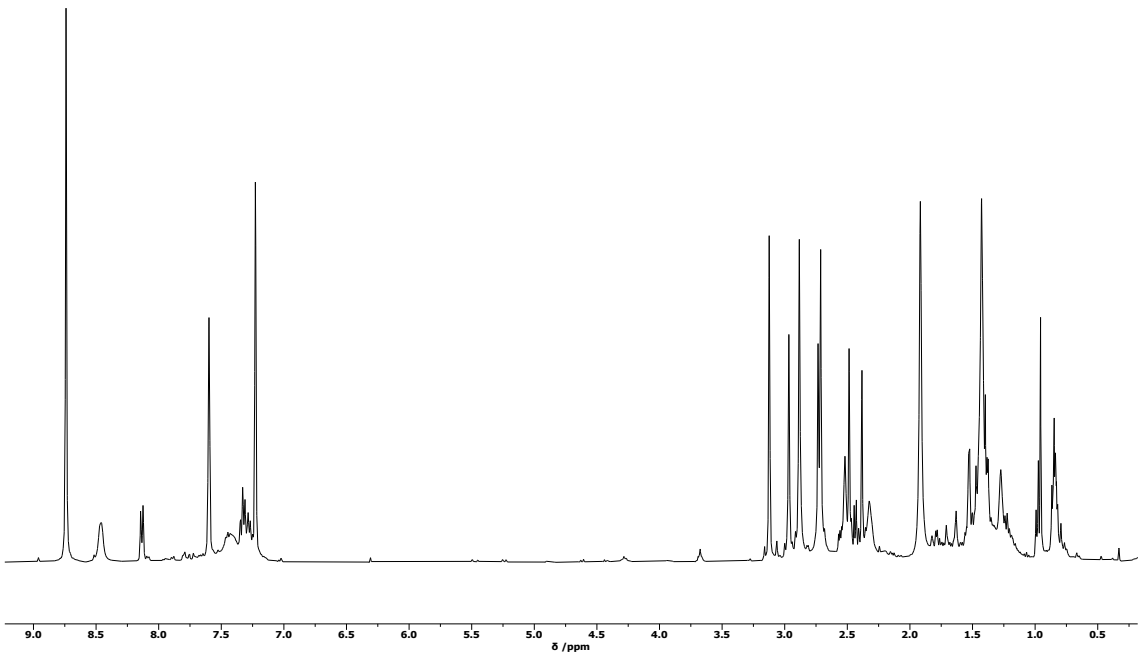

Figure A.16 ^{1}H NMR spectrum of *rac*-^{Me,Ph}SB($^{t}Bu_2$ArO,I*)Li_2 (**13f**) (pyridine-d_5, 400 MHz, 298 K).

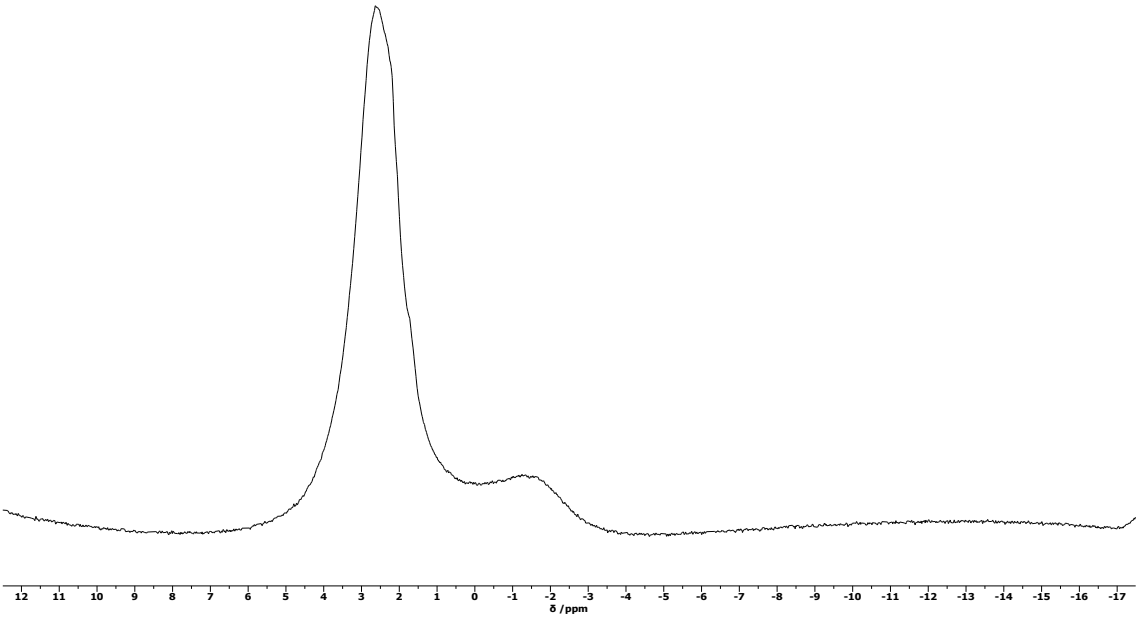

Figure A.17 ^{7}Li NMR spectrum of *rac*-^{Me,Ph}SB(^{t}Bu$_2$ArO,I*)Li$_2$ (**13f**) (pyridine-d_5, 156 MHz, 298 K).

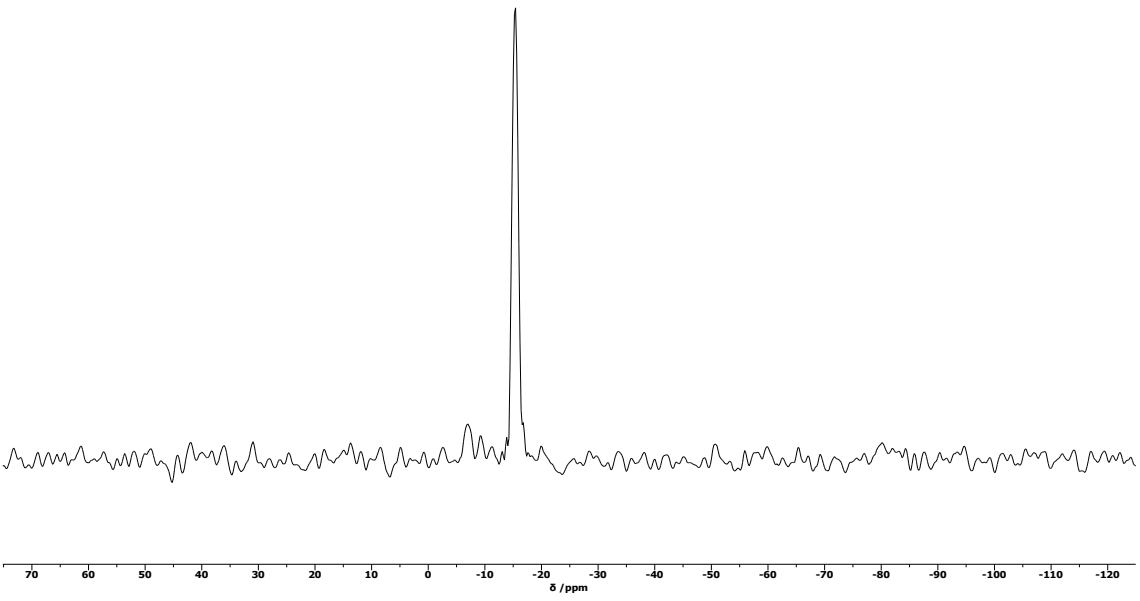

Figure A.18 ^{29}Si NMR spectrum of *rac*-^{Me,Ph}SB(^{t}Bu$_2$ArO,I*)Li$_2$ (**13f**) (^{1}H-observed HMBC, pyridine-d_5, 80 MHz, 298 K).

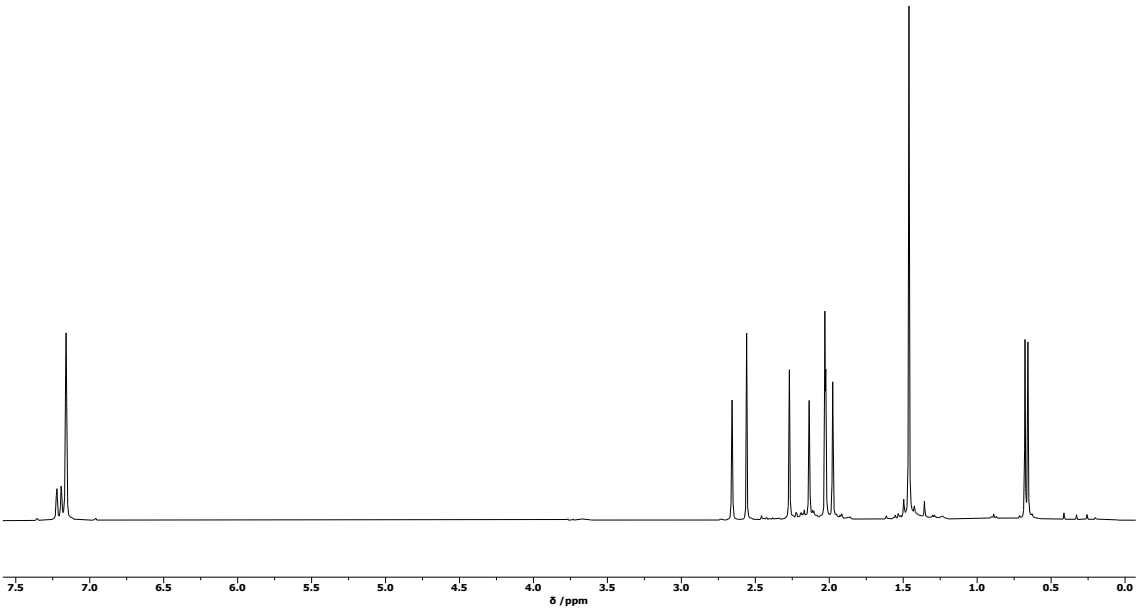

Figure A.19 ^{1}H NMR spectrum of ^{Me_2}SB($^{t\text{Bu,Me}}$ArO,I*)TiCl$_2$ (**1**) (benzene-d_6, 400 MHz, 298 K).

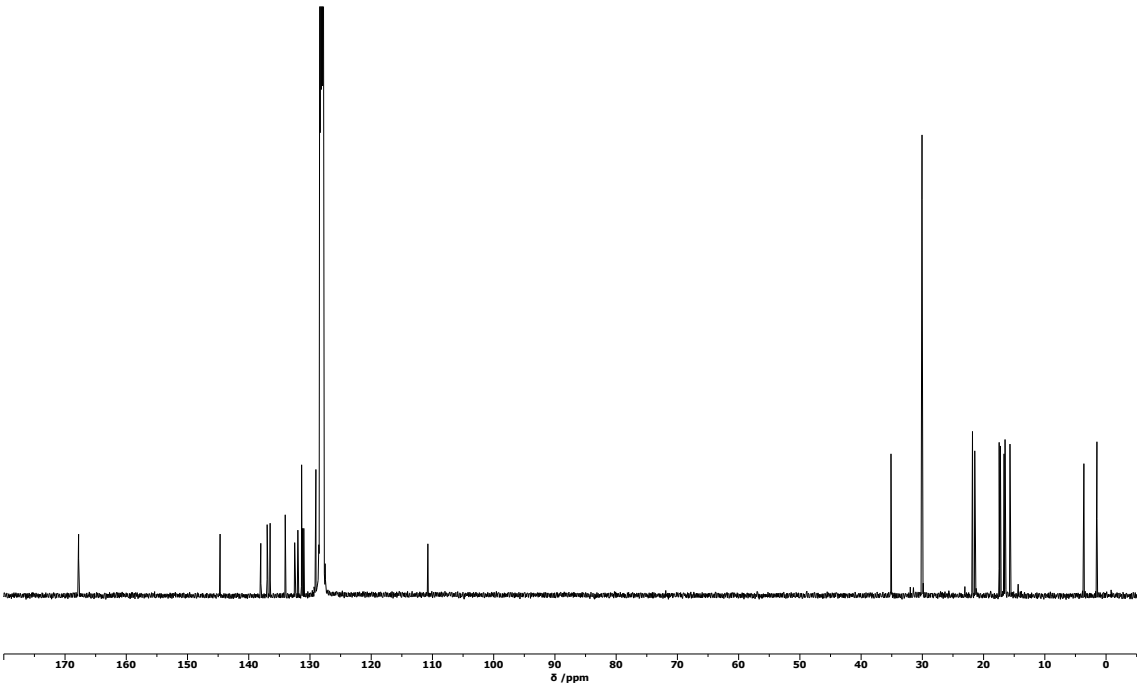

Figure A.20 ^{13}C{^{1}H} NMR spectrum of ^{Me_2}SB($^{t\text{Bu,Me}}$ArO,I*)TiCl$_2$ (**1**) (benzene-d_6, 126 MHz, 298 K).

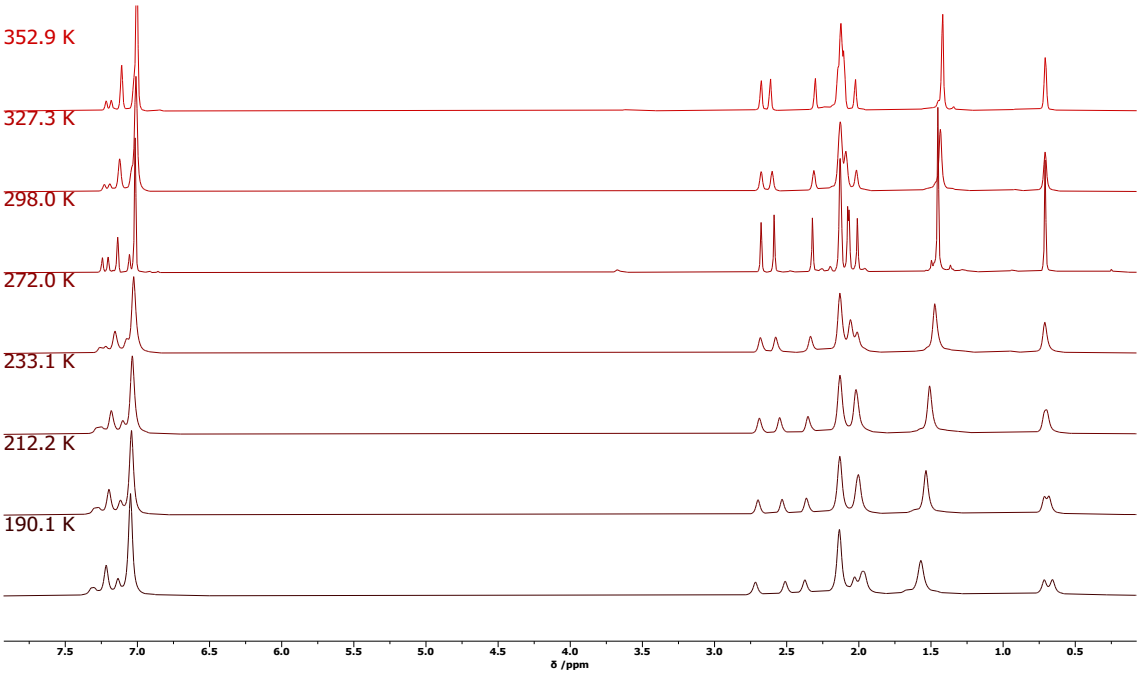

Figure A.21 ^{1}H VT NMR spectra of ^{Me_2}SB($^{t\text{Bu,Me}}$ArO,I*)TiCl$_2$ (**1**) as a function of temperature (toluene-d_8, 500 MHz, 190–353 K).

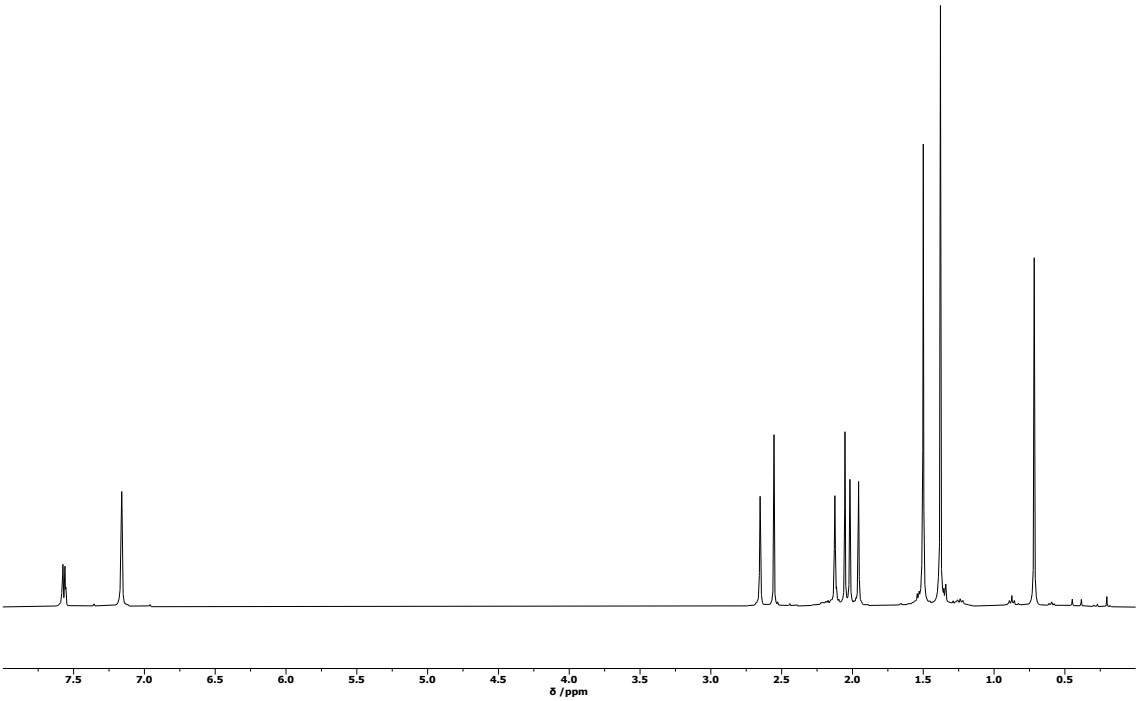

Figure A.22 ^{1}H NMR spectrum of ^{Me_2}SB($^{t\text{Bu}_2}$ArO,I*)TiCl$_2$ (**2**) (benzene-d_6, 400 MHz, 298 K).

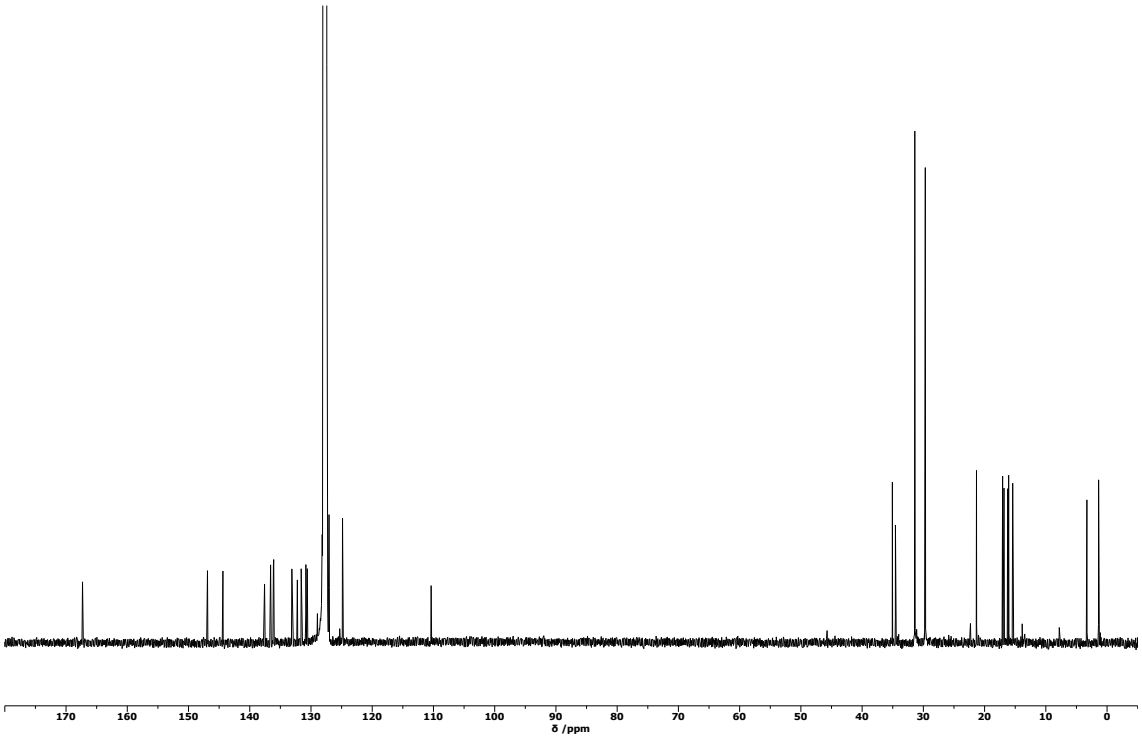

Figure A.23 $^{13}C\{^{1}H\}$ NMR spectrum of $^{Me_2}SB(^{t Bu_2}ArO,I^*)TiCl_2$ (**2**) (benzene-d_6, 126 MHz, 298 K).

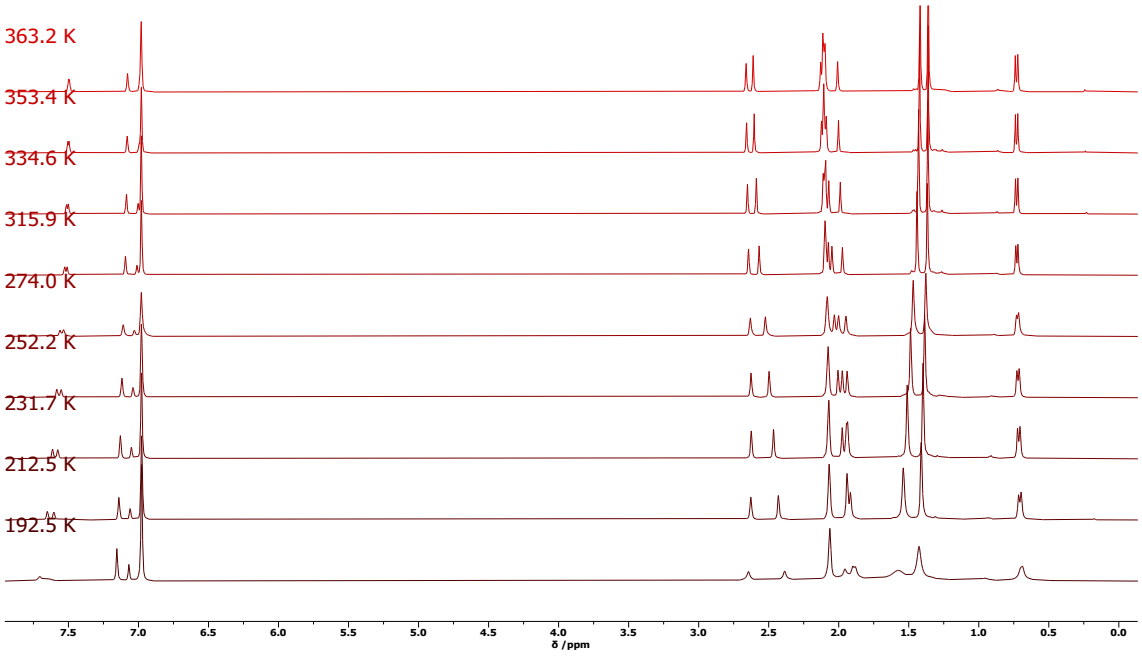

Figure A.24 ^{1}H VT NMR spectra of $^{Me_2}SB(^{t Bu_2}ArO,I^*)TiCl_2$ (**2**) as a function of temperature (toluene-d_8, 500 MHz, 193–363 K).

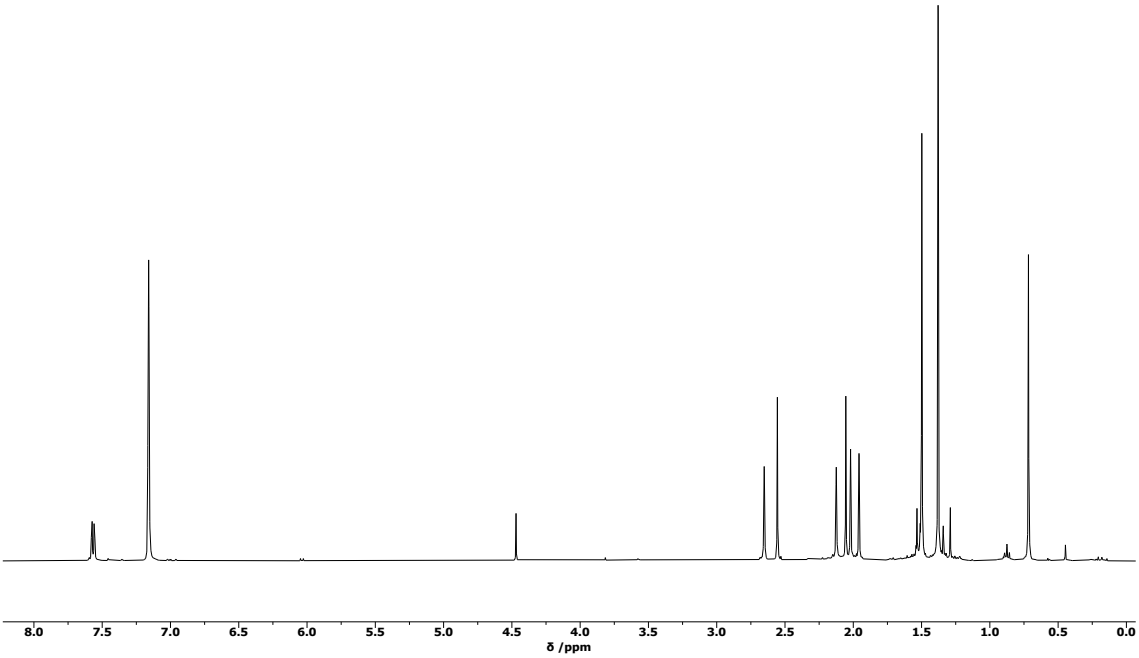

Figure A.25 ^{1}H NMR spectra of ^{Me_2}SB($^{t Bu_2}$ArO,I*)TiCl$_2$ (**2**) and H_2 (1 bar) after heating at 80 °C for 1 hour, showing that no reaction occurs (benzene-d_6, 400 MHz, 300 K).

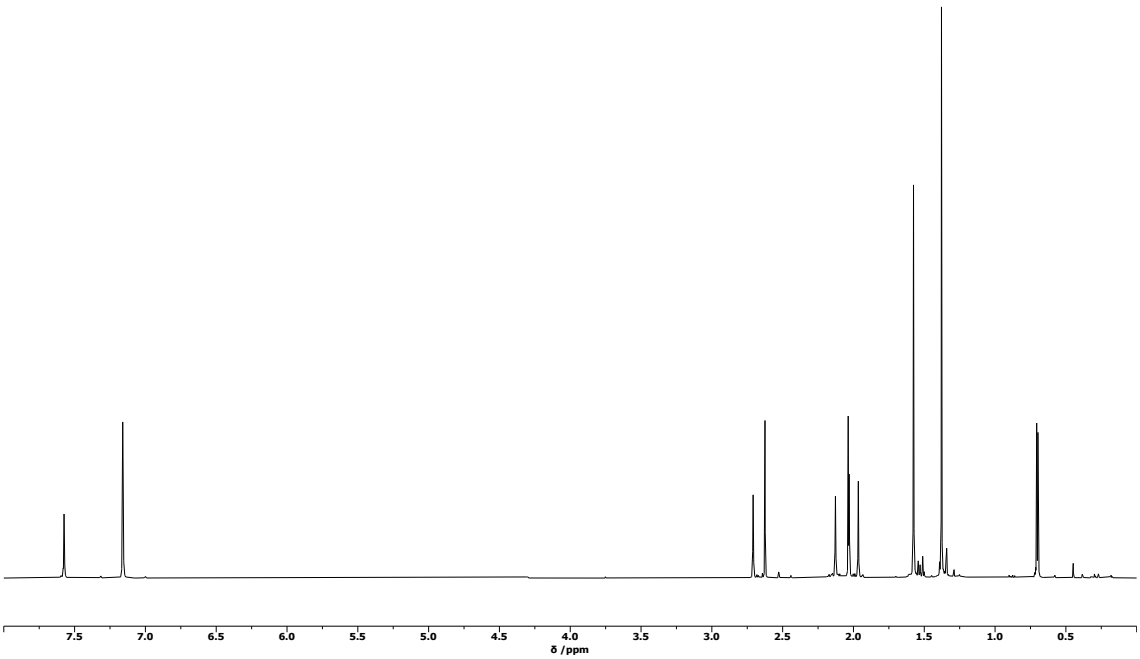

Figure A.26 ^{1}H NMR spectrum of ^{Me_2}SB($^{t Bu_2}$ArO,I*)TiBr$_2$ (**3**) (benzene-d_6, 500 MHz, 298 K).

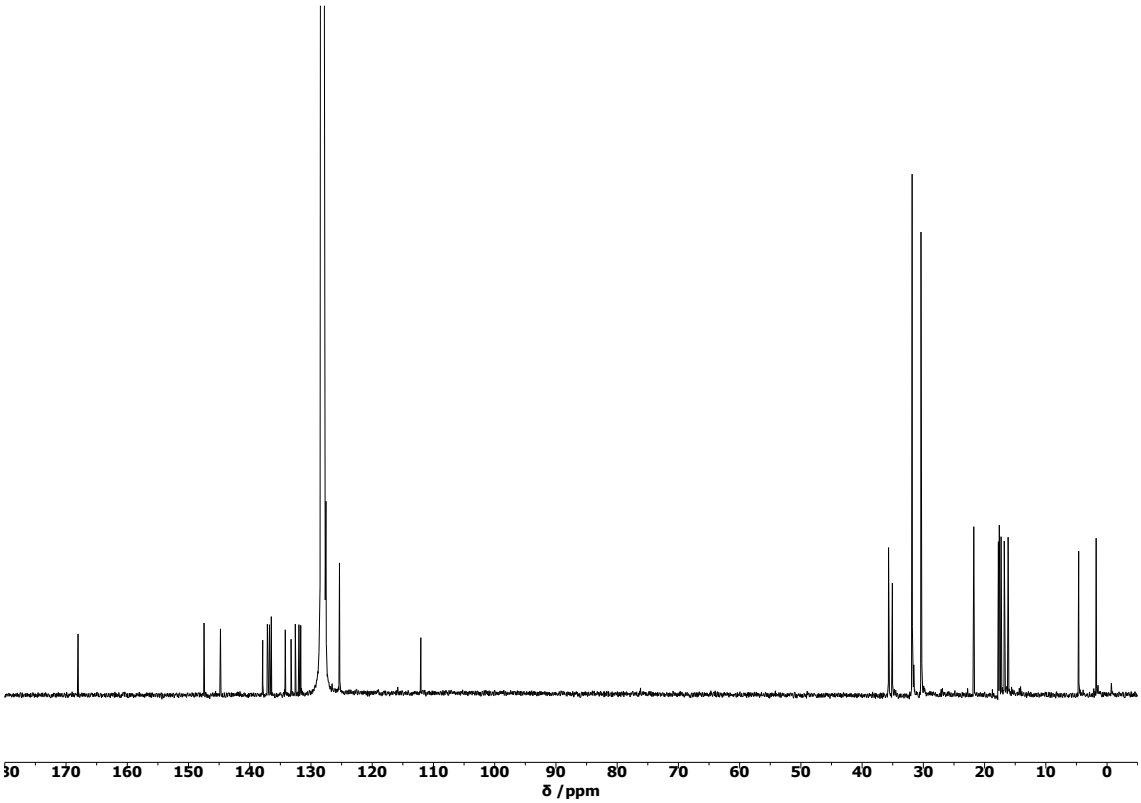

Figure A.27 $^{13}C\{^{1}H\}$ NMR spectrum of $^{Me_2}SB(^{t Bu_2}ArO,I^*)TiBr_2$ (**3**) (benzene-d_6, 126 MHz, 298 K).

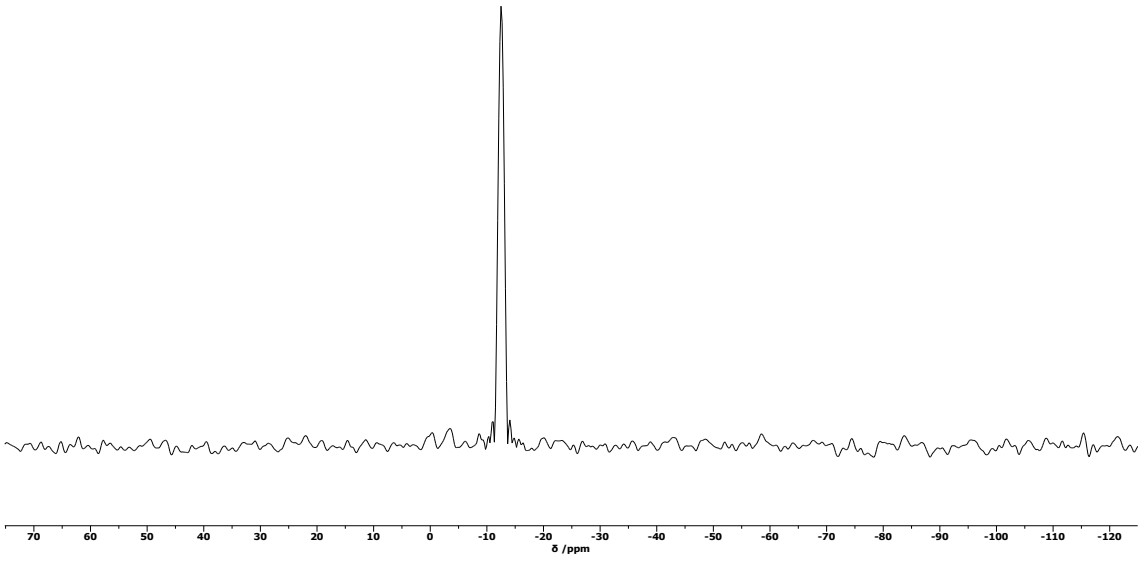

Figure A.28 ^{29}Si NMR spectrum of $^{Me_2}SB(^{t Bu_2}ArO,I^*)TiBr_2$ (**3**) (^{1}H-observed HMBC, benzene-d_6, 80 MHz, 298 K).

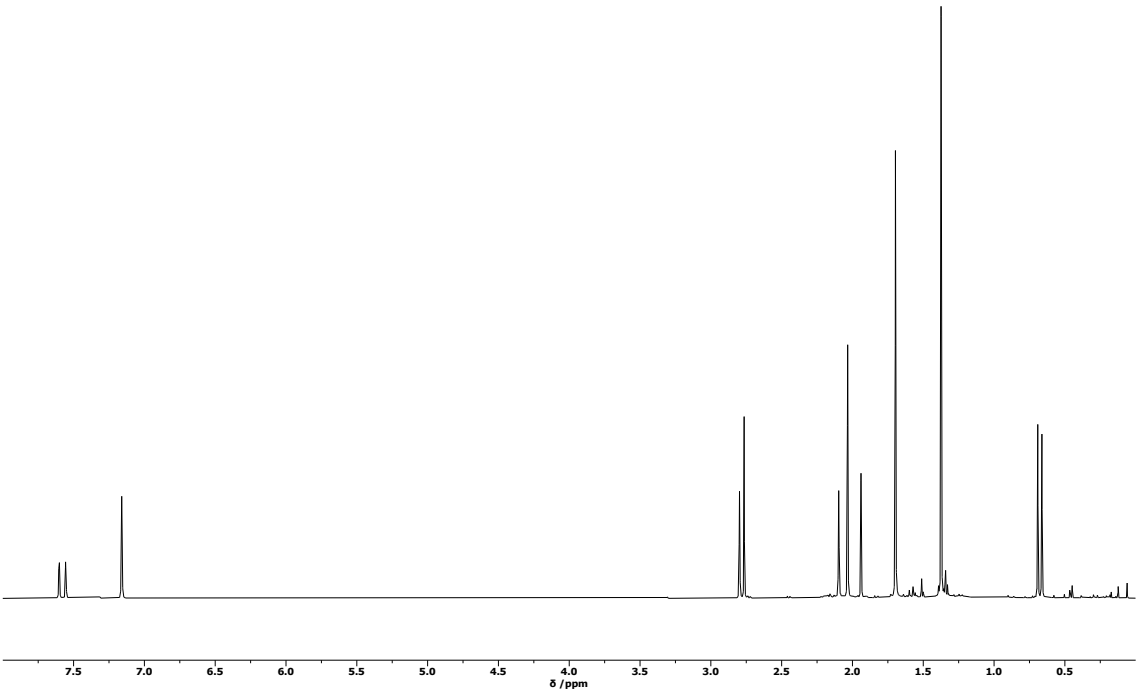

Figure A.29 ^{1}H NMR spectrum of ^{Me_2}SB($^{t Bu_2}$ArO,I*)TiI$_2$ (**4**) (benzene-d_6, 500 MHz, 298 K).

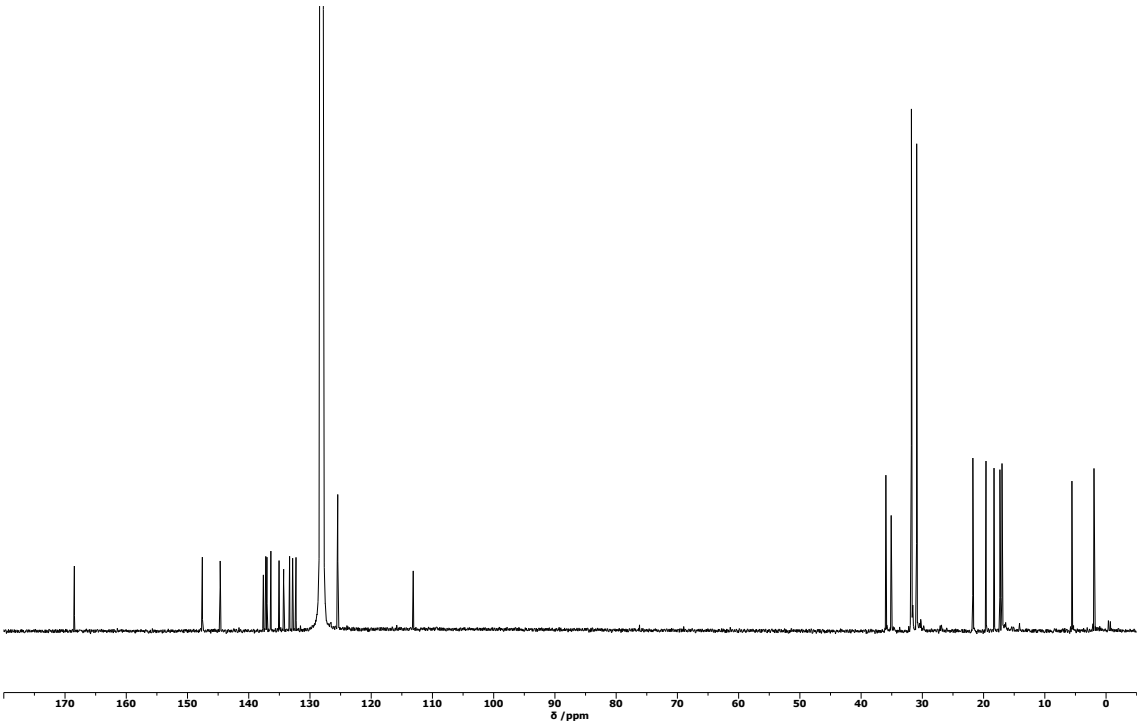

Figure A.30 ^{13}C{^{1}H} NMR spectrum of ^{Me_2}SB($^{t Bu_2}$ArO,I*)TiI$_2$ (**4**) (benzene-d_6, 126 MHz, 298 K).

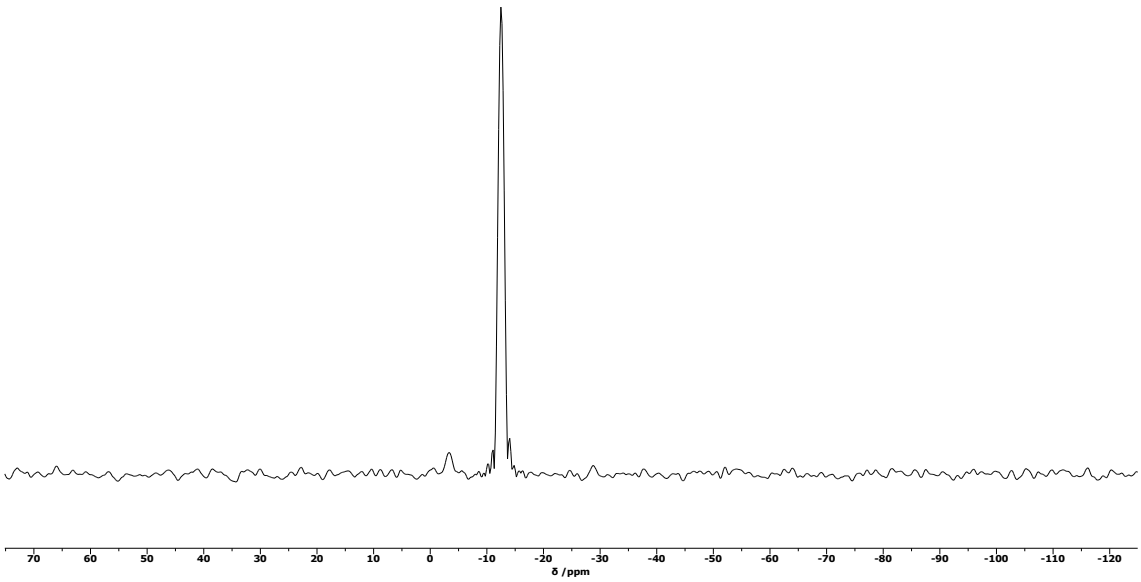

Figure A.31 ^{29}Si NMR spectrum of ^{Me_2}SB($^{t Bu_2}$ArO,I*)TiI$_2$ (**4**) (^{1}H-observed HMBC, benzene-d_6, 80 MHz, 298 K).

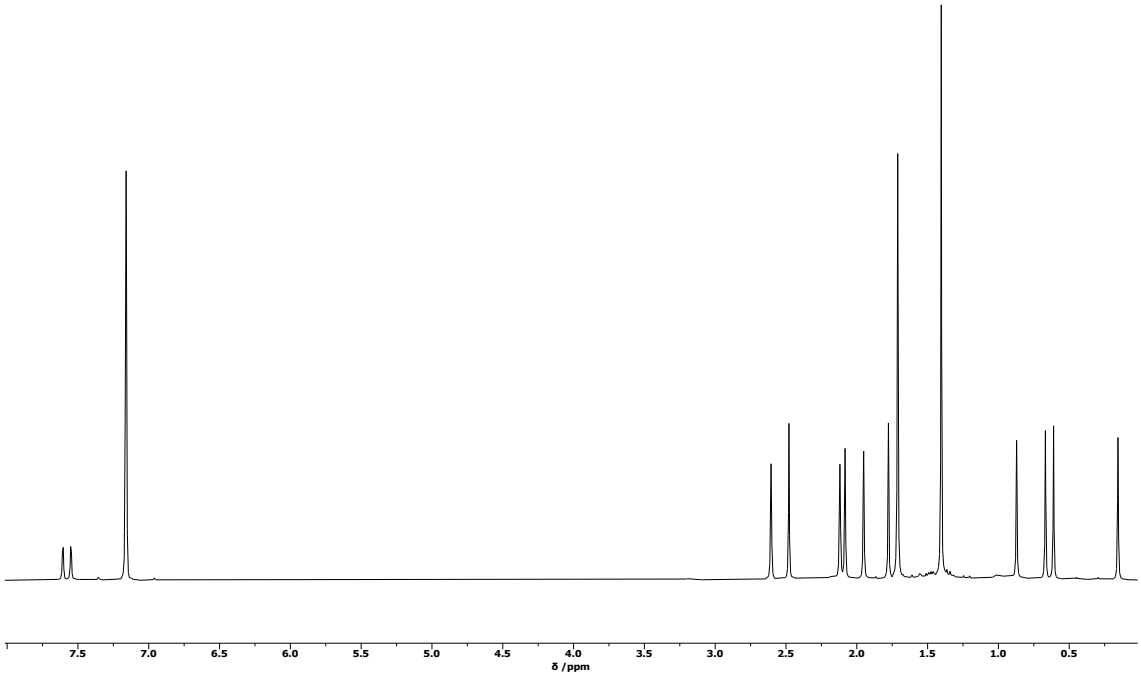

Figure A.32 ^{1}H NMR spectrum of ^{Me_2}SB($^{t Bu_2}$ArO,I*)TiMe$_2$ (**5**) (benzene-d_6, 400 MHz, 298 K).

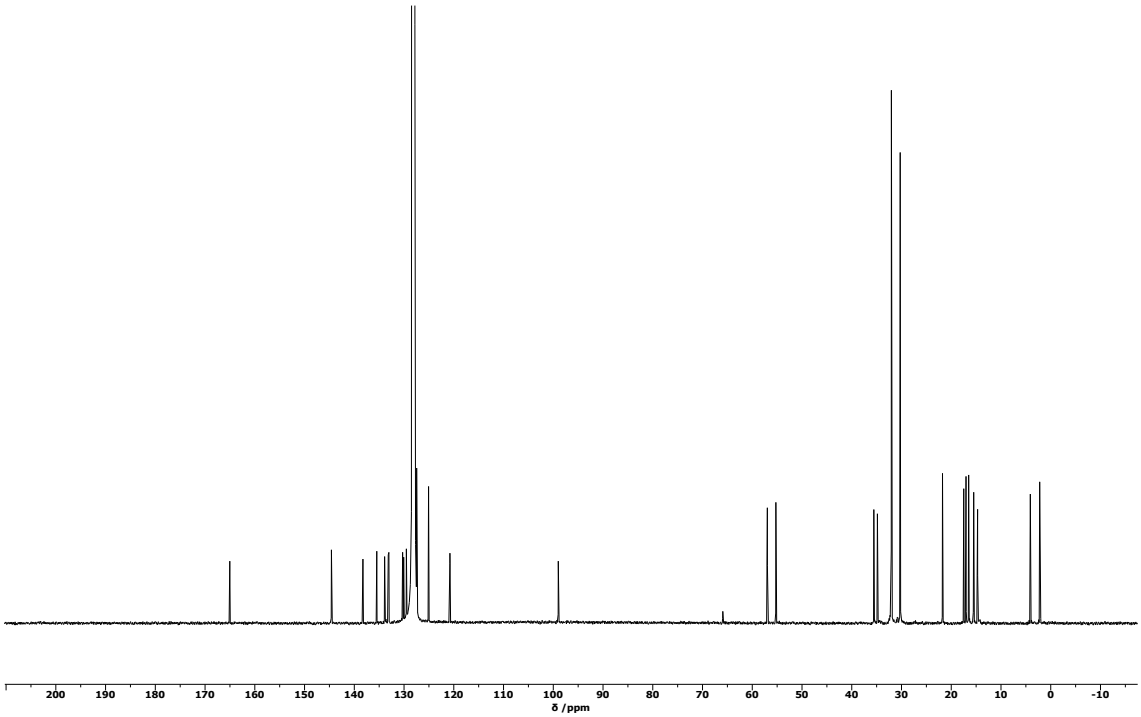

Figure A.33 $^{13}C\{^{1}H\}$ NMR spectrum of $^{Me_2}SB(^{t}Bu_2ArO,I^*)TiMe_2$ (**5**) (benzene-d_6, 126 MHz, 298 K).

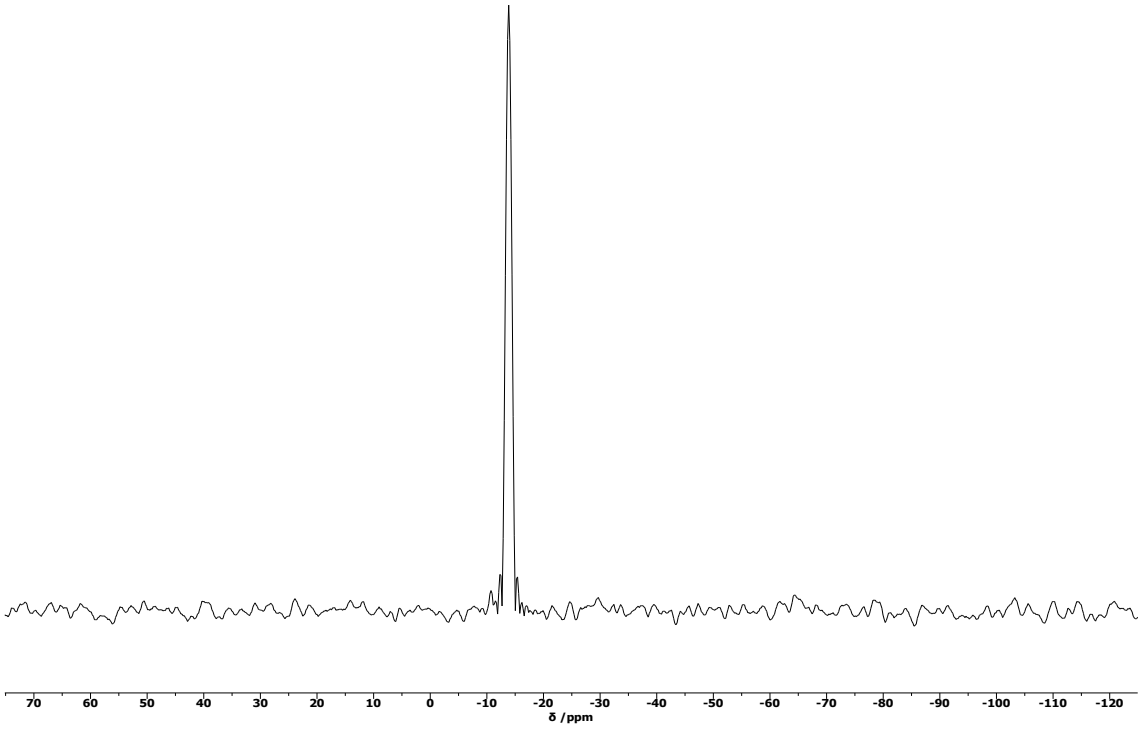

Figure A.34 ^{29}Si NMR spectrum of $^{Me_2}SB(^{t}Bu_2ArO,I^*)TiMe_2$ (**5**) (^{1}H-observed HMBC, benzene-d_6, 80 MHz, 298 K).

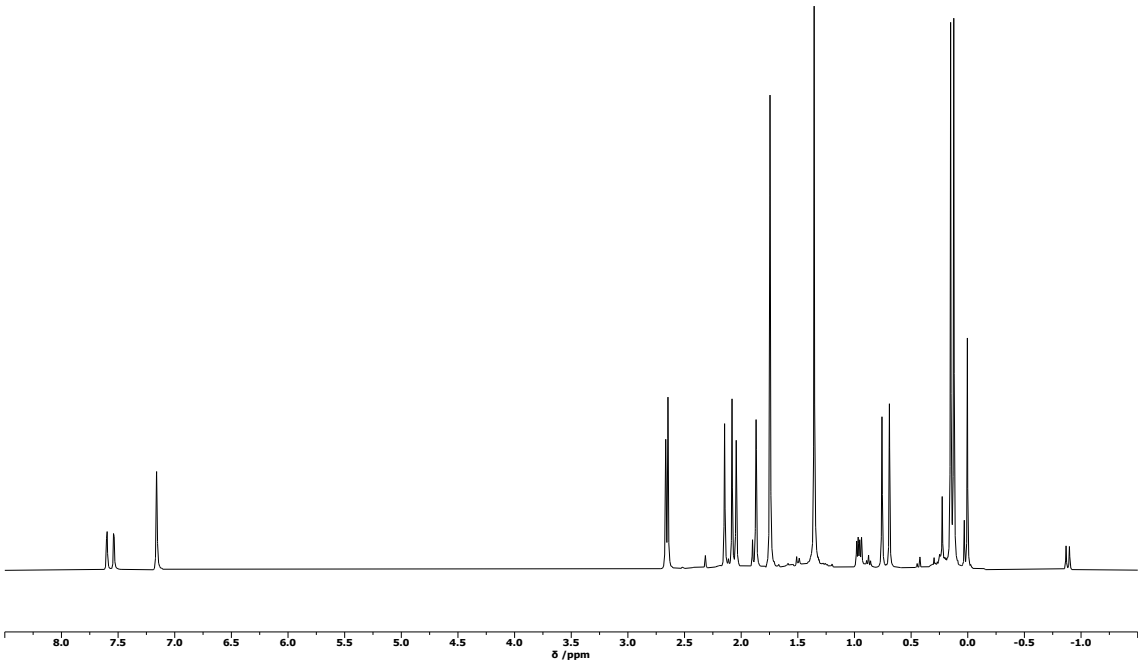

Figure A.35 ^{1}H NMR spectrum of ^{Me_2}SB(^{t}Bu$_2$ArO,I*)Ti(CH$_2$SiMe$_3$)$_2$ (**6**) (benzene-d_6, 400 MHz, 297 K).

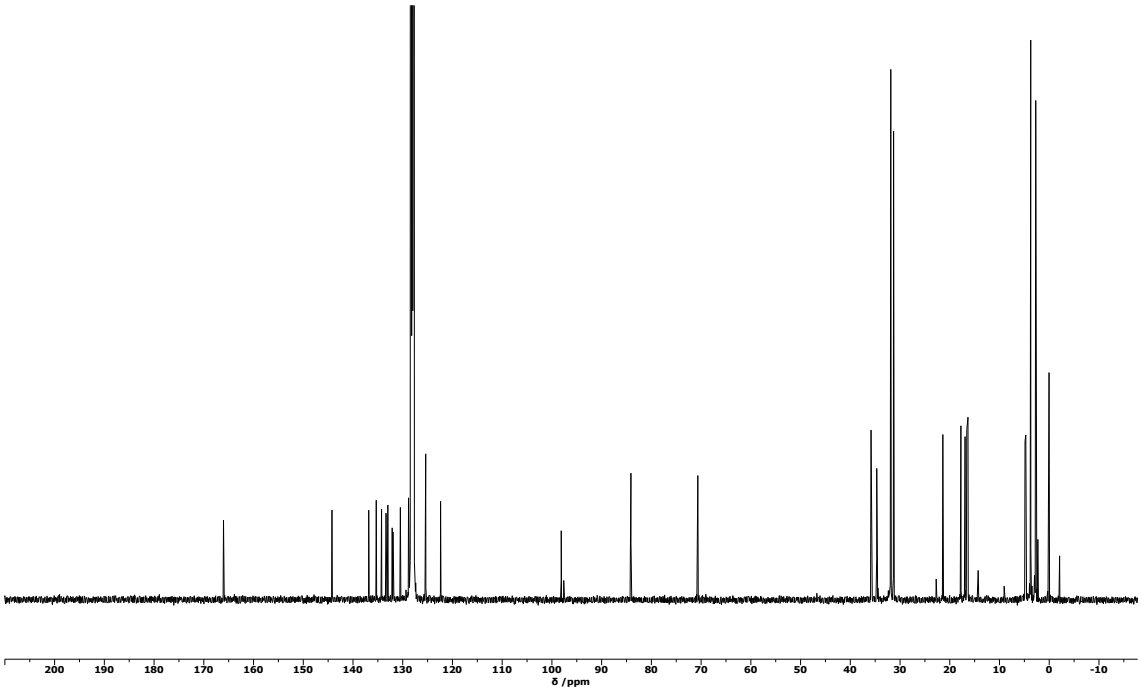

Figure A.36 ^{13}C{^{1}H} NMR spectrum of ^{Me_2}SB(^{t}Bu$_2$ArO,I*)Ti(CH$_2$SiMe$_3$)$_2$ (**6**) (benzene-d_6, 101 MHz, 298 K).

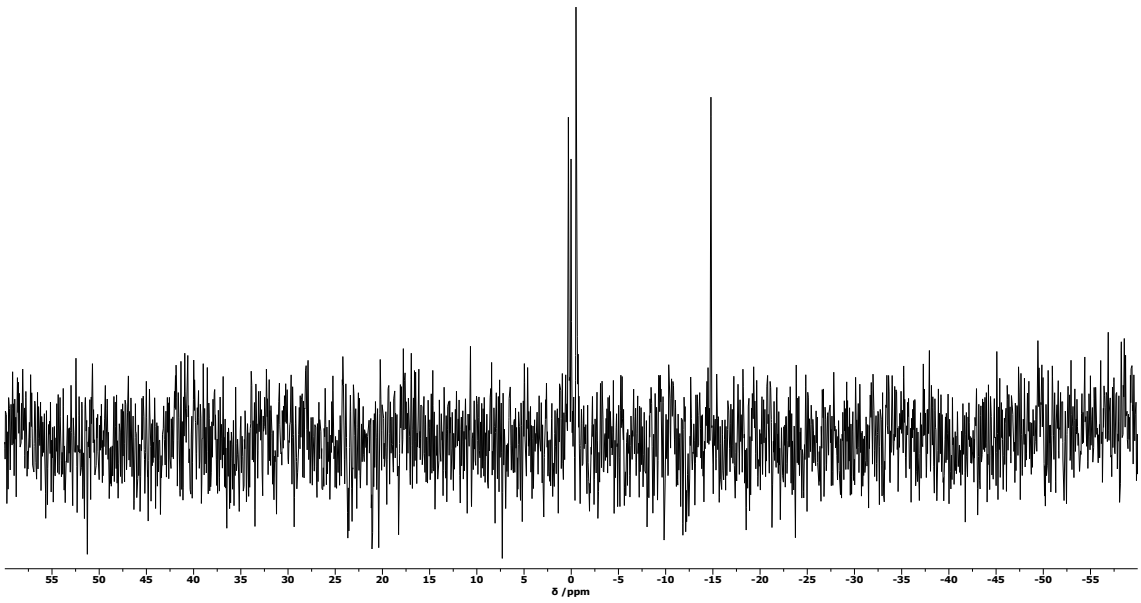

Figure A.37 ^{29}Si NMR spectrum of ^{Me_2}SB($^{t Bu_2}$ArO,I*)Ti(CH_2SiMe_3)$_2$ (**6**) (benzene-d_6, 80 MHz, 297 K).

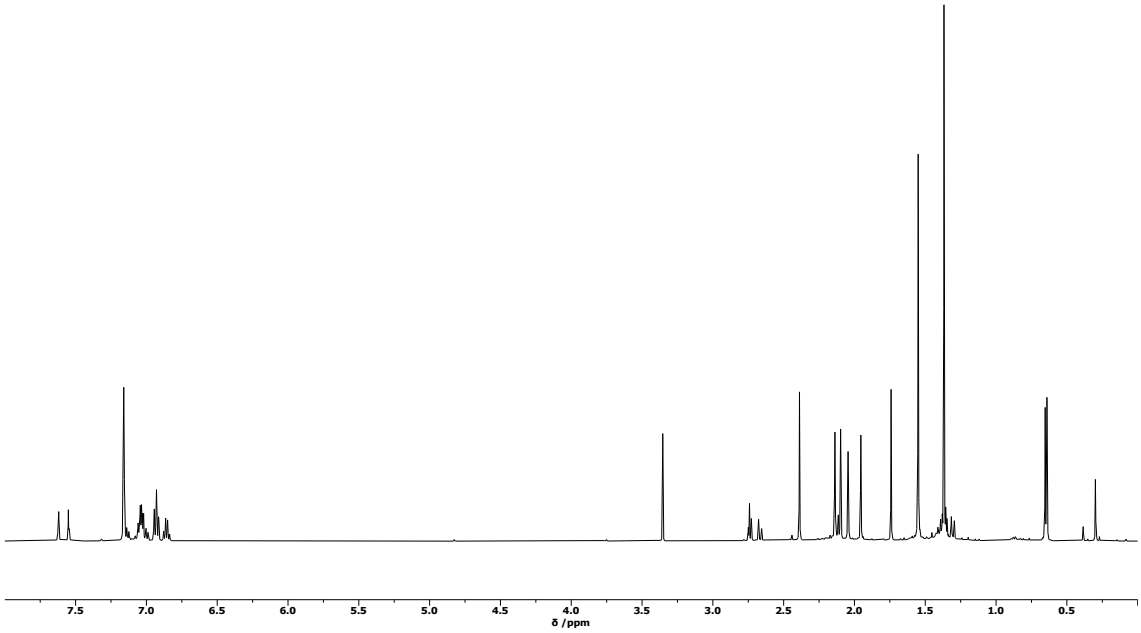

Figure A.38 ^{1}H NMR spectrum of ^{Me_2}SB($^{t Bu_2}$ArO,I*)TiBn$_2$ (**7**) (benzene-d_6, 500 MHz, 298 K).

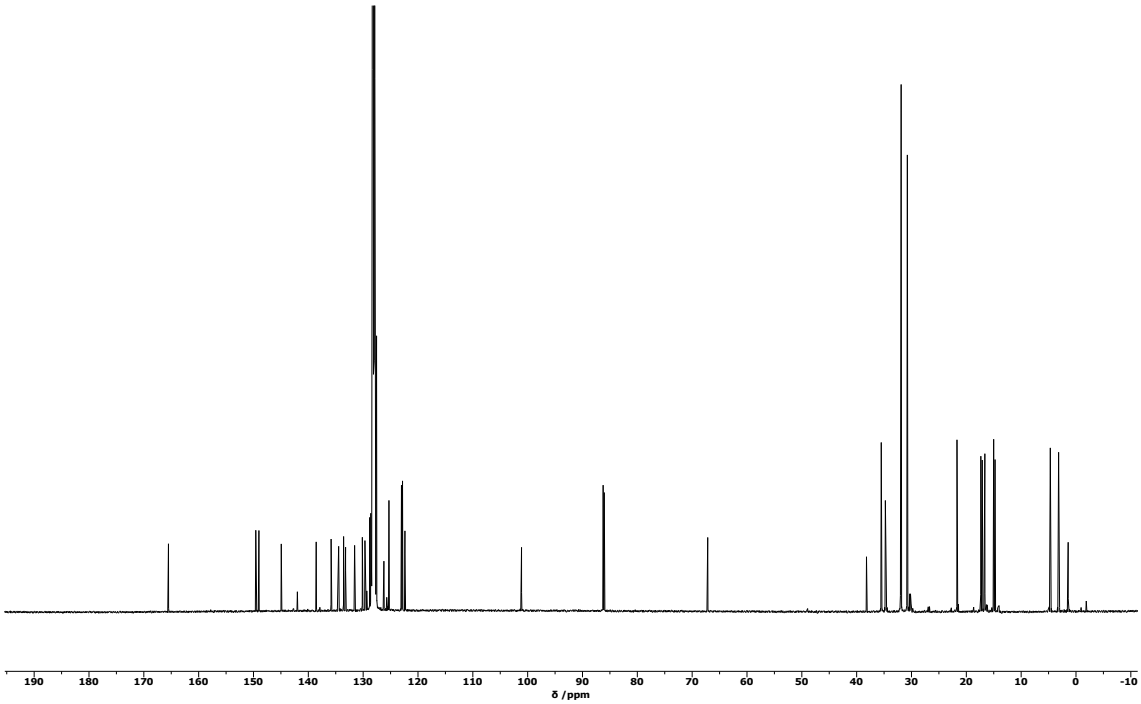

Figure A.39 $^{13}C\{^{1}H\}$ NMR spectrum of $^{Me_2}SB(^{tBu_2}ArO,I^*)TiBn_2$ (**7**) (benzene-d_6, 151 MHz, 298 K).

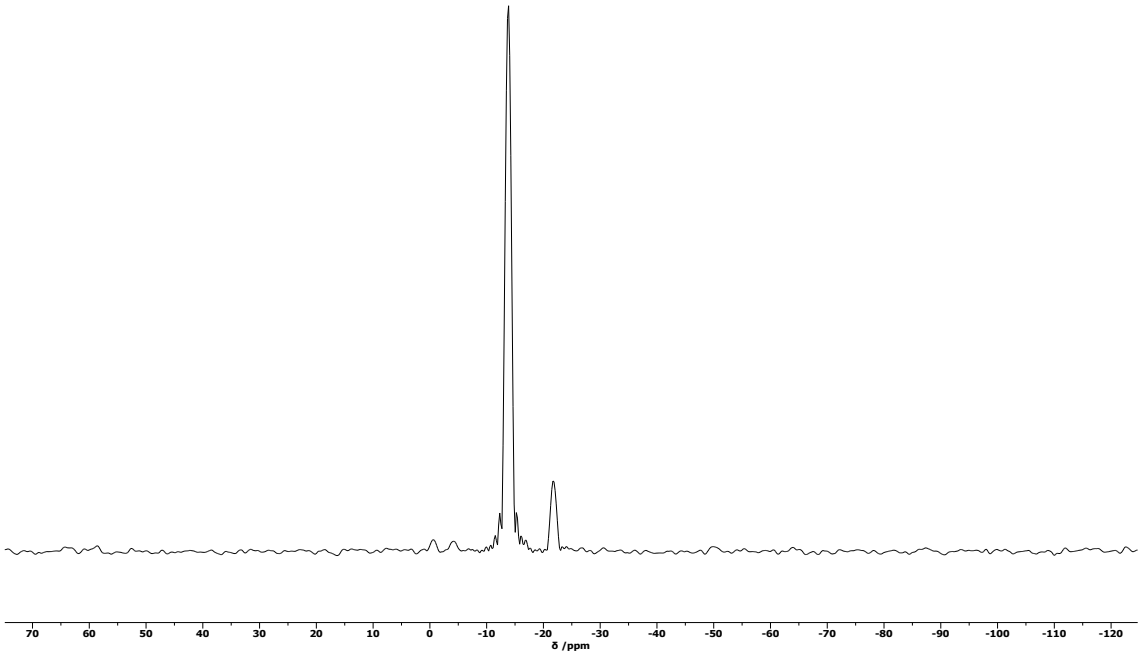

Figure A.40 ^{29}Si NMR spectrum of $^{Me_2}SB(^{tBu_2}ArO,I^*)TiBn_2$ (**7**) (^{1}H-observed HMBC, benzene-d_6, 80 MHz, 298 K).

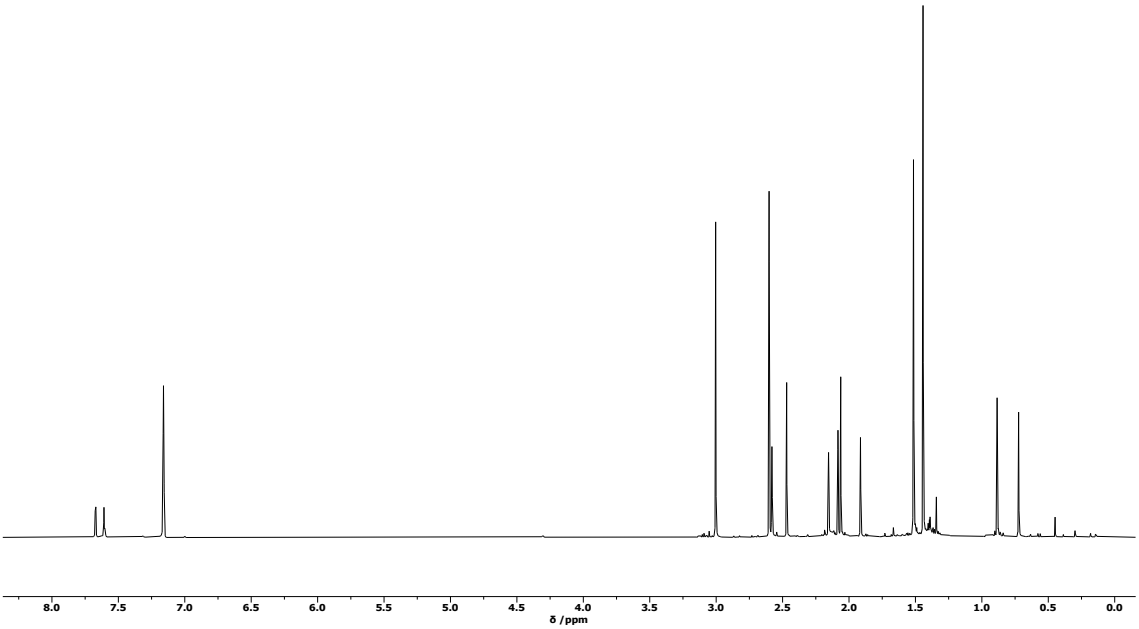

Figure A.41 ^{1}H NMR spectrum of ^{Me_2}SB(^{t}Bu$_2$ArO,I*)Ti(NMe$_2$)$_2$ (**8**) (benzene-d_6, 500 MHz, 298 K).

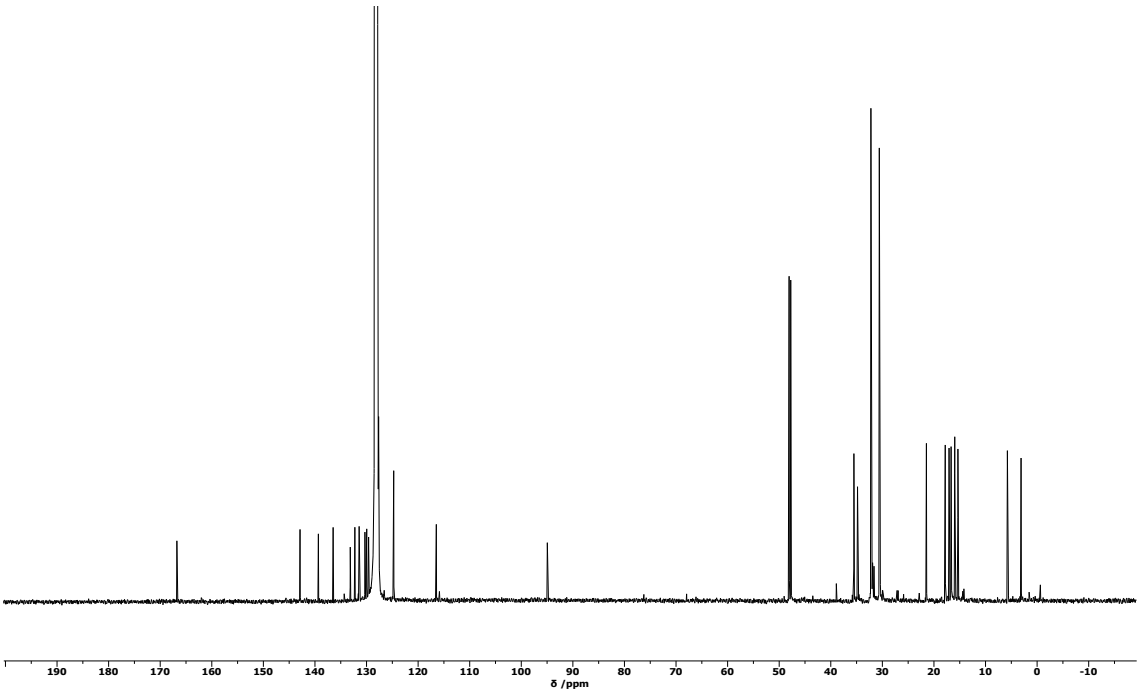

Figure A.42 ^{13}C{^{1}H} NMR spectrum of ^{Me_2}SB(^{t}Bu$_2$ArO,I*)Ti(NMe$_2$)$_2$ (**8**) (benzene-d_6, 126 MHz, 298 K).

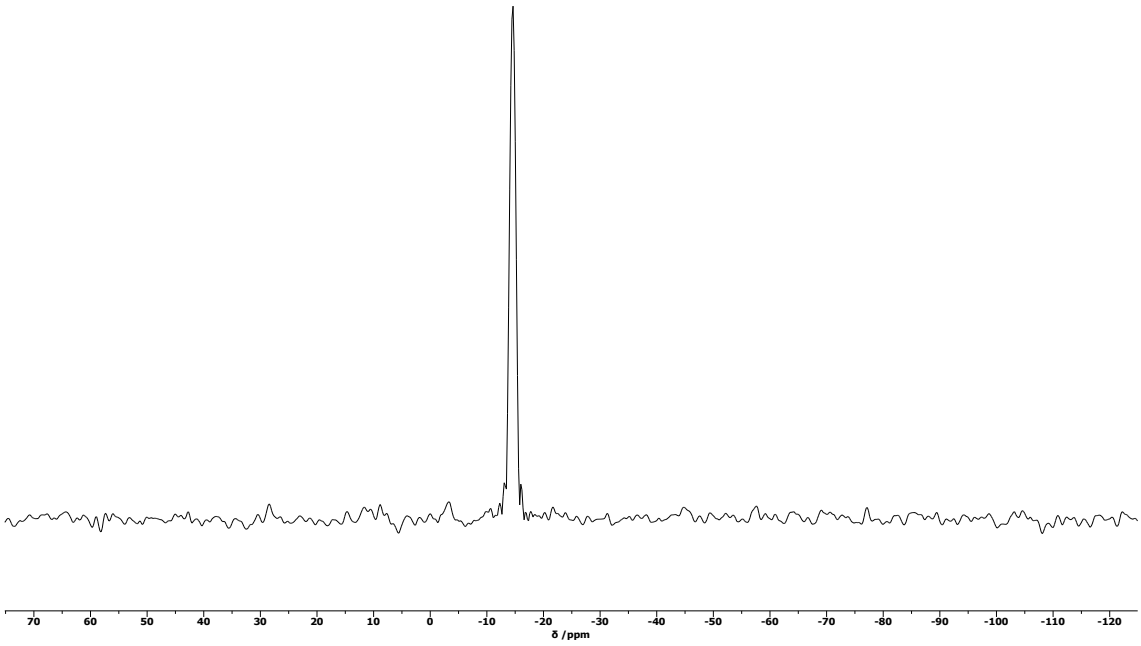

Figure A.43 ^{29}Si NMR spectrum of ^{Me_2}SB($^{t Bu_2}$ArO,I*)Ti(NMe$_2$)$_2$ (**8**) (^{1}H-observed HMBC, benzene-d_6, 80 MHz, 298 K).

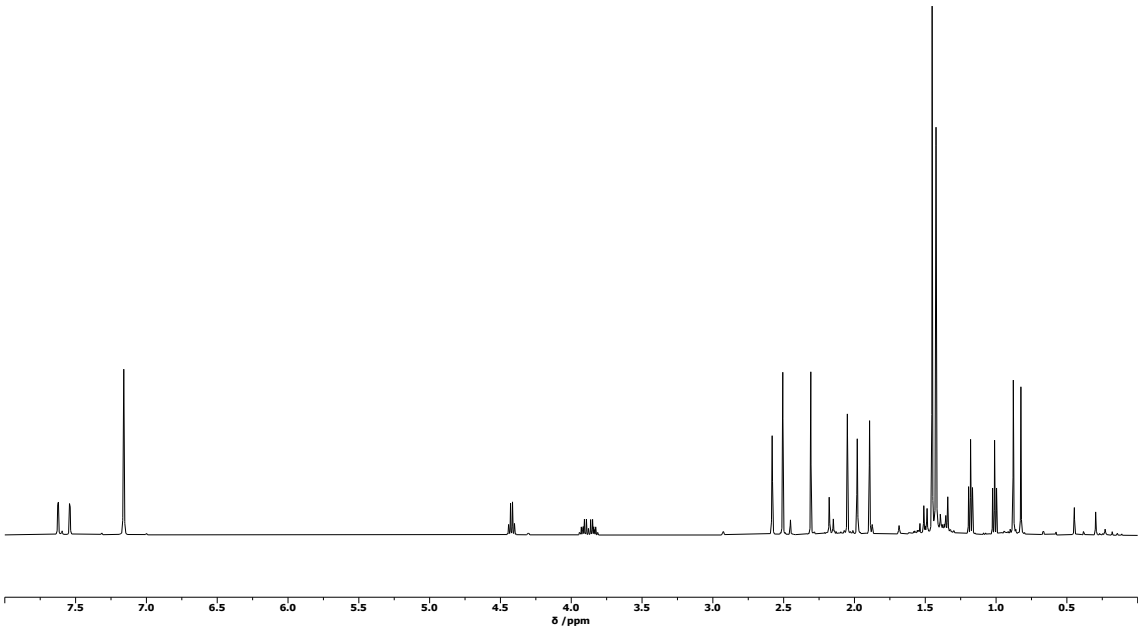

Figure A.44 ^{1}H NMR spectrum of ^{Me_2}SB($^{t Bu_2}$ArO,I*)Ti(OEt)$_2$ (**9**) (benzene-d_6, 500 MHz, 298 K).

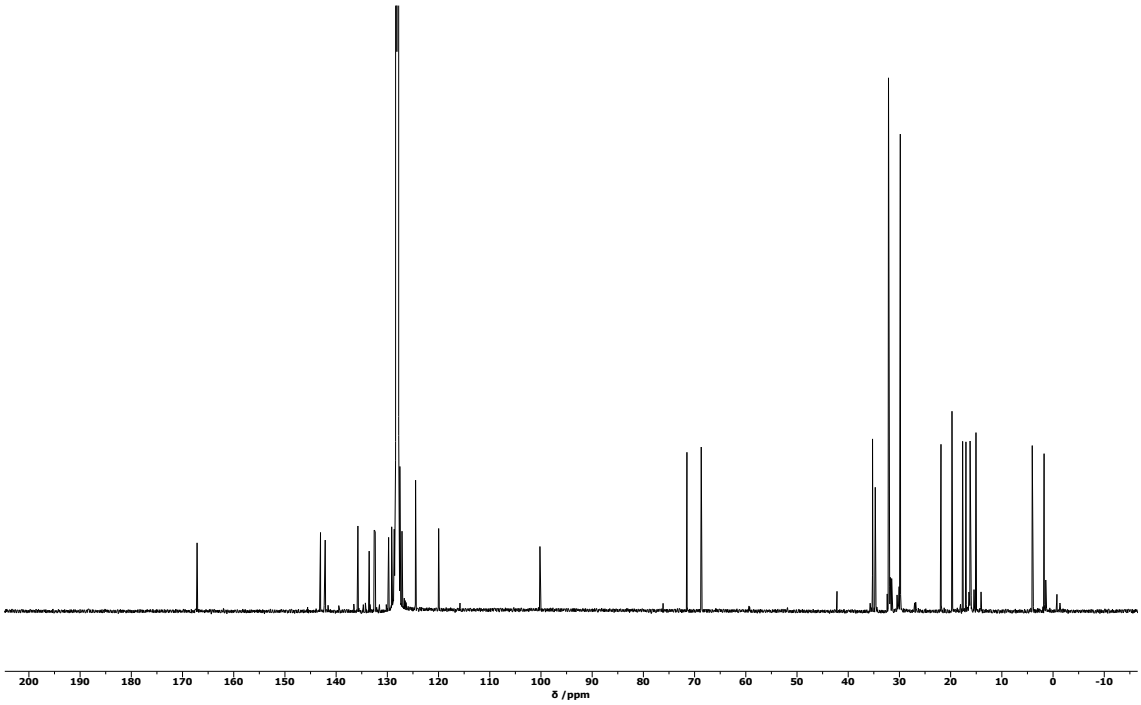

Figure A.45 $^{13}C\{^{1}H\}$ NMR spectrum of $^{Me_2}SB(^{t Bu_2}ArO,I^*)Ti(OEt)_2$ (**9**) (benzene-d_6, 126 MHz, 298 K).

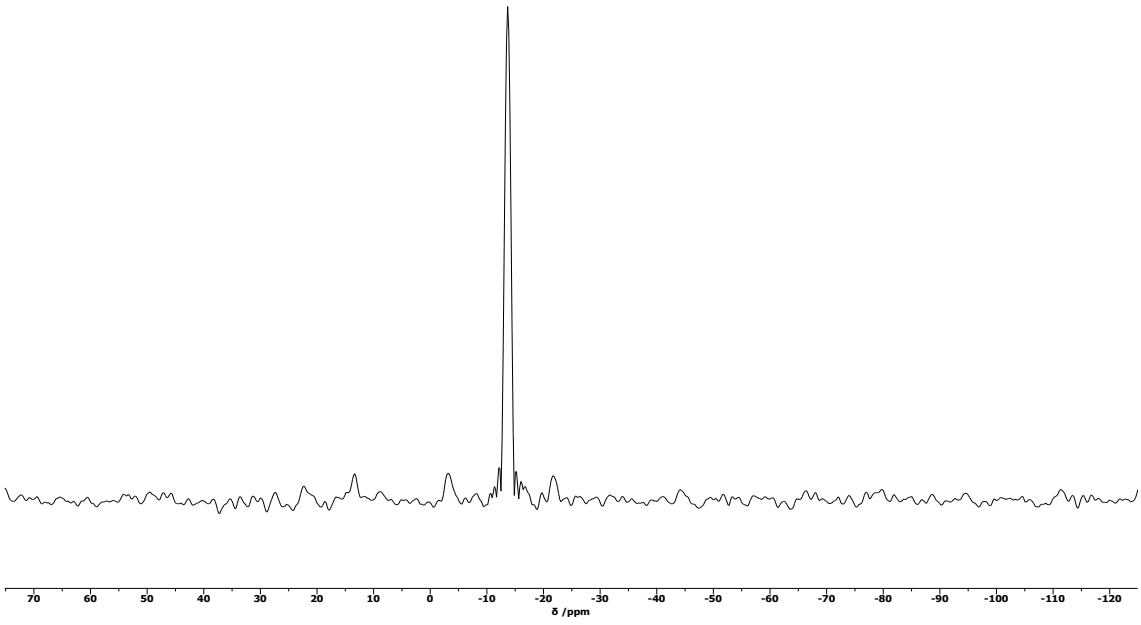

Figure A.46 ^{29}Si NMR spectrum of $^{Me_2}SB(^{t Bu_2}ArO,I^*)Ti(OEt)_2$ (**9**) (^{1}H-observed HMBC, benzene-d_6, 80 MHz, 298 K).

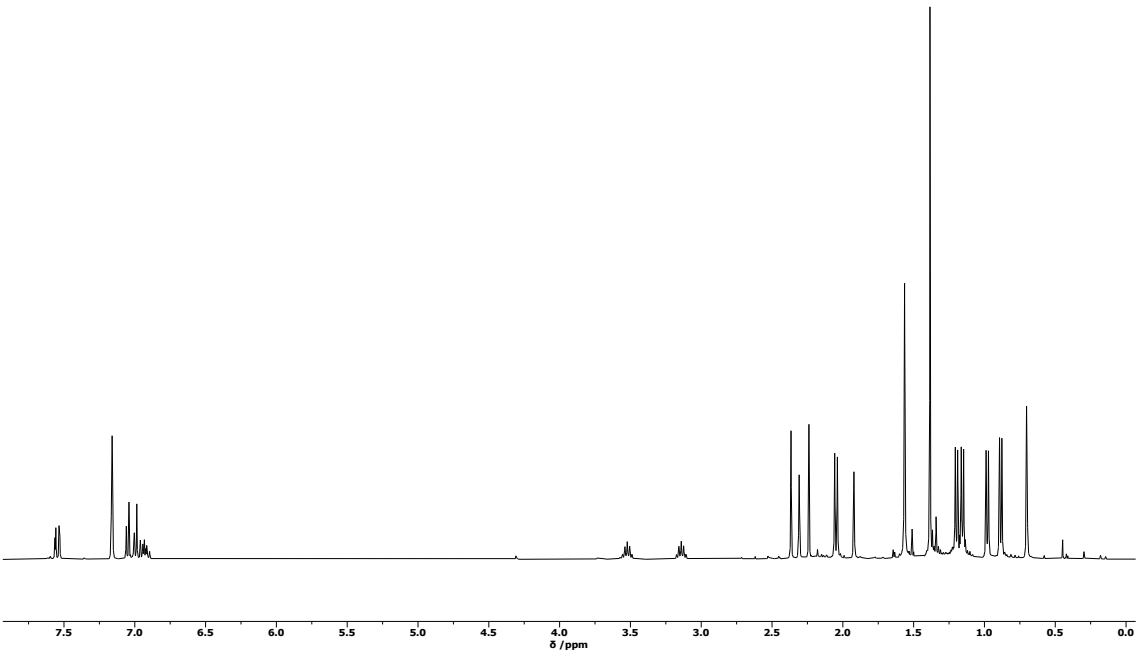

Figure A.47 ^{1}H NMR spectrum of ^{Me_2}SB($^{t Bu_2}$ArO,I*)Ti(ODipp)$_2$ (**10**) (benzene-d_6, 400 MHz, 298 K).

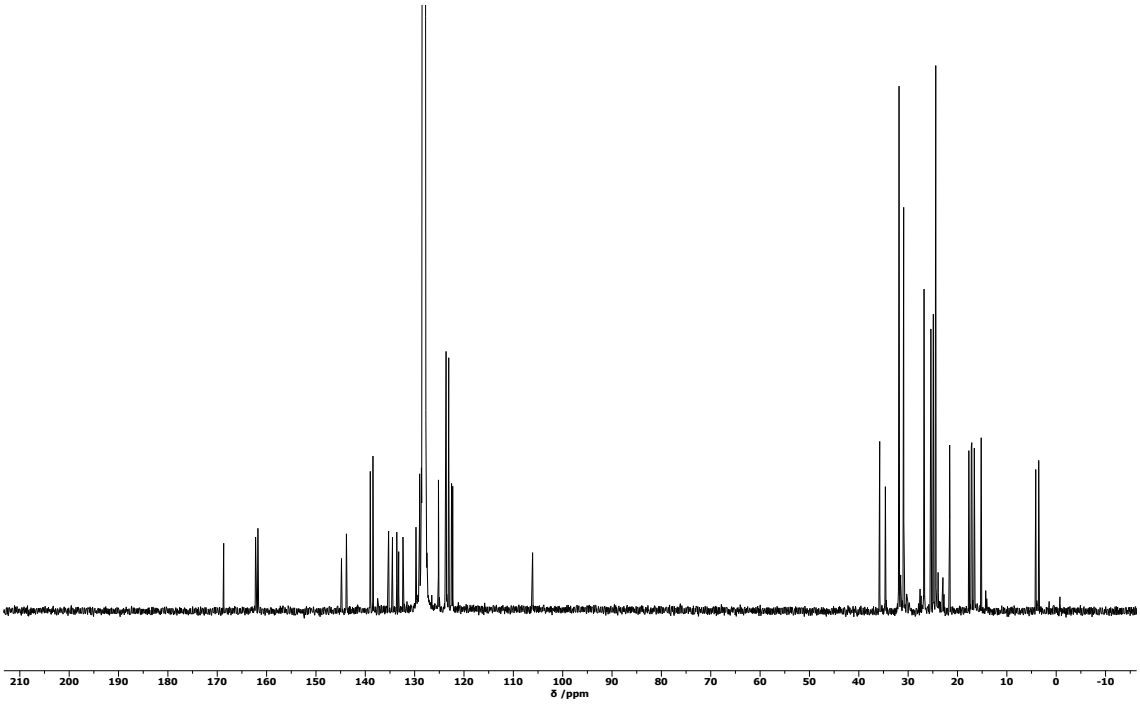

Figure A.48 ^{13}C{^{1}H} NMR spectrum of ^{Me_2}SB($^{t Bu_2}$ArO,I*)Ti(ODipp)$_2$ (**10**) (benzene-d_6, 126 MHz, 298 K).

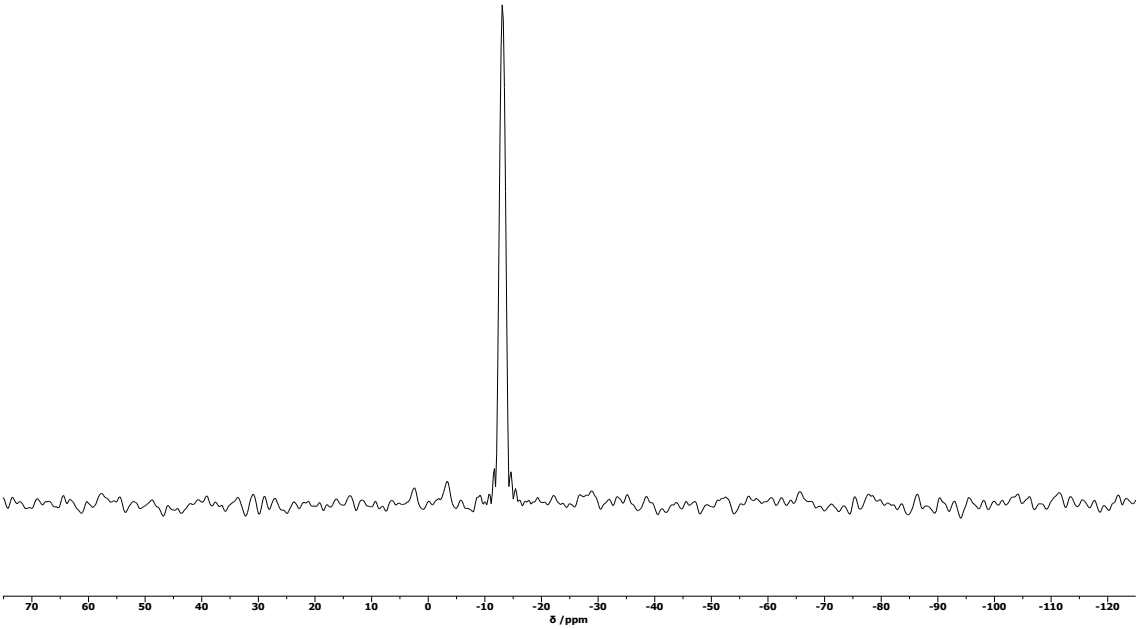

Figure A.49 ^{29}Si NMR spectrum of ^{Me_2}SB($^{t Bu_2}$ArO,I*)Ti(ODipp)$_2$ (**10**) (^{1}H-observed HMBC, benzene-d_6, 80 MHz, 298 K).

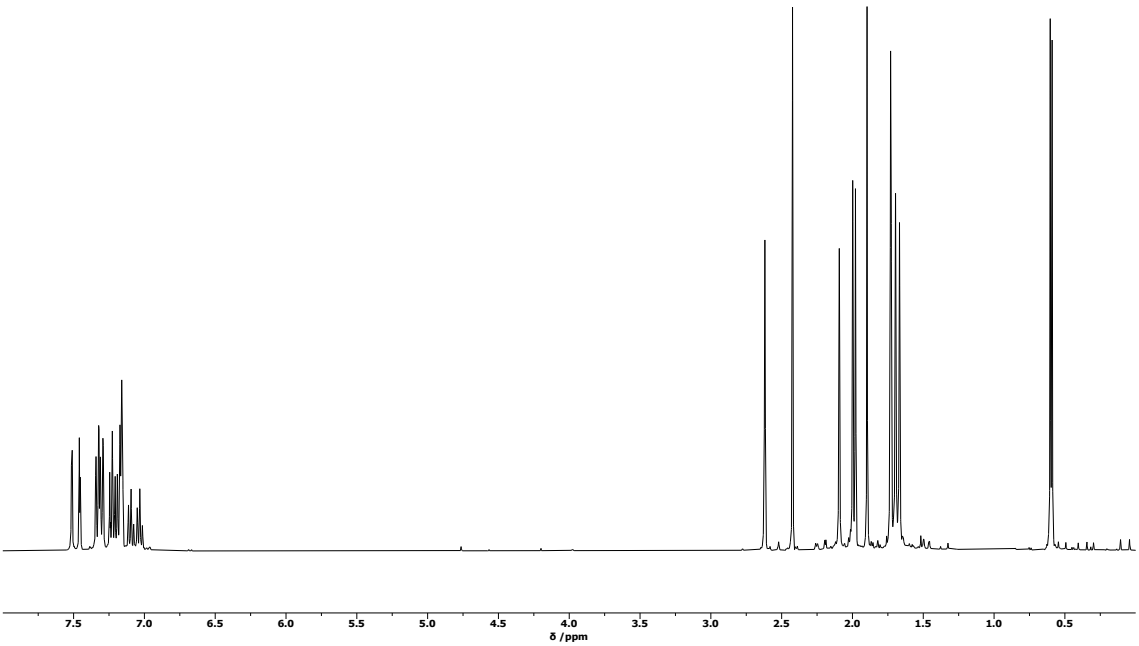

Figure A.50 ^{1}H NMR spectrum of ^{Me_2}SB(^{Cumyl_2}ArO,I*)TiCl$_2$ (**11**) (benzene-d_6, 400 MHz, 298 K).

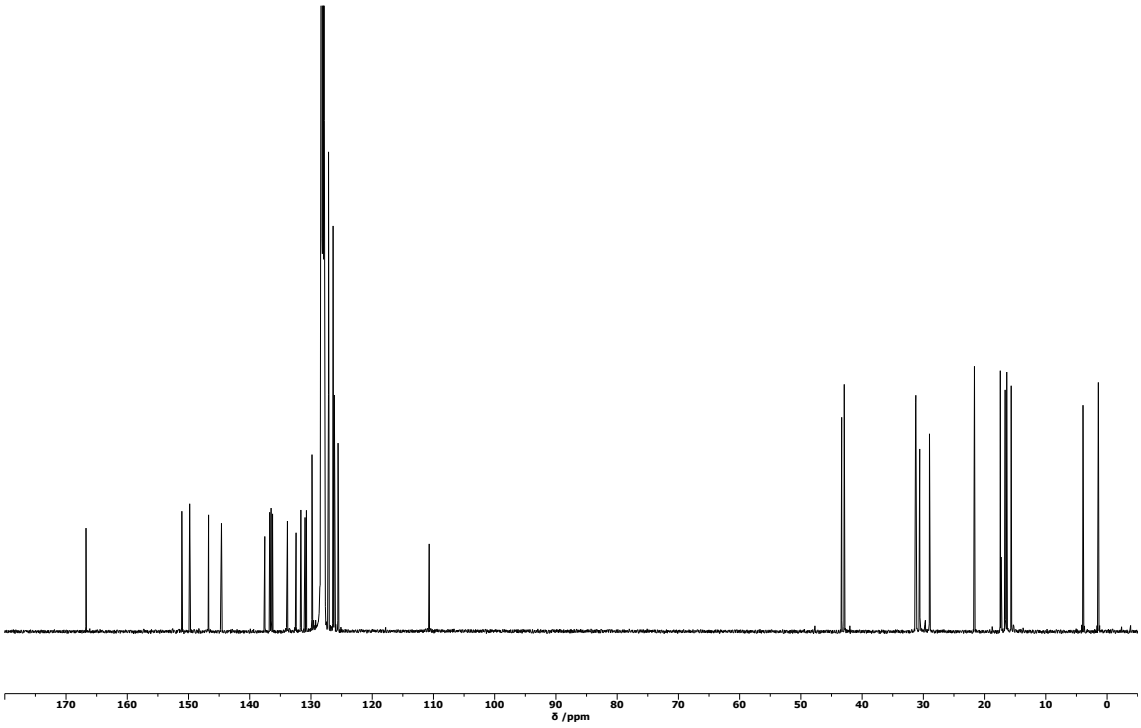

Figure A.51 $^{13}C\{^{1}H\}$ NMR spectrum of $^{Me_2}SB(^{Cumyl_2}ArO,I^*)TiCl_2$ (**11**) (benzene-d_6, 126 MHz, 298 K).

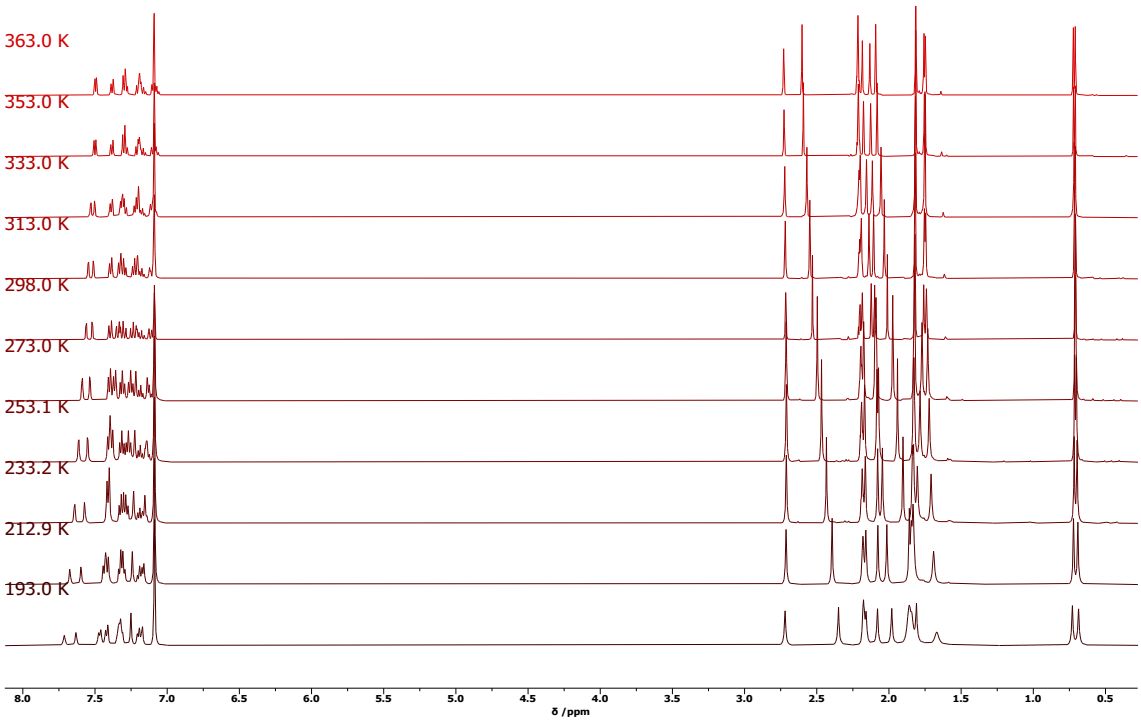

Figure A.52 ^{1}H VT NMR spectra of $^{Me_2}SB(^{Cumyl_2}ArO,I^*)TiCl_2$ (**11**) as a function of temperature (toluene-d_8, 500 MHz, 193–363 K).

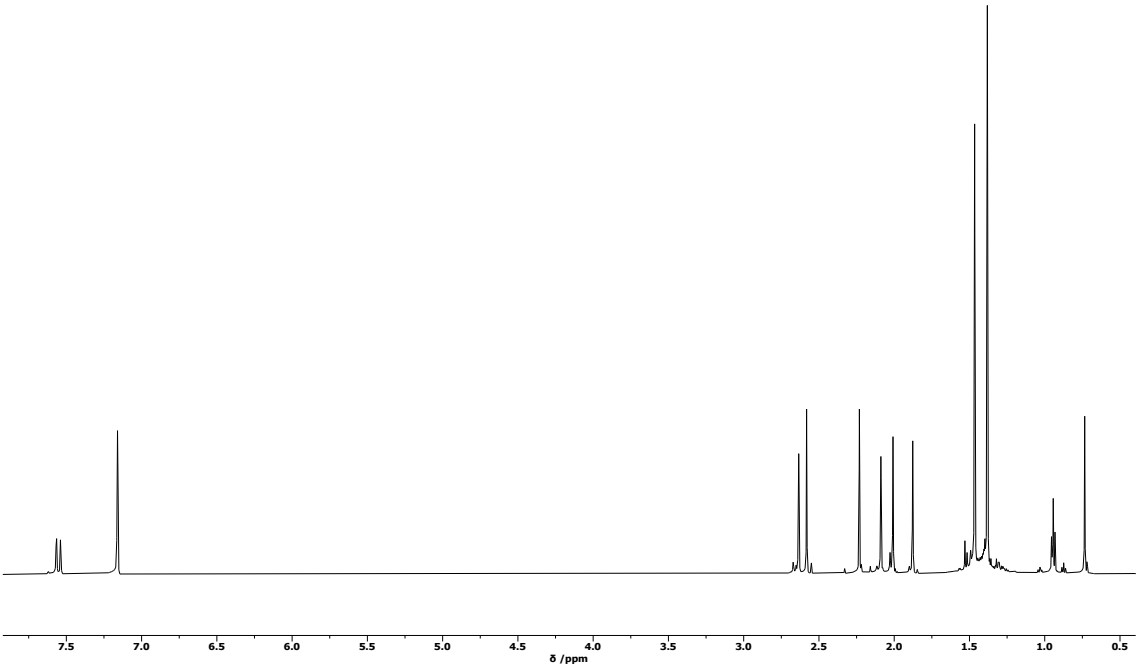

Figure A.53 ^{1}H NMR spectrum of *rac*-^{Me,nPr}SB(^{tBu2}ArO,I*)TiCl$_2$ (**12**) (benzene-d_6, 600 MHz, 298 K).

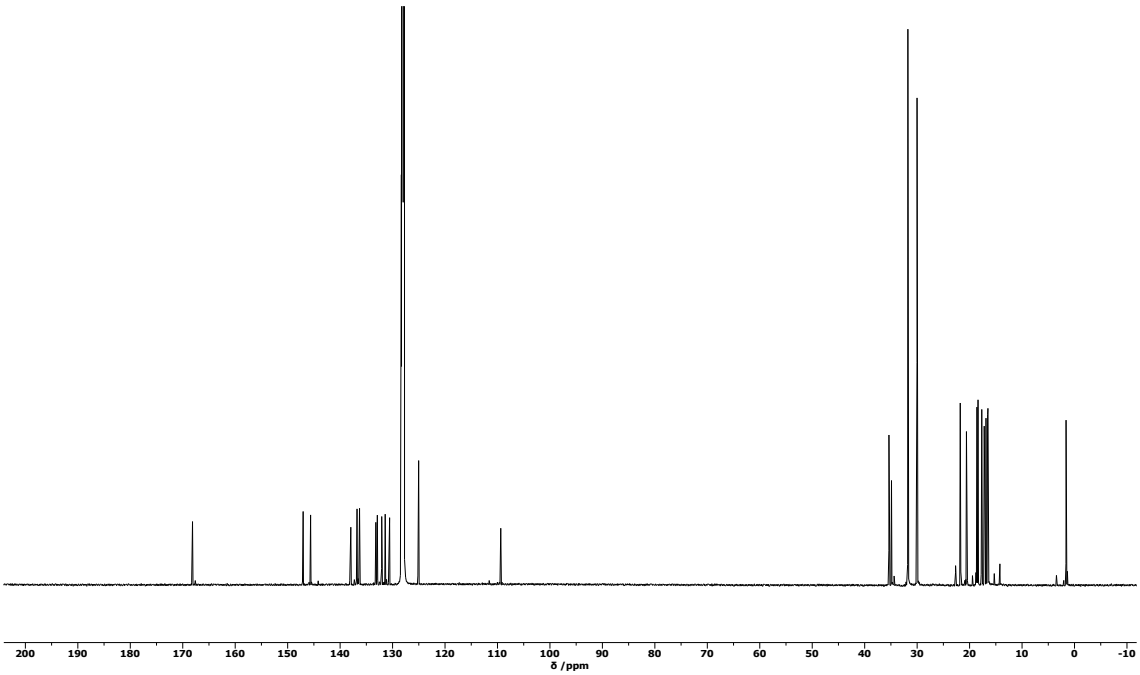

Figure A.54 ^{13}C{^{1}H} NMR spectrum of *rac*-^{Me,nPr}SB(^{tBu2}ArO,I*)TiCl$_2$ (**12**) (benzene-d_6, 151 MHz, 298 K).

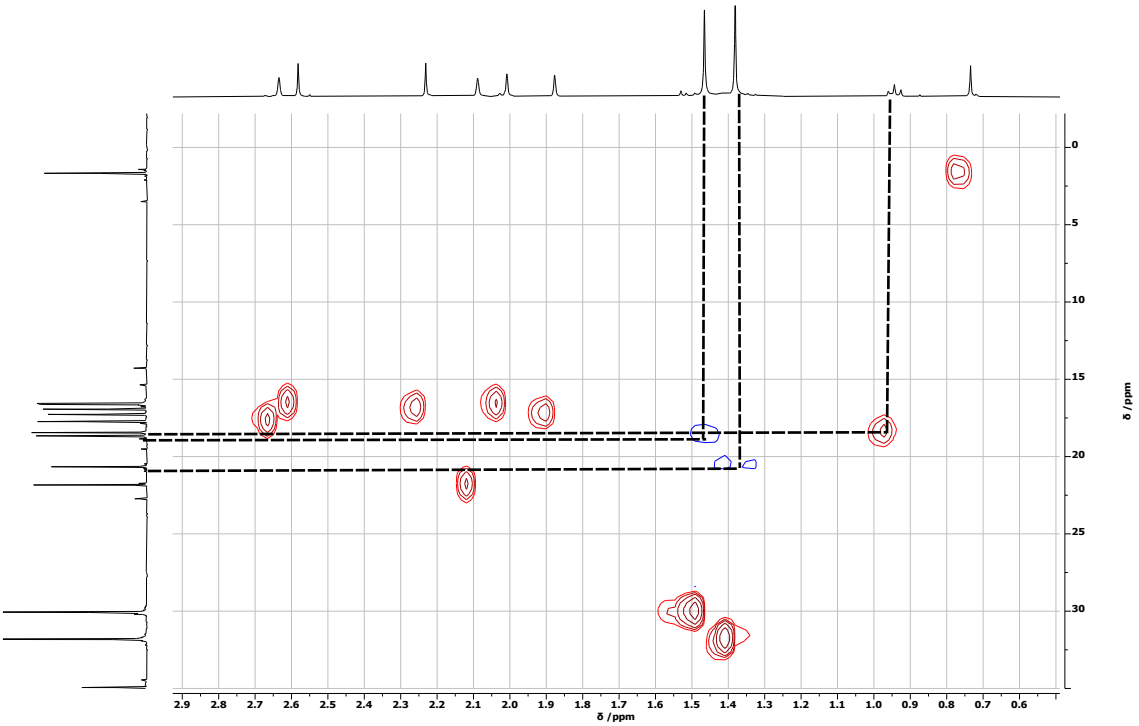

Figure A.55 $^{1}H–^{13}C$ HSQC NMR spectrum of *rac*-^{Me,nPr}SB(^{tBu2}ArO,I*)TiCl$_2$ (**12**) (benzene-d_6, 400 MHz, 298 K), with resonances corresponding to $SiCH_2CH_2CH_3$ highlighted.

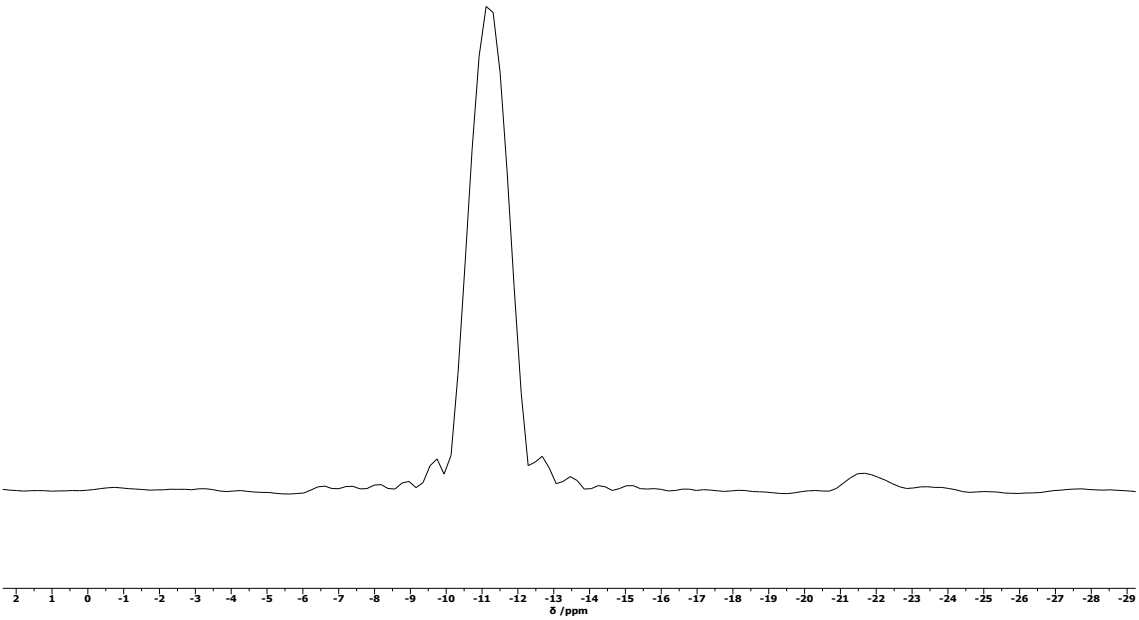

Figure A.56 ^{29}Si NMR spectrum of *rac*-^{Me,nPr}SB(^{tBu2}ArO,I*)TiCl$_2$ (**12**) (^{1}H-observed HMBC, benzene-d_6, 80 MHz, 298 K).

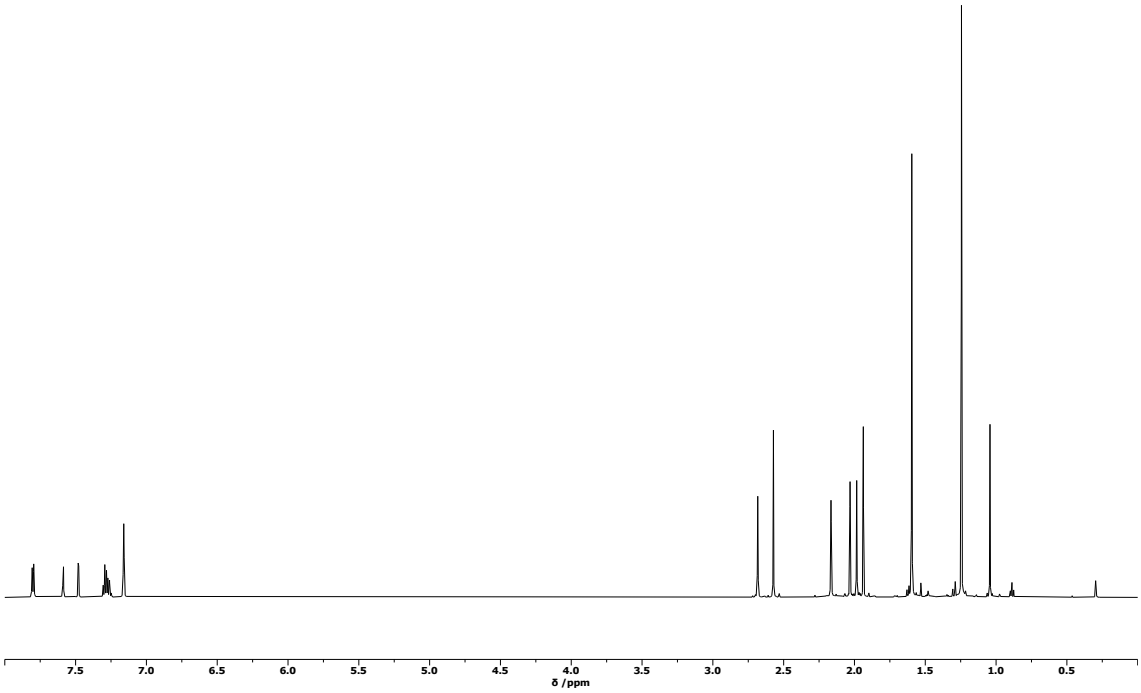

Figure A.57 ^{1}H NMR spectrum of *rac*-^{Me,Ph}SB(^{t}Bu$_2$ArO,I*)TiCl$_2$ (**13**) (benzene-d_6, 600 MHz, 298 K).

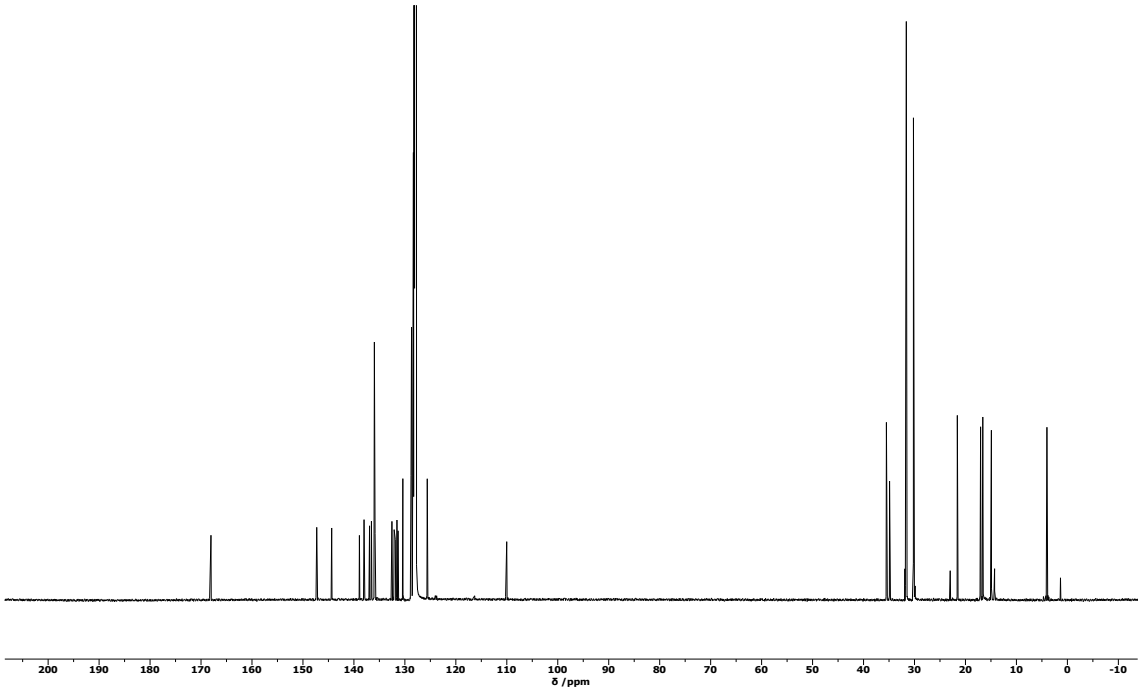

Figure A.58 ^{13}C{^{1}H} NMR spectrum of *rac*-^{Me,Ph}SB(^{t}Bu$_2$ArO,I*)TiCl$_2$ (**13**) (benzene-d_6, 151 MHz, 298 K).

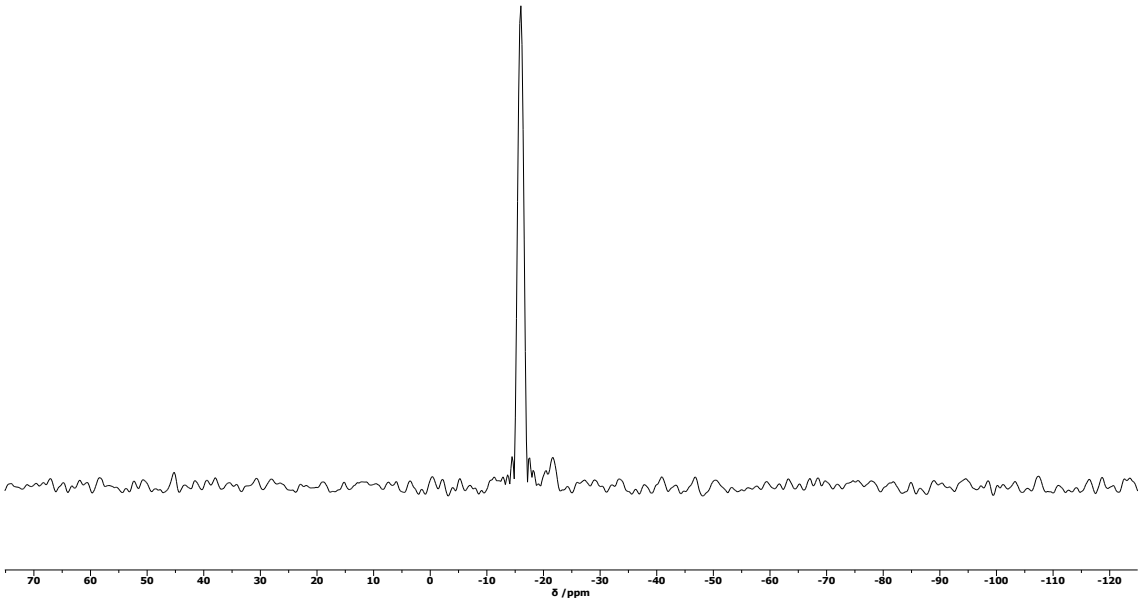

Figure A.59 ^{29}Si NMR spectrum of *rac*-^{Me,Ph}SB(^{t}Bu$_2$ArO,I*)TiCl$_2$ (**13**) (^{1}H-observed HMBC, benzene-d_6, 80 MHz, 298 K).

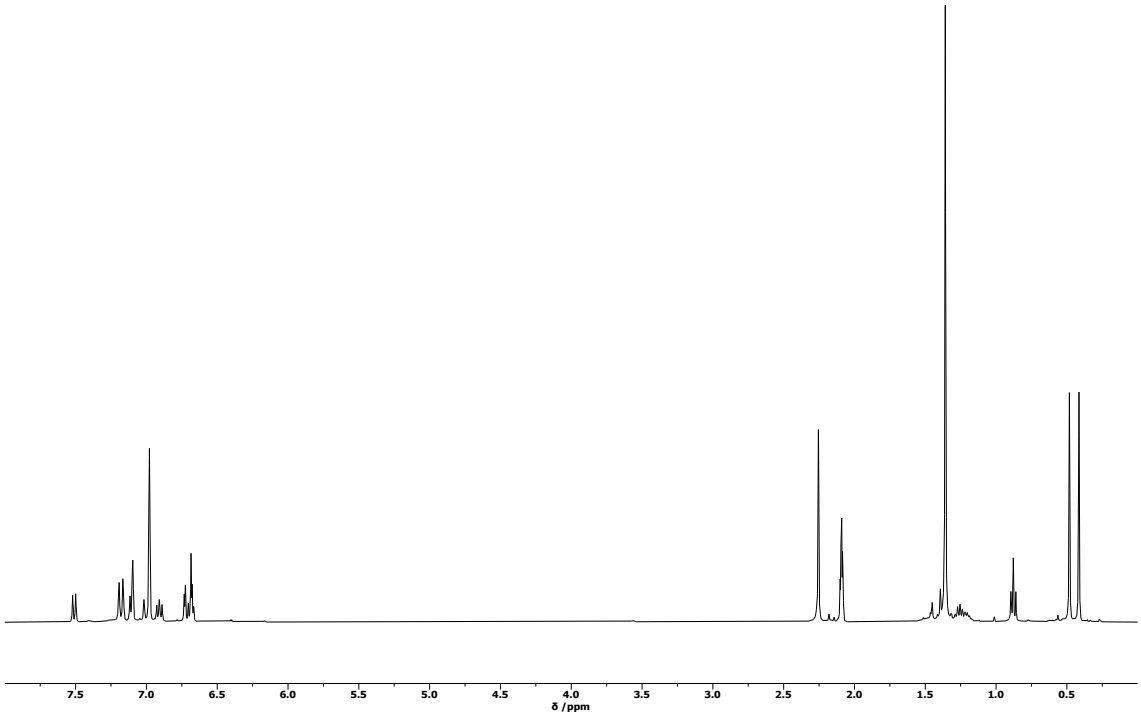

Figure A.60 ^{1}H NMR spectrum of ^{Me}$_2$SB(^{t}Bu,MeArO,Ind)TiCl$_2$ (**14**) (toluene-d_8, 400 MHz, 298 K).

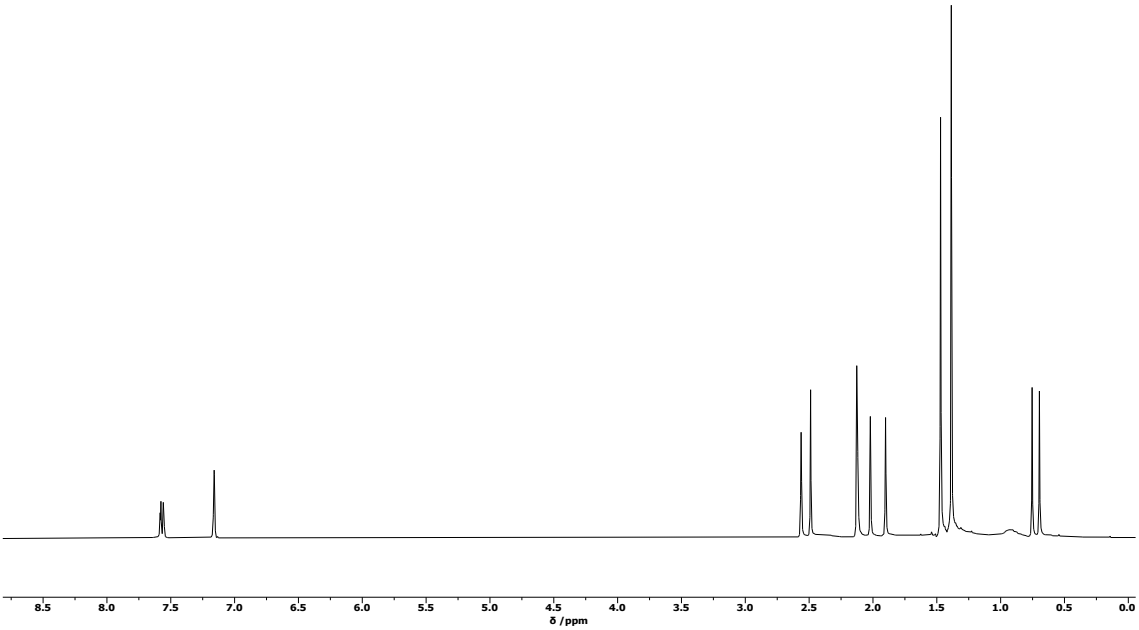

Figure A.61 ^{1}H NMR spectrum of ^{Me_2}SB($^{t Bu_2}$ArO,I*)ZrCl$_2$ (**15**) (benzene-d_6, 400 MHz, 298 K).

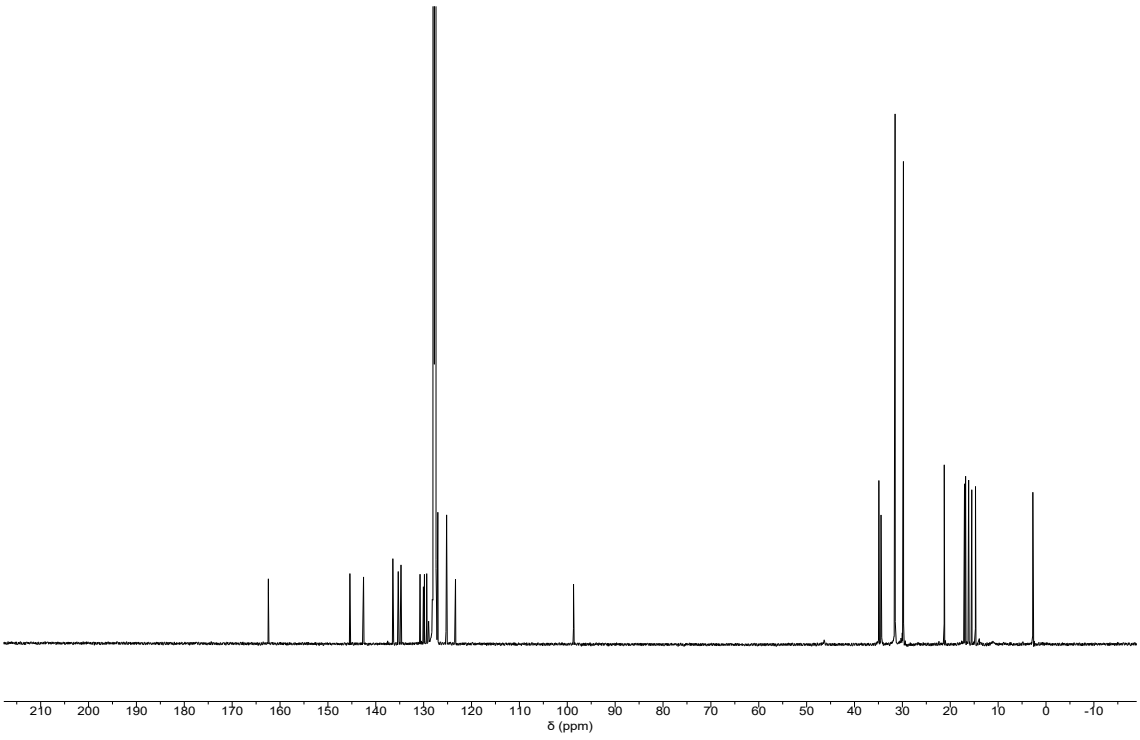

Figure A.62 ^{13}C{^{1}H} NMR spectrum of ^{Me_2}SB($^{t Bu_2}$ArO,I*)ZrCl$_2$ (**15**) (benzene-d_6, 126 MHz, 298 K).

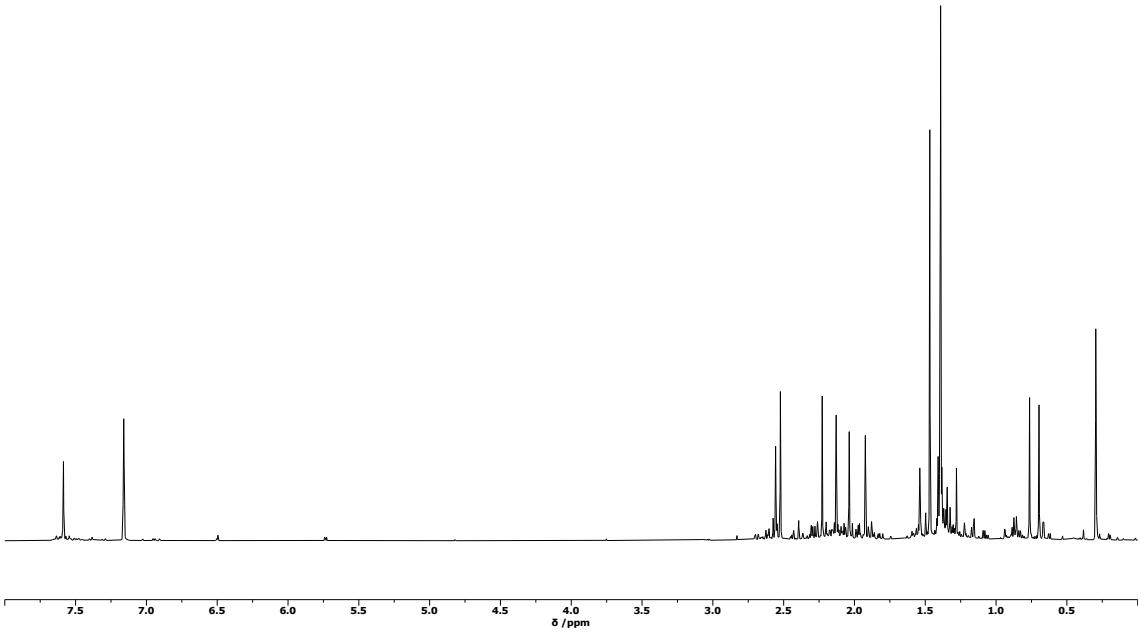

Figure A.63 ^{1}H NMR spectrum of ^{Me_2}SB($^{t Bu_2}$ArO,I*)HfCl$_2$ (**16**) (benzene-d_6, 600 MHz, 298 K).

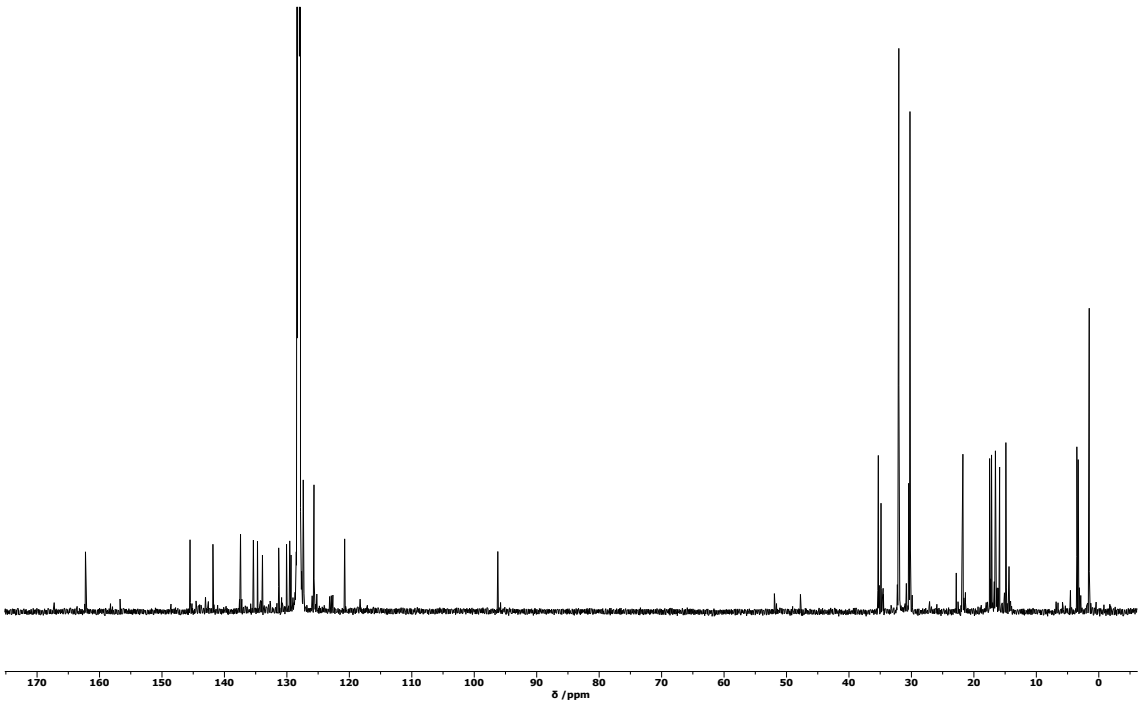

Figure A.64 ^{13}C{^{1}H} NMR spectrum of ^{Me_2}SB($^{t Bu_2}$ArO,I*)HfCl$_2$ (**16**) (benzene-d_6, 151 MHz, 298 K).

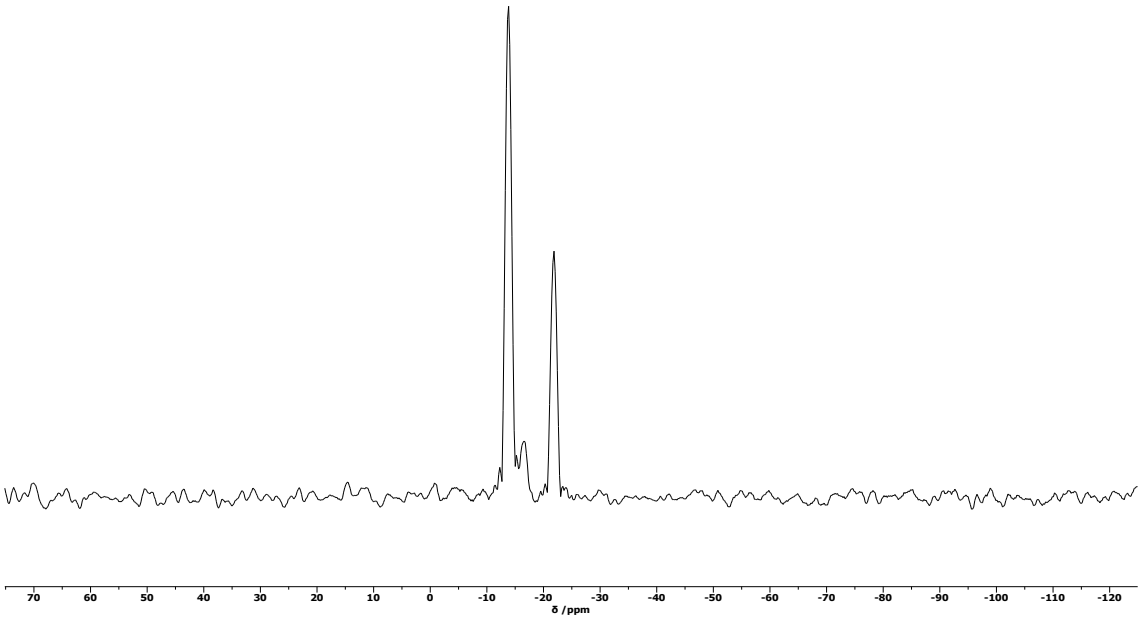

Figure A.65 ^{29}Si NMR spectrum of ^{Me2}SB(^{t}Bu$_2$ArO,I*)HfCl$_2$ (**16**) (^{1}H-observed HMBC, benzene-d_6, 80 MHz, 298 K).

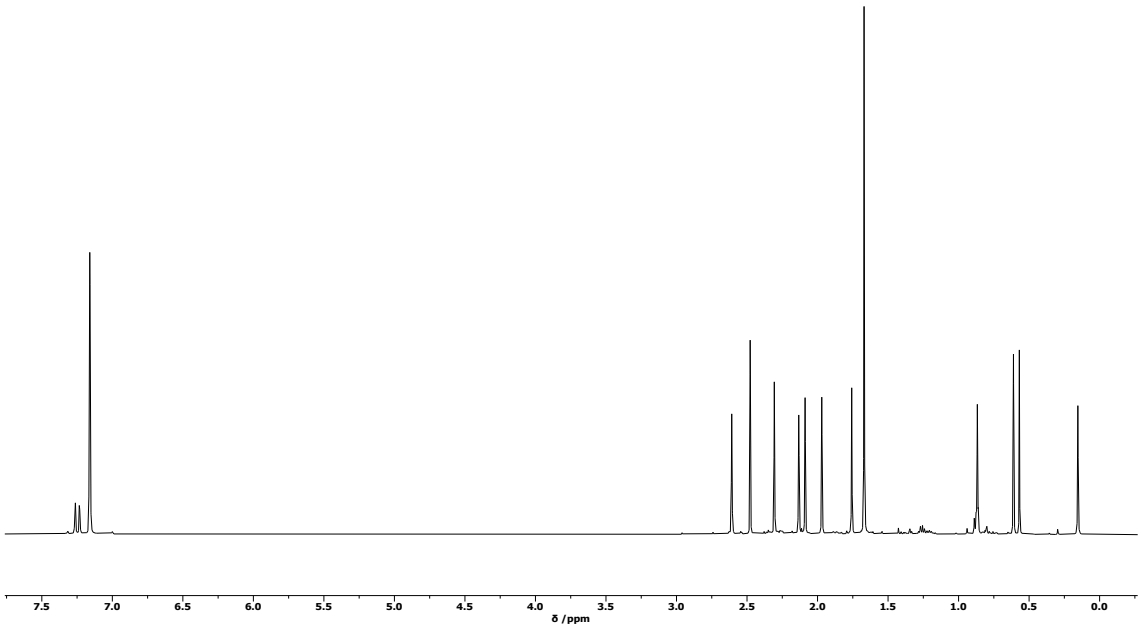

Figure A.66 ^{1}H NMR spectrum of ^{Me2}SB(^{t}Bu,MeArO,I*)TiMe$_2$ (**17**) (benzene-d_6, 500 MHz, 298 K).

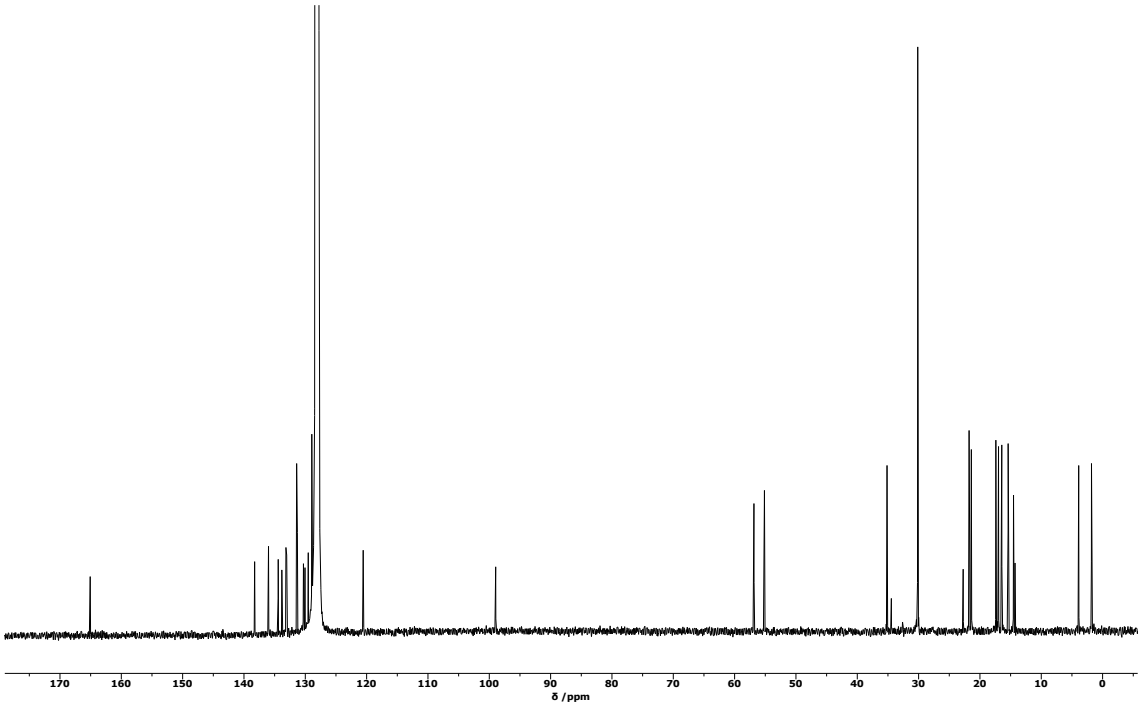

Figure A.67 $^{13}C\{^{1}H\}$ NMR spectrum of $^{Me_2}SB(^{tBu,Me}ArO,I^*)TiMe_2$ (**17**) (benzene-d_6, 126 MHz, 298 K).

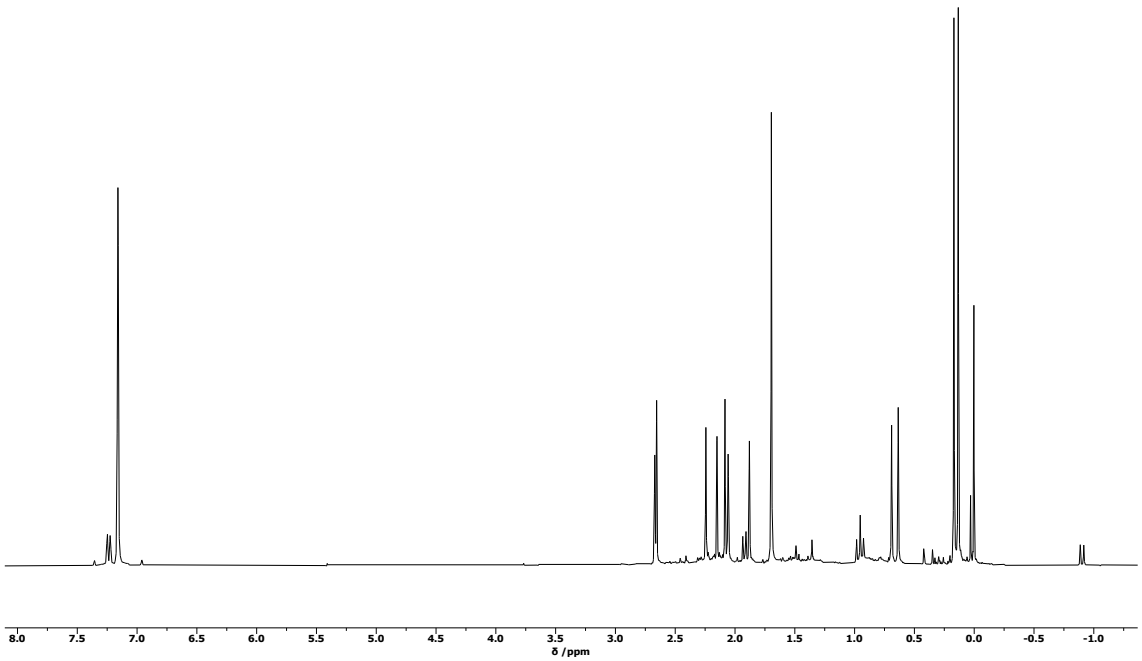

Figure A.68 ^{1}H NMR spectrum of $^{Me_2}SB(^{tBu,Me}ArO,I^*)Ti(CH_2SiMe_3)_2$ (**18**) (benzene-d_6, 400 MHz, 298 K).

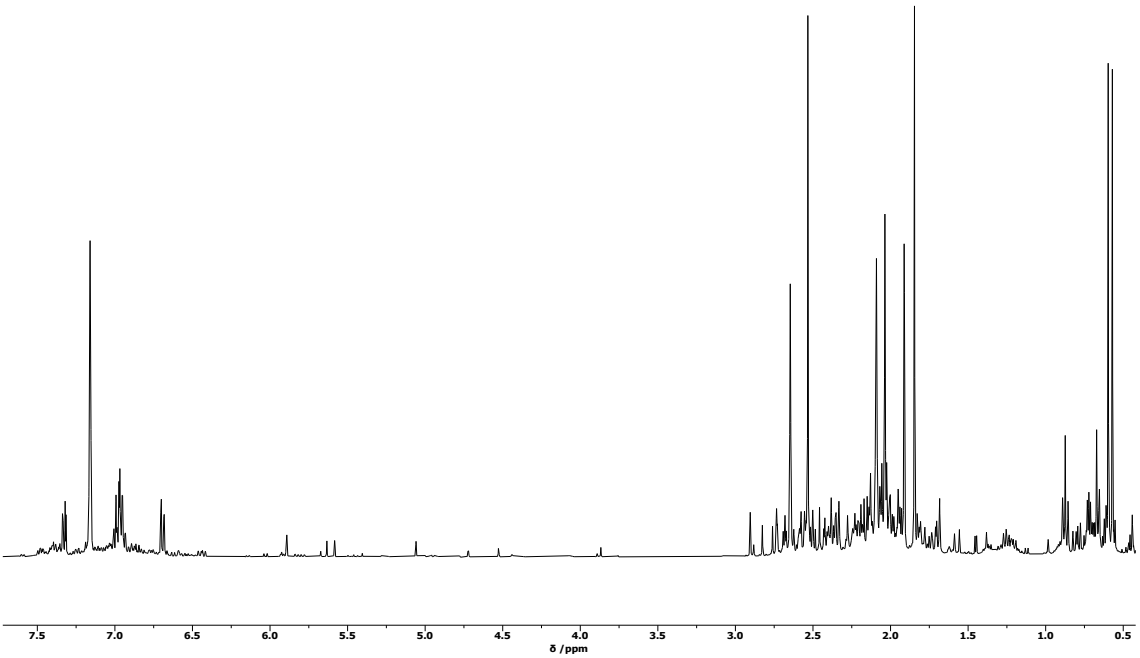

Figure A.69 ^{1}H NMR spectrum containing resonances for ^{Me_2}SB(^{H_2}ArO,I*)TiCl$_2$ (**19**) (benzene-d_6, 400 MHz, 298 K).

A.1.2. Crystallographic parameters

Experiments were carried out with Cu *K*α radiation. H-atom parameters were constrained.

	(1)	**(2)**	**(3)**	**(4)**	**(5)**
Crystal data					
Chemical formula	$C_{28}H_{38}Cl_2OSiTi$	$C_{31}H_{44}Cl_2OSiTi$	$C_{31}H_{44}Br_2OSiTi·C_6H_6$	$3(C_{31}H_{44}I_2OSiTi)·C_4H_{10}O$	$C_{33}H_{50}OSiTi$
M_r	537.50	579.55	746.60	2361.39	538.74
Crystal system, space group	Orthorhombic, *Pbca*	Triclinic, $P\bar{1}$	Triclinic, $P\bar{1}$	Triclinic, $P\bar{1}$	Triclinic, $P\bar{1}$
Temperature (K)	150	150	150	100	150
a, *b*, *c* (Å)	9.3542 (1), 15.5831 (2), 37.8666 (4)	8.7639 (2), 14.1232 (3), 14.1951 (4)	9.0454 (2), 9.2217 (1), 23.2505 (4)	10.2384 (1), 22.7315 (2), 23.8545 (1)	9.0440 (2), 13.9610 (5), 14.0102 (5)
α, β, γ (°)	90, 90, 90	116.403 (2), 90.929 (2), 104.547 (2)	92.3663 (12), 99.4751 (15), 107.5194 (14)	71.1207 (6), 87.0574 (6), 87.2403 (6)	114.214 (3), 92.161 (2), 103.906 (2)
V (Å^3)	5519.72 (11)	1506.59 (7)	1815.70 (6)	5243.24 (7)	1547.39 (10)
Z	8	2	2	2	2
μ (mm^{-1})	4.96	4.58	5.08	16.43	2.87
Crystal size (mm)	0.17 × 0.04 × 0.04	0.21 × 0.18 × 0.07	0.18 × 0.09 × 0.05	0.27 × 0.12 × 0.02	0.25 × 0.16 × 0.14
Data collection					
Diffractometer	Oxford Diffraction SuperNova	SuperNova, Dual, Cu at home/near, Atlas	Oxford Diffraction SuperNova	XtaLAB Synergy R, DW system, HyPix-Arc 150	Oxford Diffraction SuperNova
Absorption correction	Multi-scan *CrysAlis PRO* (Rigaku Oxford Diffraction, 2017)	Multi-scan *CrysAlis PRO* 1.171.39.46 (Rigaku Oxford Diffraction, 2018) Empirical absorption correction using spherical harmonics,	Multi-scan *CrysAlis PRO* (Rigaku Oxford Diffraction, 2017)	Multi-scan *CrysAlis PRO* (Rigaku Oxford Diffraction, 2017)	Multi-scan *CrysAlis PRO* (Rigaku Oxford Diffraction, 2017)

		implemented in SCALE3 ABSPACK scaling algorithm.			
T_{min}, T_{max}	0.68, 0.82	0.804, 1.000	0.56, 1.00	0.35, 0.72	0.56, 0.67
No. of measured, independent and observed reflections	19453, 5709, 4968 [$I > 2.0\sigma(I)$]	27747, 6147, 5606 [$I > 2\sigma(I)$]	29485, 7525, 6961 [$I > 2.0\sigma(I)$]	246637, 21488, 15686 [$I > 2.0\sigma(I)$]	22230, 6393, 5844 [$I > 2.0\sigma(I)$]
R_{int}	0.035	0.037	0.029	0.134	0.033
θ_{max} (°)	76.1	74.5	76.1	76.2	76.1
$(\sin\theta/\lambda)_{max}$ (Å^{-1})	0.630	0.625	0.630	0.630	0.630
Refinement					
$R[F^2 > 2\sigma(F^2)]$, $wR(F^2)$, S	0.033, 0.086, 1.02	0.043, 0.122, 1.04	0.033, 0.091, 1.00	0.063, 0.188, 0.98	0.033, 0.097, 0.91
No. of reflections	5706	6147	7525	21488	6392
No. of parameters	298	339	379	1018	325
No. of restraints	0	0	0	0	0
	Method = Modified Sheldrick $w = 1/[\sigma^2(F^2) + (0.03P)^2 + 3.46P]$, where $P = (\max(F_o^2,0) + 2F_c^2)/3$	$w = 1/[\sigma^2(F_o^2) + (0.0819P)^2 + 0.4881P]$ where $P = (F_o^2 + 2F_c^2)/3$	Method = Modified Sheldrick $w = 1/[\sigma^2(F^2) + (0.05P)^2 + 1.88P]$, where $P = (\max(F_o^2,0) + 2F_c^2)/3$	Method = Modified Sheldrick $w = 1/[\sigma^2(F^2) + (0.13P)^2 + 9.02P]$, where $P = (\max(F_o^2,0) + 2F_c^2)/3$	Method = Modified Sheldrick $w = 1/[\sigma^2(F^2) + (0.07P)^2 + 0.48P]$, where $P = (\max(F_o^2,0) + 2F_c^2)/3$
$(\Delta/\sigma)_{max}$	0.002	0.001	0.001	0.001	0.001
$\Delta\rangle_{max}$, $\Delta\rangle_{min}$ (e Å^{-3})	0.38, -0.34	0.58, -0.31	0.68, -0.60	3.20, -2.26	0.50, -0.35

	(6)	**(8)**	**(10)**	**(11)**	**(12)**
Crystal data					
Chemical formula	$C_{39}H_{66}OSi_3Ti \cdot C_5H_{12}$	$2(C_{35}H_{56}N_2OSiTi) \cdot C_5H_{12}$	$C_{55}H_{78}O_3SiTi$	$C_{41}H_{48}Cl_2OSiTi$	$C_{33}H_{48}Cl_2OSiTi$
M_r	755.23	1265.70	863.16	703.72	607.63
Crystal system, space group	Triclinic, $P\bar{1}$	Triclinic, $P\bar{1}$	Triclinic, $P\bar{1}$	Triclinic, $P\bar{1}$	Orthorhombic, $Pn2_1a$
Temperature (K)	150	150	150	150	100
a, b, c (Å)	11.3033 (4), 13.1608 (6), 17.5863 (5)	10.5569 (3), 11.8446 (3), 15.2700 (4)	10.0716 (3), 12.3398 (3), 21.4451 (8)	10.6362 (8), 13.3872 (8), 16.0218 (12)	17.3507 (1), 23.1111 (1), 16.6347 (1)
α, β, γ (°)	106.682 (3), 90.040 (3), 112.380 (4)	100.985 (2), 90.922 (2), 99.828 (2)	88.842 (3), 76.694 (3), 71.553 (3)	66.408 (6), 73.901 (6), 71.856 (6)	90, 90, 90
V (Å^3)	2299.34 (16)	1844.58 (8)	2456.41 (14)	1955.9 (3)	6670.41 (6)
Z	2	2	2	2	8
μ (mm^{-1})	2.53	2.49	2.02	3.62	4.16
Crystal size (mm)	0.32 × 0.20 × 0.04	0.10 × 0.07 × 0.05	0.26 × 0.13 × 0.05	0.16 × 0.04 × 0.02	0.49 × 0.03 × 0.02
Data collection					
Diffractometer	SuperNova, Dual, Cu at home/near, Atlas	Oxford Diffraction SuperNova	SuperNova, Dual, Cu at home/near, Atlas	Oxford Diffraction SuperNova	XtaLAB Synergy R, DW system, HyPix-Arc 150
Absorption correction	Gaussian *CrysAlis PRO* 1.171.41.93a (Rigaku Oxford Diffraction, 2020) Numerical absorption correction based on gaussian integration over a multifaceted crystal model Empirical	–	Gaussian *CrysAlis PRO* 1.171.41.93a (Rigaku Oxford Diffraction, 2020) Numerical absorption correction based on gaussian integration over a multifaceted crystal model Empirical	Multi-scan *CrysAlis PRO* (Rigaku Oxford Diffraction, 2017)	Multi-scan *CrysAlis PRO* (Rigaku Oxford Diffraction, 2017)

	absorption correction using spherical harmonics, implemented in SCALE3 ABSPACK scaling algorithm.		absorption correction using spherical harmonics, implemented in SCALE3 ABSPACK scaling algorithm.		
T_{min}, T_{max}	0.528, 1.000	–	0.629, 1.000	0.77, 0.93	0.56, 0.92
No. of measured, independent and observed reflections	23343, 9374, 7646 [$I > 2\sigma(I)$]	29935, 7605, 6767 [$I > 2.0\sigma(I)$]	26222, 10032, 8724 [$I > 2\sigma(I)$]	14761, 5911, 4306 [$I > 2.0\sigma(I)$]	119728, 13499, 10601 [$I > 2.0\sigma(I)$]
R_{int}	0.042	0.029	0.031	0.049	0.127
θ_{max} (°)	74.5	76.0	74.5	61.5	75.2
$(\sin\theta/\lambda)_{max}$ (Å^{-1})	0.625	0.629	0.625	0.570	0.627
Refinement					
$R[F^2 > 2\sigma(F^2)]$, $wR(F^2)$, S	0.053, 0.149, 1.04	0.033, 0.093, 0.90	0.036, 0.095, 1.02	0.047, 0.124, 0.96	0.071, 0.207, 0.99
No. of reflections	9374	7604	10032	5910	13499
No. of parameters	464	397	563	415	686
No. of restraints	21	3	0	0	1
	$w = 1/[\sigma^2(F_o^2) + (0.0729P)^2 + 1.5926P]$ where $P = (F_o^2 + 2F_c^2)/3$	Method = Modified Sheldrick $w = 1/[\sigma^2(F^2) + (0.06P)^2 + 0.71P]$, where $P = (\max(F_o^2,0) + 2F_c^2)/3$	$w = 1/[\sigma^2(F_o^2) + (0.0505P)^2 + 0.4454P]$ where $P = (F_o^2 + 2F_c^2)/3$	Method = Modified Sheldrick $w = 1/[\sigma^2(F^2) + (0.06P)^2 + 1.1P]$, where $P = (\max(F_o^2,0) + 2F_c^2)/3$	Method = Modified Sheldrick $w = 1/[\sigma^2(F^2) + (0.16P)^2 + 0.0P]$, where $P = (\max(F_o^2,0) + 2F_c^2)/3$
$(\Delta/\sigma)_{max}$	0.001	0.001	0.001	0.0004	0.001
$\Delta\rangle_{max}$, $\Delta\rangle_{min}$ (e Å^{-3})	1.41, -0.89	0.34, -0.27	0.31, -0.30	0.65, -0.58	1.54, -0.59

	(13)	**(15)**	**(16)**
Crystal data			
Chemical formula	$C_{36}H_{46}Cl_2OSiTi$	$C_{31}H_{44}Cl_2OSiZr \cdot C_6H_6$	$C_{31}H_{44}Cl_2HfOSi$
M_r	641.62	701.01	710.17
Crystal system, space group	Monoclinic, $P2_1/c$	Triclinic, $P\bar{1}$	Triclinic, $P\bar{1}$
Temperature (K)	150	150	150
a, b, c (Å)	24.6520 (11), 9.3785 (5), 16.9267 (15)	8.6681 (1), 9.2302 (2), 23.6646 (3)	8.8737 (2), 9.2262 (1), 23.7302 (4)
α, β, γ (°)	90, 98.503 (6), 90	87.5766 (13), 83.2225 (12), 73.6327 (14)	87.0816 (14), 80.5280 (15), 72.9297 (16)
V (Å^3)	3870.4 (4)	1803.86 (5)	1831.89 (6)
Z	4	2	2
μ (mm^{-1})	3.61	4.37	7.05
Crystal size (mm)	0.30 × 0.21 × 0.06	0.22 × 0.16 × 0.03	0.12 × 0.12 × 0.04
Data collection			
Diffractometer	SuperNova, Dual, Cu at home/near, Atlas	Oxford Diffraction SuperNova	Oxford Diffraction SuperNova
Absorption correction	Gaussian *CrysAlis PRO* 1.171.41.93a (Rigaku Oxford Diffraction, 2020) Numerical absorption correction based on gaussian integration over a multifaceted crystal model Empirical absorption correction using spherical harmonics, implemented in SCALE3 ABSPACK scaling algorithm.	Multi-scan *CrysAlis PRO* (Rigaku Oxford Diffraction, 2017)	Multi-scan *CrysAlis PRO* (Rigaku Oxford Diffraction, 2017)
T_{min}, T_{max}	0.416, 1.000	0.49, 0.88	0.42, 0.75
No. of measured, independent and	49770, 7914, 5835 [$I > 2\sigma(I)$]	38067, 7483, 6960 [$I > 2.0\sigma(I)$]	31554, 7550, 7215 [$I > 2.0\sigma(I)$]

observed reflections			
R_{int}	0.112	0.035	0.040
θ_{max} (°)	74.5	76.2	76.2
$(\sin\theta/\lambda)_{max}$ (Å^{-1})	0.625	0.630	0.630
Refinement			
$R[F^2 > 2\sigma(F^2)]$, $wR(F^2)$, S	0.150, 0.376, 1.05	0.032, 0.086, 1.02	0.041, 0.101, 1.03
No. of reflections	7914	7483	7550
No. of parameters	383	379	353
No. of restraints	0	0	0
	$w = 1/[\sigma^2(F_o^2) + (0.0955P)^2 + 51.9365P]$ where $P = (F_o^2 + 2F_c^2)/3$	Method = Modified Sheldrick $w = 1/[\sigma^2(F^2) + (0.04P)^2 + 2.89P]$, where $P = (\max(F_o^2,0) + 2F_c^2)/3$	Method = Modified Sheldrick $w = 1/[\sigma^2(F^2) + (0.03P)^2 + 10.74P]$, where $P = (\max(F_o^2,0) + 2F_c^2)/3$
$(\Delta/\sigma)_{max}$	0.001	0.002	0.001
$\Delta\rangle_{max}$, $\Delta\rangle_{min}$ (e Å^{-3})	1.33, -0.97	0.83, -0.57	2.11, -1.21

Computer programs: SuperNova, (Oxford Diffraction, 2010), *CrysAlis PRO* 1.171.39.46 (Rigaku OD, 2018), *CrysAlis PRO* 1.171.41.93a (Rigaku OD, 2020), *CrysAlis PRO* (Rigaku Oxford Diffraction, 2017), *SUPERFLIP* (Palatinus & Chapuis, 2007), *SUPERFLIP* Palatinus, L.; Chapuis, G. J. Appl. Cryst. 2007, 40, 786-790., *CRYSTALS* (Betteridge *et al.*, 2003), *SHELXL2014* (Sheldrick, 2014), *SHELXL2018*/3 (Sheldrick, 2018), *CAMERON* (Watkin *et al.*, 1996), *ORTEP-3 for Windows* (Farrugia, 1997), *ORTEP-3 for Windows* Farrugia, L. J. J. Appl. Cryst. 1997, 30, 565., *WinGX* publication routines (Farrugia, 1999).

.

A.1.3. Supplementary X-ray crystal structures

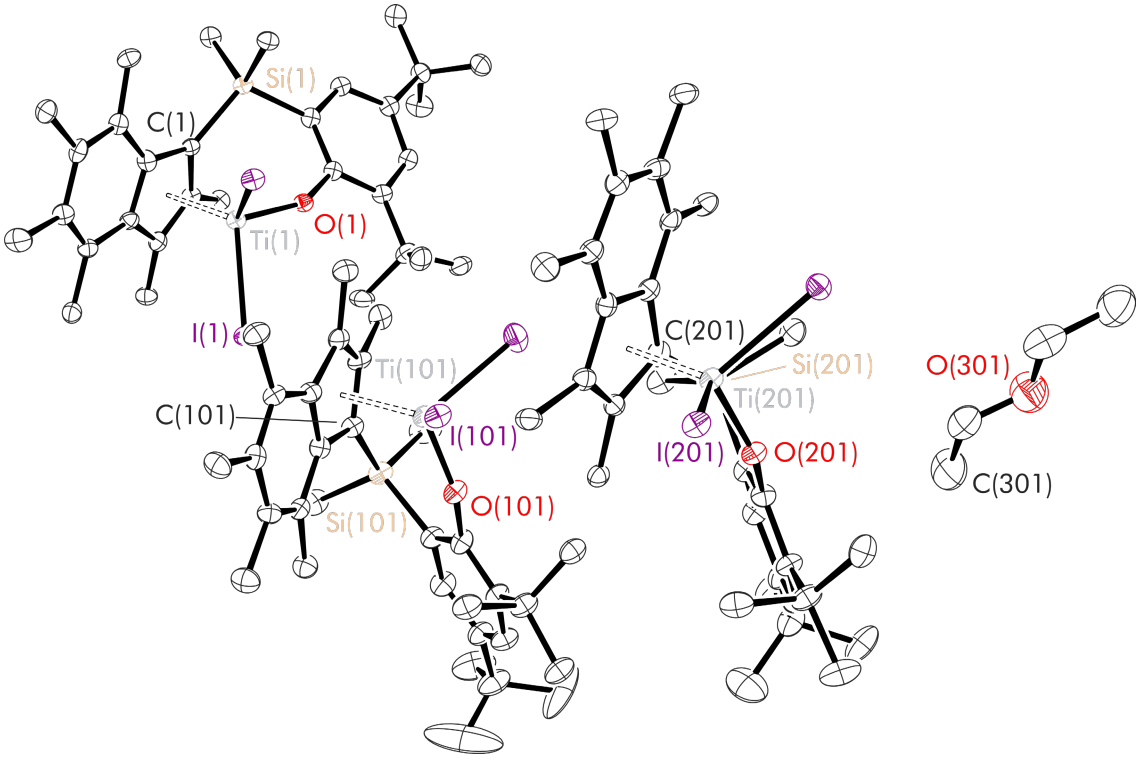

Figure A.70 Solid-state ellipsoid plot of ^{Me_2}SB($^{t\text{Bu}_2}$ArO,I*)TiI$_2$ (**4**). Whole asymmetric unit (Z' = 3) shown with (left to right) residue 1 containing Ti(1) (B-type conformation), 2 containing Ti(101) (A-type conformation), and 3 containing Ti(201) (B-type conformation). Residue 4 is an ether of crystallisation. All hydrogen atoms omitted for clarity; thermal ellipsoids drawn at 30% probability.

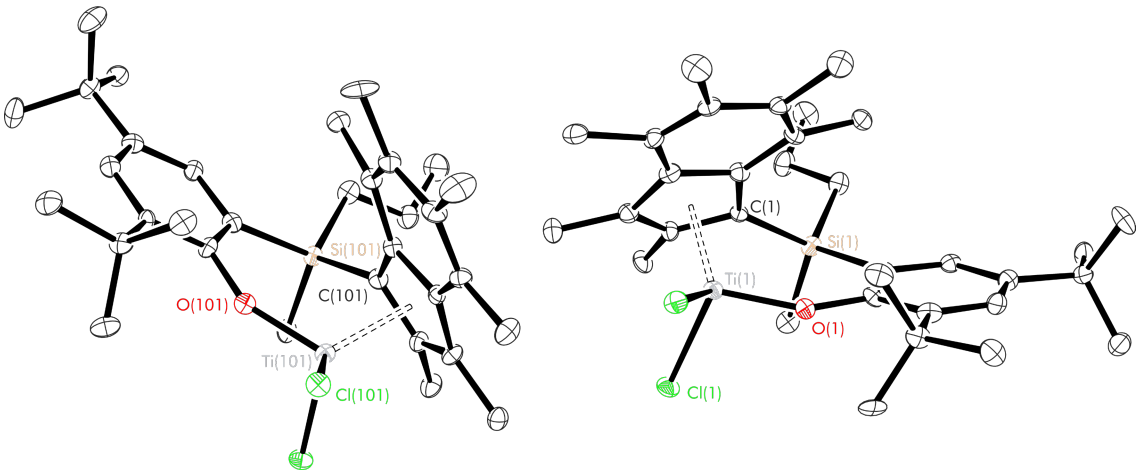

Figure A.71 Solid-state ellipsoid plot of $^{Me,n\text{Pr}}$SB($^{t\text{Bu}_2}$ArO,I*)TiCl$_2$ (**12**). Whole asymmetric unit (Z' = 2) shown with both residues having similar structures. All hydrogen atoms omitted for clarity; thermal ellipsoids drawn at 30% probability.

A.1.4. NMR spectra of cationic complexes

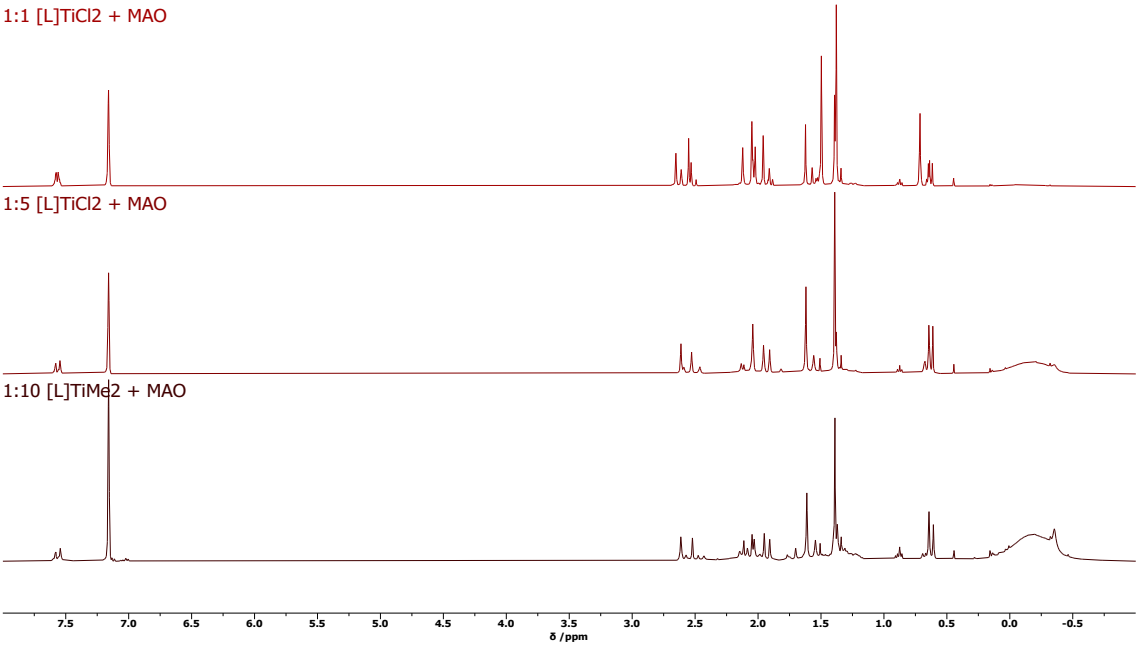

Figure A.72 ^{1}H NMR spectra of the reaction between ^{Me_2}SB(^{t}Bu$_2$ArO,I*)TiCl$_2$ (**2**) and MAO as a function of [MAO]/[Ti] (benzene-d_6, 400 MHz, 298 K).

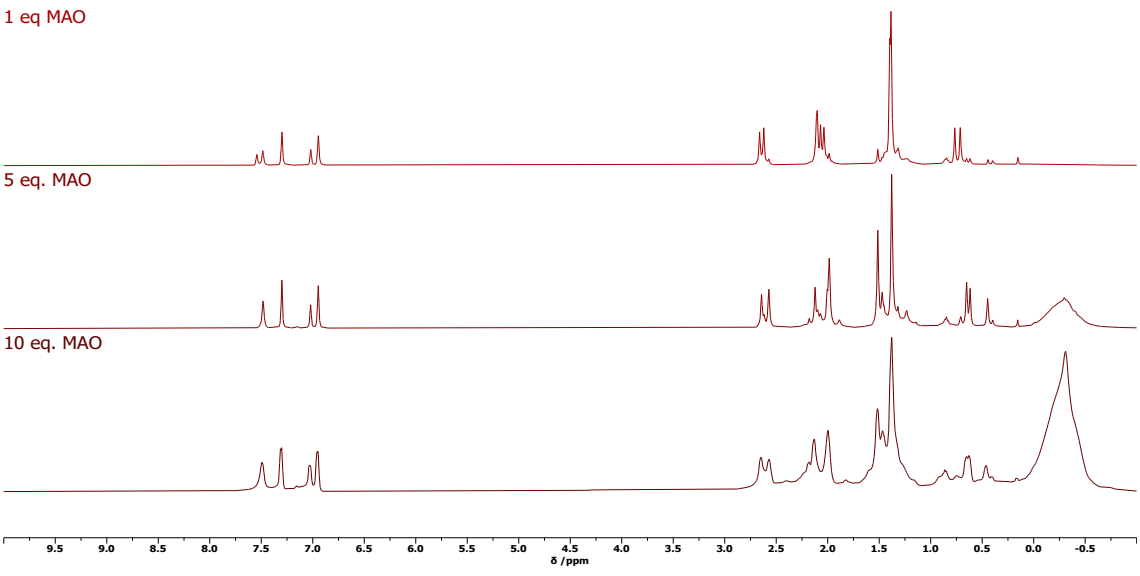

Figure A.73 ^{1}H NMR spectra of the reaction between ^{Me_2}SB(^{t}Bu$_2$ArO,I*)TiCl$_2$ (**2**) and MAO as a function of [MAO]/[Ti] (bromobenzene-d_5, 400 MHz, 297 K).

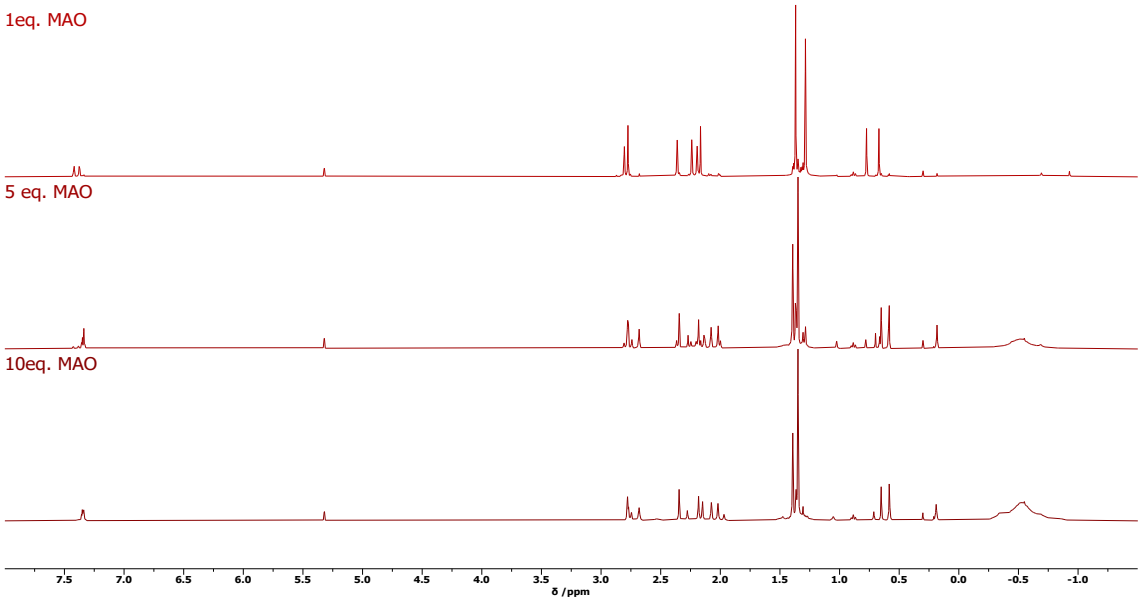

Figure A.74 ^{1}H NMR spectra of the reaction between ^{Me_2}SB($^{t Bu_2}$ArO,I*)TiCl$_2$ (**2**) and MAO as a function of [MAO]/[Ti] (dichloromethane-d_2, 400 MHz, 298 K).

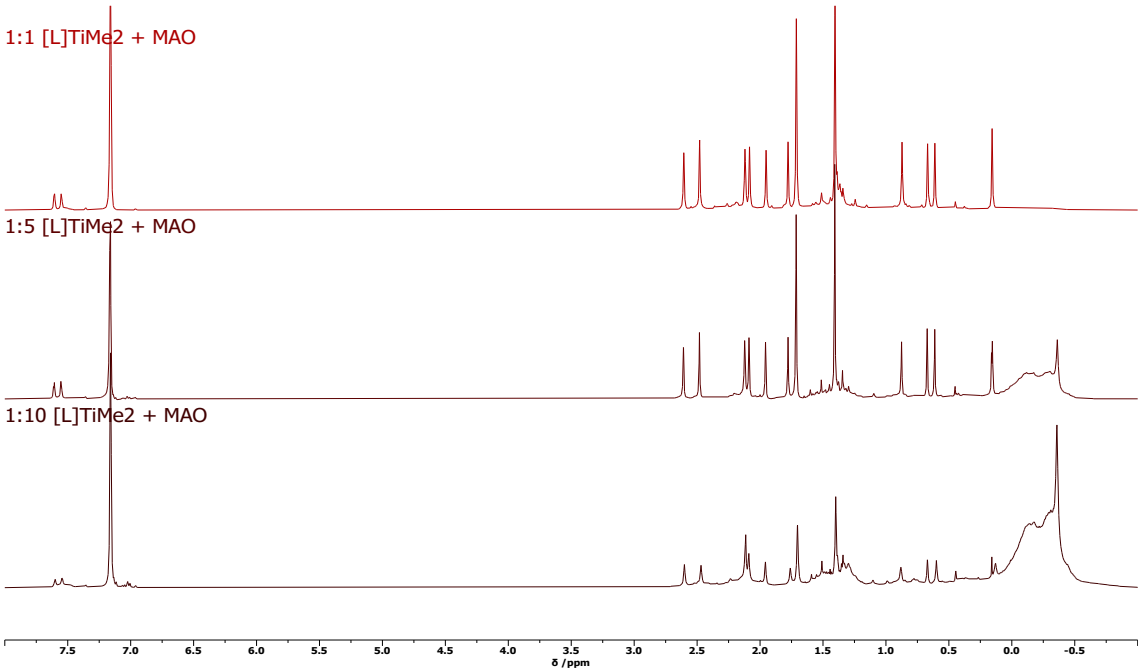

Figure A.75 ^{1}H NMR spectra of the reaction between ^{Me_2}SB($^{t Bu_2}$ArO,I*)TiMe$_2$ (**5**) and MAO as a function of [MAO]/[Ti] (benzene-d_6, 400 MHz, 298 K).

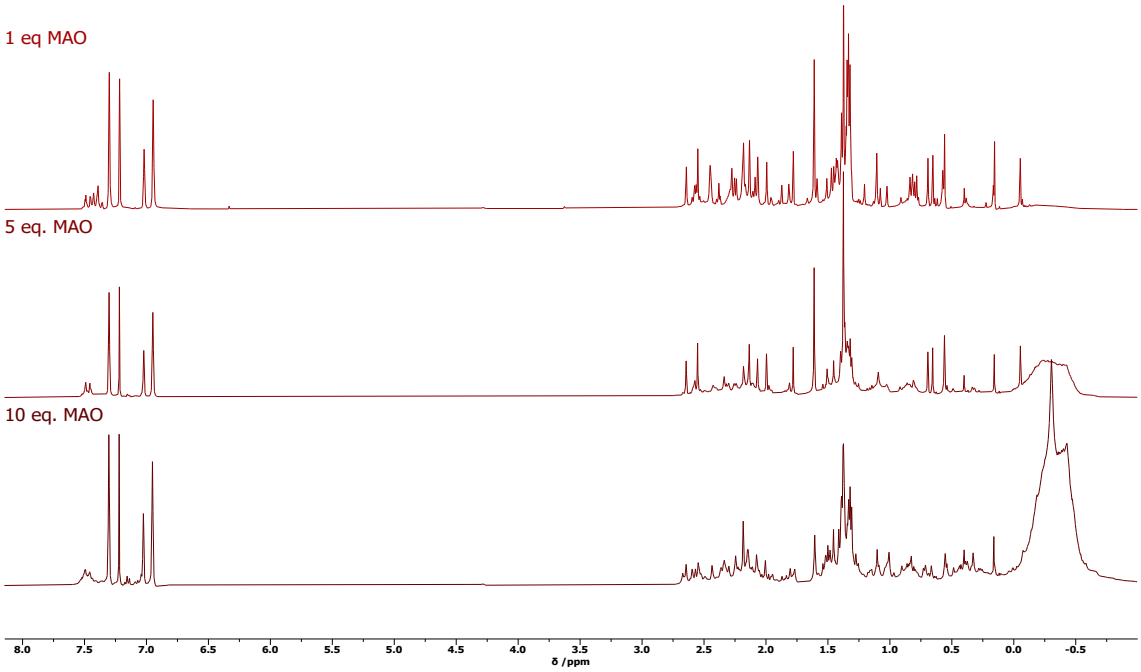

Figure A.76 ^{1}H NMR spectra of the reaction between $^{Me}_{2}$SB(^{t}Bu$_2$ArO,I*)TiMe$_2$ (**5**) and MAO as a function of [MAO]/[Ti] (bromobenzene-d_5, 400 MHz, 298 K).

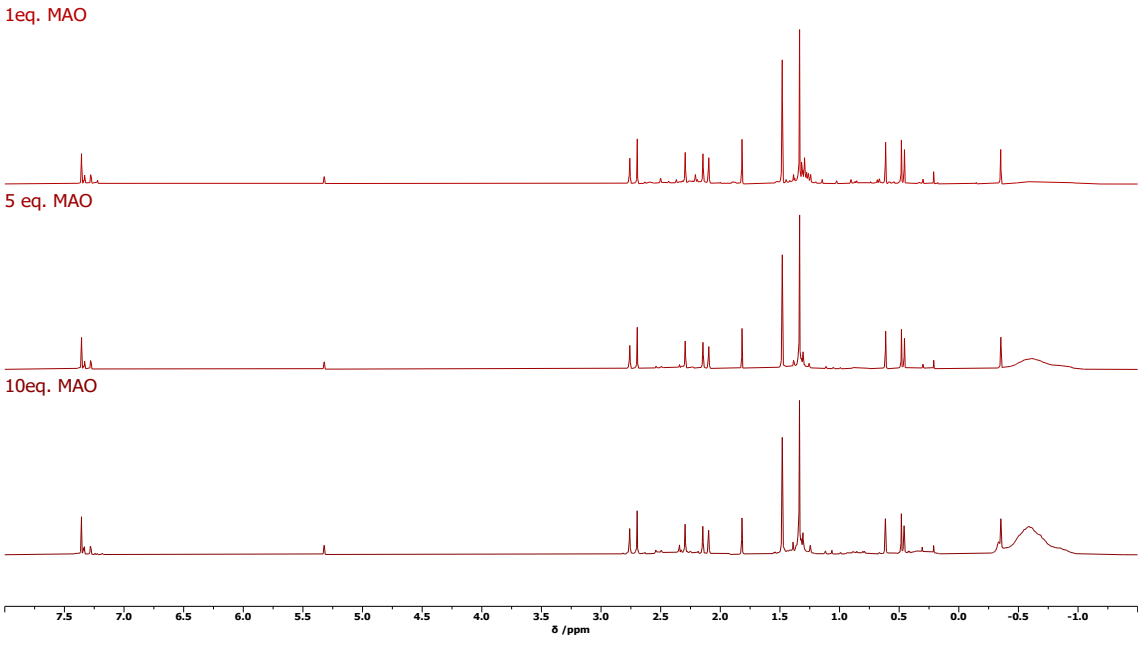

Figure A.77 ^{1}H NMR spectra of the reaction between $^{Me}_{2}$SB(^{t}Bu$_2$ArO,I*)TiMe$_2$ (**5**) and MAO as a function of [MAO]/[Ti] (dichloromethane-d_2, 400 MHz, 297 K).

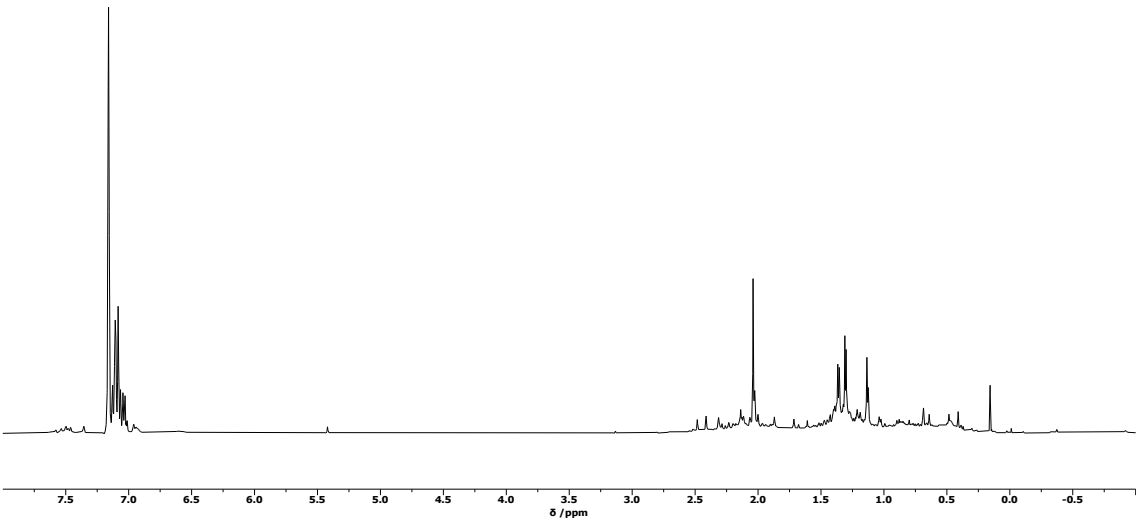

Figure A.78 ^{1}H NMR spectra of the reaction between ^{Me_2}SB($^{t Bu_2}$ArO,I*)TiMe$_2$ (**5**) and [Ph$_3$C][BAr$^F{}_4$] (benzene-d_6, 400 MHz, 297 K). A single ^{11}B resonance at δ –16 ppm and ^{19}F resonances at δ –132, –162, and –166 ppm were observed.

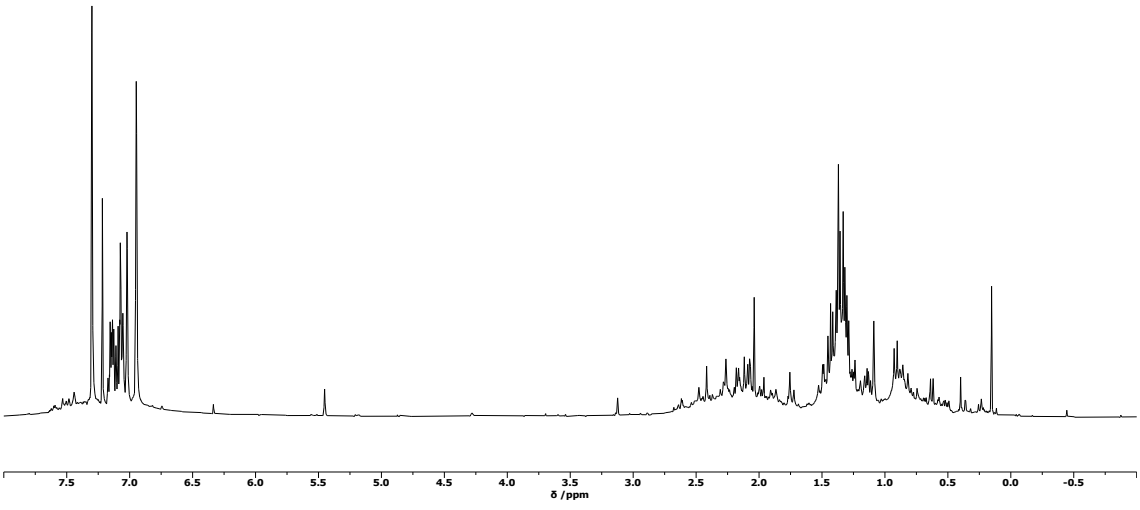

Figure A.79 ^{1}H NMR spectra of the reaction between ^{Me_2}SB($^{t Bu_2}$ArO,I*)TiMe$_2$ (**5**) and [Ph$_3$C][BAr$^F{}_4$] (bromobenzene-d_5, 400 MHz, 297 K).

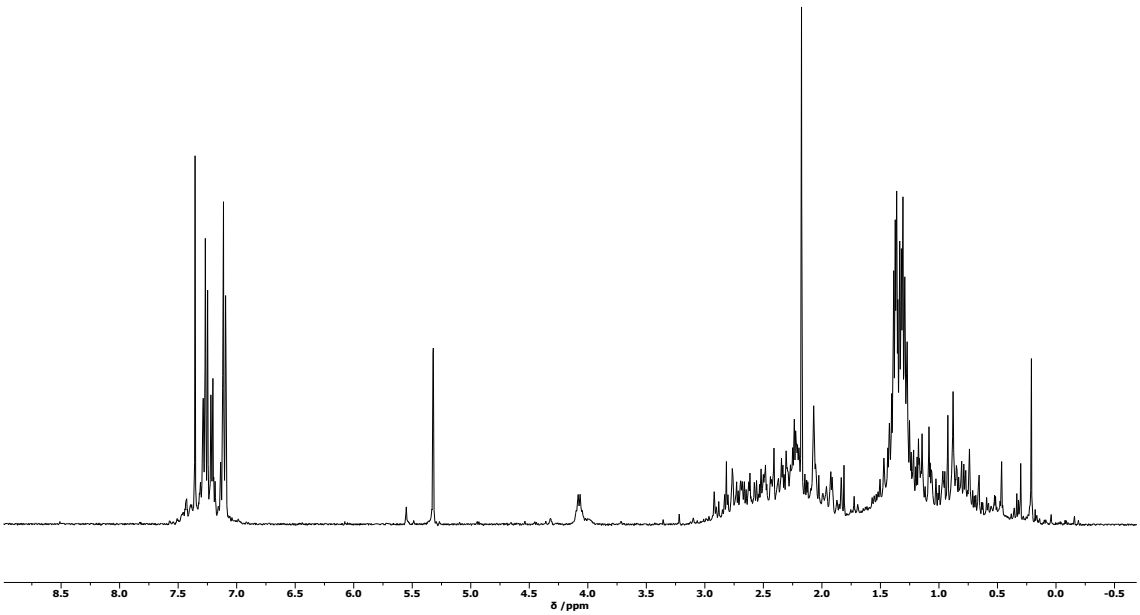

Figure A.80 ^{1}H NMR spectra of the reaction between ^{Me_2}SB($^{t Bu_2}$ArO,I*)TiMe$_2$ (**5**) and [Ph$_3$C][BAr$^F{}_4$] (dichloromethane-d_2, 400 MHz, 297 K). A single ^{11}B resonance at δ –17 ppm and ^{19}F resonances at δ –133, –164, and –167 ppm were observed.

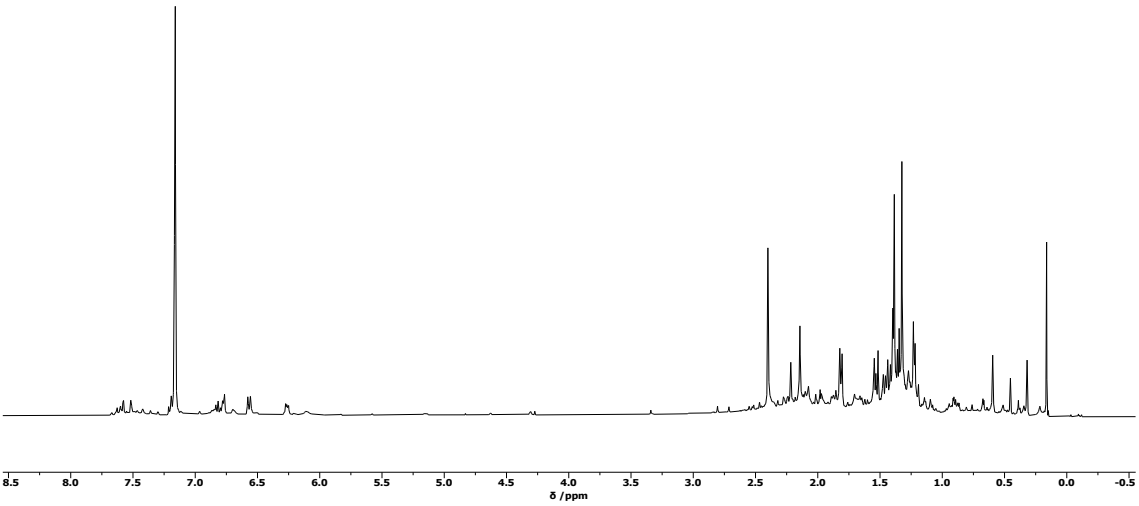

Figure A.81 ^{1}H NMR spectra of the reaction between ^{Me_2}SB($^{t Bu_2}$ArO,I*)TiMe$_2$ (**5**) and [PhNHMe$_2$][BAr$^F{}_4$] (benzene-d_6, 400 MHz, 298 K). ^{19}F resonances at δ –132, –162, and –166 ppm were observed.

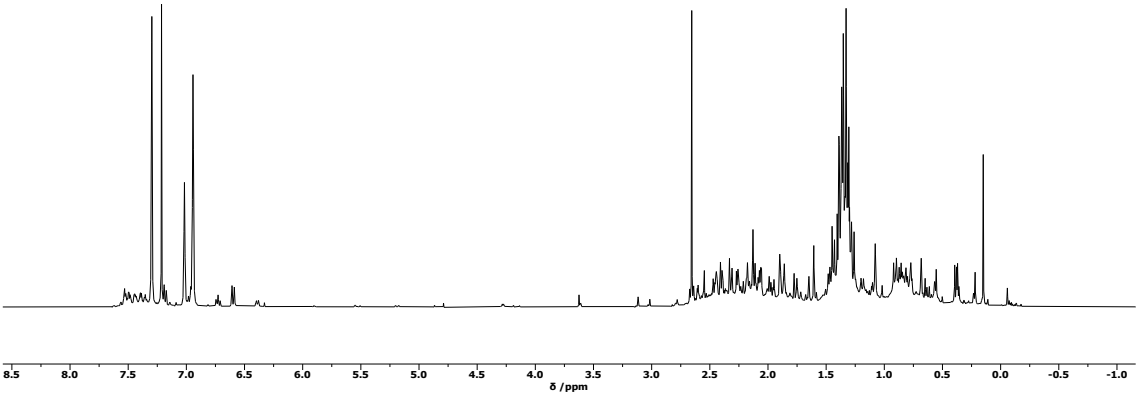

Figure A.82 ^{1}H NMR spectra of the reaction between ^{Me2}SB(^{t}Bu$_2$ArO,I*)TiMe$_2$ (**5**) and [PhNHMe$_2$][BAr$^{F}_4$] (bromobenzene-d_5, 400 MHz, 298 K). ^{19}F resonances at δ –131, –162, and –166 ppm were observed.

A.1.5. ssNMR spectra of solid catalysts

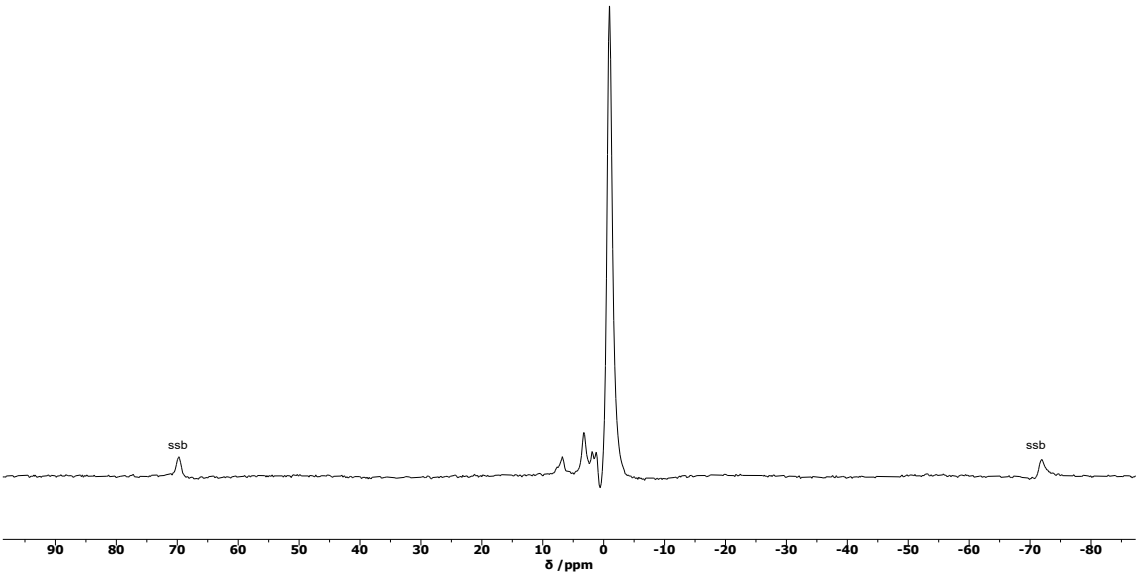

Figure A.83 ^{1}H ssNMR spectrum of sMAO-^{Me2}SB(^{t}Bu$_2$ArO,I*)TiCl$_2$ (**2$_{sMAO}$**) (60 kHz, 850 MHz, 298 K).

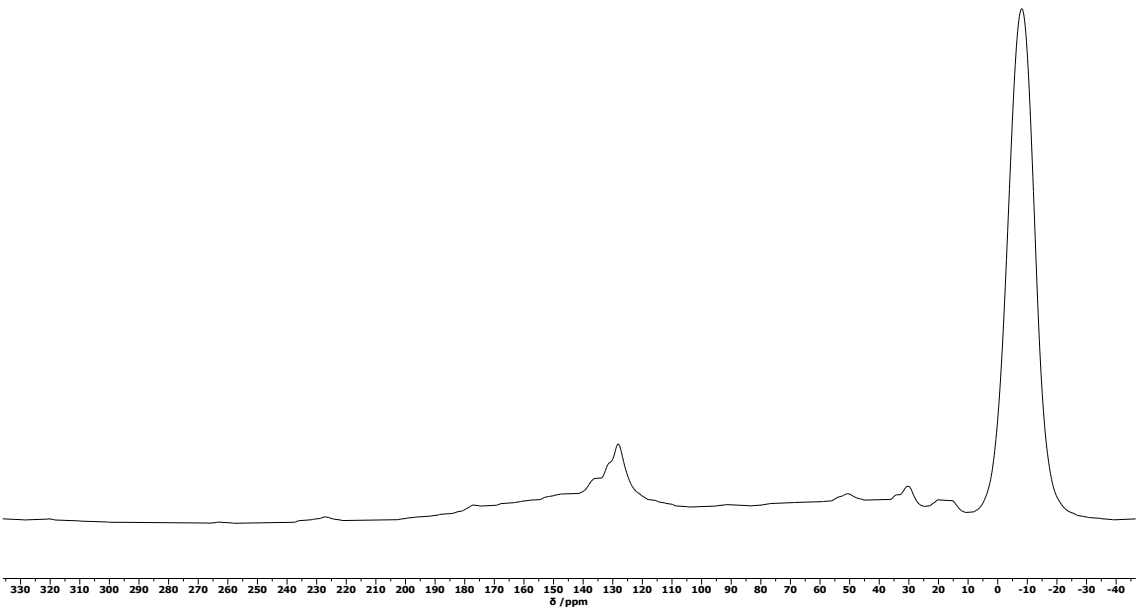

Figure A.84 ^{13}C CPMAS ssNMR spectrum of sMAO-^{Me2}SB(^{tBu2}ArO,I*)TiCl$_2$ (**2$_{sMAO}$**) (10 kHz, 101 MHz, 298 K).

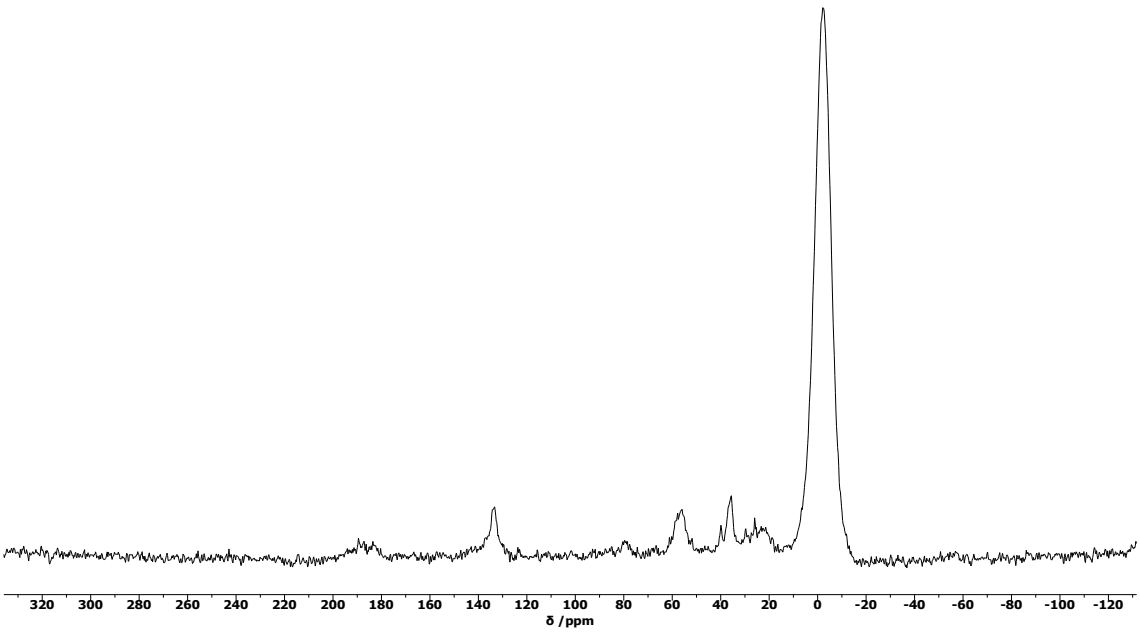

Figure A.85 ^{13}C CPMAS ssNMR spectrum of sMAO-^{Me2}SB(^{tBu2}ArO,I*)TiCl$_2$ (**2$_{sMAO}$**) (60 kHz, 214 MHz, 298 K).

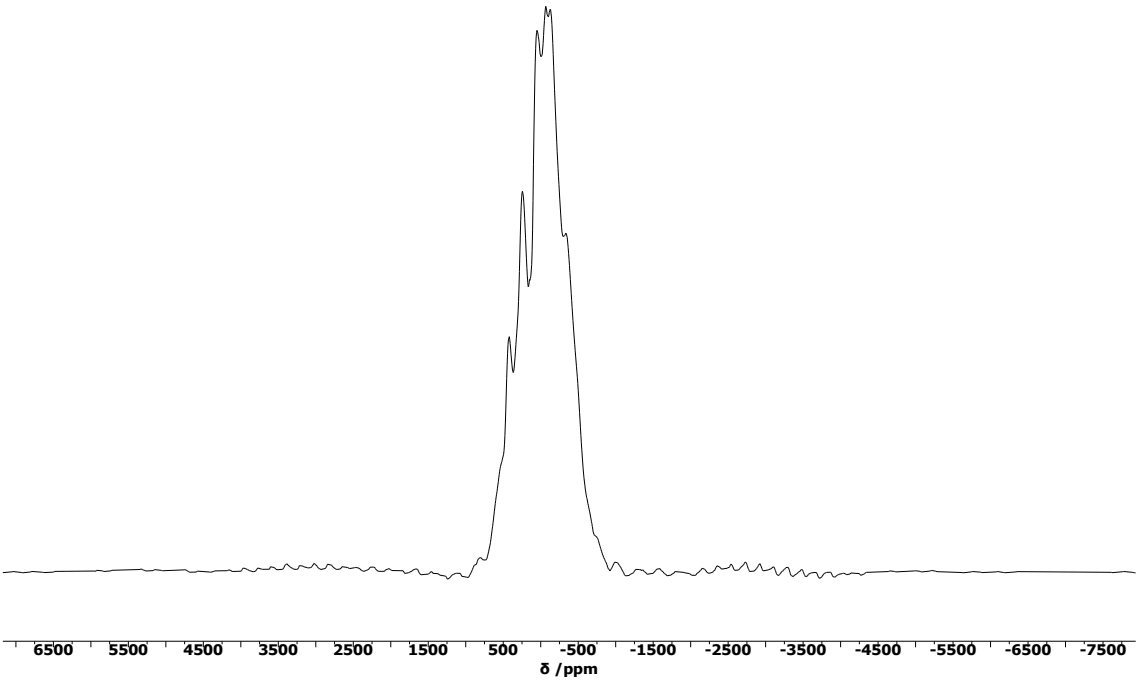

Figure A.86 ^{27}Al Hahn echo ssNMR spectrum of sMAO-^{Me2}SB(^{tBu2}ArO,I*)TiCl$_2$ (**2$_{sMAO}$**) (20 kHz, 104 MHz, 298 K).

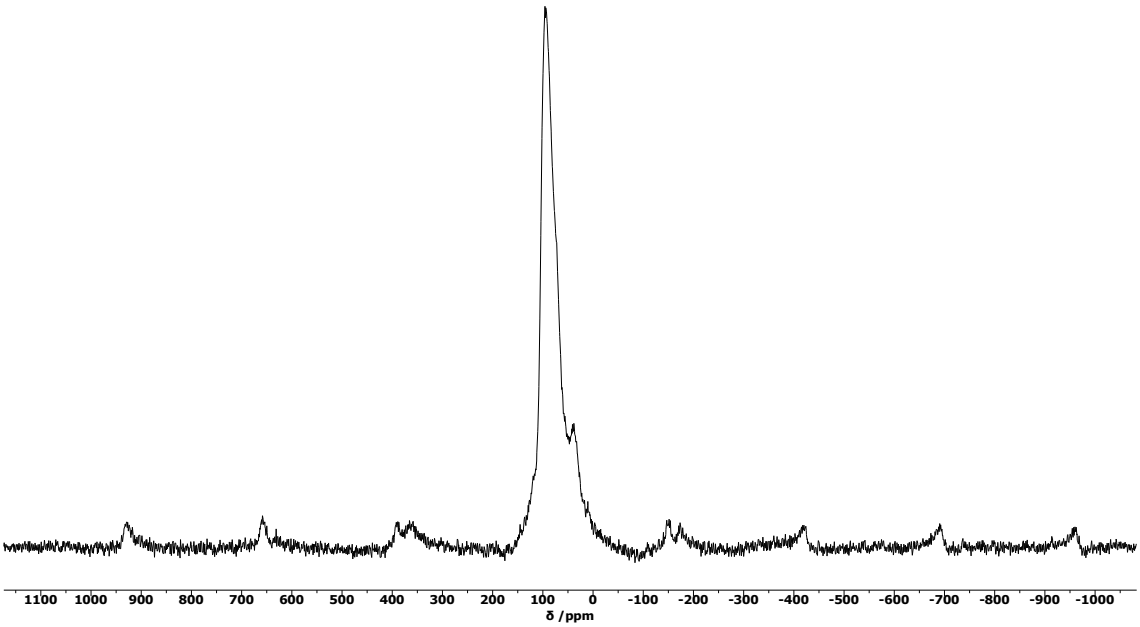

Figure A.87 ^{27}Al DPMAS ssNMR spectrum of sMAO-^{Me2}SB(^{tBu2}ArO,I*)TiCl$_2$ (**2$_{sMAO}$**) (60 kHz, 222 MHz, 298 K).

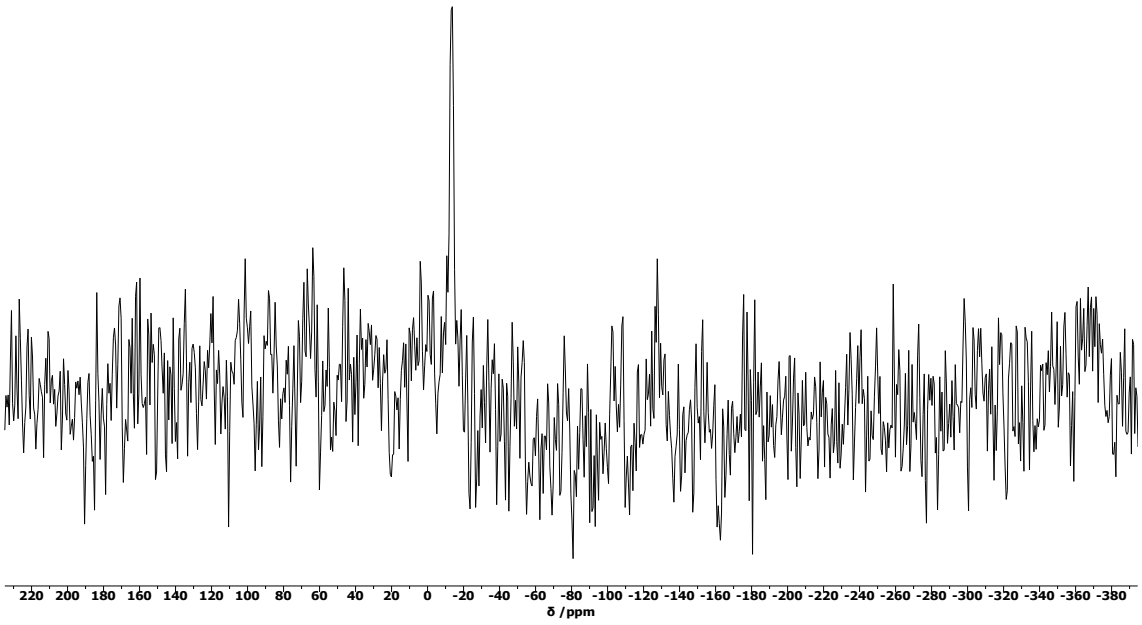

Figure A.88 ^{29}Si CPMAS ssNMR spectrum of sMAO-^{Me2}SB(^{t}Bu$_2$ArO,I*)TiCl$_2$ (**2$_{sMAO}$**) (10 kHz, 79 MHz, 298 K).

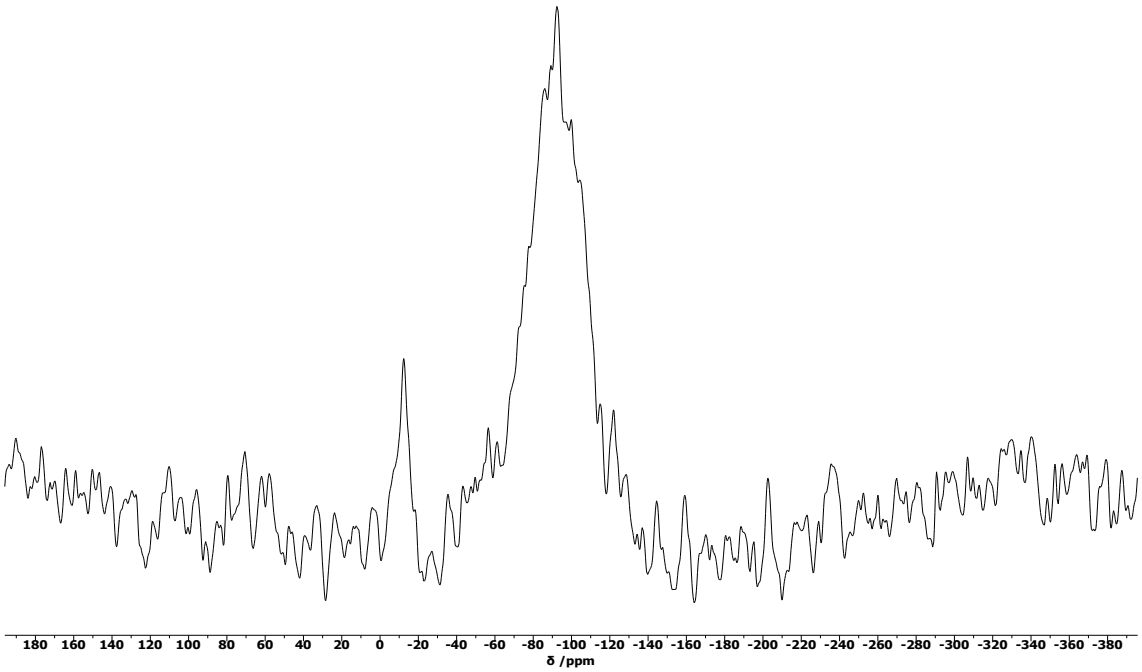

Figure A.89 ^{29}Si CPMAS ssNMR spectrum of sMAO-^{Me2}SB(^{t}Bu$_2$ArO,I*)TiCl$_2$ (**2$_{sMAO}$**) (60 kHz, 169 MHz, 298 K).

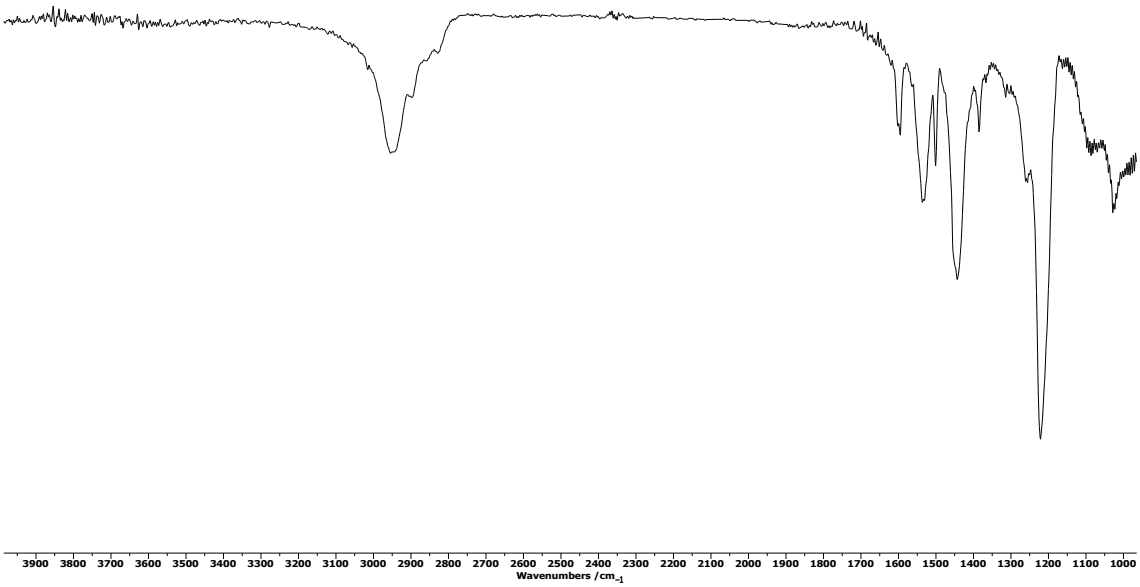

Figure A.90 FTIR spectrum of sMAO-^{Me2}SB(^{t}Bu$_2$ArO,I*)TiCl$_2$ (**2$_{sMAO}$**) (KBr).

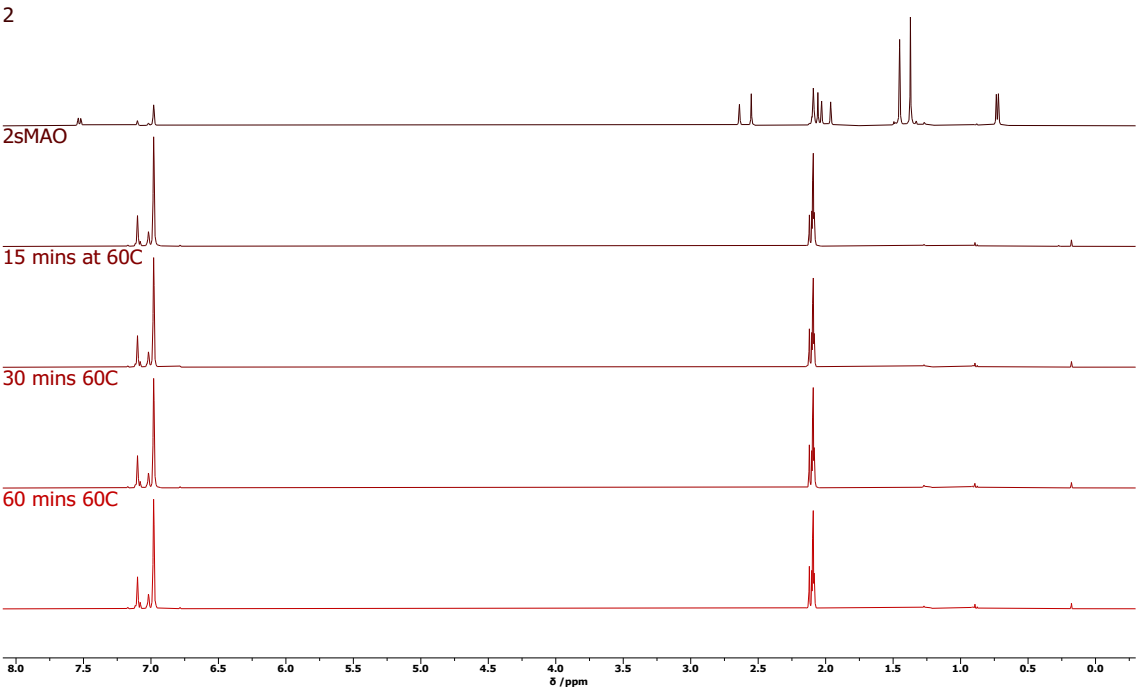

Figure A.91 ^{1}H NMR spectrum of sMAO-^{Me2}SB(^{t}Bu$_2$ArO,I*)TiCl$_2$ (**2$_{sMAO}$**) (toluene-d_8, 400 MHz, 298 K) demonstrating that no leaching occurs.

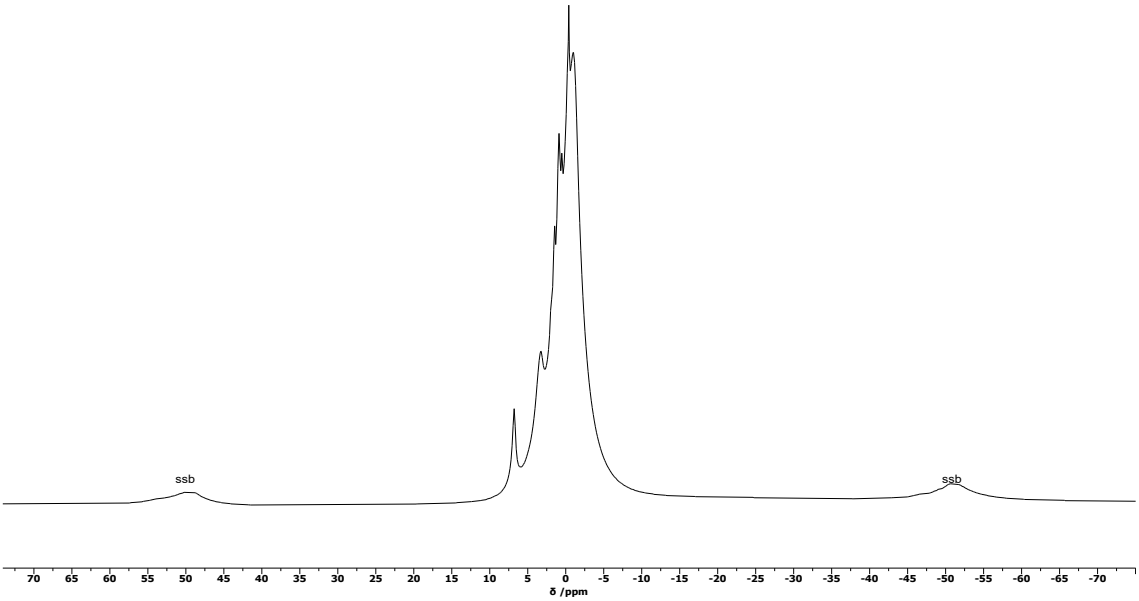

Figure A.92 ^{1}H ssNMR spectrum of SSMAO-^{Me2}SB(^{t}Bu^{2}ArO,I*)TiCl$_2$ (**2**$_{\mathbf{SSMAO}}$) (20 kHz, 400 MHz, 298 K).

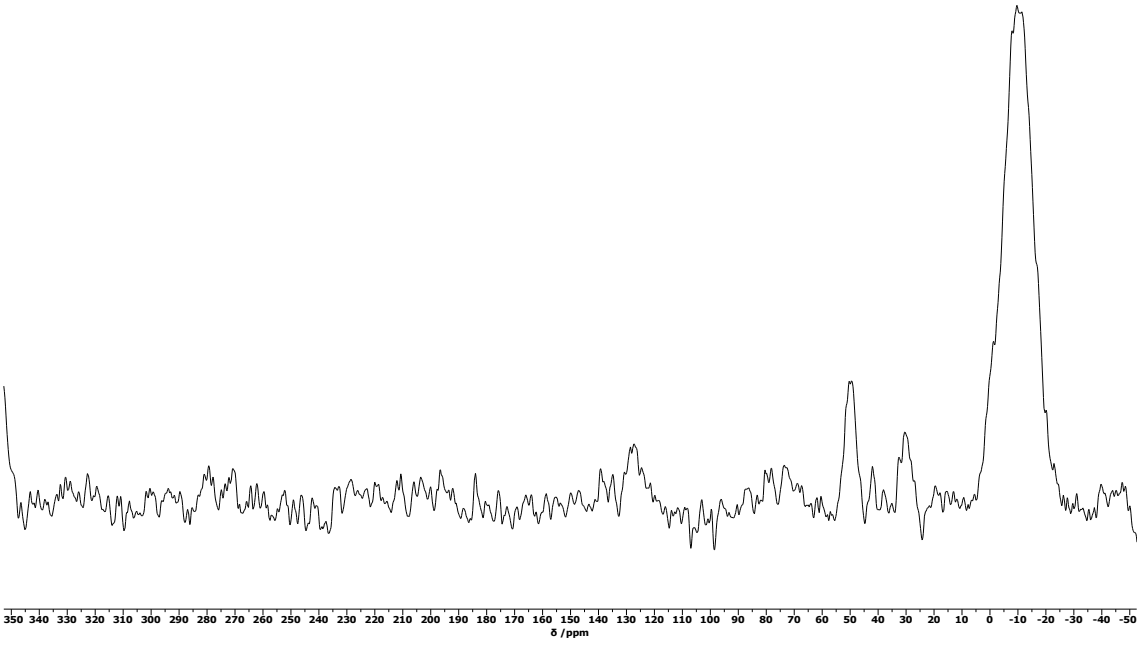

Figure A.93 ^{13}C CPMAS ssNMR spectrum of SSMAO-^{Me2}SB(^{t}Bu^{2}ArO,I*)TiCl$_2$ (**2**$_{\mathbf{SSMAO}}$) (10 kHz, 101 MHz, 298 K).

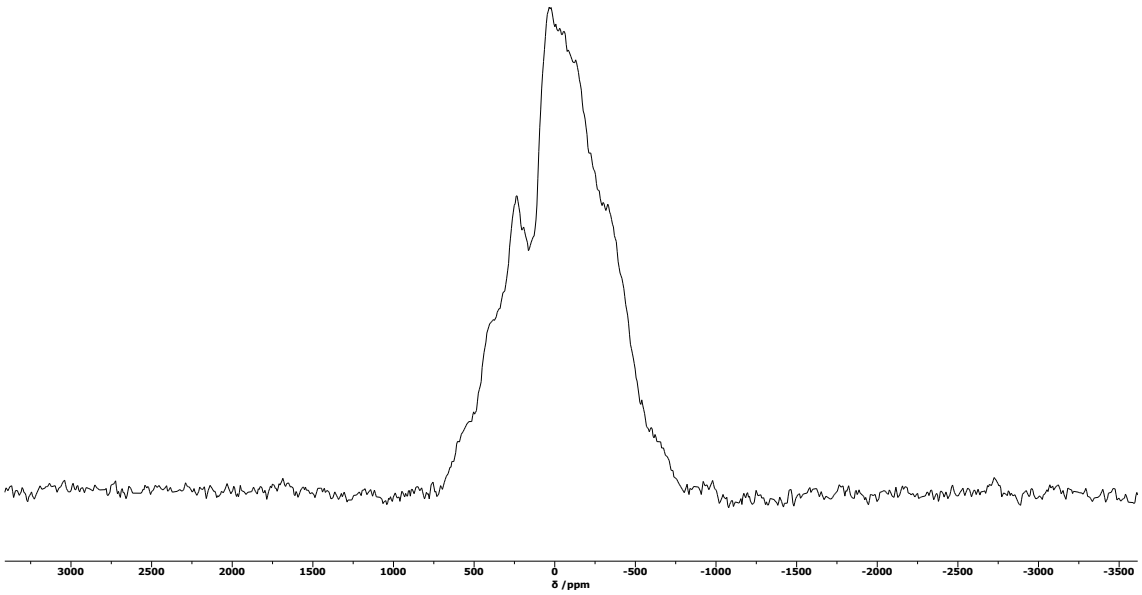

Figure A.94 ^{27}Al Hahn echo ssNMR spectrum of SSMAO-^{Me2}SB(^{tBu2}ArO,I*)TiCl$_2$ (**2$_{SSMAO}$**) (20 kHz, 104 MHz, 298 K).

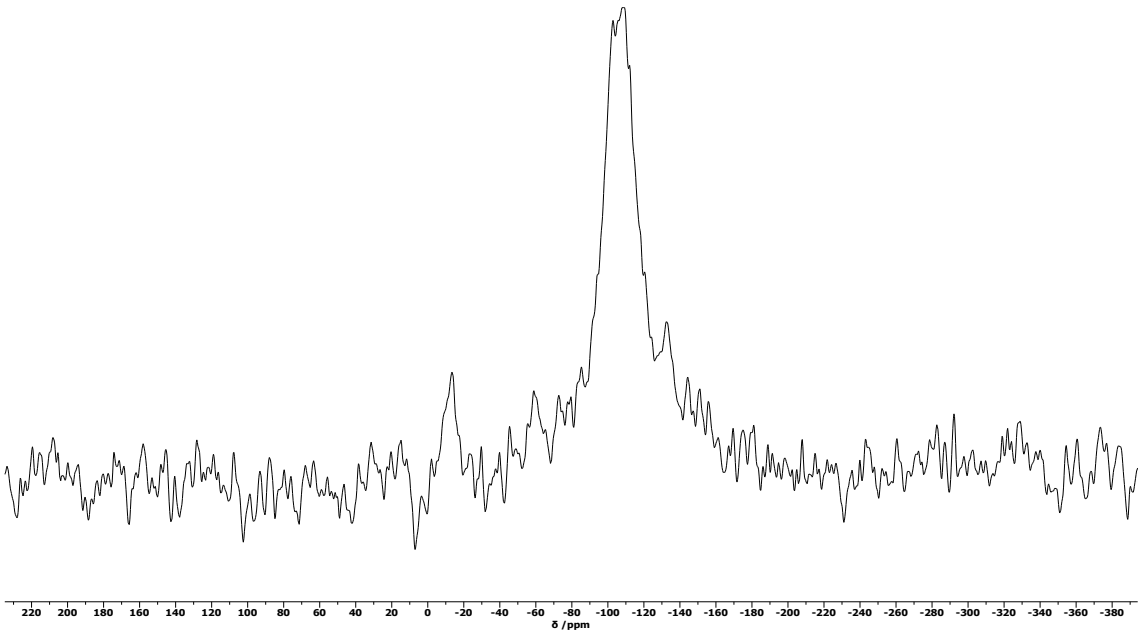

Figure A.95 ^{29}Si CPMAS ssNMR spectrum of SSMAO-^{Me2}SB(^{tBu2}ArO,I*)TiCl$_2$ (**2$_{SSMAO}$**) (10 kHz, 79 MHz, 298 K).

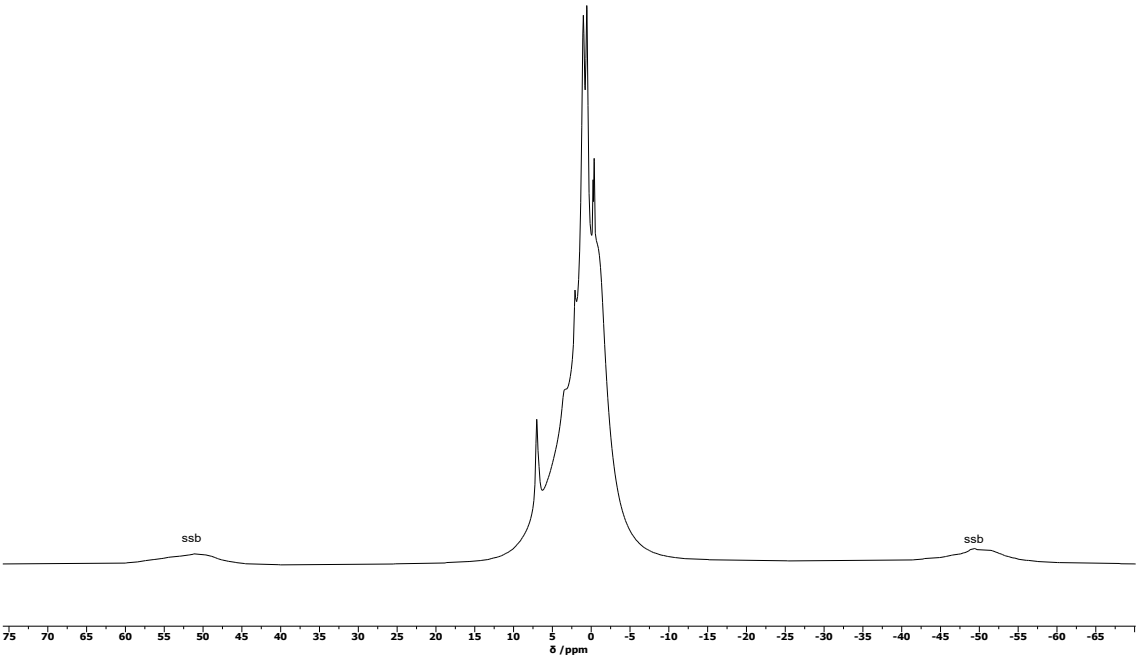

Figure A.96 ^{1}H ssNMR spectrum of LDHMAO-^{Me2}SB(^{tBu2}ArO,I*)TiCl$_2$ (**2$_{LDHMAO}$**) (20 kHz, 400 MHz, 298 K).

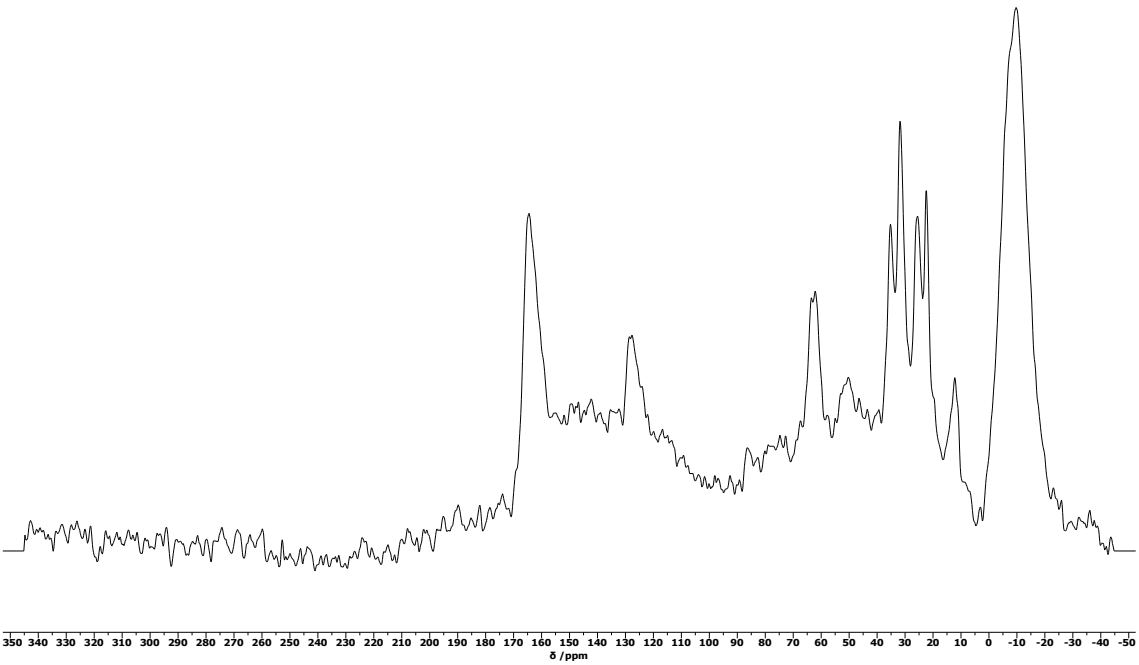

Figure A.97 ^{13}C CPMAS ssNMR spectrum of LDHMAO-^{Me2}SB(^{tBu2}ArO,I*)TiCl$_2$ (**2$_{LDHMAO}$**) (10 kHz, 101 MHz, 298 K).

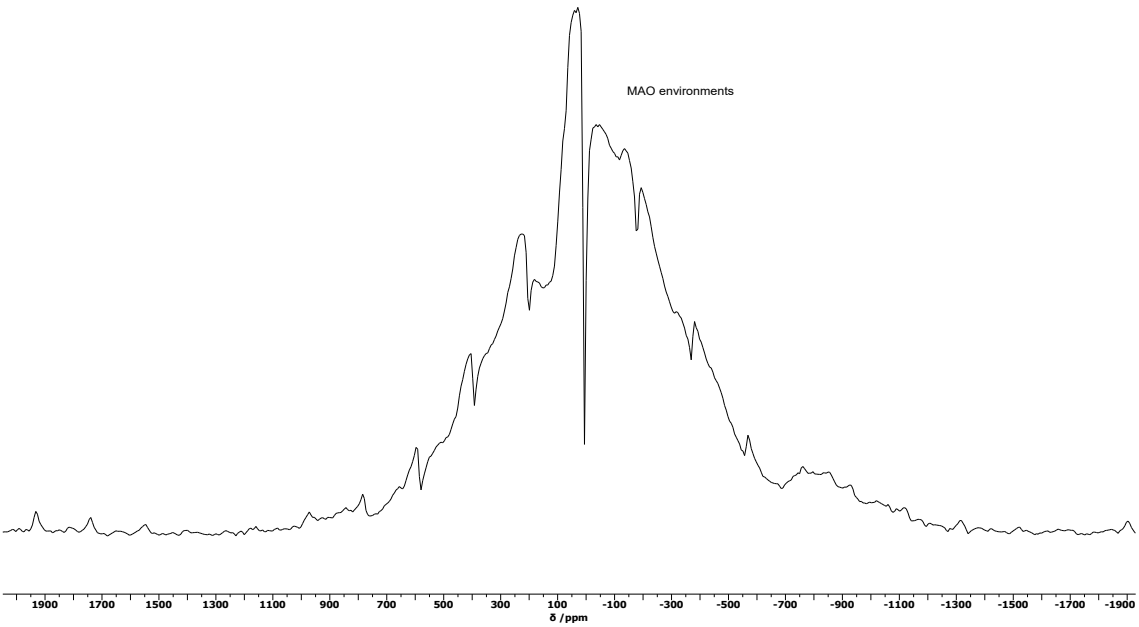

Figure A.98 ^{27}Al Hahn echo ssNMR spectrum of LDHMAO-^{Me2}SB(^{tBu2}ArO,I*)TiCl$_2$ (**2$_{LDHMAO}$**) (20 kHz, 104 MHz, 298 K).

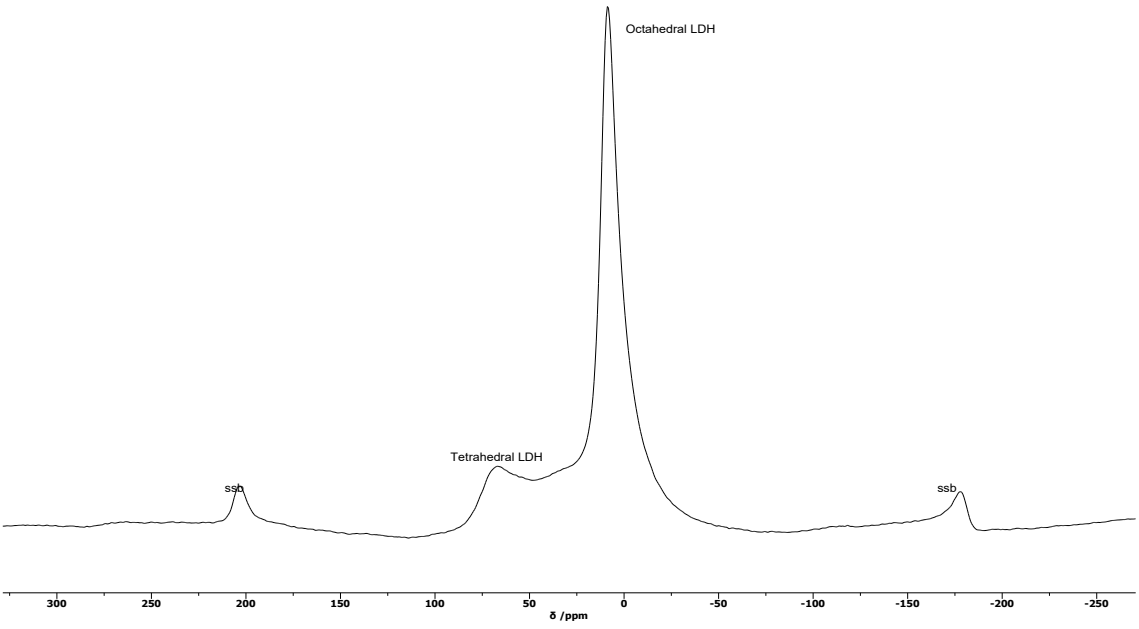

Figure A.99 ^{27}Al DPMAS ssNMR spectrum of LDHMAO-^{Me2}SB(^{tBu2}ArO,I*)TiCl$_2$ (**2$_{LDHMAO}$**) (20 kHz, 104 MHz, 298 K).

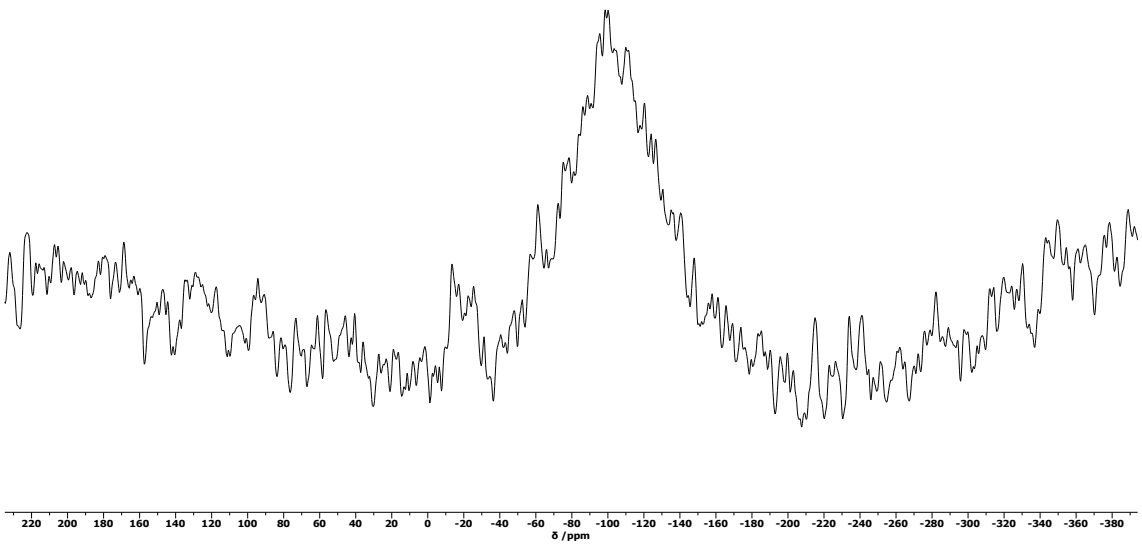

Figure A.100 ^{29}Si CPMAS ssNMR spectrum of LDHMAO-^{Me2}SB(^{t}Bu$_2$ArO,I*)TiCl$_2$ (**2$_{LDHMAO}$**) (10 kHz, 79 MHz, 298 K). The broad resonance at δ –100 ppm arises from residual silica impurities in the rotor.

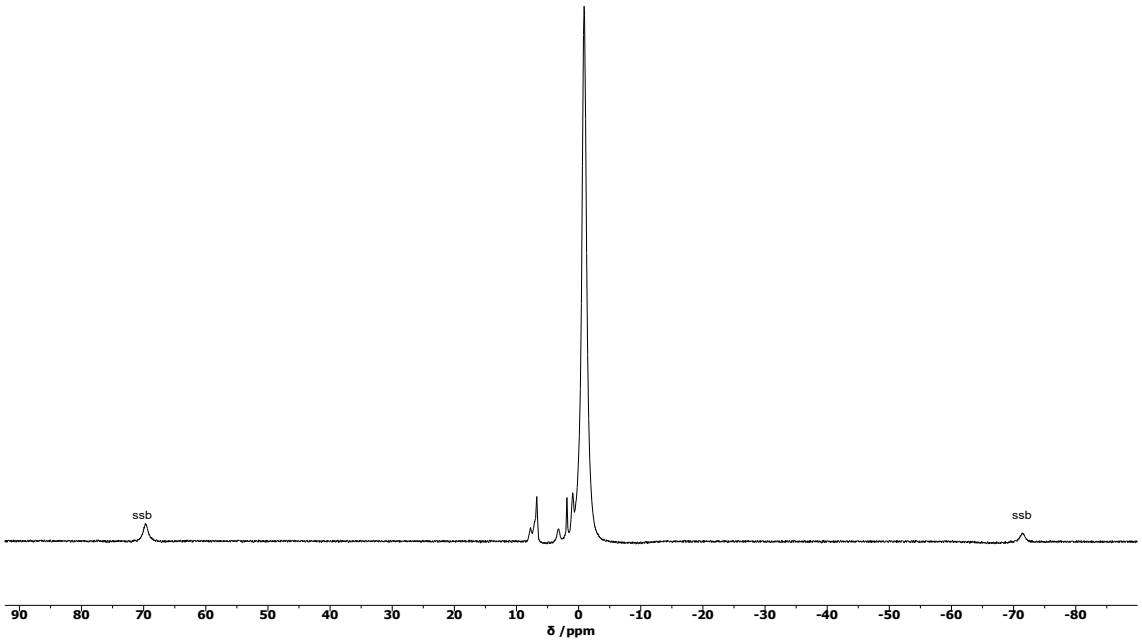

Figure A.101 ^{1}H ssNMR spectrum of sMAO-^{Me2}SB(^{t}Bu$_2$ArO,I*)TiMe$_2$ (**5$_{sMAO}$**) (60 kHz, 850 MHz, 298 K).

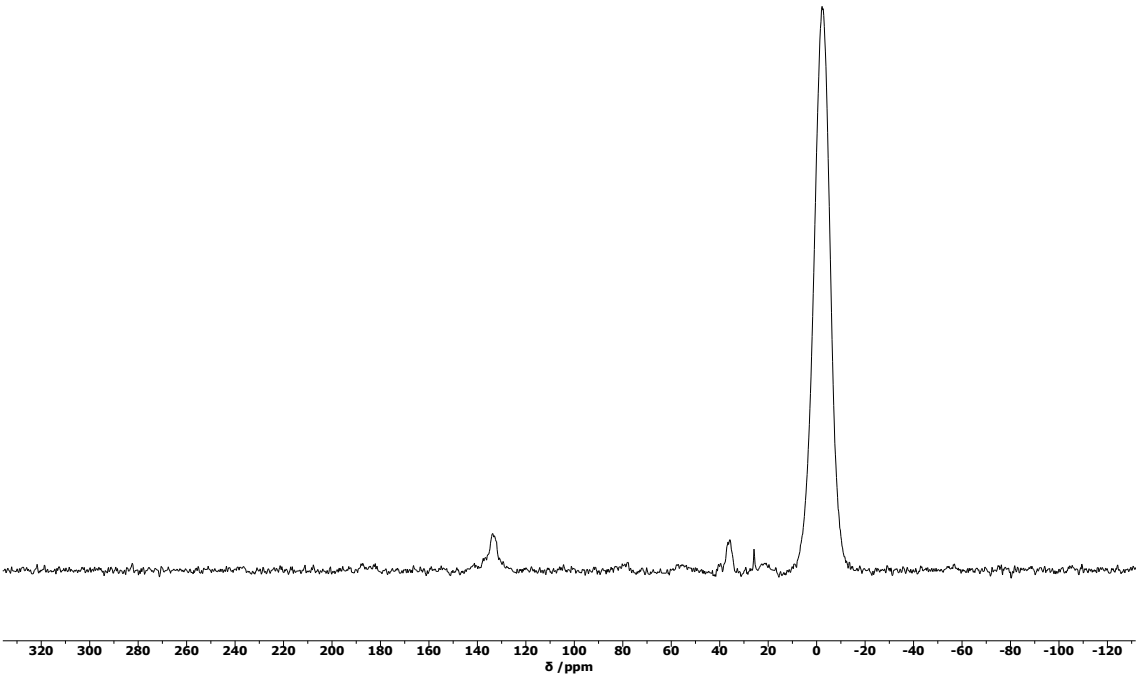

Figure A.102 ^{13}C CPMAS ssNMR spectrum of sMAO-^{Me2}SB(^{tBu2}ArO,I*)TiMe$_2$ (**5$_{sMAO}$**) (60 kHz, 214 MHz, 298 K).

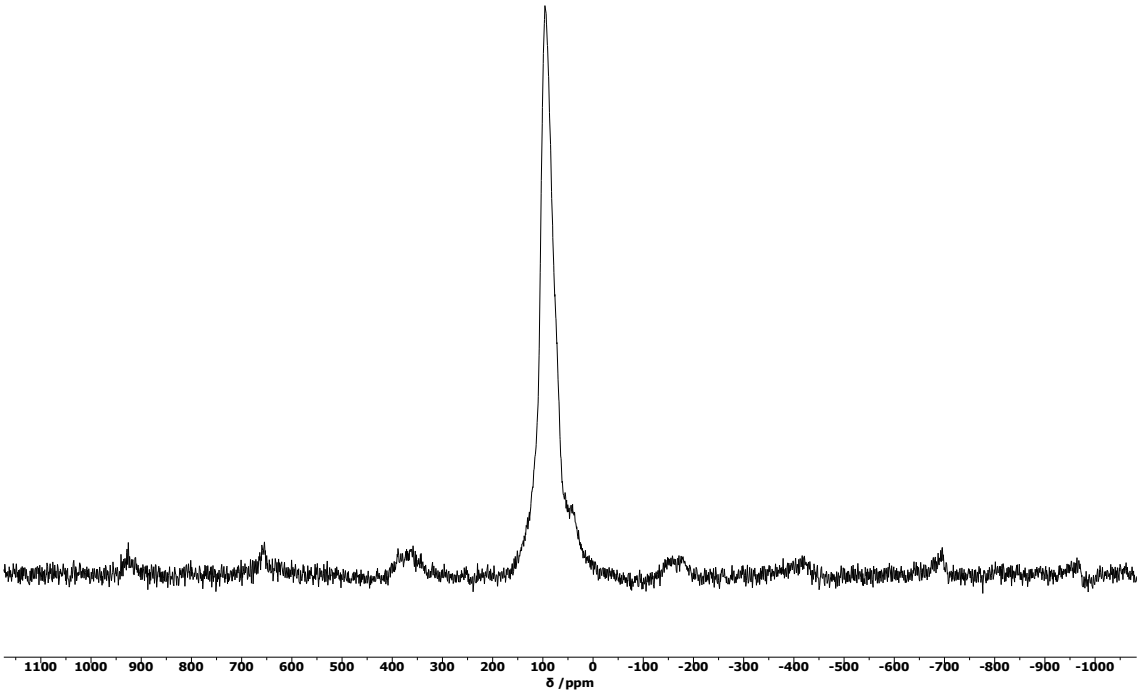

Figure A.103 ^{27}Al DPMAS ssNMR spectrum of sMAO-^{Me2}SB(^{tBu2}ArO,I*)TiMe$_2$ (**5$_{sMAO}$**) (60 kHz, 222 MHz, 298 K).

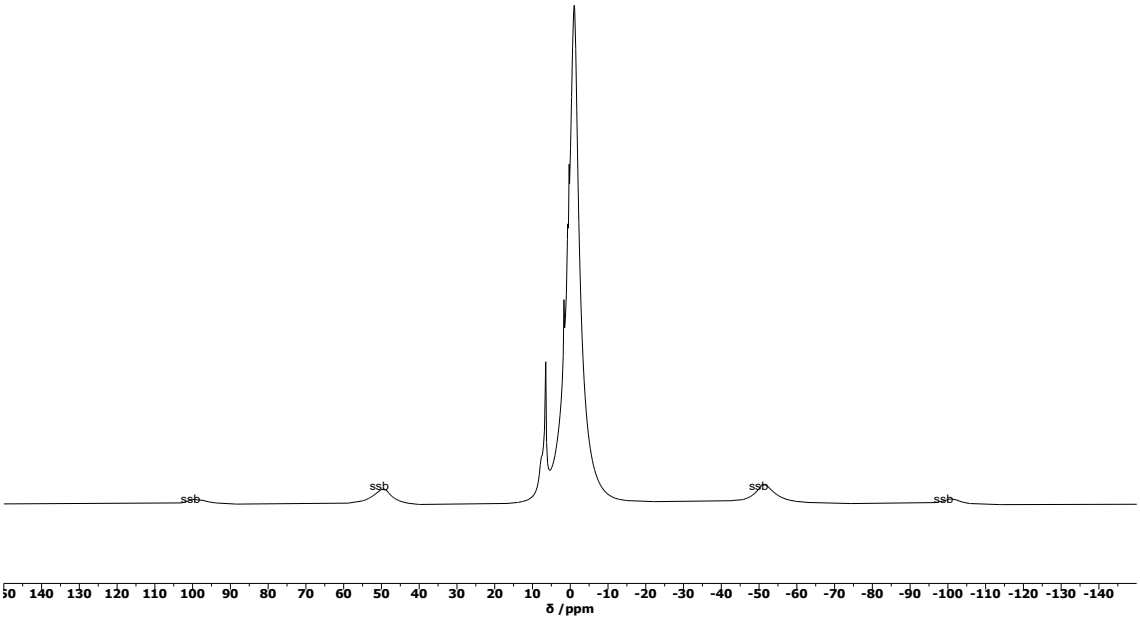

Figure A.104 ^{1}H ssNMR spectrum of sMAO-^{Me2}SB(^{Cumyl2}ArO,I*)TiCl$_2$ (**11$_{sMAO}$**) (20 kHz, 400 MHz, 298 K).

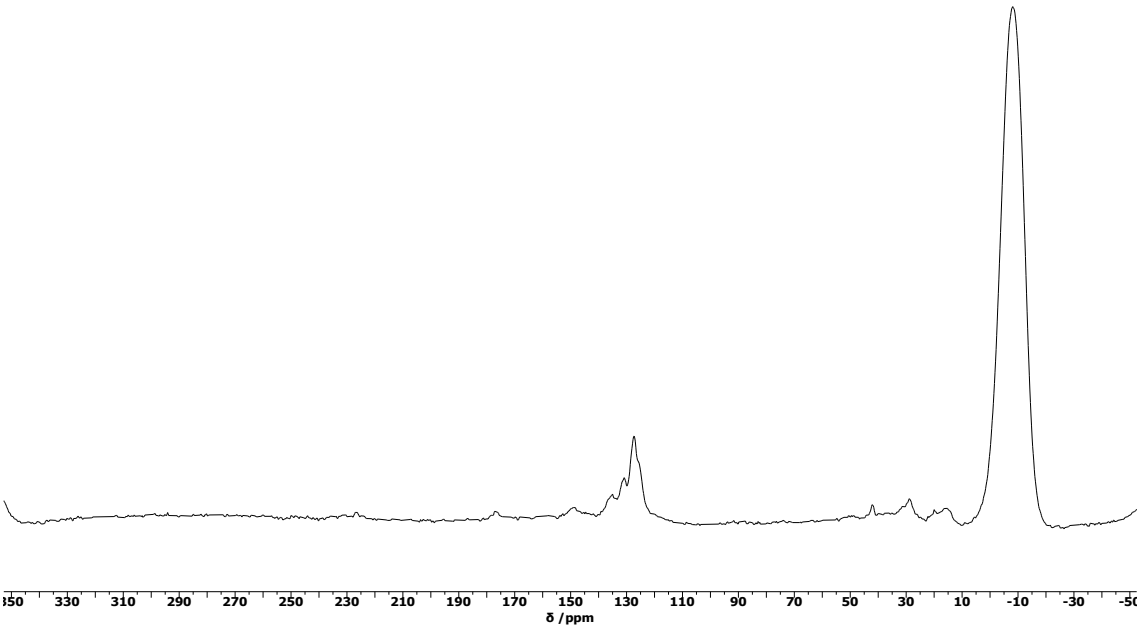

Figure A.105 ^{13}C CPMAS ssNMR spectrum of sMAO-^{Me2}SB(^{Cumyl2}ArO,I*)TiCl$_2$ (**11$_{sMAO}$**) (10 kHz, 101 MHz, 298 K).

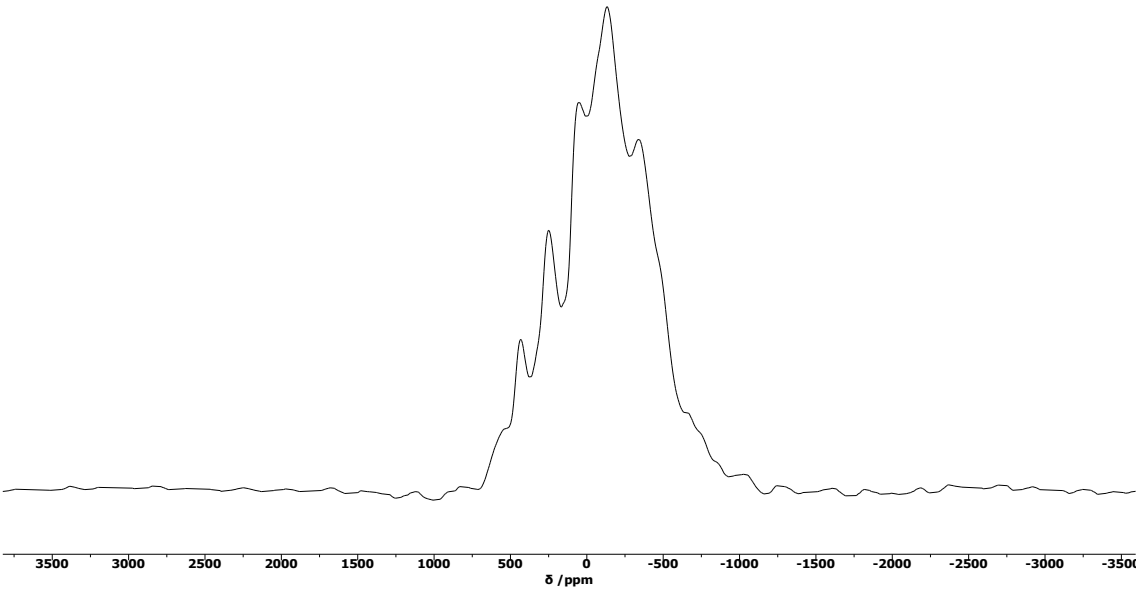

Figure A.106 ^{27}Al Hahn echo ssNMR spectrum of sMAO-^{Me2}SB(^{Cumyl2}ArO,I*)TiCl$_2$ (**11$_{sMAO}$**) (20 kHz, 104 MHz, 298 K).

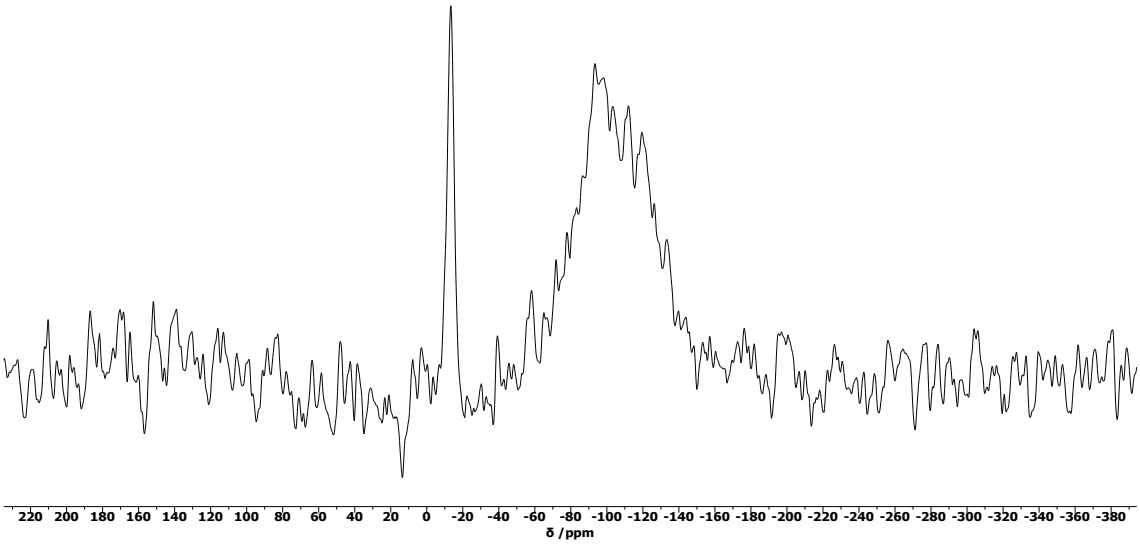

Figure A.107 ^{29}Si CPMAS ssNMR spectrum of of sMAO-^{Me2}SB(^{Cumyl2}ArO,I*)TiCl$_2$ (**11$_{sMAO}$**) (10 kHz, 79 MHz, 298 K).

A.2. Supplementary data for Chapter Three

A.2.1. Homogeneous polymerisation data

Table A.1 Solution-phase polymerisation data using selected PHENI* catalysts. Polymerisation conditions: 715 nmol complex, 2 bar ethylene, MAO ([Al_{MAO}]/[Ti] = 1000) or TB/TIBA ([TB]:[TIBA]:[Ti] = 1:200:1), 50 mL hexanes.

Complex	Temperature /°C	Time /mins	Activity /kg mol_{Ti}^{-1} h^{-1} bar^{-1}	M_w /kDa	PDI
2/MAO	30	5.00	1079 ± 53	694.6	3.0
	40	5.00	1474 ± 53	750.1	2.8
	50	5.00	2586 ± 914	708.9	2.7
	60	5.00	3842 ± 825	527.4	3.6
	70	5.00	4774 ± 707	607.6	3.6
	80	5.00	4501 ± 1247	410.0	3.3
	90	5.00	3602 ± 618	362.1	3.4
5/TB/TIBA	30	0.93	14195 ± 3932	2557.2	3.1
	40	0.83	16188 ± 1328	2242.8	3.3
	50	0.52	26976 ± 1699	1326.5	3.4
	60	0.46	22475 ± 6342	2554.3	2.6
	70	0.66	17943 ± 5495	1422.9	3.5
	80	0.57	12218 ± 1718	2577.6	3.5
	90	0.75	14759 ± 3787	2360.0	3.6
11/MAO	30	1.23	17575 ± 1599	1699.8	3.5
	40	0.91	23336 ± 1223	1335.7	3.0
	50	1.03	20011 ± 4694	1005.0	3.9
	60	0.60	22658 ± 3273	617.9	3.4
	70	0.97	23158 ± 784	494.3	3.6
	80	1.37	12711 ± 5261	467.6	3.1
	90	0.85	16017 ± 5239	466.2	3.2

A.2.2. Heterogeneous polymerisation data

Table A.2 Slurry-phase polymerisation data using selected PHENI* catalysts. Polymerisation conditions: 2 bar ethylene, 10 mg catalyst, either 150 mg TIBA or [Ti]/[TB] = 1, 50 mL hexanes.

Catalyst	Temperature /°C	Time /mins	Activity /kg mol_{Ti}^{-1} h^{-1} bar^{-1}	M_w /kDa	PDI
1$_{sMAO}$/TIBA	50	30	3078 ± 34	2513.8	2.8
	60	30	3231 ± 150	2087.9	3.0
	70	30	2776 ± 190	1876.4	3.8
	80	30	2674 ± 70	1494.5	5.1
	90	30	1723 ± 192	1313.6	5.7
2$_{sMAO}$/TIBA	30	30	2834 ± 338	3376.0	3.4
	40	30	3518 ± 129	3117.2	4.4
	50	30	3614 ± 123	2352.6	4.4
	60	30	3719 ± 106	2087.5	5.2
	70	30	3367 ± 151	2033.7	5.5
	80	30	2450 ± 121	1550.9	6.9
	90	30	2180 ± 17	1516.9	6.4
2$_{sMAO}$/TB	30	30	192 ± 27	1797.7	3.0
	40	30	256 ± 71	1963.0	2.5
	50	30	392 ± 21	2266.7	2.8
	60	30	102 ± 41	972.8	3.2
	70	30	118 ± 14	1041.8	3.4
	80	30	154 ± 23	1050.7	3.3
	90	30	111 ± 51	1002.4	3.4
2$_{SSMAO}$/TIBA	30	30	236 ± 24	2567.9	2.0

	40	30	327 ± 8	2821.1	2.0
	50	30	311 ± 89	2692.2	2.0
	60	30	437 ± 21	2643.8	1.7
	70	30	446 ± 44	2619.5	2.2
	80	30	430 ± 15	2287.5	2.8
	90	30	310 ± 1	2023.9	3.8
2$_{\mathbf{LDHMAO}}$/TIBA	30	30	642 ± 49	4195.0	1.7
	40	30	732 ± 27	4081.6	1.8
	50	30	871 ± 91	4200.9	1.6
	60	30	872 ± 95	3978.8	2.1
	70	30	820 ± 73	3893.7	1.8
	80	30	638 ± 84	3370.0	2.8
	90	30	619 ± 29	3230.0	2.7
3$_{\mathbf{sMAO}}$/TIBA	50	30	3126 ± 86	2631.2	2.3
	60	30	3133 ± 33	2437.7	3.0
	70	30	2984 ± 16	2184.5	3.1
	80	30	2881 ± 365	1491.5	4.2
	90	30	2186 ± 50	1385.0	5.0
4$_{\mathbf{sMAO}}$/TIBA	50	30	2345 ± 42	2768.4	2.1
	60	30	2493 ± 263	2696.2	2.6
	70	30	2548 ± 130	2303.2	3.4
	80	30	2103 ± 186	1970.1	4.0
	90	30	1583 ± 68	1443.8	5.1
5$_{\mathbf{sMAO}}$/TIBA	50	30	2630 ± 227	3454.7	2.6
	60	30	2817 ± 291	2173.7	3.0
	70	30	2166 ± 50	3100.3	3.0

	80	30	1945 ± 275	2383.0	3.7
	90	30	1187 ± 6	2094.3	5.4
6$_{sMAO}$/TIBA	50	30	2536 ± 113	2244.4	2.2
	60	30	2593 ± 52	2113.9	1.7
	70	30	2484 ± 282	2622.7	3.5
	80	30	2071 ± 352	2005.0	3.9
	90	30	1470 ± 149	1658.7	5.2
7$_{sMAO}$/TIBA	50	30	1638 ± 20	2368.0	1.9
	60	30	1868 ± 110	2274.0	1.9
	70	30	1751 ± 200	2213.8	2.3
	80	30	1616 ± 132	1828.9	3.4
	90	30	1517 ± 17	1443.0	4.3
8$_{sMAO}$/TIBA	50	30	1486 ± 243	2929.6	2.0
	60	30	1869 ± 161	2522.9	2.3
	70	30	1933 ± 252	2173.3	2.9
	80	30	1630 ± 45	1926.4	3.5
	90	30	1424 ± 59	1475.9	4.9
9$_{sMAO}$/TIBA	50	30	1379 ± 232	2793.8	2.4
	60	30	1371 ± 49	2608.6	2.4
	70	30	1697 ± 101	2463.0	3.0
	80	30	1596 ± 8	1954.4	4.6
	90	30	1256 ± 38	1559.5	4.5
10$_{sMAO}$/TIBA	50	30	682 ± 93	2416.5	1.7
	60	30	759 ± 43	2524.9	2.2
	70	30	785 ± 5	2263.7	2.4
	80	30	725 ± 35	1904.2	3.0

	90	30	623 ± 20	1452.7	4.8
11$_{sMAO}$/TIBA	50	30	2114 ± 2	1862.5	3.5
	60	30	1983 ± 39	1777.0	3.5
	70	30	1597 ± 126	1392.8	3.7
	80	30	1317 ± 297	1108.2	3.9
	90	30	1022 ± 154	873.5	3.7
12$_{sMAO}$/TIBA	50	30	3662 ± 430	2810.1	2.5
	60	30	3897 ± 23	2337.0	3.1
	70	30	3767 ± 358	2052.3	4.0
	80	30	3453 ± 16	1728.7	4.4
	90	30	2361 ± 619	1346.1	5.6
13$_{sMAO}$/TIBA	50	30	3840 ± 320	1596.2	3.2
	60	30	3705 ± 540	1365.9	3.1
	70	30	3332 ± 38	1146.2	3.9
	80	30	2442 ± 269	708.2	4.4
	90	30	1351 ± 350	1087.0	4.1
14$_{sMAO}$/TIBA	50	30	155 ± 3	1192.2	25.5
	60	30	144 ± 2	1091.7	20.9
	70	30	114 ± 16	878.2	23.7
	80	30	103 ± 13	719.5	35.9
	90	30	60 ± 7	501.5	20.8
15$_{sMAO}$/TIBA	50	30	353 ± 40	162.0 / 2110.8 (87:13)	6.0 / 1.9
	60	30	338 ± 14	120.0 / 1303.2 (80:20)	3.8 / 3.4
	70	30	265 ± 3	163.0 / 1367.3	4.6 / 2.7

				(81:19)	
	80	30	216 ± 44	141.0 / 1193.4 (79:21)	3.4 / 3.4
	90	30	212 ± 1	254.0 / 1664.3 (86:14)	7.9 / 2.0

Table A.3 Slurry-phase polymerisation data using selected PHENI* catalysts. Polymerisation conditions: 2 bar ethylene, 10 mg catalyst, 150 or 750 mg TIBA, 50 or 250 mL hexanes.

Catalyst	Temperature /°C	Solvent /mL	Time /mins	Activity /kg mol_{Ti}^{-1} h^{-1} bar^{-1}	M_w /kDa	PDI
$\mathbf{2}_{\mathbf{sMAO}}$/TIBA	60	50	5	6997 ± 220	1942.0	6.4
$\mathbf{2}_{\mathbf{sMAO}}$/TIBA	60	50	15	5191 ± 209	2429.6	5.3
$\mathbf{2}_{\mathbf{sMAO}}$/TIBA	60	50	30	3719 ± 106	2087.5	5.2
$\mathbf{2}_{\mathbf{sMAO}}$/TIBA	60	50	60	2782 ± 424	2776.3	4.8
$\mathbf{2}_{\mathbf{sMAO}}$/TIBA	60	50	120	2188 ± 51	3198.3	3.7
$\mathbf{2}_{\mathbf{sMAO}}$/TIBA	60	250	5	6853	2284.5	2.4
$\mathbf{2}_{\mathbf{sMAO}}$/TIBA	60	250	120	2461	2221.1	2.3

Table A.4 Slurry-phase polymerisation data using selected PHENI* catalysts. Polymerisation conditions: 2 bar ethylene, 10 mg catalyst, [Al]/[Ti] = 1000, 50 mL hexanes.

Catalyst	Temperature /°C	Time /mins	Activity /kg mol_{Ti}^{-1} h^{-1} bar^{-1}	M_w /kDa	PDI
$\mathbf{2}_{\mathbf{sMAO}}$/TIBA	60	30	3719 ± 106	2087.5	5.2
$\mathbf{2}_{\mathbf{sMAO}}$/TEA	60	30	721 ± 312	791.1	14.1
$\mathbf{2}_{\mathbf{sMAO}}$/TMA	60	30	1099 ± 8	1355.2	7.9
$\mathbf{2}_{\mathbf{sMAO}}$/MAO	60	30	1684 ± 476	2631.3	5.5

Table A.5 Slurry-phase polymerisation data using selected PHENI* catalysts. Polymerisation conditions: 2 bar ethylene, 10 mg catalyst, 50 mL hexanes.

Catalyst	Temperature /°C	$[TIBA]_0/[Ti]_0$	Activity /kg mol_{Ti}^{-1} h^{-1} bar^{-1}	M_w /kDa	PDI
$\mathbf{2}_{sMAO}$/TIBA	60	0	242 ± 24	1695.1	3.7
$\mathbf{2}_{sMAO}$/TIBA	60	125	3965 ± 421	2654.0	6.9
$\mathbf{2}_{sMAO}$/TIBA	60	250	4018 ± 39	2807.2	3.3
$\mathbf{2}_{sMAO}$/TIBA	60	500	4325 ± 177	2330.4	6.4
$\mathbf{2}_{sMAO}$/TIBA	60	1059	3719 ± 106	2087.5	5.2
$\mathbf{2}_{sMAO}$/TIBA	60	2500	3829 ± 157	1853.3	7.3
$\mathbf{2}_{sMAO}$/TIBA	60	5000	3684 ± 79	1671.4	6.8

Table A.6 Slurry-phase polymerisation data using selected PHENI* catalysts. Polymerisation conditions: 2 bar ethylene, 150 mg TIBA, 50 mL hexanes.

Catalyst	Temperature /°C	Catalyst mass /mg	Activity /kg mol_{Ti}^{-1} h^{-1} bar^{-1}	M_w /kDa	PDI
$\mathbf{2}_{sMAO}$/TIBA	60	5	3403 ± 3	2575.1	4.3
$\mathbf{2}_{sMAO}$/TIBA	60	10	3719 ± 106	2087.5	5.2
$\mathbf{2}_{sMAO}$/TIBA	60	15	3020 ± 495	1949.6	5.7
$\mathbf{2}_{sMAO}$/TIBA	60	20	2779 ± 7	1871.6	5.9

Table A.7 Slurry-phase hydrogen response polymerisation data using selected PHENI* catalysts. Polymerisation conditions: 2 bar ethylene/hydrogen (98:2), 10 mg catalyst, 150 mg TIBA, 50 mL hexanes.

Catalyst	Temperature /°C	Time /mins	Activity /kg mol_{Ti}^{-1} h^{-1} bar^{-1}	M_w /kDa	PDI
$\mathbf{2}_{\mathbf{sMAO}}$/TIBA	50	30	1689 ± 242	110	9.5
	60	30	1765 ± 83	91.3	7.2
	70	30	1168 ± 28	109.6	6.9
	80	30	1164 ± 190	89.3	5.4
	90	30	1095 ± 239	85.2	4.5

A.2.3. Ethylene uptake profiles

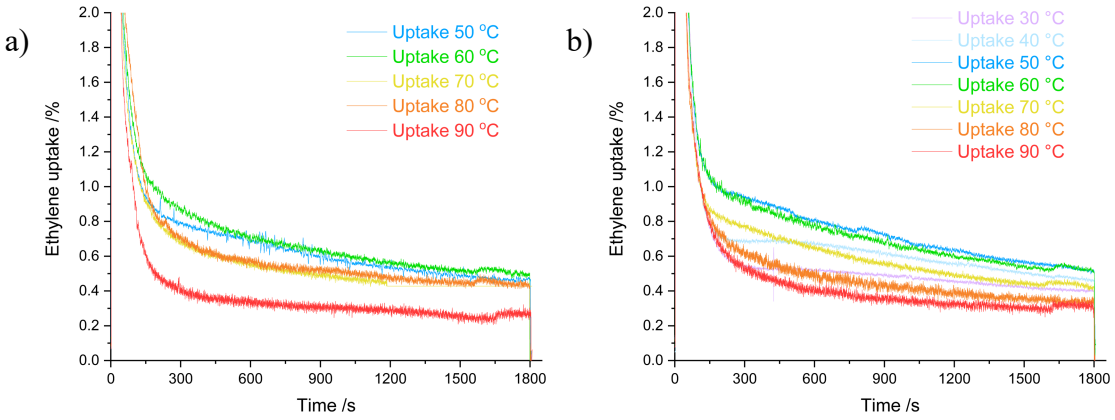

Figure A.108 Ethylene uptake as a function of reaction time for a) **1**$_{sMAO}$/TIBA, and b) **2**$_{sMAO}$/TIBA. Polymerisation conditions: 10 mg catalyst, 2 bar ethylene, 50 mL hexanes, 30 minutes, and 150 mg TIBA.

A.2.4. Gel-permeation chromatography

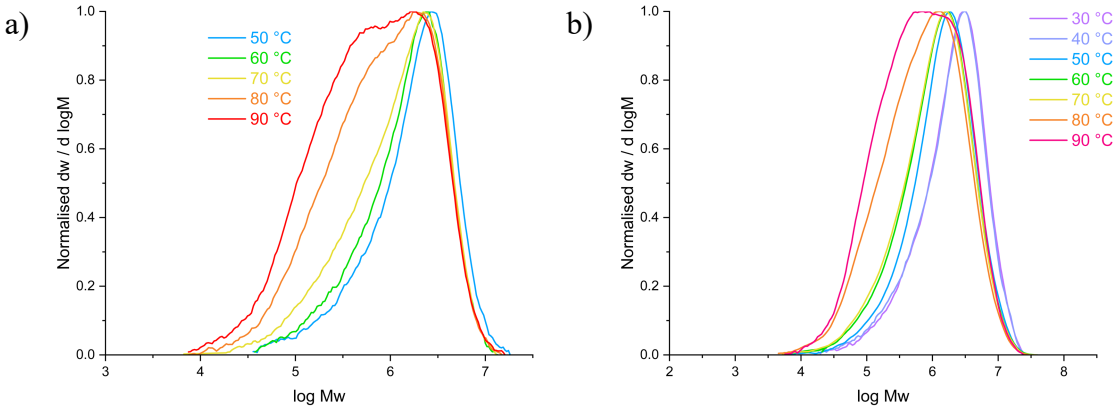

Figure A.109 Gel-permeation chromatograms of polyethylene produced by a) **1**$_{sMAO}$/TIBA, or b) **2**$_{sMAO}$/TIBA as a function of temperature. Polymerisation conditions: 10 mg catalyst, 2 bar ethylene, 50 mL hexanes, 30 minutes, and 150 mg TIBA.

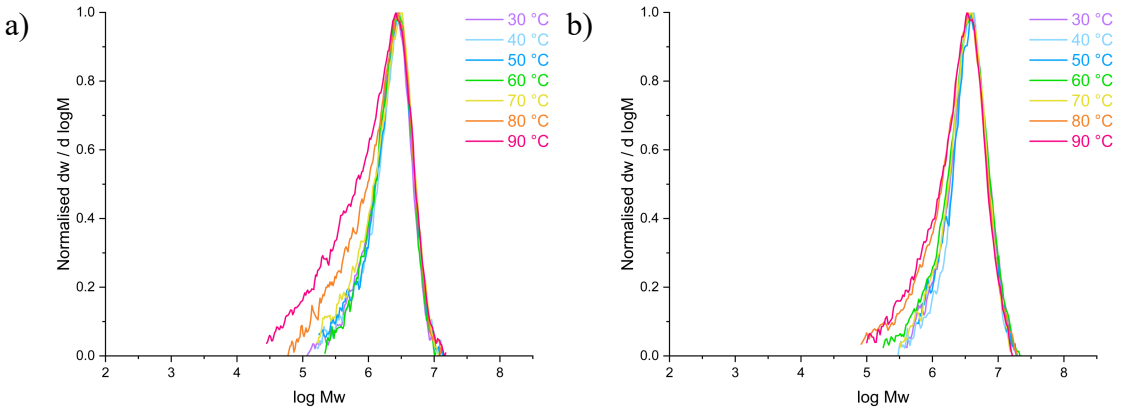

Figure A.110 Gel-permeation chromatograms of polyethylene produced by a) **2**$_{SSMAO}$/TIBA, or b) **2**$_{LDHMAO}$/TIBA as a function of temperature. Polymerisation conditions: 10 mg catalyst, 2 bar ethylene, 50 mL hexanes, 30 minutes, and 150 mg TIBA.

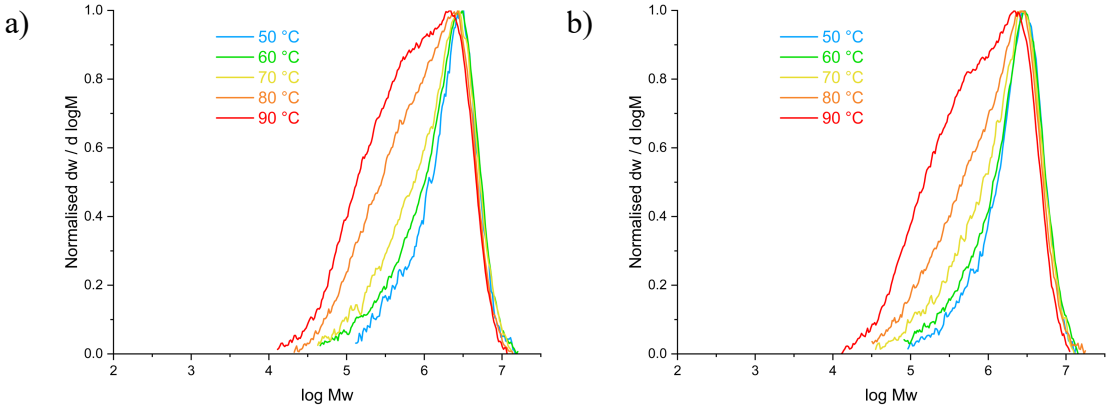

Figure A.111 Gel-permeation chromatograms of polyethylene produced by a) **3**$_{sMAO}$/TIBA, or b) **4**$_{sMAO}$/TIBA as a function of temperature. Polymerisation conditions: 10 mg catalyst, 2 bar ethylene, 50 mL hexanes, 30 minutes, and 150 mg TIBA.

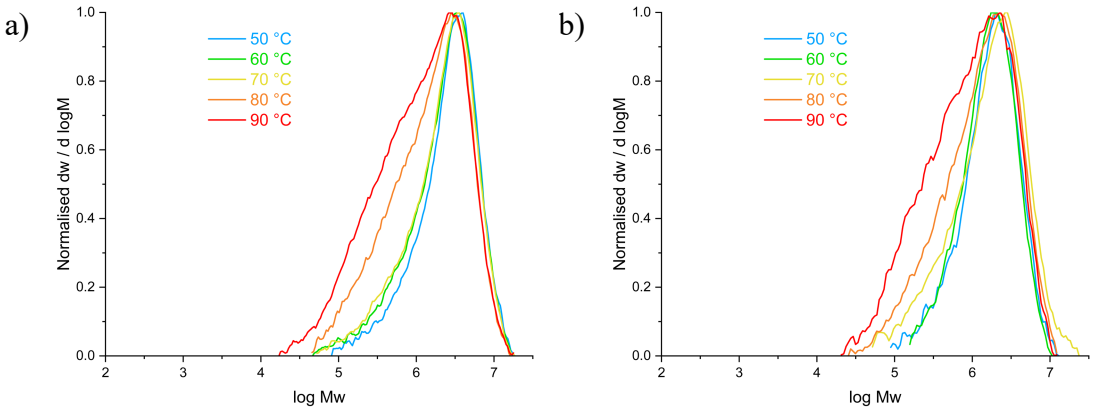

Figure A.112 Gel-permeation chromatograms of polyethylene produced by a) $\mathbf{5}_{\mathbf{sMAO}}$/TIBA, or b) $\mathbf{6}_{\mathbf{sMAO}}$/TIBA as a function of temperature. Polymerisation conditions: 10 mg catalyst, 2 bar ethylene, 50 mL hexanes, 30 minutes, and 150 mg TIBA.

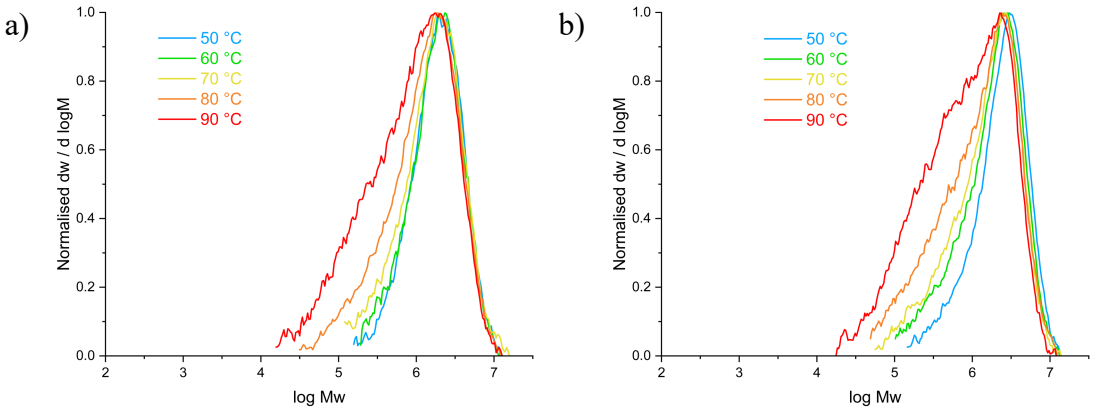

Figure A.113 Gel-permeation chromatograms of polyethylene produced by a) $\mathbf{7}_{\mathbf{sMAO}}$/TIBA, or b) $\mathbf{8}_{\mathbf{sMAO}}$/TIBA as a function of temperature. Polymerisation conditions: 10 mg catalyst, 2 bar ethylene, 50 mL hexanes, 30 minutes, and 150 mg TIBA.

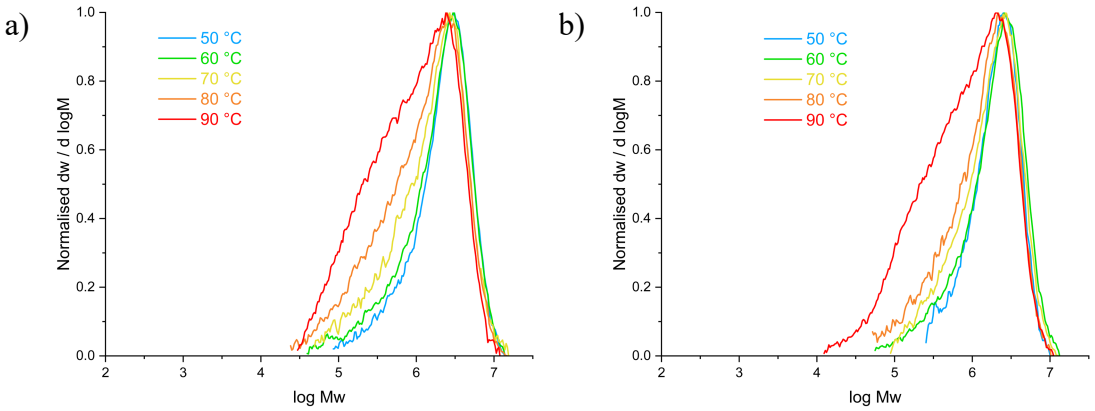

Figure A.114 Gel-permeation chromatograms of polyethylene produced by a) **9**$_{sMAO}$/TIBA, or b) **10**$_{sMAO}$/TIBA as a function of temperature. Polymerisation conditions: 10 mg catalyst, 2 bar ethylene, 50 mL hexanes, 30 minutes, and 150 mg TIBA.

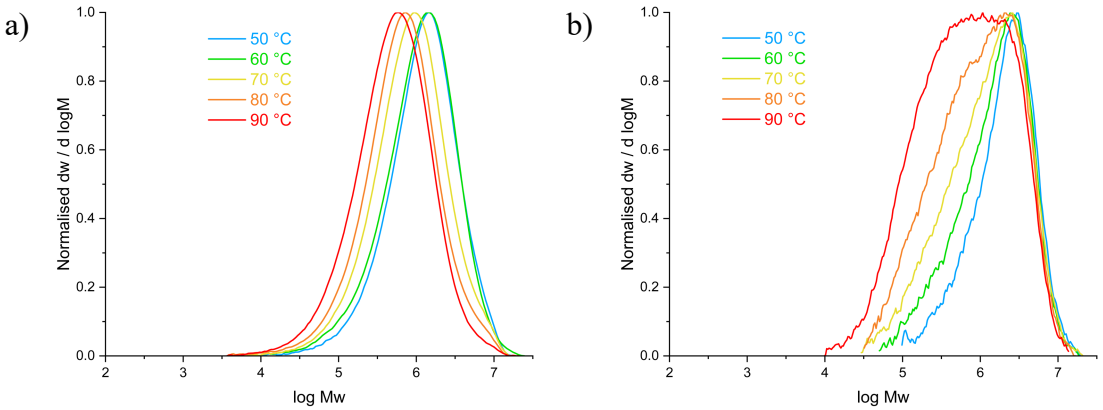

Figure A.115 Gel-permeation chromatograms of polyethylene produced by a) **11**$_{sMAO}$/TIBA, or b) **12**$_{sMAO}$/TIBA as a function of temperature. Polymerisation conditions: 10 mg catalyst, 2 bar ethylene, 50 mL hexanes, 30 minutes, and 150 mg TIBA.

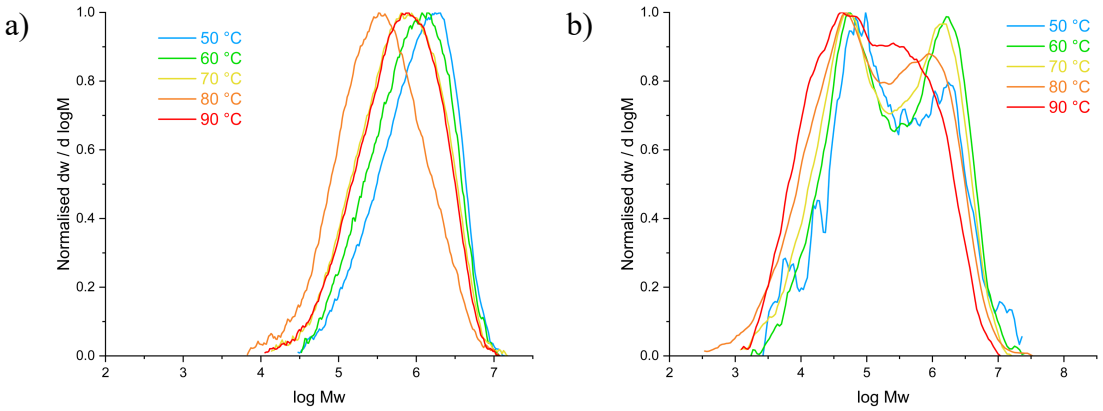

Figure A.116 Gel-permeation chromatograms of polyethylene produced by a) **13**$_{sMAO}$/TIBA, or b) **14**/TIBA as a function of temperature. Polymerisation conditions: 10 mg catalyst, 2 bar ethylene, 50 mL hexanes, 30 minutes, and 150 mg TIBA.

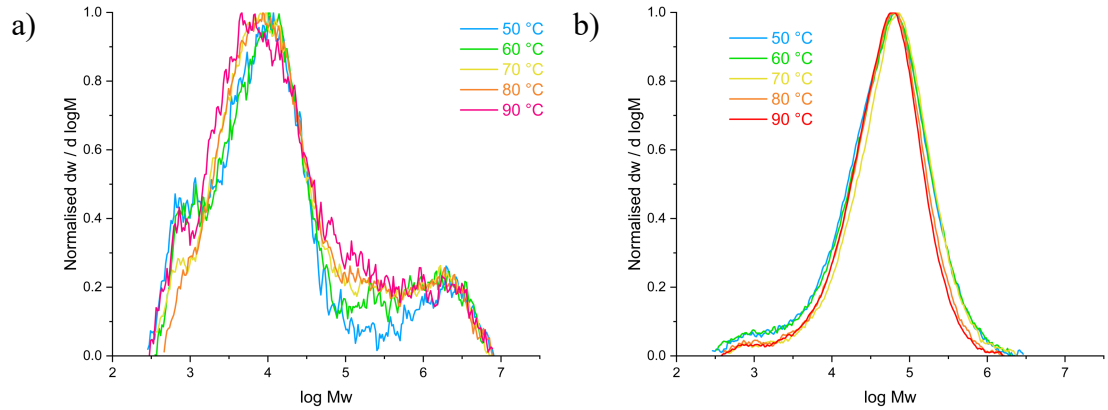

Figure A.117 Gel-permeation chromatograms of polyethylene produced by a) **15**$_{sMAO}$/TIBA, or b) **2**$_{sMAO}$/TIBA as a function of temperature. Polymerisation conditions: 10 mg catalyst, 50 mL hexanes, 30 minutes, 150 mg TIBA, and a) 2 bar ethylene, or b) 2 bar ethylene/hydrogen (98:2).

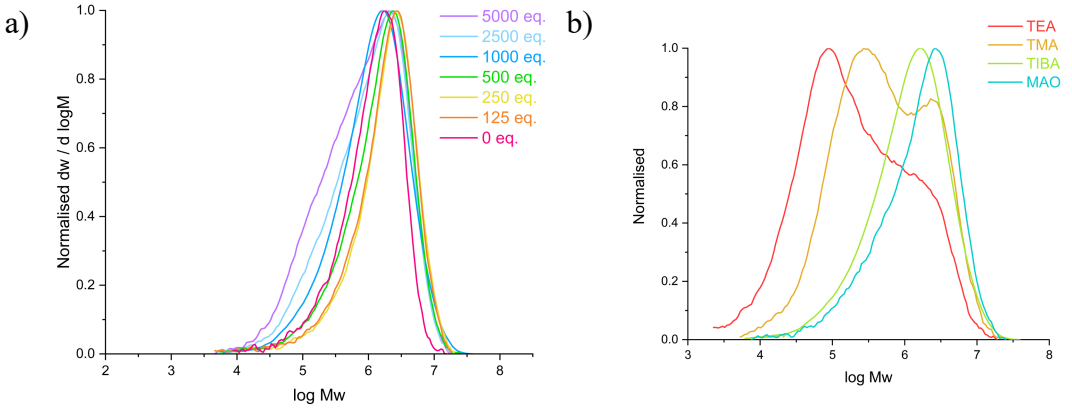

Figure A.118 Gel-permeation chromatograms of polyethylene produced by $\mathbf{2}_{\mathbf{sMAO}}$ as a function of a) [TIBA][Ti] or b) scavenger. Polymerisation conditions: 10 mg catalyst, 2 bar ethylene, 50 mL hexanes, 30 minutes, and 60 °C.

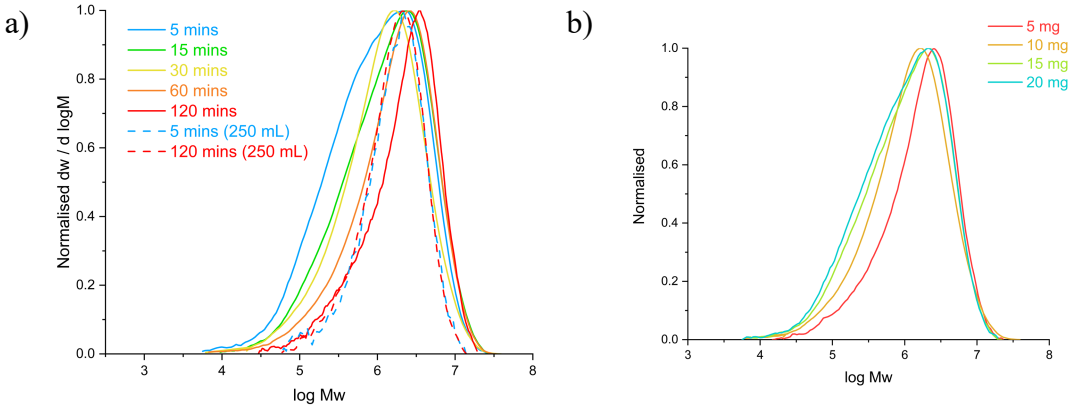

Figure A.119 Gel-permeation chromatograms of polyethylene produced by $\mathbf{2}_{\mathbf{sMAO}}$ as a function of a) time or b) catalyst amount. Polymerisation conditions: 5–20 mg catalyst, 2 bar ethylene, 50–250 mL hexanes, 5–120 minutes, 150–750 mg TIBA, and 60 °C.

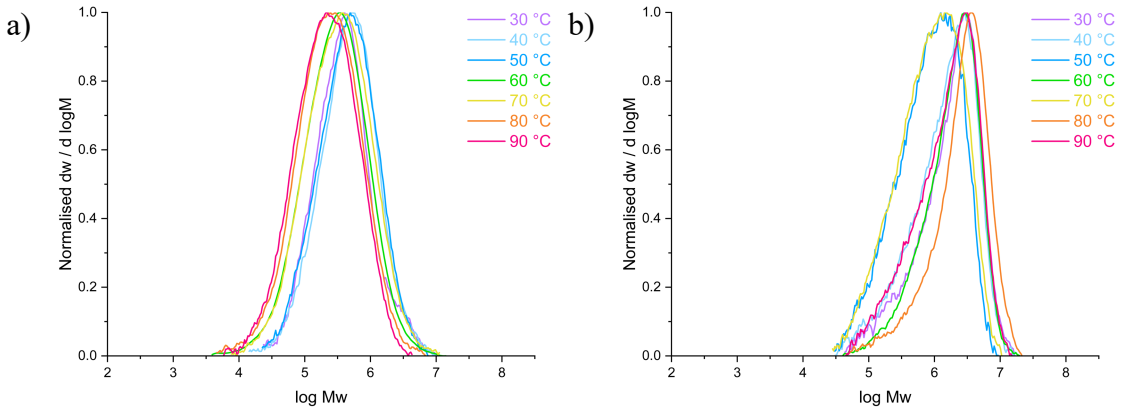

Figure A.120 Gel-permeation chromatograms of polyethylene produced by a) **2**/MAO, or b) **2**/TB as a function of temperature. Polymerisation conditions: 715 nmol complex, MAO ($[Al_{MAO}]/[Ti] = 1000$) or TB/TIBA ([TB]:[TIBA]:[Ti] = 1:200:1), 2 bar ethylene, 50 mL hexanes, and 5 minutes or until stirring ceased.

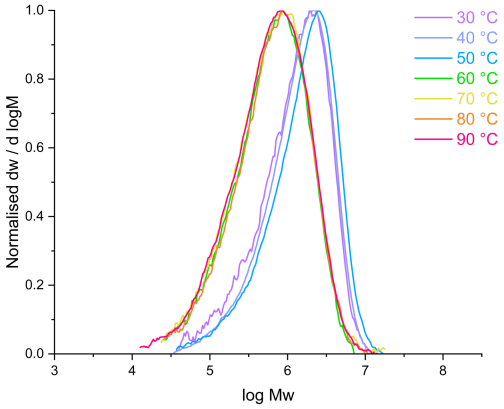

Figure A.121 Gel-permeation chromatogram of polyethylene produced by $\mathbf{2}_{\mathbf{sMAO}}$/TB as a function of temperature. Polymerisation conditions: 10 mg catalyst, 2 bar ethylene, 50 mL hexanes, 30 minutes, and [TB]/[Ti] = 1.

A.2.5. Differential scanning calorimetry

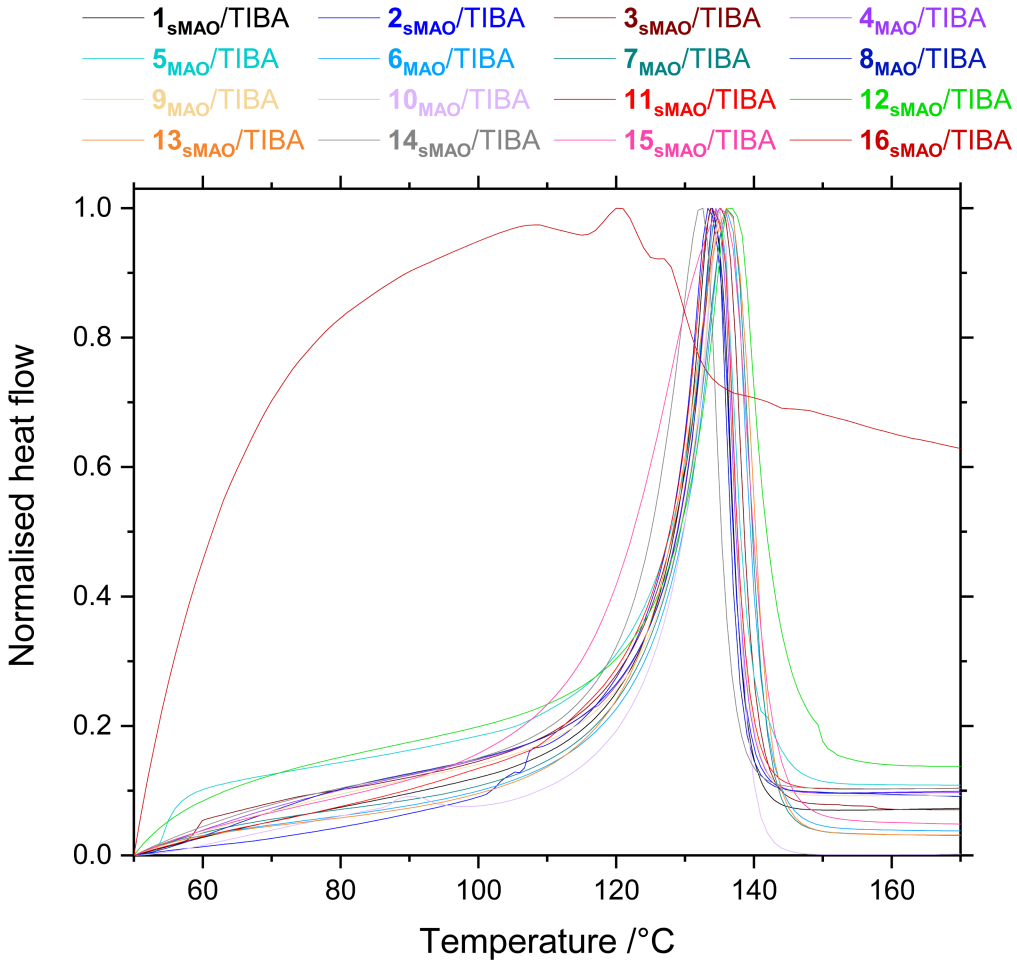

Figure A.122 Differential scanning calorimetry plot of polyethylene produced by **1$_{sMAO}$–16$_{sMAO}$**. Polymerisation conditions: 10 mg catalyst, 150 mg TIBA, 2 bar ethylene, 50 mL hexanes, 30 minutes, and 60 °C.

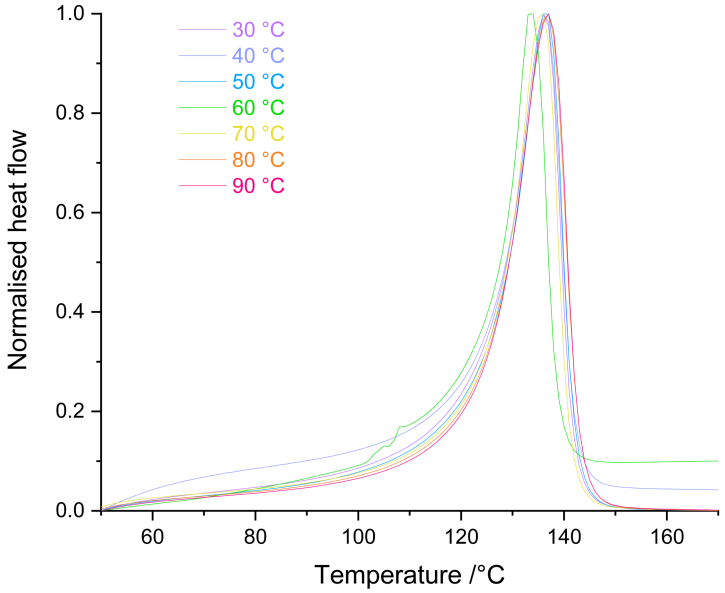

Figure A.123 Differential scanning calorimetry plot of polyethylene produced by **2**$_{sMAO}$/TIBA as a function of polymerisation temperature. Polymerisation conditions: 10 mg catalyst, 150 mg TIBA, 2 bar ethylene, 50 mL hexanes, 30 minutes, and 30–90 °C.

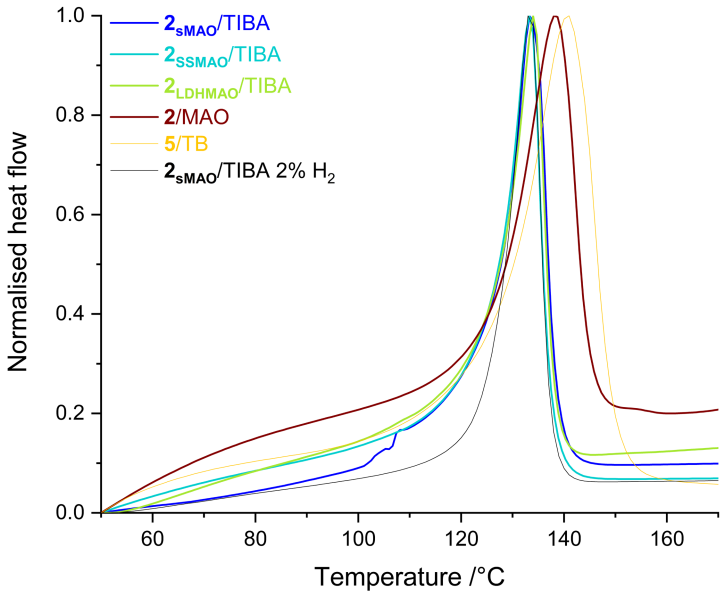

Figure A.124 Differential scanning calorimetry plot of polyethylene produced by **2**$_{sMAO}$/TIBA, **2**$_{SSMAO}$/TIBA, **2**$_{LDHMAO}$/TIBA, **2**/MAO, and **5**/TB. Slurry-phase polymerisation conditions: 10 mg catalyst, 150 mg TIBA, 2 bar ethylene or ethylene/hydrogen (98:2), 50 mL hexanes, 30 minutes, and 60 °C. Solution-phase polymerisation conditions: 715 nmol complex, MAO ([Al$_{MAO}$]/[Ti] = 1000) or TB/TIBA ([TB]:[TIBA]:[Ti] = 1:200:1), 2 bar ethylene, 50 mL hexanes, and 5 minutes or until stirring ceased.

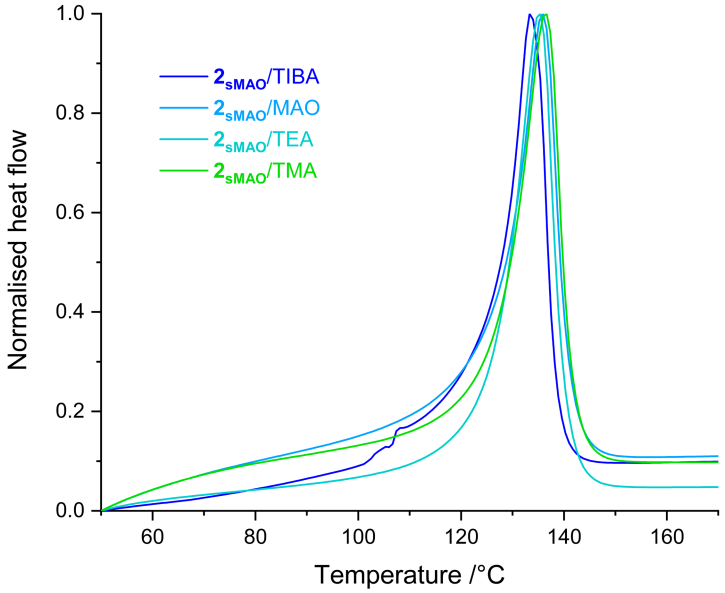

Figure A.125 Differential scanning calorimetry plot of polyethylene produced by **2**$_{sMAO}$/TIBA, **2**$_{sMAO}$/MAO, **2**$_{sMAO}$/TEA, and **2**$_{sMAO}$/TMA. Polymerisation conditions: 10 mg catalyst, [Al]/[Ti] = 1000, 2 bar ethylene, 50 mL hexanes, 30 minutes, and 60 °C.

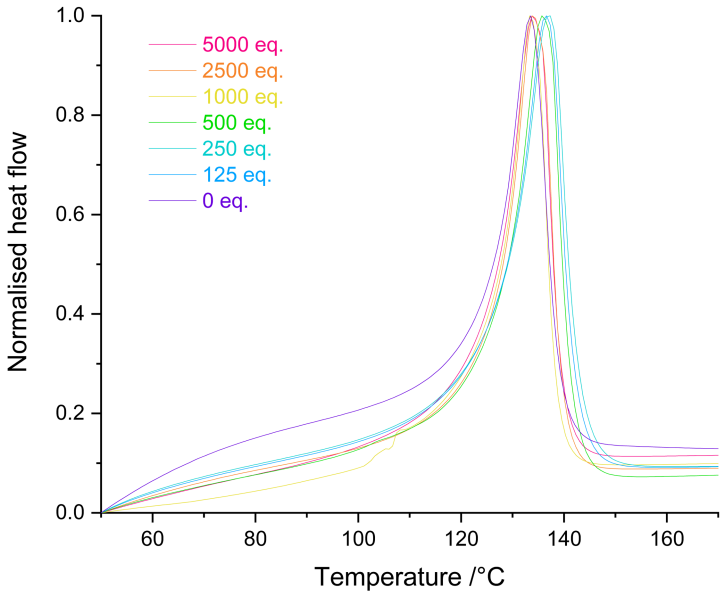

Figure A.126 Differential scanning calorimetry plot of polyethylene produced by **2**$_{sMAO}$/TIBA as a function of [Al]/[Ti]. Polymerisation conditions: 10 mg catalyst, [TIBA]/[Ti] = 0–5000, 2 bar ethylene, 50 mL hexanes, 30 minutes, and 30–90 °C.

A.2.6. High-throughput (Xplore s.r.l.)

N.B. OX59 = **14**$_{sMAO}$; OX60 = **2**$_{sMAO}$; OX61 = **1**$_{sMAO}$; OX62 = **11**$_{sMAO}$; OX63 = **15**$_{sMAO}$; OX64 = **6**$_{sMAO}$. OX60-400 is **2**$_{sMAO}$ synthesised using [Al$_{sMAO}$]/[Ti] = 400.

HTExplore s.r.l.
A Spin-off of UNIVERSITA' DEGLI STUDI DI NAPOLI FEDERICO II

Legal Address: Via Rodolfo Morandi, 12 – 80124 Napoli (Italy) – VAT Number 07435531210
Operation Address: c/o Dip. Scienze Chimiche, Università di Napoli Federico II – Via Cintia – 80126 Napoli (Italy)
☎ +39-081-674051 ♦ 🖷 +39-081-674057 ♦ E-mail: info@htexplore.com ♦ Web: www.htexplore.com

13 November 2020

To: SCG Chemicals Co. Ltd
Attn. Dr. Tossapol Khamnaen, Dr. Jean-Charles Buffet

Report for Project SCG 03-2020
(V. Busico, R. Cipullo, L. Rongo, A. Mingione)

In this screening campaign, seven supported metallocene catalysts provided by SCG (in collaboration with U-Oxford), with ID Codes OX59, OX60, OX61, OX62, OX60-400, OX63 and OX64, were screened at HTExplore in ethene homopolymerization and ethene/1-hexene copolymerization in hydrocarbon slurry. In particular, the effects of 1-hexene volume in the feed (v_H in the range of 0 to 250 μL per cell) and polymerization temperature (40, 60, 80°C) were evaluated. The DoE proposed by Dr. J. C. Buffet, comprising 2 PPR48 libraries, is shown in Chart 1.

Lib #1

	1	2	3	4	5	6
A	**OX59** *T* = 40 °C no 1-hexene	**OX59** *T* = 60 °C no 1-hexene	**OX59** *T* = 80 °C no 1-hexene	**OX59** *T* = 40 °C 125 μL 1-hexene	**OX59** *T* = 40 °C 250 μL 1-hexene	**OX59** *T* = 60 °C 250 μL 1-hexene
B	**OX60** *T* = 40 °C no 1-hexene	**OX60** *T* = 60 °C no 1-hexene	**OX60** *T* = 80 °C no 1-hexene	**OX60** *T* = 40 °C 125 μL 1-hexene	**OX60** *T* = 40 °C 250 μL 1-hexene	**OX60** *T* = 60 °C 250 μL 1-hexene
C	**OX61** *T* = 40 °C no 1-hexene	**OX61** *T* = 60 °C no 1-hexene	**OX61** *T* = 80 °C no 1-hexene	**OX61** *T* = 40 °C 125 μL 1-hexene	**OX61** *T* = 40 °C 250 μL 1-hexene	**OX61** *T* = 60 °C 250 μL 1-hexene
D	**OX62** *T* = 40 °C no 1-hexene	**OX62** *T* = 60 °C no 1-hexene	**OX62** *T* = 80 °C no 1-hexene	**OX62** *T* = 40 °C 125 μL 1-hexene	**OX62** *T* = 40 °C 250 μL 1-hexene	**OX62** *T* = 60 °C 250 μL 1-hexene
E	**OX59** *T* = 40 °C no 1-hexene	**OX59** *T* = 60 °C no 1-hexene	**OX59** *T* = 80 °C no 1-hexene	**OX59** *T* = 40 °C 125 μL 1-hexene	**OX59** *T* = 40 °C 250 μL 1-hexene	**OX59** *T* = 60 °C 250 μL 1-hexene
F	**OX60** *T* = 40 °C no 1-hexene	**OX60** *T* = 60 °C no 1-hexene	**OX60** *T* = 80 °C no 1-hexene	**OX60** *T* = 40 °C 125 μL 1-hexene	**OX60** *T* = 40 °C 250 μL 1-hexene	**OX60** *T* = 60 °C 250 μL 1-hexene
G	**OX61** *T* = 40 °C no 1-hexene	**OX61** *T* = 60 °C no 1-hexene	**OX61** *T* = 80 °C no 1-hexene	**OX61** *T* = 40 °C 125 μL 1-hexene	**OX61** *T* = 40 °C 250 μL 1-hexene	**OX61** *T* = 60 °C 250 μL 1-hexene
H	**OX62** *T* = 40 °C no 1-hexene	**OX62** *T* = 60 °C no 1-hexene	**OX62** *T* = 80 °C no 1-hexene	**OX62** *T* = 40 °C 125 μL 1-hexene	**OX62** *T* = 40 °C 250 μL 1-hexene	**OX62** *T* = 60 °C 250 μL 1-hexene

Lib #2

	1	2	3	4	5	6
A	**OX60-400** *T* = 40 °C no 1-hexene	**OX60-400** *T* = 60 °C no 1-hexene	**OX60-400** *T* = 80 °C no 1-hexene	**OX60-400** *T* = 40 °C 125 μL 1-hexene	**OX60-400** *T* = 40 °C 250 μL 1-hexene	**OX60-400** *T* = 60 °C 250 μL 1-hexene
B	**OX63** *T* = 40 °C no 1-hexane	**OX63** *T* = 60 °C no 1-hexene	**OX63** *T* = 80 °C no 1-hexene	**OX63** *T* = 40 °C 125 μL 1-hexene	**OX63** *T* = 40 °C 250 μL 1-hexene	**OX63** *T* = 60 °C 250 μL 1-hexene
C	**OX64** *T* = 40 °C no 1-hexene	**OX64** *T* = 60 °C no 1-hexene	**OX64** *T* = 80 °C no 1-hexene	**OX64** *T* = 40 °C 125 μL 1-hexene	**OX64** *T* = 40 °C 250 μL 1-hexene	**OX64** *T* = 60 °C 250 μL 1-hexene
D	**OX** *T* = 40 °C	**OX60** *T* = 60 °C 125 μL 1-hexene	**OX60** *T* = 80 °C 250 μL 1-hexene	**OX** *T* = 40 °C	**OX** *T* = 40 °C	**OX** *T* = 60 °C
E	**OX60-400** *T* = 40 °C no 1-hexene	**OX60-400** *T* = 60 °C no 1-hexene	**OX60-400** *T* = 80 °C no 1-hexene	**OX60-400** *T* = 40 °C 125 μL 1-hexene	**OX60-400** *T* = 40 °C 250 μL 1-hexene	**OX60-400** *T* = 60 °C 250 μL 1-hexene
F	**OX63** *T* = 40 °C no 1-hexene	**OX63** *T* = 60 °C no 1-hexene	**OX63** *T* = 80 °C no 1-hexene	**OX63** *T* = 40 °C 125 μL 1-hexene	**OX63** *T* = 40 °C 250 μL 1-hexene	**OX63** *T* = 60 °C 250 μL 1-hexene
G	**OX64** *T* = 40 °C no 1-hexene	**OX64** *T* = 60 °C no 1-hexene	**OX64** *T* = 80 °C no 1-hexene	**OX64** *T* = 40 °C 125 μL 1-hexene	**OX64** *T* = 40 °C 250 μL 1-hexene	**OX64** *T* = 60 °C 250 μL 1-hexene
H	**OX** *T* = 40 °C	**OX60** *T* = 60 °C 125 μL 1-hexene	**OX60** *T* = 80 °C 250 μL 1-hexene	**OX** *T* = 40 °C	**OX** *T* = 40 °C	**OX** *T* = 60 °C

Chart 1. DoE of the project, as proposed by Dr. J.C. Buffet (e-mail dated 20 October 2020).

Based on the above DoE, a first PPR library (Lib. ID 104950) was carried on 27 October. Notwithstanding a previous preparation library, the observation of an unusually high ratio between polymer yield and ethene uptake, broad PDI values for several polymer samples, and a non-obvious relationship between v_H and copolymer composition at the three explored temperatures prompted us to discuss the results with Dr. Buffet. Some possible pitfalls were jointly identified, and some correcting actions were agreed for the subsequent library (in particular, decrease catalyst loadings and v_H values). As a matter of fact, a revised DoE was provided by Dr. Buffet (Chart 2).

Lib.#2 - revised

	1	2	3	4	5	6
A	OX60-400 *T* = 40 °C no 1-hexene	OX60-400 *T* = 60 °C no 1-hexene	OX60-400 *T* = 80 °C no 1-hexene	OX60-400 *T* = 40 °C 125 µL 1-hexene	OX60-400 *T* = 60 °C 250 µL 1-hexene	OX60-400 *T* = 80 °C 250 µL 1-hexene
B	OX60 *T* = 40 °C no 1-hexene	OX60 *T* = 60 °C no 1-hexene	OX63 *T* = 80 °C no 1-hexene	OX62 *T* = 40 °C no 1-hexene	OX63 *T* = 60 °C 125 µL 1-hexene	OX63 *T* = 80 °C 125 µL 1-hexene
C	OX64 *T* = 40 °C no 1-hexene	OX64 *T* = 60 °C no 1-hexene	OX64 *T* = 80 °C no 1-hexene	OX64 *T* = 40 °C 125 µL 1-hexene	OX64 *T* = 60 °C 250 µL 1-hexene	OX64 *T* = 80 °C 250 µL 1-hexene
D	OX60 *T* = 40 °C 75 µL 1-hexene	OX60 *T* = 60 °C 75 µL 1-hexene	OX60 *T* = 80 °C 75 µL 1-hexene	OX62 *T* = 40 °C 75 µL 1-hexene	OX62 *T* = 60 °C 75 µL 1-hexene	OX62 *T* = 80 °C 75 µL 1-hexene
E	OX60-400 *T* = 40 °C no 1-hexene	OX60-400 *T* = 60 °C no 1-hexene	OX60-400 *T* = 80 °C no 1-hexene	OX60-400 *T* = 40 °C 125 µL 1-hexene	OX60-400 *T* = 60 °C 250 µL 1-hexene	OX60-400 *T* = 80 °C 250 µL 1-hexene
F	OX60 *T* = 40 °C no 1-hexene	OX60 *T* = 60 °C no 1-hexene	OX63 *T* = 80 °C no 1-hexene	OX62 *T* = 40 °C no 1-hexene	OX63 *T* = 60 °C 125 µL 1-hexene	OX63 *T* = 80 °C 125 µL 1-hexene
G	OX64 *T* = 40 °C no 1-hexene	OX64 *T* = 60 °C no 1-hexene	OX64 *T* = 80 °C no 1-hexene	OX64 *T* = 40 °C 125 µL 1-hexene	OX64 *T* = 60 °C 250 µL 1-hexene	OX64 *T* = 80 °C 250 µL 1-hexene
H	OX60 *T* = 40 °C 75 µL 1-hexene	OX60 *T* = 60 °C 75 µL 1-hexene	OX60 *T* = 80 °C 75 µL 1-hexene	OX62 *T* = 40 °C 75 µL 1-hexene	OX62 *T* = 60 °C 75 µL 1-hexene	OX62 *T* = 80 °C 75 µL 1-hexene

Chart 2. Revised DoE for Lib. #2, as proposed by Dr. J. C. Buffet (e-mail dated 30 October 2020).

In view of the above, we decided to repeat Lib#1 to make its DoE consistent with the revised one in Chart 2. The two libraries were on 02 November 2020 (Lib. #1, ID 104953) and 03 November 2020 (Lib. #2, ID 104954). The polymerization conditions and the main polymerization and polymer characterization results are reported in Tables 1-2 and Figures 1-4.

From the productivity standpoint, the catalysts were seemingly well-behaved. For ethene homopolymerization at 80°C, the absolute values measured in the PPR were in decent agreement with those declared by U-Oxford (Figure 1), and linearly dependent on the injected catalyst amounts. The reproducibility of duplicate experiments was within PPR specifications. Last but not least, the kinetic profiles (Figure 2) were fairly stable (or, at most, moderately decaying) up to a reaction time of 1 h. Two catalysts (namely OX60-400 and OX-64), though, turned out to be almost inactive in ethene/1-hexene copolymerization at $T \geq 60$°C.

On the other hand, the morphology of ethene/1-hexene copolymers prepared at $T \geq 60$°C was awful, the products appearing as partly flowable swollen gels largely wrapped around the PPR stir paddles.

Most polymers could not be dissolved for the high-temperature GPC and CEF characterizations. The ^{13}C NMR spectra of all copolymers featured a very poor line shape, likely due to extensive chain entanglement.

The GPC curves (Figure 3) were very broad or even multimodal, with PDI values up >50 (!) for ethene/1-hexene copolymer samples produced at T = 80°C. The average M_w values were rather high (typically between 0.5 and 1.5 MDa). Importantly, the traces highlighted the co-presence of a very low MW component (evidently able to flow when solvent-swollen) and a UHMW component (to which we ascribe the aforementioned sample dissolution problems).

The ^{13}C NMR characterization results for the ethene/1-hexene copolymers are peculiar (Figure 4). At T = 40°C, with the only exception of the products of catalyst OX59, comonomer incorporation was comparatively low. At $T \geq 60$°C, on the other hand, with the only exception of catalyst OX63, much greater comonomer contents were observed.

Overall, notwithstanding the inadequate number of experiments, we feel confident to conclude that catalyst behavior was heavily affected by physical effects. In our opinion, at T = 40°C both the homopolymers and the copolymers encapsulated the catalyst granules, and the observed kinetics (including comonomer incorporation) was limited by mass transfer phenomena. At $T \geq$ 60°C, instead, the copolymers were largely swollen or even dissolved by the reaction diluent, and the polymerization was poorly controlled. We trace the dramatic broadening of the molar mass distributions, at least in part, to this effect.

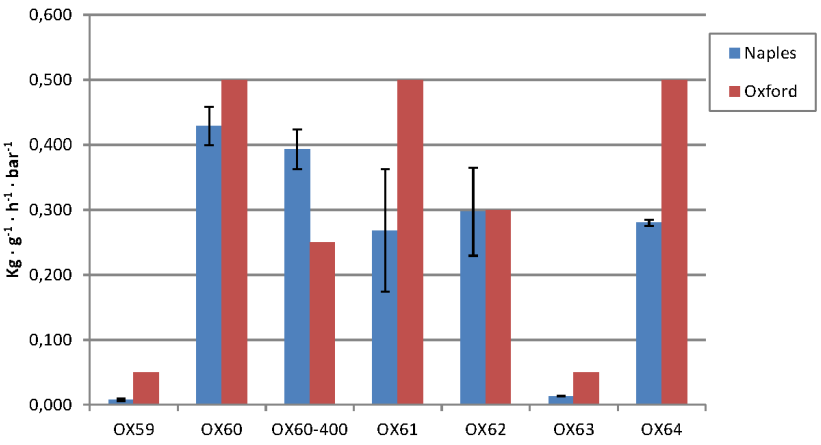

Figure 1. Comparison between catalyst productivity values in ethene homopolymerization at 80°C as measured by HTExplore ("*Naples*") and U-Oxford ("*Oxford*").

Table 1. Results of Library **#104953** (02 November 2020).
Experimental conditions: 5.0 mL total liquid volume per cell, heptane diluent; $p(C_2H_4)$ = 120 psi; TIBA scavenger, n_{Al} = 10 μmol.

Catalyst	T °C	v_H μL	Cell	m_{Cat} mg	t s	Yield mg	R_p Kg · g_{Cat}^{-1} · h^{-1} · bar^{-1}	M_n kDa	M_w kDa	PDI	x_H mol%	AF wt%	$T_{el,max}$ °C
OX59	40	0	3A	0.80	3602	73	0.011						
			3E	0.80	3602	73	0.011						
		75	5A	0.80	3602	31	0.005				2.4	5.8	75.2/111.5
			5E	0.80	3602	29	0.004						
		125	6A	0.80	3603	21	0.003						
			6E	0.80	3600	21	0.003				5.2	56.5	76.0/110.7
	60	0	2A	0.80	3602	100	0.015						
			2E	0.80	3602	83	0.012						
		125	4A	0.80	3600	24	0.004				4.9(0.4)	53.8	78.5/108.5
			4E	0.80	3600	18	0.003						
	80	0	1A	0.80	3602	63	0.0095	63	600	9.6		Not eluted	
			1E	0.80	3600	41	0.0062	56	506	9.0			
OX60	40	0	3B	0.05	3600	53	0.13						
			3F	0.10	3603	95	0.12						
		75	5B	0.05	3601	43	0.10				0.4	Not eluted	
			5F	0.10	3072	65	0.09						
		125	6B	0.05	3602	39	0.09				0.8	Not eluted	
			6F	0.10	3397	65	0.08						
	60	0	2B	0.05	3601	144	0.35						
			2F	0.05	3601	117	0.28						
		125	4B	0.05	3602	46	0.11						
			4F	0.10	3600	61	0.07				4.5	16.7	75.7/95.9
	80	0	1B	0.05	3079	162	0.46					Not eluted	
			1F	0.05	3400	156	0.40						
OX61	40	0	3C	0.05	3602	26	0.06						
			3G	0.15	3602	62	0.05						
		75	5C	0.05	3601	13	0.03						
			5G	0.15	3600	40	0.03				0.3	Not eluted	
		125	6C	0.05	3601	15	0.04						
			6G	0.15	3602	38	0.03				0.85	Not eluted	
	60	0	2C	0.05	3602	71	0.17						
			2G	0.05	3603	56	0.13						
		125	4C	0.05	3601	24	0.06						
			4G	0.15	3602	42	0.03				4.5	Not eluted	
	80	0	1C	0.05	3612	151	0.36					Not eluted	
			1G	0.05	3603	72	0.17						
OX62	40	0	3D	0.05	3606	39	0.09						
			3H	0.10	3601	64	0.08						
		75	5D	0.05	3600	30	0.07						
			5H	0.10	3601	53	0.06				0.4		
		125	6D	0.05	3600	29	0.07						
			6H	0.10	3600	48	0.06				1.1	Not eluted	
	60	0	2D	0.05	3603	108	0.26						
			2H	0.05	3600	81	0.20						
		125	4D	0.05	3600	58	0.14						
			4H	0.10	2576	76	0.13				4.1	11.6	84.4
	80	0	1D	0.05	3600	151	0.36					Not eluted	
			1H	0.05	3600	95	0.23						

Table 2. Results of Library **#104954** (03 November 2020).
Experimental conditions: 5.0 mL total liquid volume per cell, heptane diluent; $p(C_2H_4)$ = 120 psi; TIBA scavenger, n_{Al} = 10 μmol.

Catalyst	T °C	v_H μL	Cell	m_{Cat} Mg	t s	Yield mg	R_p Kg · g_{Cat}^{-1} · h^{-1} · bar^{-1}	M_n kDa	M_w kDa	PDI	x_H mol%	AF wt%	$T_{el,max}$ °C
OX-60	40	0	3B	0.10	3603	86	0.10						
			3F	0.10	3602	86	0.10						
		75	3D	0.10	3602	62	0.08						
			3H	0.10	3602	60	0.07				0.4		
	60	0	2B	0.05	3607	114	0.28						
			2F	0.05	3601	111	0.27						
		75	2D	0.10	1351	74	0.24				1.5		
			2H	0.10	1326	73	0.24						
	80	75	1D	0.10	4164	33	0.03	229	664	2.9	3.1	Not eluted	
			1H	0.10	3516	28	0.03	244	667	2.7			
OX60-400	40	0	3A	0.15	3602	123	0.10						
			3E	0.15	3602	132	0.11						
		125	6A	0.15	2686	68	0.07				0.9		
			6E	0.15	1275	36	0.08						
	60	0	2A	0.10	2776	172	0.27						
			2E	0.10	2189	135	0.27						
		250	5A	0.15	3601	13	0.01						
			5E	0.15	3602	13	0.01						
	80	0	1A	0.10	1712	167	0.42	519	1640	3.2		Not eluted	
			1E	0.10	1941	162	0.36	252	1306	5.2			
		250	4A	0.15	3600	9	0.01						
			4E	0.15	3602	7	0.01						
OX62	40	0	6B	0.10	3601	74	0.09						
			6F	0.10	3601	73	0.09						
		75	6D	0.10	3601	54	0.07						
			6H	0.10	3600	56	0.07				0.5		
	60	75	5D	0.10	1783	69	0.17						
			5H	0.10	1883	71	0.17				1.6		
	80	75	4D	0.10	3601	42	0.05	311	945	3.0	2.9	Not eluted	
			4H	0.10	3603	32	0.04	297	901	3.0			
OX63	60	125	5B	0.80	3602	52	0.01				1.3		
			5F	0.80	3601	51	0.01						
	80	0	1B	0.80	3601	95	0.01	11	658	59		Not eluted	
			1F	0.80	3602	84	0.01	12	592	48			
		125	4B	0.80	3601	36	0.01	20	859	43	1.2	Not eluted	
			4F	0.80	3601	31	0.01	25	769	31			
OX64	40	0	3C	0.10	3601	93	0.11						
			3G	0.10	3601	87	0.11						
		125	6C	0.10	3601	34	0.04				1.0		
			6G	0.10	3603	33	0.04						
	60	0	2C	0.05	3601	99	0.24						
			2G	0.05	3568	94	0.23						
		250	5C	0.10	3601	4	0.01						
			5G	0.10	3603	5	0.01						
	80	0	1C	0.05	3602	118	0.28	200	1198	6.0		Not eluted	
			1G	0.05	3602	114	0.27	194	1048	5.4			
		250	4C	0.10	3602	3	0.01						
			4G	0.10	3601	4	0.01						

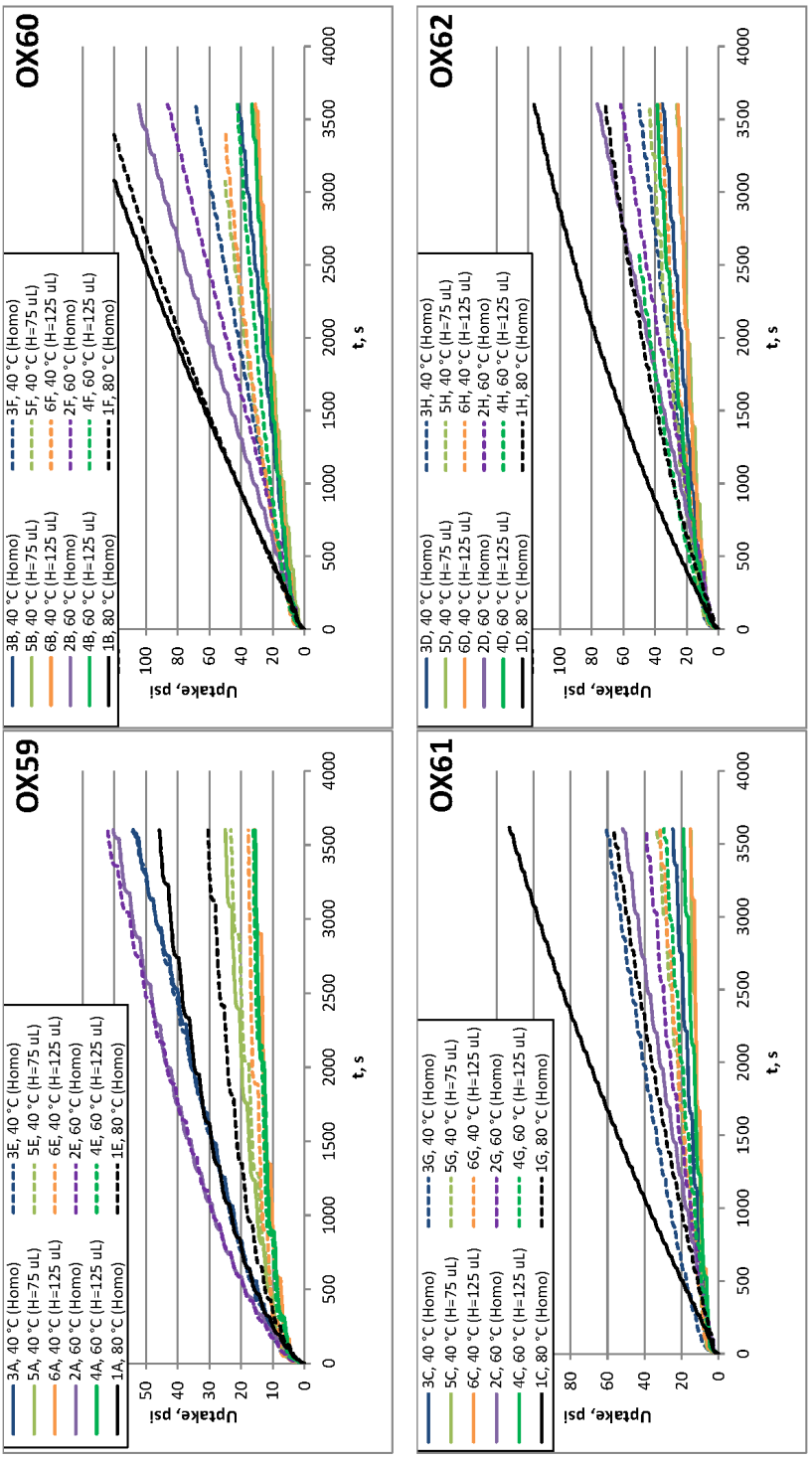

Figure 2-A. Ethene uptake profiles for Library **104953** (Table 1).

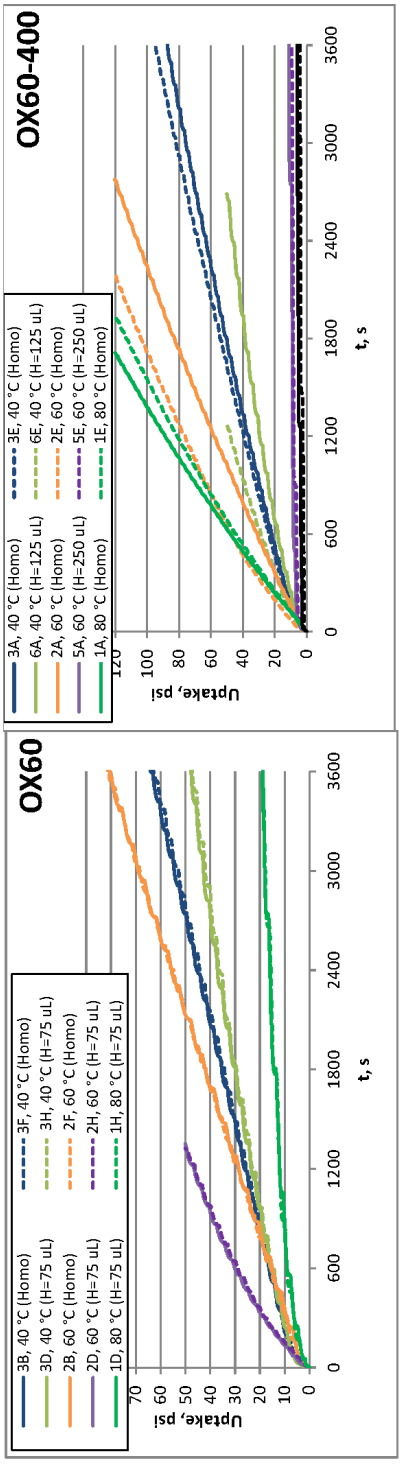

Figure 2-B. Ethene uptake profiles for Library **104954** (Table 2).

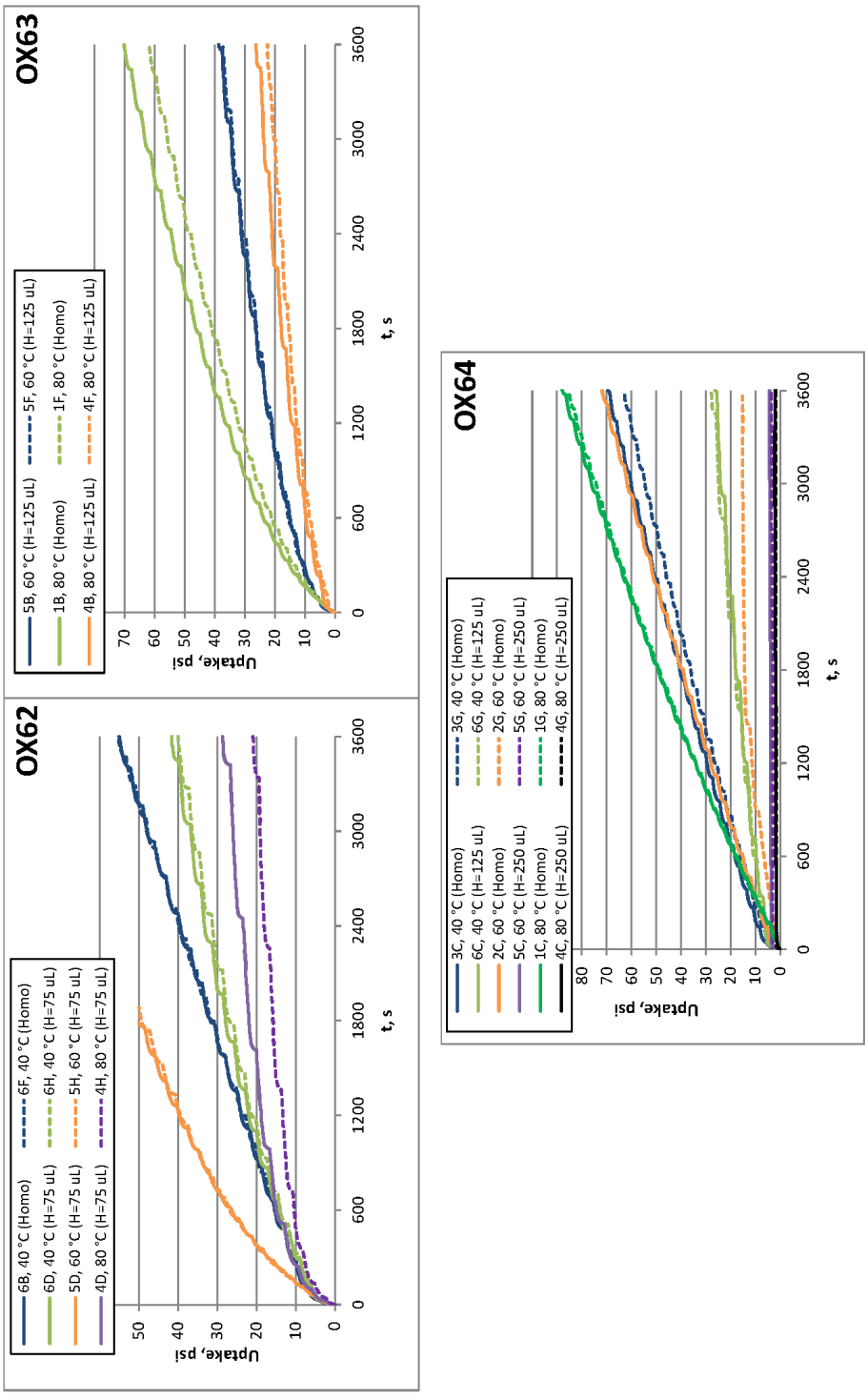

Figure 2-B (cont). Ethene uptake profiles for Library **104954** (Table 2).

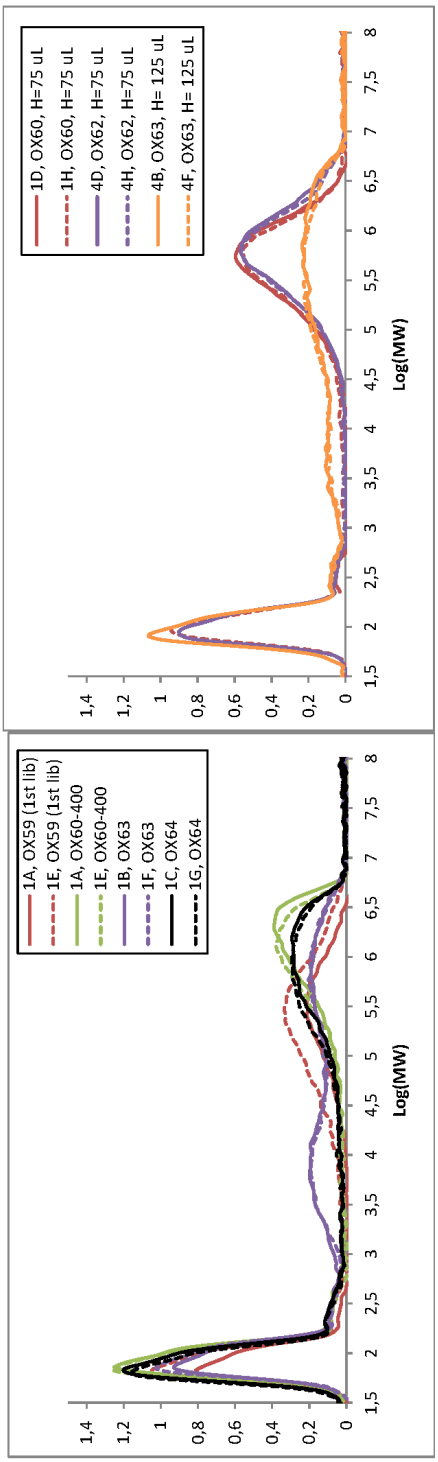

Figure 3. GPC traces for selected ethene homopolymers (*left*) and ethene/1-hexene copolymers (*right*) produced.

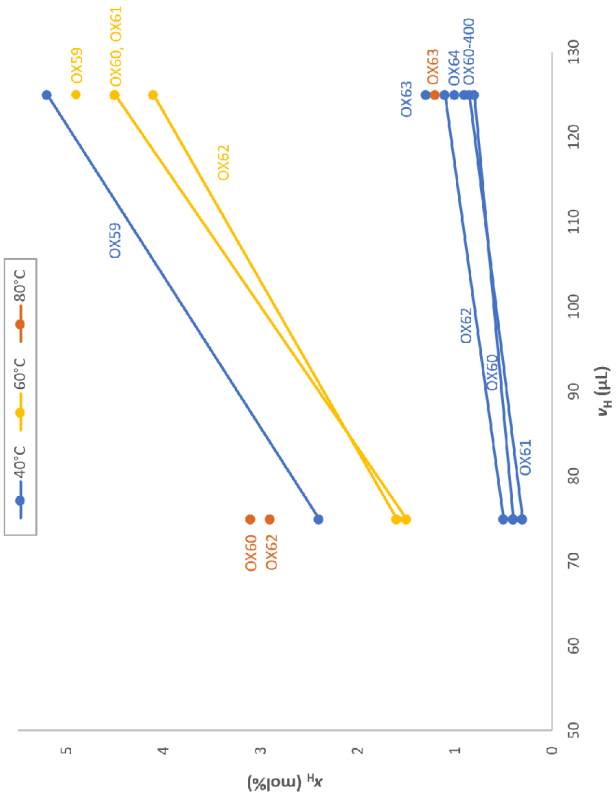

Figure 4. Average ^{13}C NMR mole fraction of 1-hexene units (x_H) as a function of 1-hexene volume in the feed (v_H) for ethene/1-hexene copolymers produced in Libraries **#104953** and **#104954** (Tables 1-2).

Despite the large molecular weights and poor solubility, polymer samples were successfully analysed by gel-permeation chromatography at Norner AS.

Table A.8 GPC results for PE synthesised at Xplore s.r.l. Incorporation measured by GPC-IR.

Catalyst	Temperature /°C	1-hexene /µL	M_w /kDa	PDI	Incorporation (wt%)
1$_{sMAO}$/TIBA (OX61)	40	0	4555.4	1.8	
	40	125	2201.5	2.9	19.0
	60	0	4704.2	2.0	
	80	0	4422.8	2.1	
2$_{sMAO}$/TIBA (OX60)	40	0	4255.7	2.0	
	40	125	2211.8	2.8	–
	60	0	4707.8	2.0	
	80	0	4609.5	2.1	
6$_{sMAO}$/TIBA (OX64)	40	0	4709.1	1.8	
	40	125	2172.4	3.2	–
	60	0	4817.0	1.8	
	80	0	4471.8	2.0	
11$_{sMAO}$/TIBA (OX62)	40	0	4880.6	2.2	
	40	125	1707.4	4.9	0.7
	60	0	4545.3	2.0	
	80	0	4098.4	2.1	
14$_{sMAO}$/TIBA (OX59)	40	0	2445.6	6.0	
	40	125	482.3	22.2	3.1
	60	0	2262.7	9.2	
	80	0	1794.1	10.3	

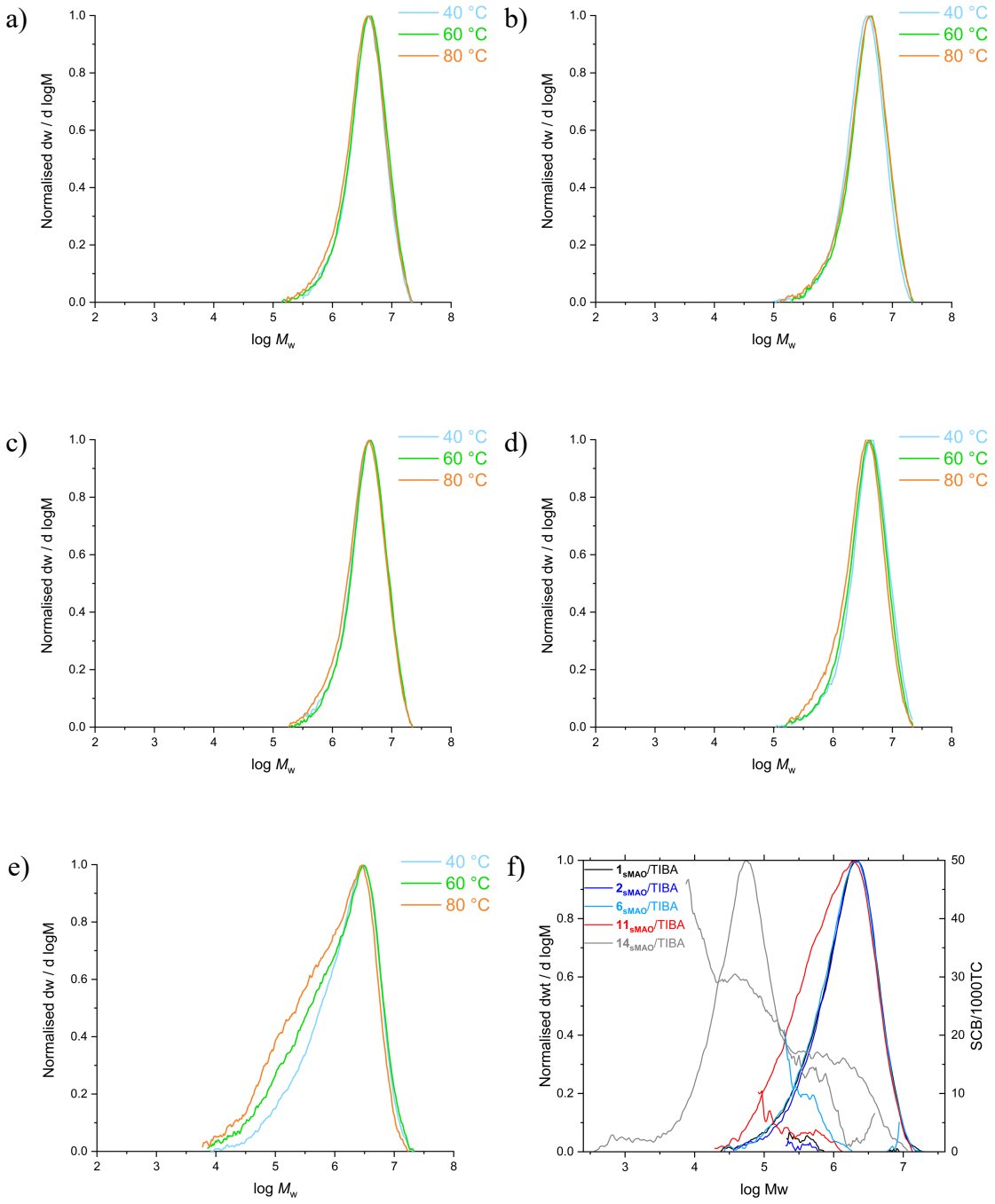

Figure A.127 Gel-permeation chromatograms of polyethylene produced by a) **1**$_{sMAO}$/TIBA, b) **2**$_{sMAO}$/TIBA, c) **6**$_{sMAO}$/TIBA, d) **11**$_{sMAO}$/TIBA, or e) **14**$_{sMAO}$/TIBA as a function of temperature. f) Gel-permeation chromatogram of E/C6 copolymer produced at T_p = 40 °C. Polymerisation conditions: 0.05–0.80 mg solid catalyst, 10 µmol TIBA, 8.3 bar ethylene, 5 mL heptane, 0–125 µL 1-hexene, and either 60 minutes or until 120 psi ethylene uptake.

A.2.7. UHMWPE Mechanical test report (Norner AS)

Norner AS 06.12.21

Test report

TR no.	: R-211104-004	Tester	: TG		
Project no	: 221876	Pre-load	: 4	N	
Customer	: Oxford University	Speed, tensile modulus	: 1	mm/min	
Test standard	: ISO 527-2/5A	Test speed	: 50	mm/min	
Material	: CCR 298 UHMWPE	Load cell	: 5kN		
Temperature	: 22				

Test results:

No.	E_t MPa	σ_Y MPa	ε_Y %	σ_M MPa	ε_M %	σ_B MPa	ε_B %	h mm	b mm	A_0 mm²
1	714	-	-	55,8	226,8	55,8	226,8	0,92	3,86	3,55
2	654	-	-	50,7	198,6	50,3	198,7	0,92	3,86	3,55
3	639	-	-	47,1	180,8	45,8	180,9	0,96	3,88	3,72
4	541	-	-	49,4	183,4	48,8	183,4	0,98	3,87	3,79
5	585	-	-	51,6	199,2	50,5	199,2	0,97	3,89	3,77

Statistics:

Series n = 5	E_t MPa	σ_Y MPa	ε_Y %	σ_M MPa	ε_M %	σ_B MPa	ε_B %	h mm	b mm	A_0 mm²
$\bar{x}$	627	-	-	50,9	197,8	50,2	197,8	0,95	3,872	3,68
s	66,5	-	-	3,18	18,3	3,61	18,3	0,02828	0,01304	0,12
v	10,62	-	-	6,25	9,24	7,20	9,24	2,98	0,34	3,23

Series graph:

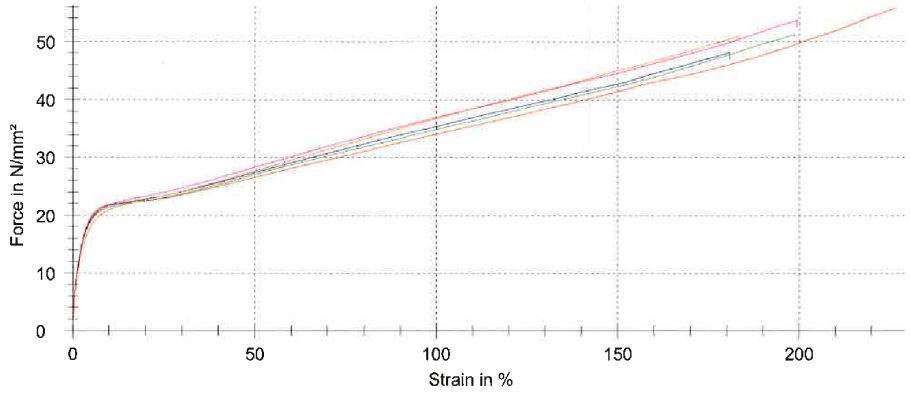

CCR 298 UHMWPE.zs2 **Page 1/1**

A.2.8. Differential scanning calorimetry (annealing)

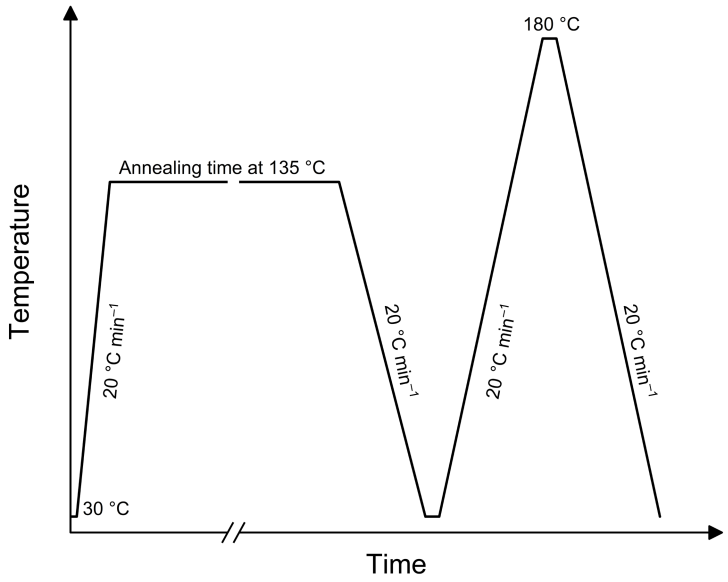

Figure A.128 DSC thermal annealing protocol used.

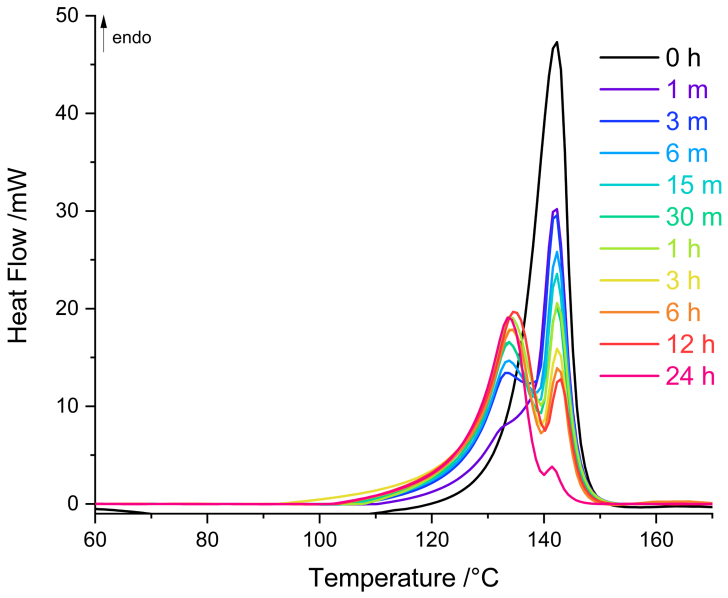

Figure A.129 Heating cycle of UHMWPE after annealing at 135 °C for different annealing times. Synthesis conditions: **2$_{sMAO}$**, T_p = 30°C, $[Al_{sMAO}]_0/[Ti]_0$ = 200, 10 mg catalyst, 150 mg TIBA, 2 bar ethylene, 50 mL hexanes, and 30 minutes. M_w = 3376.0 kDa, PDI = 3.4.

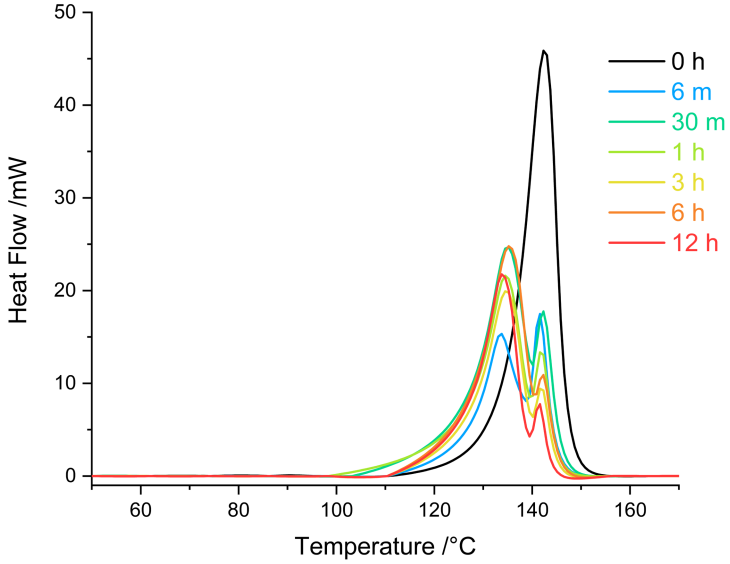

Figure A.130 Heating cycle of UHMWPE after annealing at 135 °C for different annealing times. Synthesis conditions: **2$_{sMAO}$**, T_p = 60°C, $[Al_{sMAO}]_0/[Ti]_0$ = 200, 10 mg catalyst, 150 mg TIBA, 2 bar ethylene, 50 mL hexanes, and 30 minutes. M_w = 2087.5 kDa, PDI = 5.2.

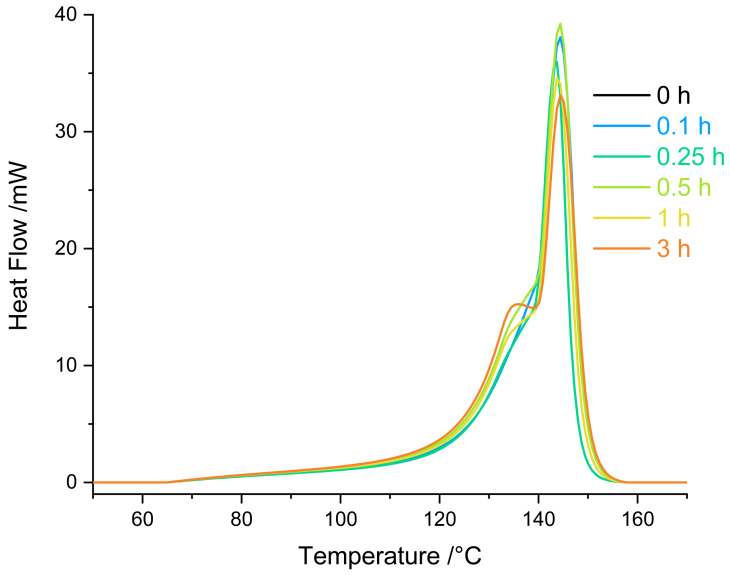

Figure A.131 Heating cycle of UHMWPE after annealing at 135 °C for different annealing times. Synthesis conditions: **3$_{sMAO}$**, T_p = 60°C, $[Al_{sMAO}]_0/[Ti]_0$ = 200, 10 mg catalyst, 150 mg TIBA, 2 bar ethylene, 50 mL hexanes, and 30 minutes. M_w = 2437.7 kDa, PDI = 3.0.

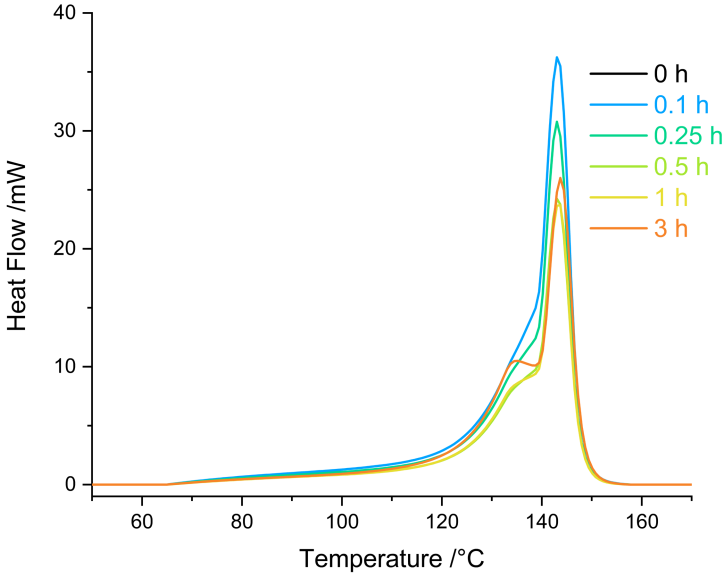

Figure A.132 Heating cycle of UHMWPE after annealing at 135 °C for different annealing times. Synthesis conditions: $\mathbf{4_{sMAO}}$, T_p = 60°C, $[Al_{sMAO}]_0/[Ti]_0$ = 200, 10 mg catalyst, 150 mg TIBA, 2 bar ethylene, 50 mL hexanes, and 30 minutes. M_w = 2696.2 kDa, PDI = 2.6.

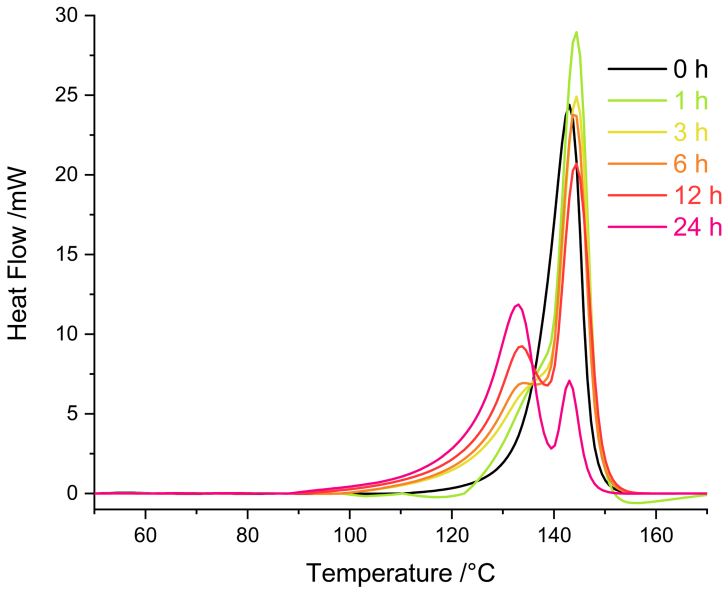

Figure A.133 Heating cycle of UHMWPE after annealing at 135 °C for different annealing times. Synthesis conditions: $\mathbf{2_{LDHMAO}}$, T_p = 30°C, $[Al_{MAO}]_0/[Ti]_0$ = 200, 10 mg catalyst, 150 mg TIBA, 2 bar ethylene, 50 mL hexanes, and 30 minutes. M_w = 4195.0 kDa, PDI = 1.7.

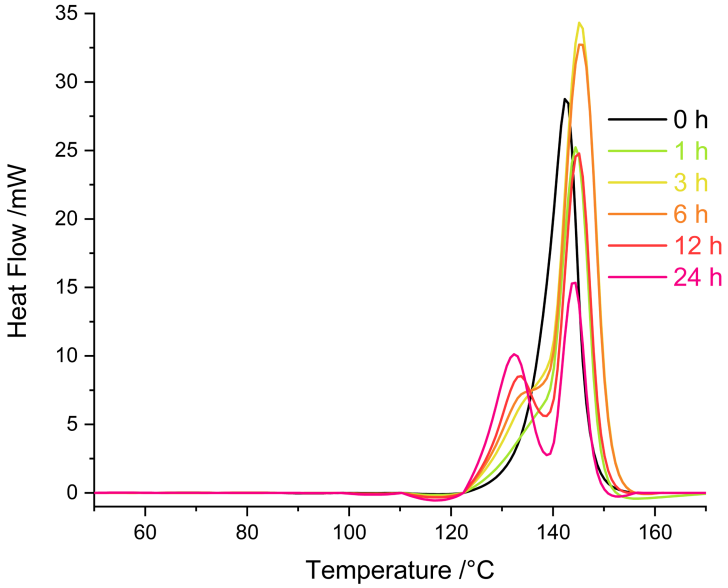

Figure A.134 Heating cycle of UHMWPE after annealing at 135 °C for different annealing times. Synthesis conditions: **2$_{LDHMAO}$**, T_p = 60°C, $[Al_{MAO}]_0/[Ti]_0$ = 200, 10 mg catalyst, 150 mg TIBA, 2 bar ethylene, 50 mL hexanes, and 30 minutes.

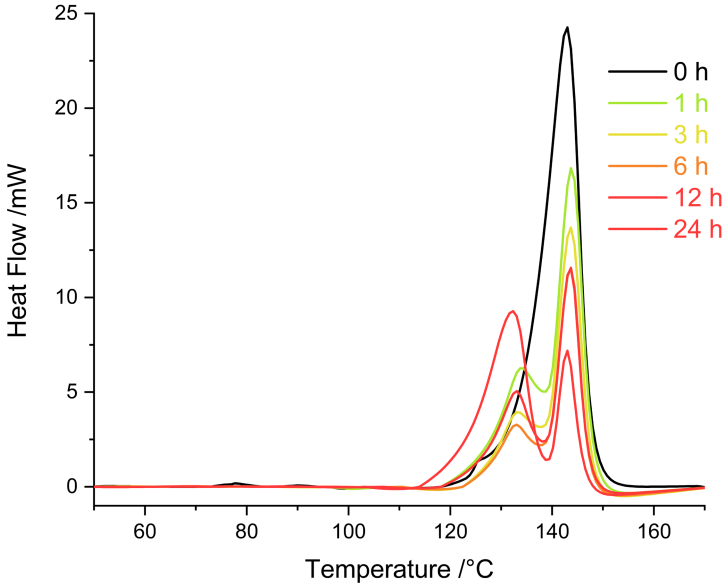

Figure A.135 Heating cycle of UHMWPE after annealing at 135 °C for different annealing times. Synthesis conditions: **2$_{LDHMAO}$**, T_p = 90°C, $[Al_{MAO}]_0/[Ti]_0$ = 200, 10 mg catalyst, 150 mg TIBA, 2 bar ethylene, 50 mL hexanes, and 30 minutes. M_w = 3230.0 kDa, PDI = 2.7.

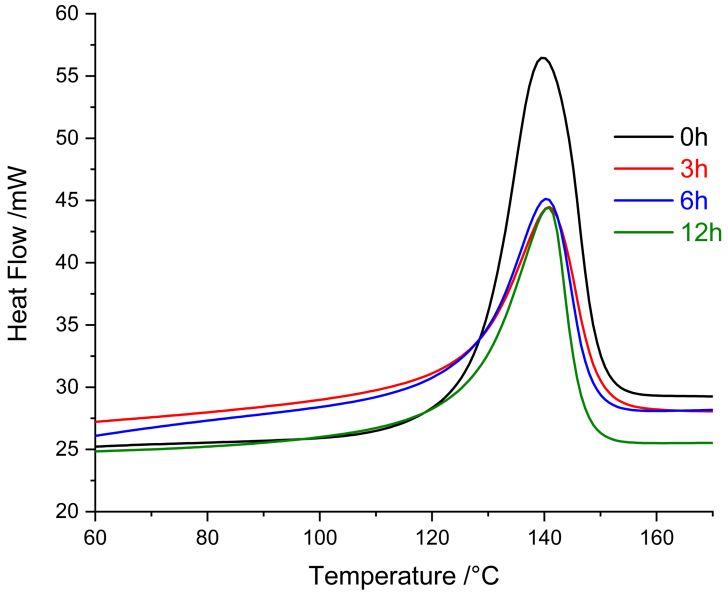

Figure A.136 Heating cycle of UHMWPE after annealing at 135 °C for different annealing times. Synthesis conditions: **2**, T_p = 30°C, $[Al_{MAO}]_0/[Ti]_0$ = 1000, 2 bar ethylene, 414 µg catalyst, 49 mL hexanes, 1 mL toluene, and 5 minutes.

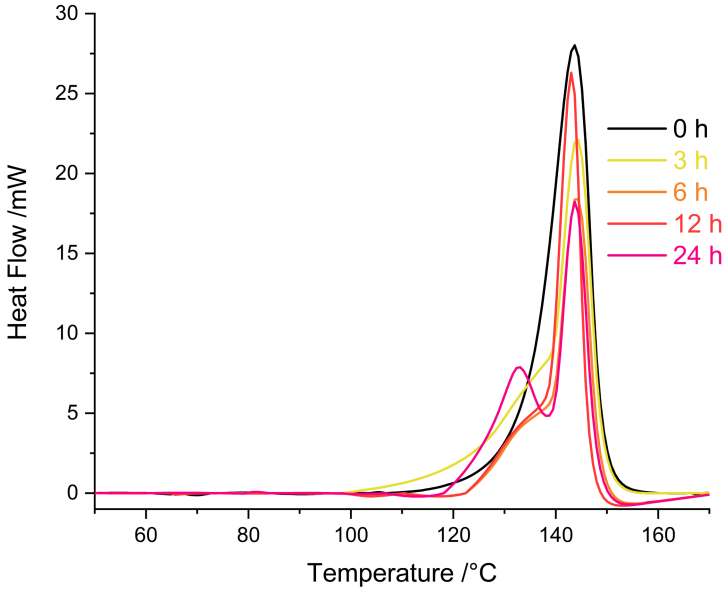

Figure A.137 Heating cycle of UHMWPE after annealing at 135 °C for different annealing times. Synthesis conditions: $\mathbf{2}_{\mathbf{SSMAO}}$, T_p = 30°C, $[Al_{MAO}]_0/[Ti]_0$ = 200, 10 mg catalyst, 150 mg TIBA, 2 bar ethylene, 50 mL hexanes, and 30 minutes. M_w = 2567.9 kDa, PDI = 2.0.

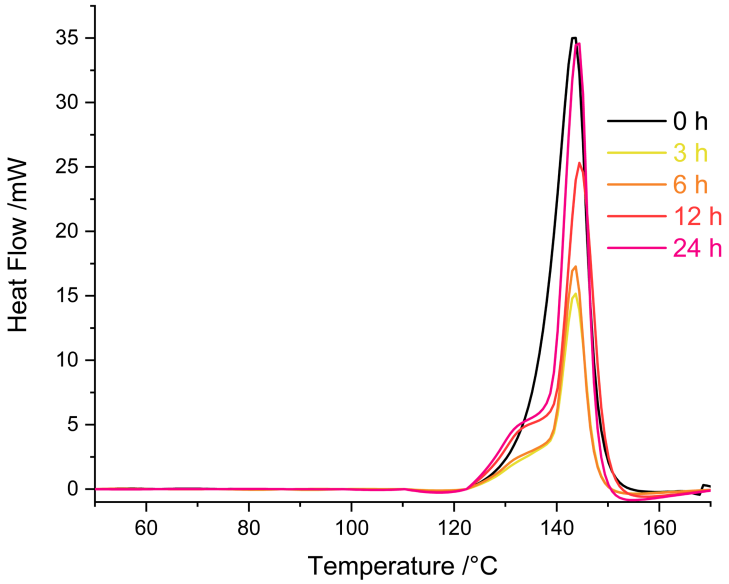

Figure A.138 Heating cycle of UHMWPE after annealing at 135 °C for different annealing times. Synthesis conditions: **2SSMAO**, T_p = 60°C, $[Al_{MAO}]_0/[Ti]_0$ = 200, 10 mg catalyst, 150 mg TIBA, 2 bar ethylene, 50 mL hexanes, and 30 minutes. M_w = 2643.8 kDa, PDI = 1.7.

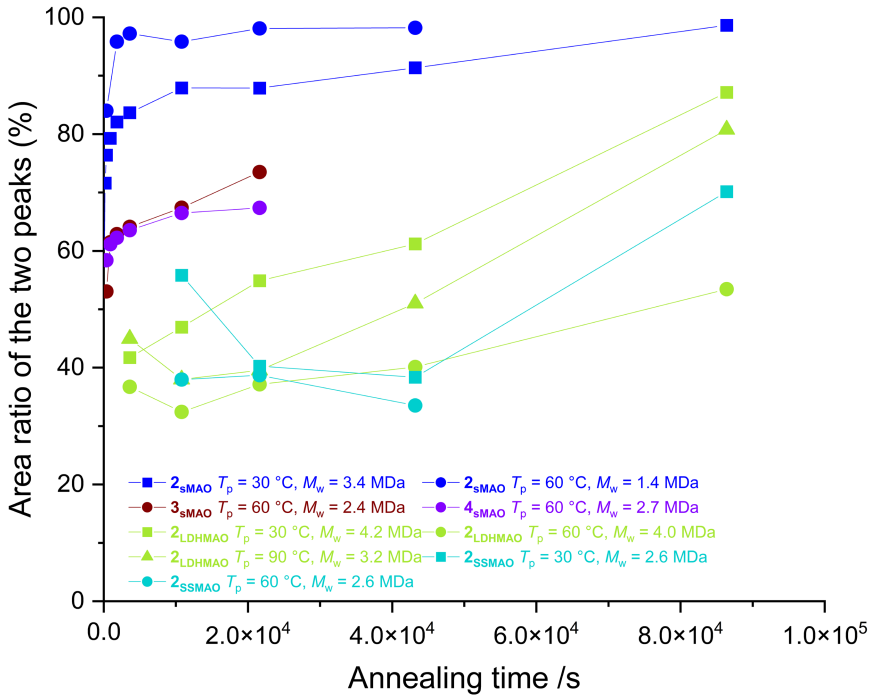

Figure A.139 Evolution of the normalised area of the DSC peaks as a function of annealing time.

A.2.9. ssNMR

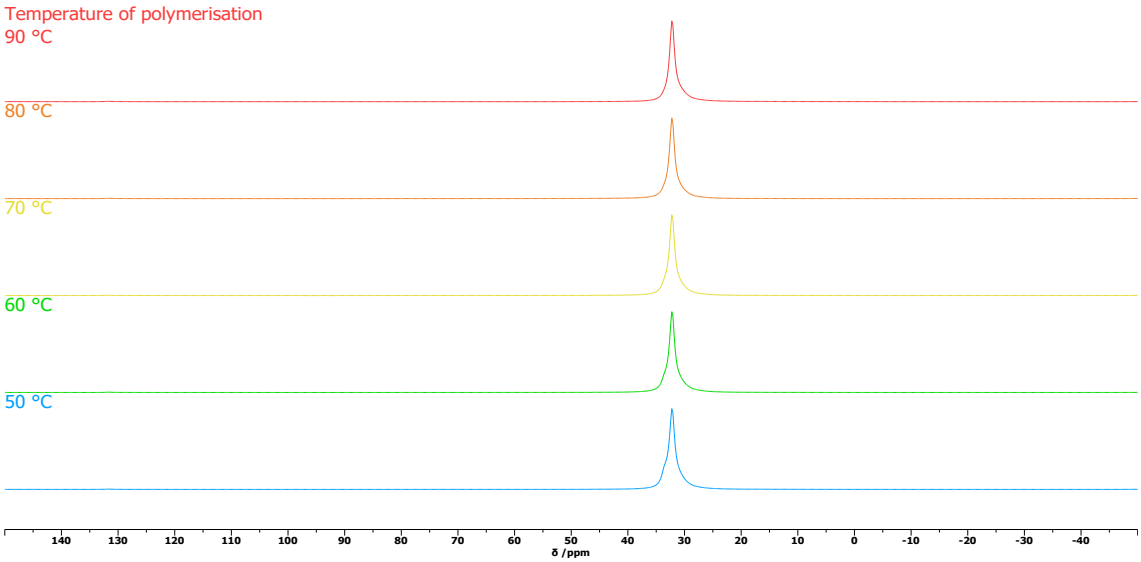

Figure A.140 ^{13}C CPMAS ssNMR spectrum (10 kHz, 101 MHz, 298 K) of polyethylene synthesised using **2**$_{sMAO}$ across a temperature of polymerisation of 50–90 °C. Polymerisation conditions: 10 mg catalyst, 2 bar ethylene, 50 mL hexanes, 150 mg TIBA, and 30 minutes.

A.2.10. Thermogravimetric analysis

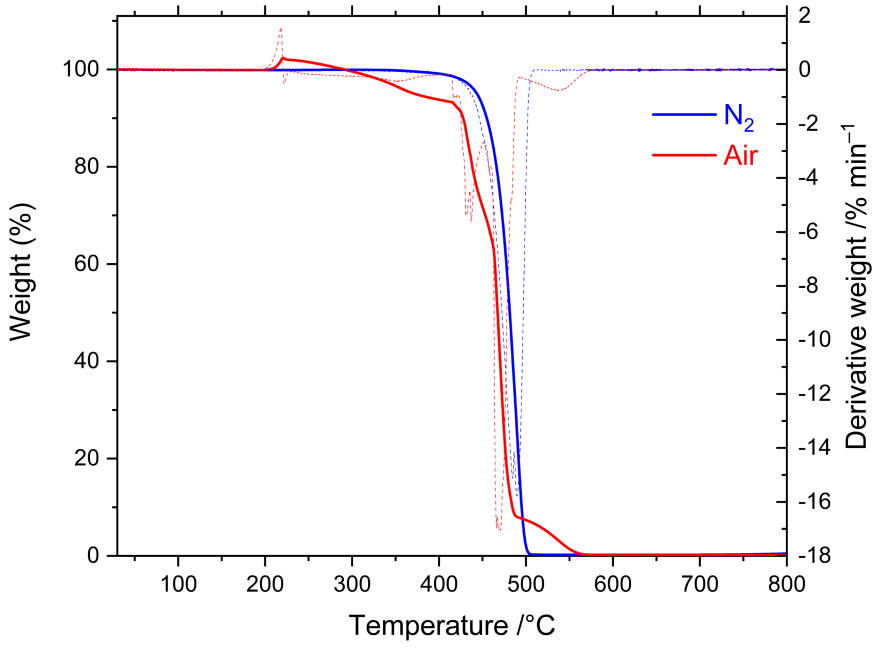

Figure A.141 Thermogravimetry plots of UHMWPE, at a heating rate of 20 K min^{-1} under an atmosphere of dry nitrogen or synthetic air (20% O_2 in N_2). Polymerisation conditions: 10 mg catalyst, 2 bar ethylene, 50 mL hexanes, 150 mg TIBA, and 30 minutes.

A.2.11.Microcompounding/film extrusion report (Nanoforce Technology Ltd.)

Micro-compounding/film extrusion of UHMWPE/PE blends

Ref to Nanoforce quotation NAN00586P.

Nanoforce Technology Ltd
Queen Mary University of London
Joseph Priestley Building
Mile End Road
London E1 4NS
Tel. +44 (0)20 7882 2726
Email: info@nanoforce.co.uk

21 Mar 2022

Aims

Dilution of new UHMW-PE with commercial LDPE and/or HDPE, which will act as a polymer diluent/lubricant for compounding this new polymer, which has virtually zero MFI. We would try to prepare **four dilutions**. **The aim is to find the highest possible concentration of UHMWPE** and collect as much material as possible.

Collection of the blended materials in **ribbons ~2 cm wide and 0.2 mm thick**. Aim to produce as much ribbon as we can in the allotted time with the available materials.

Micro-compounding with DSM Xplore 15cc

The materials were blended inside the micro-compounder in recirculation mode for about 5 min using a screw speed of 100 rpm and argon atmosphere to avoid materials oxidation/degradation. The temperature was set separately for the three zones of the micro-compounder: top part (beginning of the screws/feeding area), middle region, and bottom part (tip of the screws/die area).

The table below reports the processing parameters used to blend the materials.

Sample name	T top (°C)	T middle (°C)	T bottom (°C)	Speed (RPM)	Compounding time (min)
Pure LDPE	150	150	150	100	5
LDPE/10% UHMWPE	200	200	200	"	"
LDPE/15% UHMWPE	"	"	"	"	"
LDPE/20% UHMWPE	"	"	"	"	"
LDPE/30% UHMWPE	"	"	205	"	"
Pure HDPE	"	"	"	"	"
HDPE/10% UHMWPE	"	"	200	50	"
HDPE/15% UHMWPE	"	"	205	100	"
HDPE/20% UHMWPE	"	"	"	"	"
HDPE/30% UHMWPE	"	"	"	90	"

Collection of ribbons from the micro-compounder

After blending, the samples were collected in a ribbon shape using a flat film die attached to the micro-compounder and a dedicated take-off system. The take-off system consisted of an air blade positioned close to the die used for a fast cooling to avoid or limit any lateral shrinkage of the extruded material; a speed-controlled collection roll; and a torque-controlled winding roll.

The table below reports the processing conditions used to collect the ribbons.

Sample name	Air blade flow (LPM)	Collection roll speed (a.u.)	Winding roll torque (a.u.)	Film thickness (µm)
Pure LDPE	20	500	50	50-150
LDPE/10% UHMWPE	"	520	60	300-150
LDPE/15% UHMWPE	"	525	75	400-100
LDPE/20% UHMWPE	"	520	160	500-250
LDPE/30% UHMWPE	"	500	50	550-300
Pure HDPE	"	575	100	180-60
HDPE/10% UHMWPE	"	525	75	500-250
HDPE/15% UHMWPE	"	600	170	250-80
HDPE/20% UHMWPE	"	600	180	400-150
HDPE/30% UHMWPE	"	600	100	190-150

Nanoforce Technology Limited, Queen Mary, University of London, Joseph Priestley Building, Mile End Road, London E1 4NS
Registered in England No: 05638415

A.2.12.PE/UHMWPE characterisation

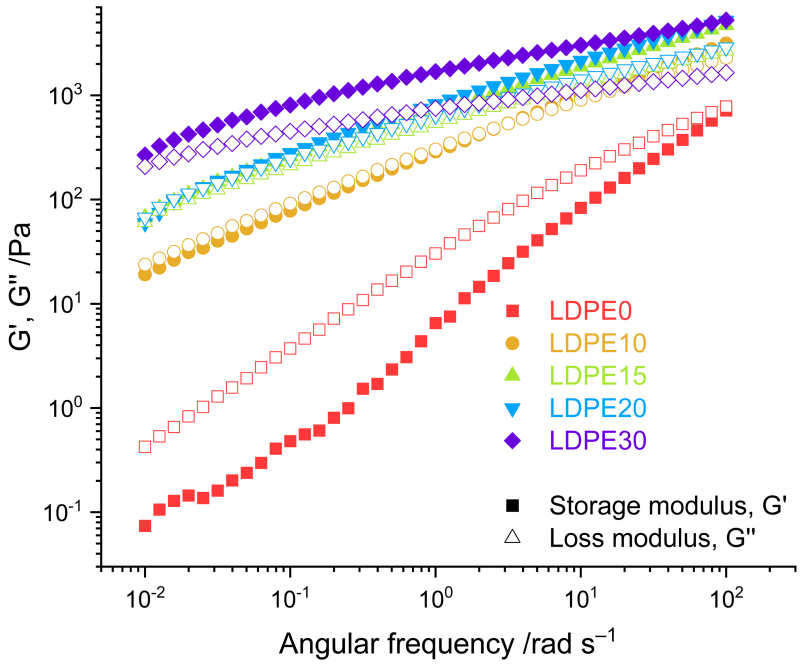

Figure A.142 Rheological storage and loss moduli as a function of shear angular frequency of LDPE/UHMWPE blends.

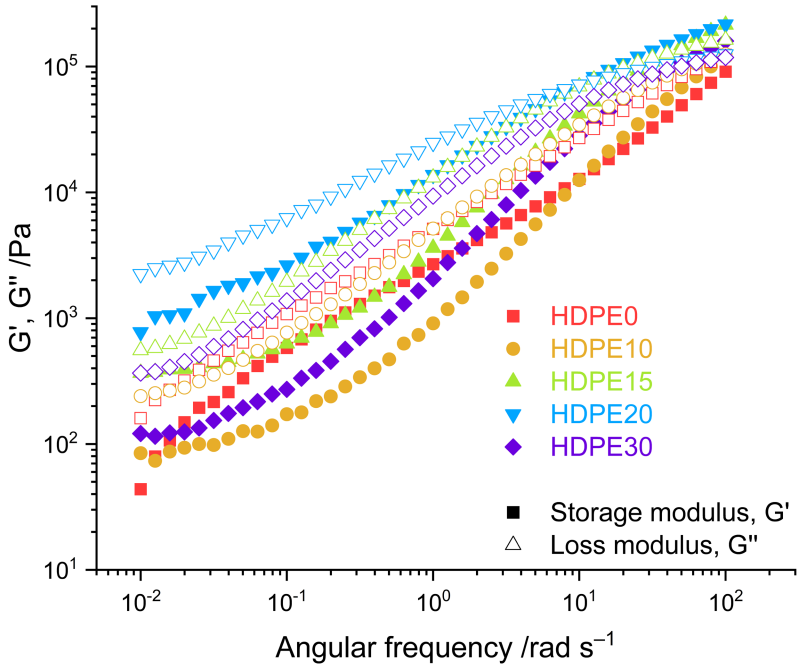

Figure A.143 Rheological storage and loss moduli as a function of shear angular frequency of HDPE/UHMWPE blends.

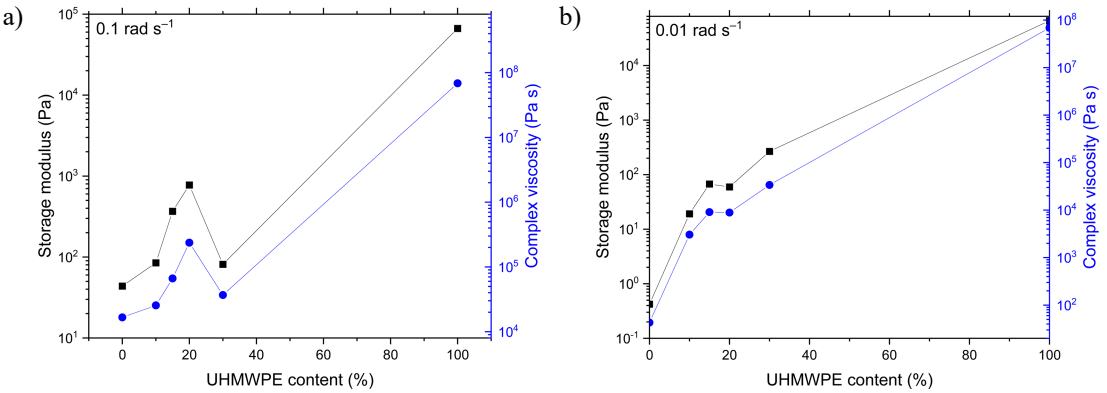

Figure A.144 Log-additivity law for rheological parameters (at $\omega = 0.1$ rad s^{-1}) for a) HDPE/UHMWPE, and b) LDHPE/UHMWPE as a function of polymer blend composition.

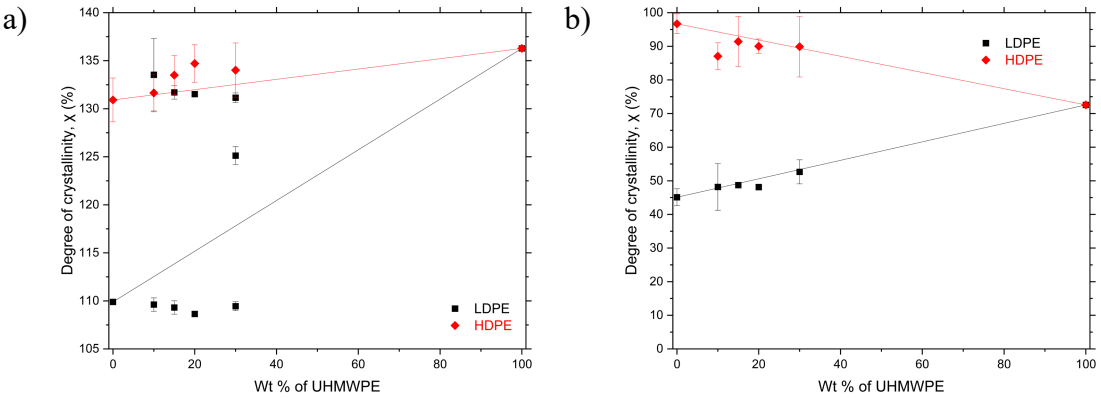

Figure A.145 Law of mixtures for a) T_m, and b) crystallinity of HDPE/UHMWPE and LDPE/UHMWPE as a function of polymer blend composition.

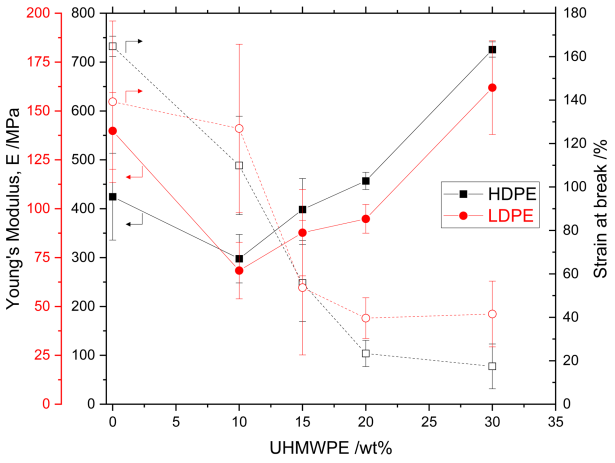

Figure A.146 Young's modulus, E, and strain at break, ε_B, of HDPE/UHMWPE and LDPE/UHMWPE as a function of polymer blend composition.

A.3. Supplementary data for Chapter Four

A.3.1. Polymerisation data

Table A.9 Propylene polymerisation data using selected PHENI* catalysts. Polymerisation conditions: 2 bar propylene.

	Catalyst /mg	T_p /°C	Time /mins	[Al_{MAO}]/[Ti]	$V_{hexanes}$ /mL	Activity /kg mol_{Ti}^{-1} h^{-1} bar^{-1}	M_w /kDa	PDI
1$_{sMAO}$/MAO	10	60	30	1000	50	2610 ± 94	471.3	2.2
	10	70	30	1000	50	1440 ± 378	368.9	2.3
	10	80	30	1000	50	1121	234.2	2.3
2$_{sMAO}$/MAO	10	60	30	1000	50	3213 ± 595	633.9	2.2
	10	70	30	1000	50	2176 ± 23	426.9	2.2
	10	80	30	1000	50	1609 ± 22	353.6	2.1
6$_{sMAO}$/MAO	10	60	30	1000	50	311 ± 186	249.5	2.1
	10	70	30	1000	50	581 ± 188	332.0	2.1
	10	80	30	1000	50	448 ± 10	227.4	2.2
11$_{sMAO}$/MAO	10	60	30	1000	50	1733 ± 326	374.9	2.3
	10	70	30	1000	50	623.9 ± 268	286.4	2.3
	10	80	30	1000	50	636.9 ± 34	196.6	2.2

12$_{\mathbf{sMAO}}$/MAO	10	30	30	1000	50	1328 ± 160	68.8/983.1	4.9/3.8
	10	40	30	1000	50	886 ± 151	866.5	2.4
	10	50	30	1000	50	1120 ± 186	755.7	2.2
	10	60	30	1000	50	586 ± 160	504.1	2.4
	10	70	30	1000	50	522 ± 95	369.9	2.2
	10	80	30	1000	50	529 ± 102	280.9	2.3
13$_{\mathbf{sMAO}}$/MAO	10	30	30	1000	50	1381 ± 569	1041.9	2.4
	10	40	30	1000	50	1833 ± 129	811.6	2.2
	10	50	30	1000	50	2151 ± 321	585.0	2.2
	10	60	30	1000	50	1497 ± 160	427.3	2.2
	10	70	30	1000	50	540 ± 140	268.8	2.2
	10	80	30	1000	50	862 ± 7	244.6	2.6
14$_{\mathbf{sMAO}}$/MAO	10	60	30	1000	50	105 ± 119	95.9	4.5
	10	70	30	1000	50	36.9 ± 0.3	63.2	3.2
	10	80	30	1000	50	18.7 ± 4.6	75.2	3.5
2$_{\mathbf{sMAO}}$/MAO	10	30	10	1000	50	7309 ± 291	1338.4	2.3
	10	40	10	1000	50	6825 ± 887	972.9	2.2
	10	50	10	1000	50	6591 ± 1119	760.0	2.2
	10	60	10	1000	50	5703 ± 28	746.7	2.2
	10	70	10	1000	50	5053 ± 1023	692.4	2.2
	10	80	10	1000	50	3262 ± 9	396.4	2.1
	10	90	10	1000	50	1129 ± 935	399.2	2.1
2$_{\mathbf{sMAO}}$/MAO	10	30	10	5000	250	9761	1176.7	2.5
	10	30	103	5000	250	3596	1409.8	1.9
2$_{\mathbf{sMAO}}$/MAO	10	30	10	0	50	312.8 ± 343	1144.4	2.5
	10	30	10	125	50	602.4 ± 105	1061.1	2.7

	10	30	10	250	50	3847 ± 868	1424.5	2.3
	10	30	10	500	50	5705 ± 1046	1346.2	2.4
	10	30	10	1000	50	7309 ± 291	1338.4	2.3
	10	30	10	2500	50	11685 ± 731	793.4	2.4
	10	30	10	5000	50	9304 ± 2681	710.8	2.4
2$_{sMAO}$/MAO	10	4	10	500	50	997.7 ± 237	1996.5	2.7
	10	23	10	500	50	2062 ± 171	1380.6	2.3
2/MAO	0.414	4	10	1000	50	1270 ± 98	1268.4	2.7
	0.414	30	10	1000	50	6117 ± 371	1085.0	2.4
	0.414	40	10	1000	50	6205 ± 187	759.0	2.4
	0.414	50	10	1000	50	4491 ± 941	567.2	2.4
	0.414	60	10	1000	50	4118 ± 478	487.4	2.4
	0.414	70	10	1000	50	2618 ± 621	324.5	2.3
	0.414	80	10	1000	50	1800 ± 650	275.3	2.3
	0.414	90	10	1000	50	1495 ± 333	189.1	2.2
2/MAO	0.414	30	10	1000	50	6117 ± 371	1085.0	2.4
	0.207	30	10	2000	50	6301 ± 1650	1407.0	2.5
	0.104	30	10	4000	50	8097 ± 2109	1346.6	2.3
	0.052	30	10	8000	50	11790 ± 570	1512.8	2.6
2/TMA	0.414	30	10	1000	50	-	-	-
2/TEA	0.414	30	10	1000	50	-	-	-
2/TIBA	0.414	30	10	1000	50	-	-	-
2$_{sMAO}$/TIBA	10	60	30	1000	50	279 ± 2		
2/MAO	0.414	30	10	0	50	-	-	-
	0.414	30	10	125	50	147.7 ± 19	480.6	2.4
	0.414	30	10	250	50	892.4 ± 276	912.0	3.7

	0.414	30	10	500	50	1367 ± 187	795.7	2.5
	0.414	30	10	1000	50	6117 ± 371	1085.0	2.4
	0.414	30	10	2000	50	11270 ± 416	706.8	2.4
	0.414	30	10	5000	50	9924 ± 830	557.6	2.4
2/MAO	0.414	30	120	5000	250	2668 ± 60	1210.6	2.7
2/MAO	0.414	30	139	5000	250	6244		

A.3.2. Gel-permeation chromatography

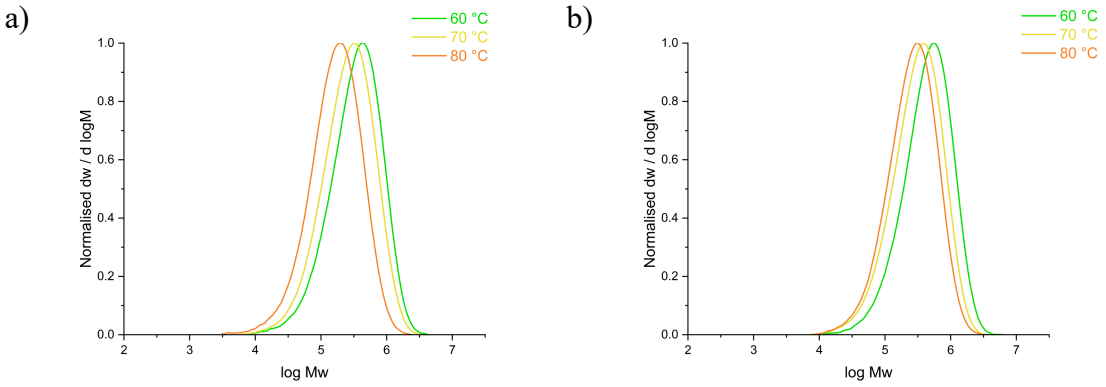

Figure A.147 Gel permeation chromatograms of PP synthesised by a) **1**$_{sMAO}$, and b) **2**$_{sMAO}$ as a function of temperature. Polymerisation conditions: 10 mg catalyst, [Al$_{MAO}$]/[Ti] = 1000, 2 bar propylene, 50 mL hexanes, and 30 minutes.

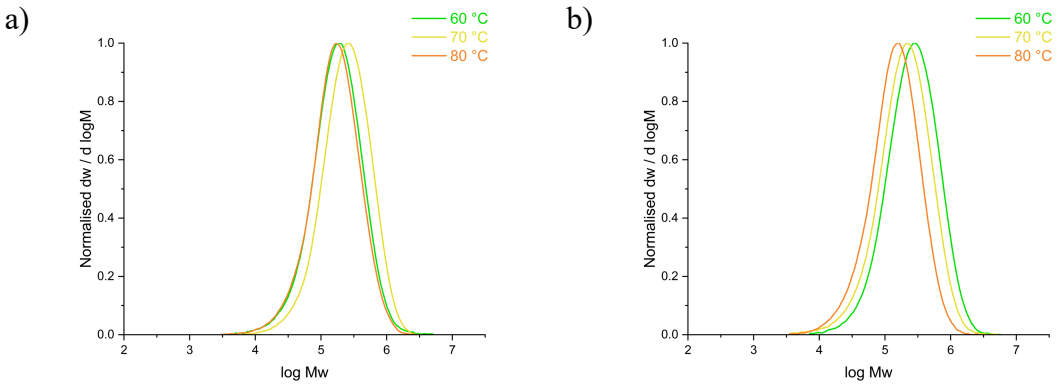

Figure A.148 Gel permeation chromatograms of PP synthesised by a) **6**$_{sMAO}$, and b) **11**$_{sMAO}$ as a function of temperature. Polymerisation conditions: 10 mg catalyst, [Al$_{MAO}$]/[Ti] = 1000, 2 bar propylene, 50 mL hexanes, and 30 minutes.

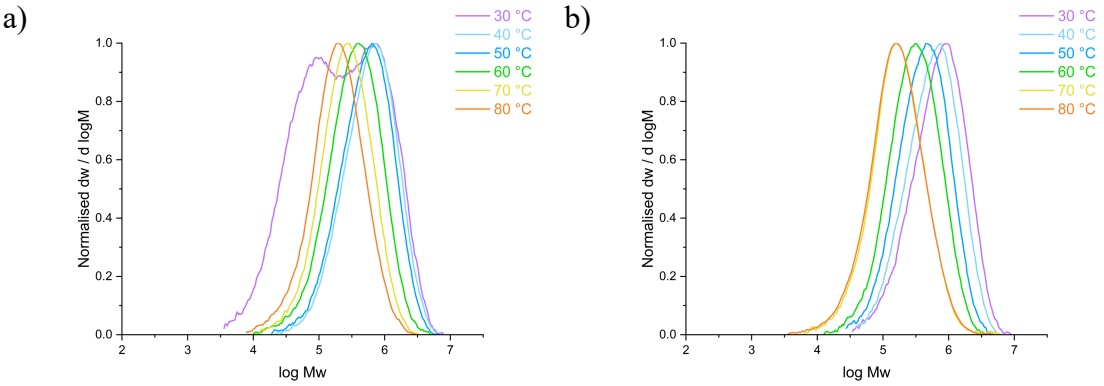

Figure A.149 Gel permeation chromatograms of PP synthesised by a) **12$_{sMAO}$**, and b) **13$_{sMAO}$** as a function of temperature. Polymerisation conditions: 10 mg catalyst, [Al$_{MAO}$]/[Ti] = 1000, 2 bar propylene, 50 mL hexanes, and 30 minutes.

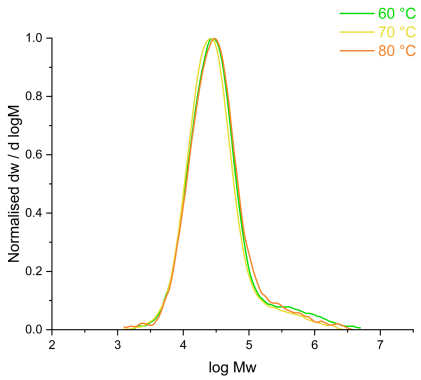

Figure A.150 Gel permeation chromatograms of PP synthesised by **14$_{sMAO}$** as a function of temperature. Polymerisation conditions: 10 mg catalyst, [Al$_{MAO}$]/[Ti] = 1000, 2 bar propylene, 50 mL hexanes, and 30 minutes.

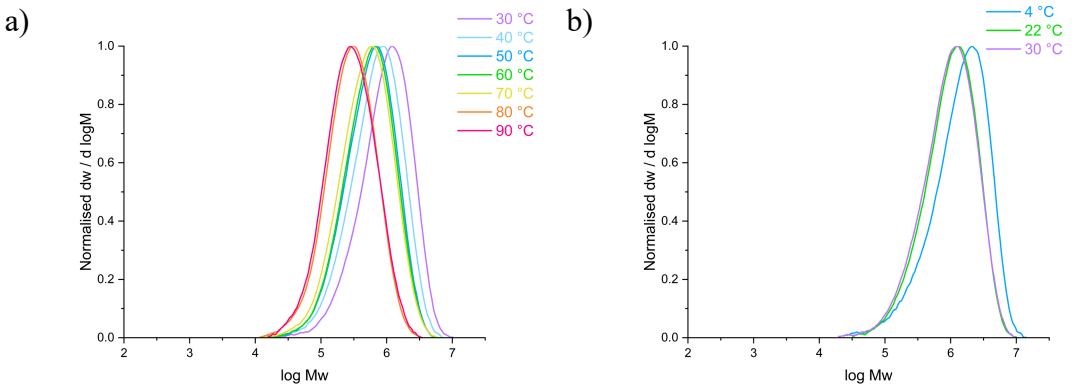

Figure A.151 Gel permeation chromatograms of PP synthesised by **2**$_{\mathbf{sMAO}}$ as a function of temperature. Polymerisation conditions: 10 mg catalyst, [Al$_{MAO}$]/[Ti] = 1000, 2 bar propylene, 50 mL hexanes, and 10 minutes.

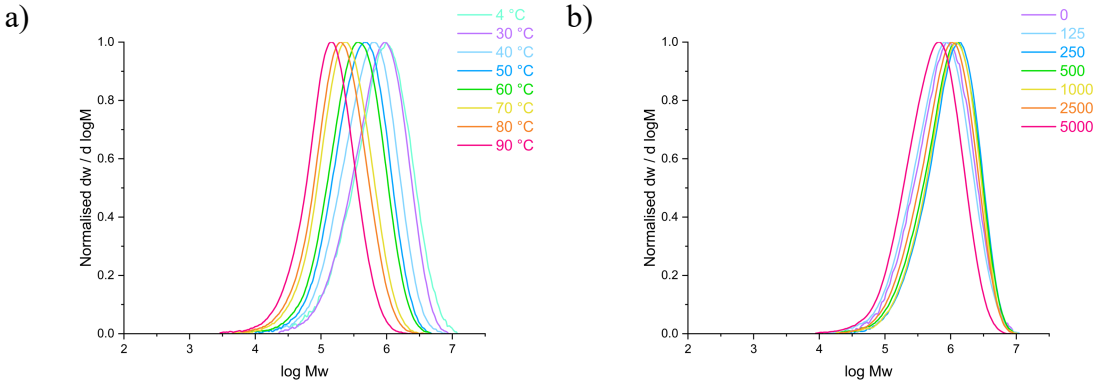

Figure A.152 Gel permeation chromatograms of PP synthesised by a) **2** as a function of temperature, and b) **2**$_{\mathbf{sMAO}}$ as a function of [Al$_{MAO}$]/[Ti]. Polymerisation conditions: 2 bar propylene, 50 mL hexanes, 10 minutes, and a) 414 µg catalyst, [Al$_{MAO}$]/[Ti] = 1000, or b) 10 mg catalyst, 60 °C.

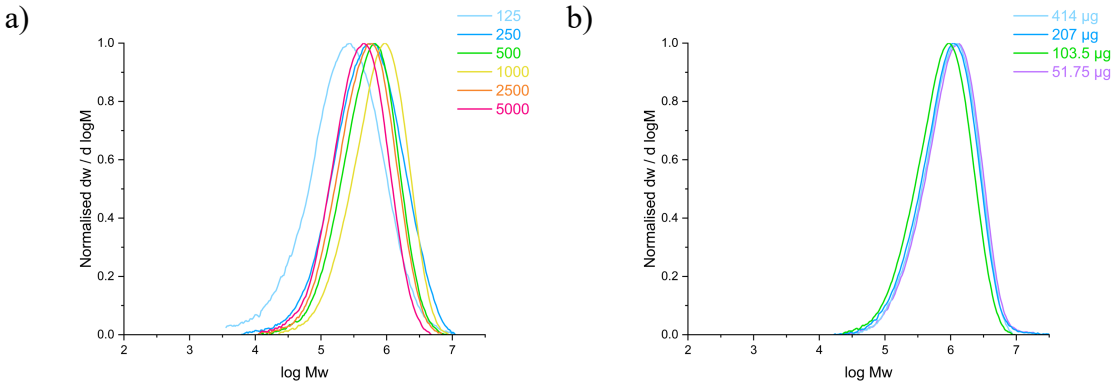

Figure A.153 Gel permeation chromatograms of PP synthesised by **2** as a function of a) $[Al_{MAO}]/[Ti]$, or b) catalyst mass. Polymerisation conditions: 2 bar propylene, 50 mL hexanes, 30 °C, 10 minutes, and a) 414 µg catalyst, or b) $[Al_{MAO}]$ = 14 mM.

A.3.3. Thermogravimetric analysis

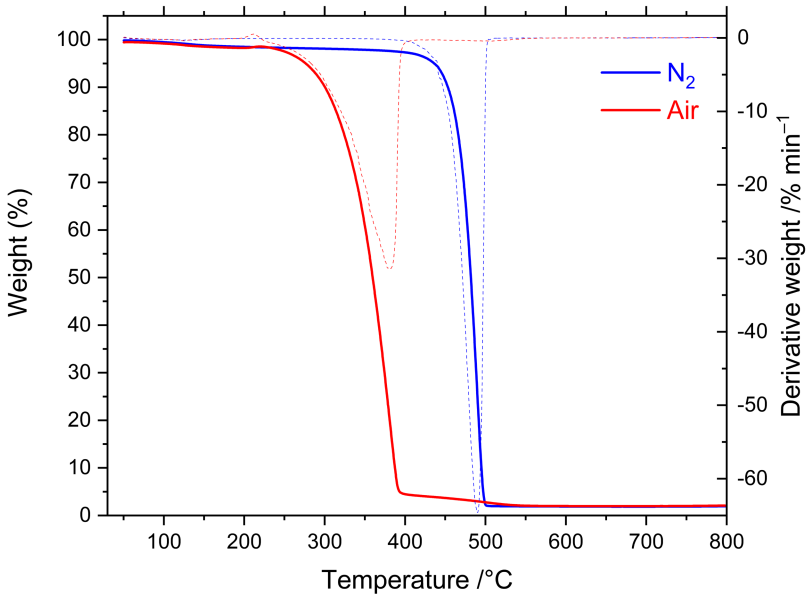

Figure A.154 Thermogravimetry plots of UHMWaPP, at a heating rate of 20 K min^{-1} under an atmosphere of dry nitrogen or synthetic air (20% O_2 in N_2). Polymerisation conditions: 414 µg catalyst, 2 bar propylene, 250 mL hexanes, $[Al_{MAO}]/[Ti]$ = 5000, 139 minutes, and 30 °C.

A.3.4. Differential scanning calorimetry

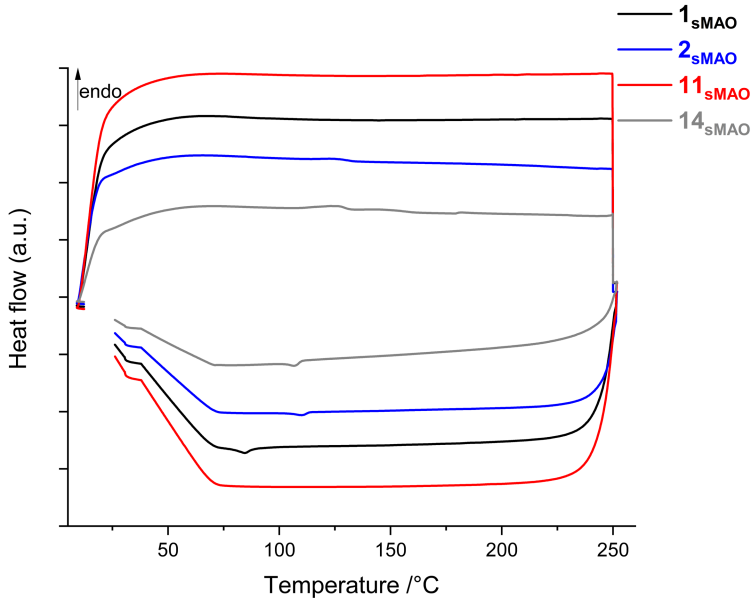

Figure A.155 Differential scanning calorimetry plots (at 20 K min^{-1}, second heating and cooling shown), of PP produced by the sMAO-supported catalysts **1**$_{sMAO}$, **2**$_{sMAO}$, **11**$_{sMAO}$, and **14**$_{sMAO}$. Polymerisation conditions: 10 mg catalyst, 2 bar propylene, 50 mL hexanes, [Al$_{MAO}$]/[Ti] = 1000, 30 minutes, and 60 °C.

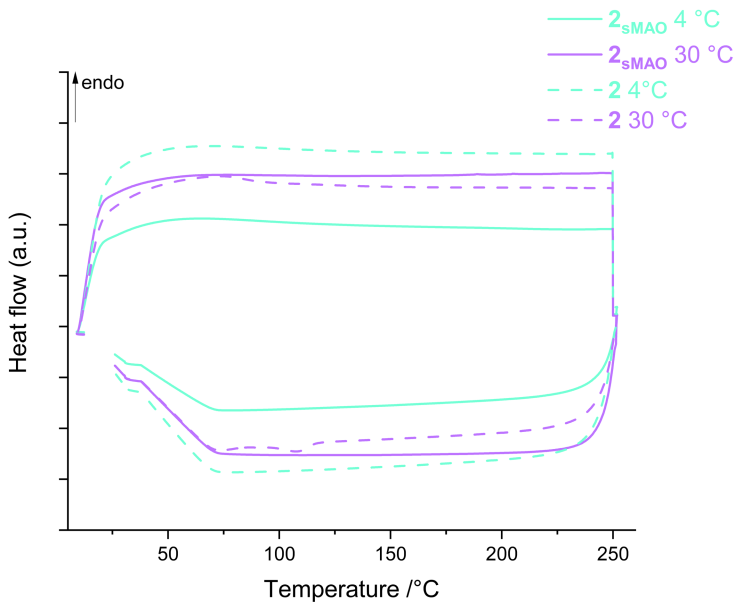

Figure A.156 Differential scanning calorimetry plots (at 20 K min^{-1}, second heating and cooling shown), of PP produced by the **2**$_{sMAO}$ and **2**. Polymerisation conditions: 10 mg **2**$_{sMAO}$ or 414 µg **2**, 2 bar propylene, 50 mL hexanes, [Al$_{MAO}$]/[Ti] = 1000, 30 minutes, and 60 °C.

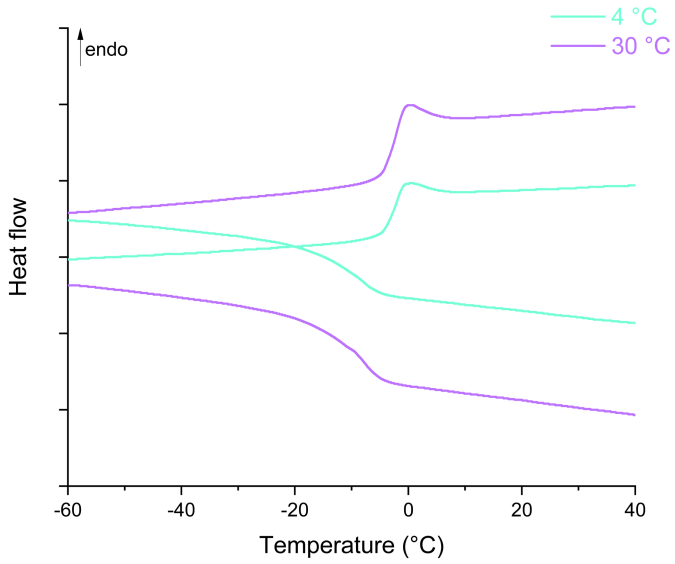

Figure A.157 Differential scanning calorimetry plots (at 10 K min^{-1}, second heating and cooling shown), of PP produced by **2**$_{sMAO}$. Polymerisation conditions: 10 mg catalyst, 2 bar propylene, 50 mL hexanes, [Al$_{MAO}$]/[Ti] = 1000, 10 minutes, and 4 or 30 °C.

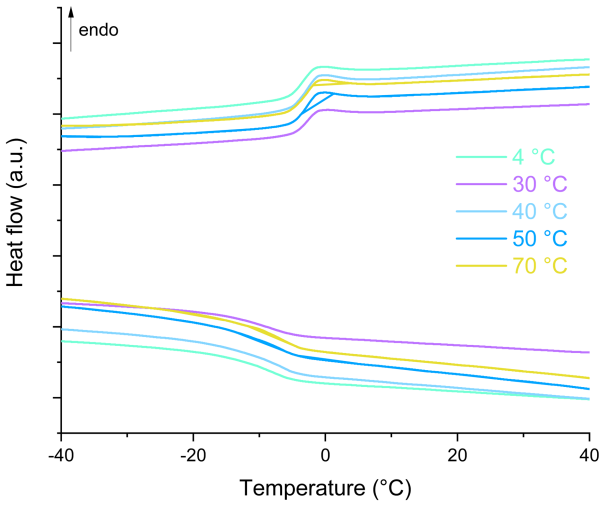

Sample	T_g /°C	$\Delta C_{p,T_g}$ /J °C^{-1} g^{-1}
1$_{sMAO}$, T_p = 60 °C	–3.20	0.527
2$_{sMAO}$, T_p = 60 °C	–3.63	0.513
11$_{sMAO}$, T_p = 60 °C	–6.46	0.452
14$_{sMAO}$, T_p = 60 °C	–12.01	0.179
2$_{sMAO}$, T_p = 4 °C	–2.86	0.391
2$_{sMAO}$, T_p = 30 °C	–2.85	0.480
2, T_p = 4 °C	–3.61	0.520
2, T_p = 30 °C	–3.03	0.418
2, T_p = 40 °C	–3.31	0.542
2, T_p = 50 °C	–3.33	0.482
2, T_p = 70 °C	–3.34	0.547

Figure A.158 Differential scanning calorimetry plots (at 10 K min^{-1}, second heating and cooling shown), of PP produced by **2**. Polymerisation conditions: 414 µg catalyst, 2 bar propylene, 50 mL hexanes, [Al$_{MAO}$]/[Ti] = 1000, 10 minutes, and 4 or 30 °C. And thermal data for polypropylenes synthesised by PHENI* complexes.

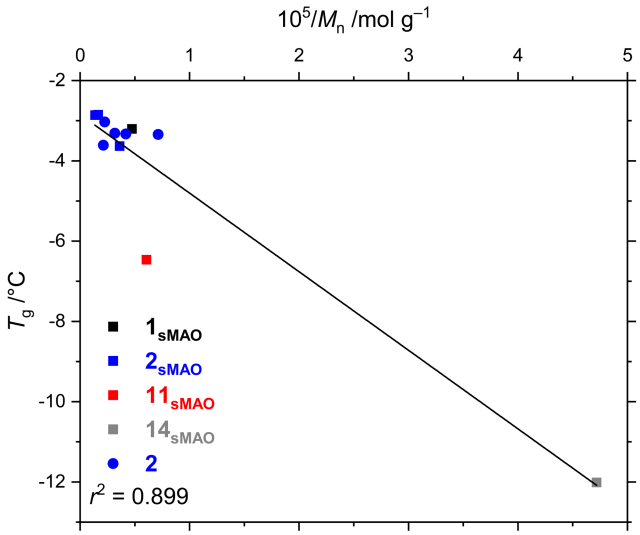

Figure A.159 T_g as a function of M_n^{-1}. Polymerisation conditions: 10 mg catalyst, 2 bar propylene, 50 mL hexanes, $[Al_{MAO}]/[Ti]$ = 1000, 30 minutes, and 60 °C.

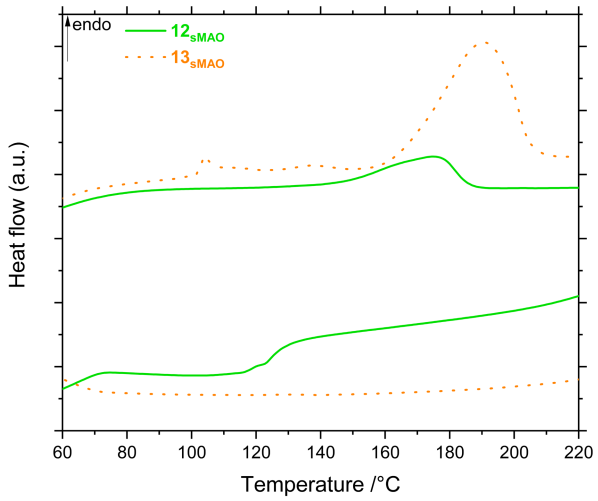

Figure A.160 Differential scanning calorimetry plots (at 20 K min^{-1}, second heating and cooling shown), of PP produced by the sMAO-supported catalysts **12**$_{sMAO}$, and **13**$_{sMAO}$. Polymerisation conditions: 10 mg catalyst, 2 bar propylene, 50 mL hexanes, $[Al_{MAO}]/[Ti]$ = 1000, 30 minutes, and 60 °C.

A.3.5. ^{13}C NMR spectroscopy

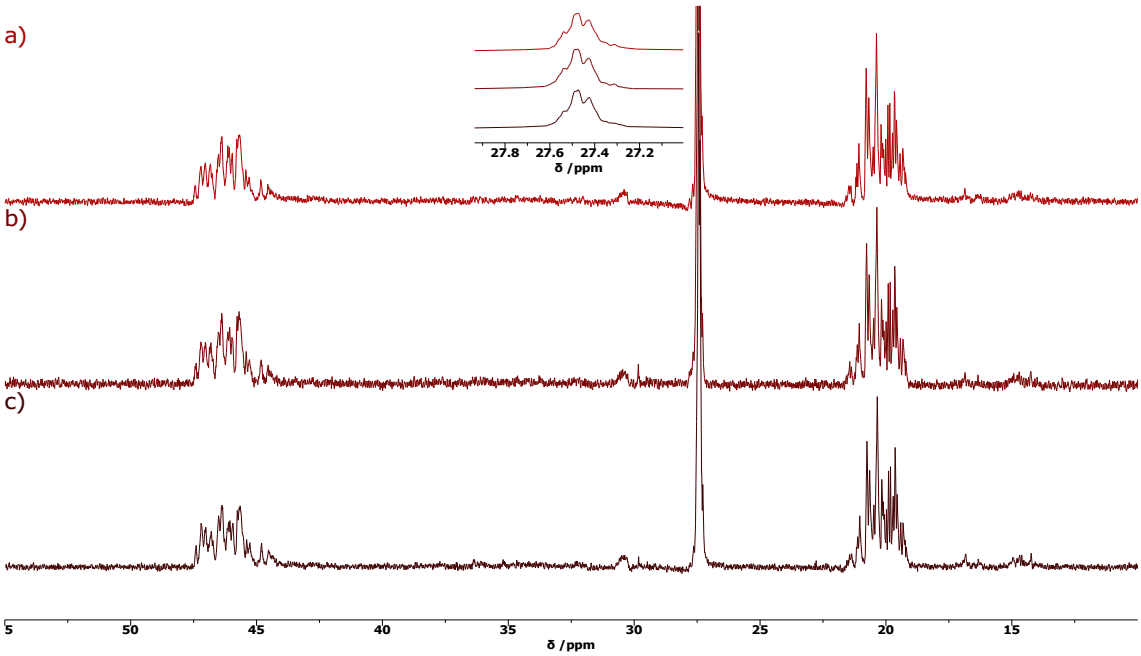

Figure A.161 $^{13}C\{^{1}H\}$ NMR spectra (151 MHz, chloroform-*d*, 298 K, $55 \leq \delta \leq 10$) of polypropylene synthesised by $\mathbf{1}_{sMAO}$ at a) 60 °C, b) 70 °C, and c) 80 °C. Polymerisation conditions: 10 mg catalyst, $[Al_{MAO}]/[Ti] = 1000$, 2 bar propylene, 50 mL hexanes, 30 minutes, and 60–80 °C.

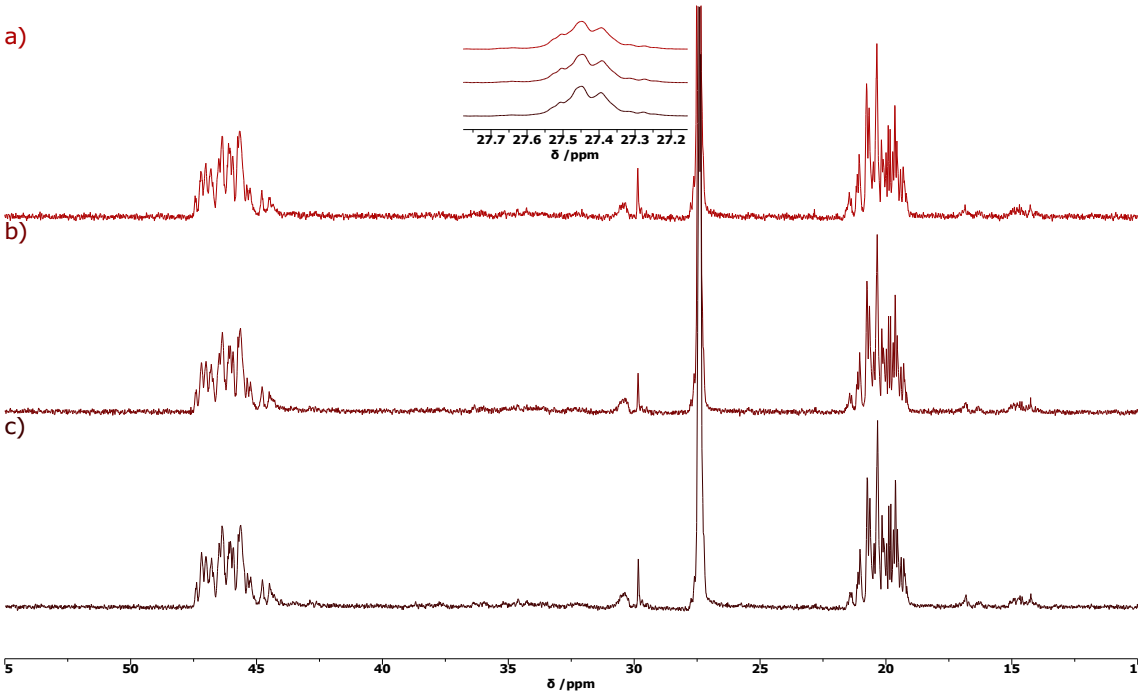

Figure A.162 $^{13}C\{^{1}H\}$ NMR spectra (126 MHz, chloroform-*d*, 298 K, $55 \leq \delta \leq 10$) of polypropylene synthesised by $\mathbf{2}_{sMAO}$ at a) 60 °C, b) 70 °C, and c) 80 °C. Polymerisation conditions: 10 mg catalyst, $[Al_{MAO}]/[Ti] = 1000$, 2 bar propylene, 50 mL hexanes, 30 minutes, and 60–80 °C.

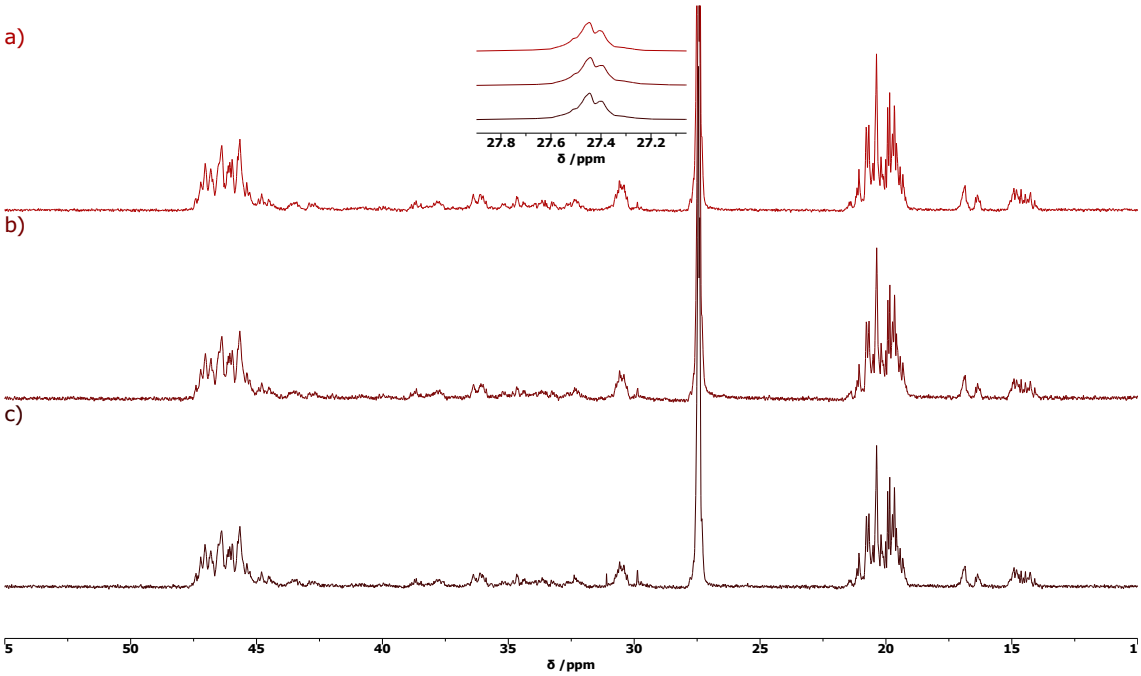

Figure A.163 $^{13}C\{^{1}H\}$ NMR spectra (126 MHz, chloroform-*d*, 298 K, $55 \leq \delta \leq 10$) of polypropylene synthesised by **11**$_{sMAO}$ at a) 60 °C, b) 70 °C, and c) 80 °C. Polymerisation conditions: 10 mg catalyst, $[Al_{MAO}]/[Ti] = 1000$, 2 bar propylene, 50 mL hexanes, 30 minutes, and 60–80 °C.

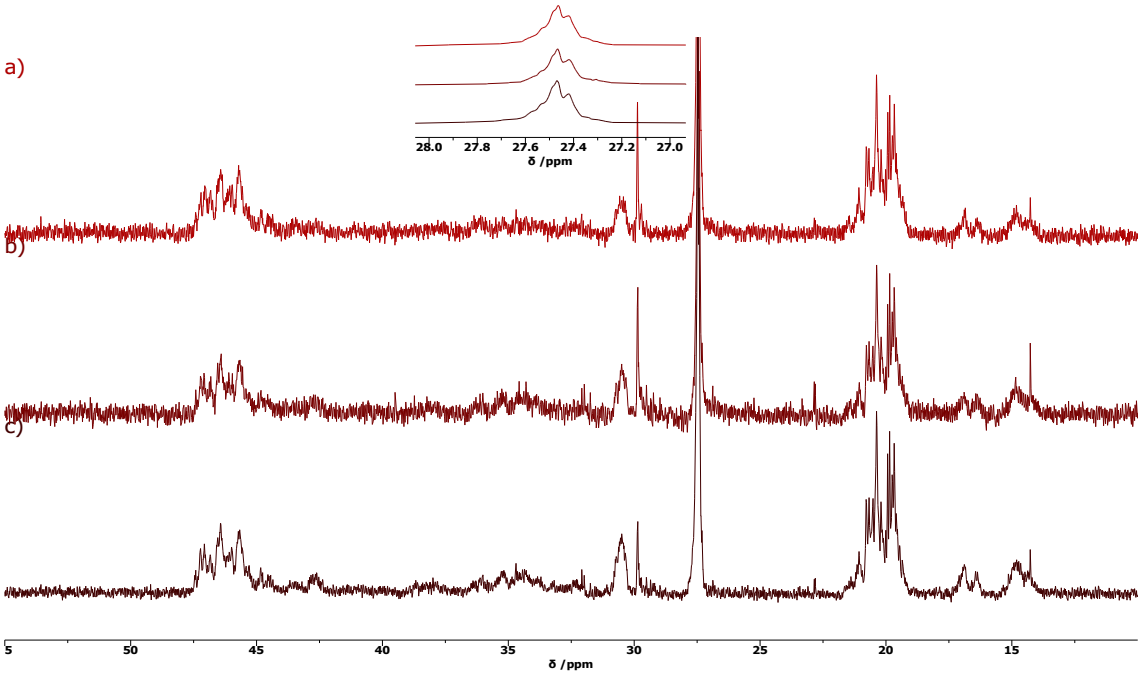

Figure A.164 $^{13}C\{^{1}H\}$ NMR spectra (151 MHz, chloroform-*d*, 298 K, $55 \leq \delta \leq 10$) of polypropylene synthesised by **14**$_{sMAO}$ at a) 60 °C, b) 70 °C, and c) 80 °C. Polymerisation conditions: 10 mg catalyst, $[Al_{MAO}]/[Ti] = 1000$, 2 bar propylene, 50 mL hexanes, 30 minutes, and 60–80 °C.

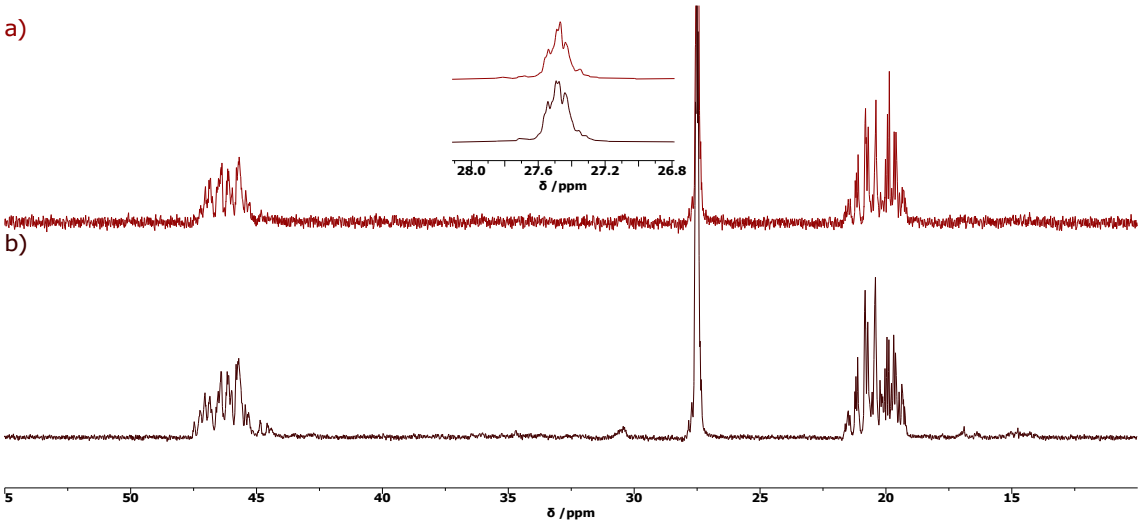

Figure A.165 $^{13}C\{^{1}H\}$ NMR spectra (151 MHz, chloroform-*d*, 298 K, $55 \leq \delta \leq 10$) of polypropylene synthesised by $\mathbf{2}_{\mathbf{sMAO}}$ at a) 4 °C, $[Al_{MAO}]/[Ti] = 500$, and b) 30 °C, $[Al_{MAO}]/[Ti] = 1000$. Polymerisation conditions: 10 mg catalyst, 2 bar propylene, 50 mL hexanes, 10 minutes, and 4–30 °C.

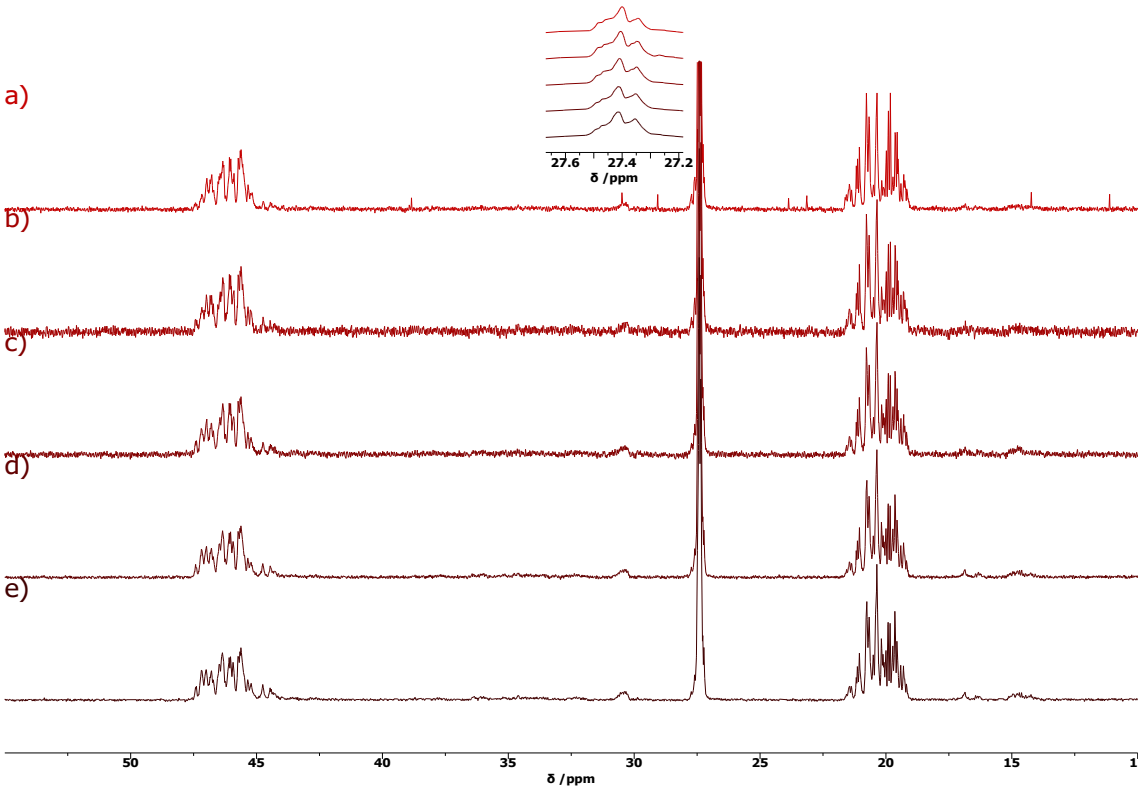

Figure A.166 $^{13}C\{^{1}H\}$ NMR spectra (151 MHz, chloroform-*d*, 298 K, $55 \leq \delta \leq 10$) of polypropylene synthesised by **2** at a) 4 °C, b) 30 °C, c) 50 °C, d) 70 °C, and e) 90 °C. Polymerisation conditions: 414 µg catalyst, 2 bar propylene, 50 mL hexanes, $[Al_{MAO}]/[Ti] = 1000$, and 10 minutes.

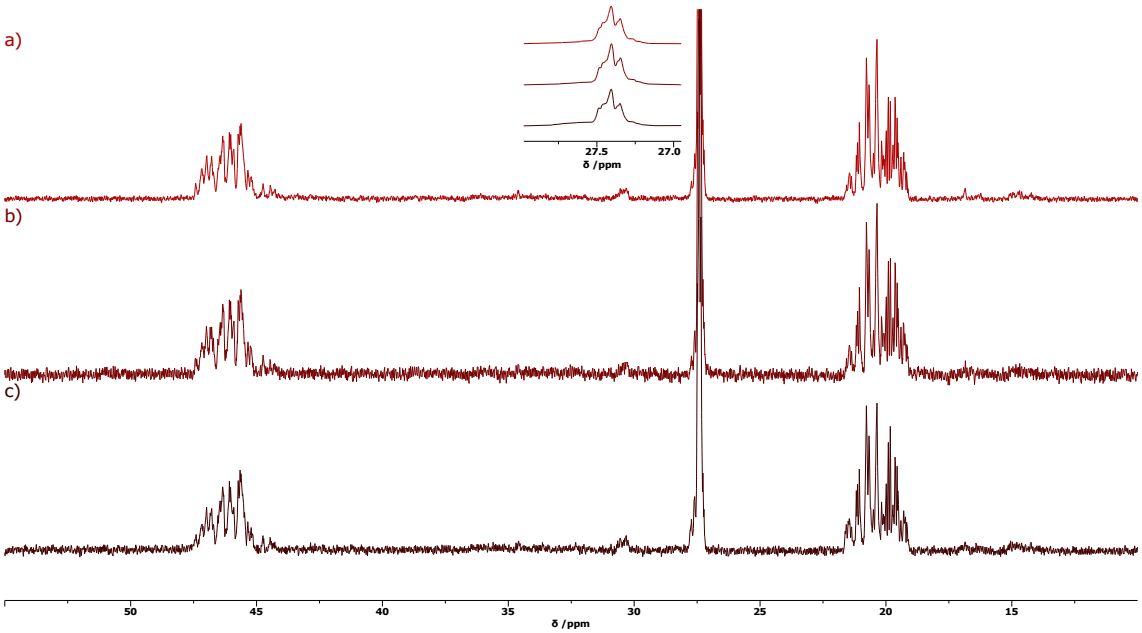

Figure A.167 $^{13}C\{^{1}H\}$ NMR spectra (151 MHz, chloroform-*d*, 298 K, $55 \leq \delta \leq 10$) of polypropylene synthesised by **2** using a) 2500, b) 1000, and c) 250 equivalents of MAO. Polymerisation conditions: 414 µg catalyst, 2 bar propylene, 50 mL hexanes, $[Al_{MAO}]/[Ti] = 250–2500$, 30 °C, and 10 minutes.

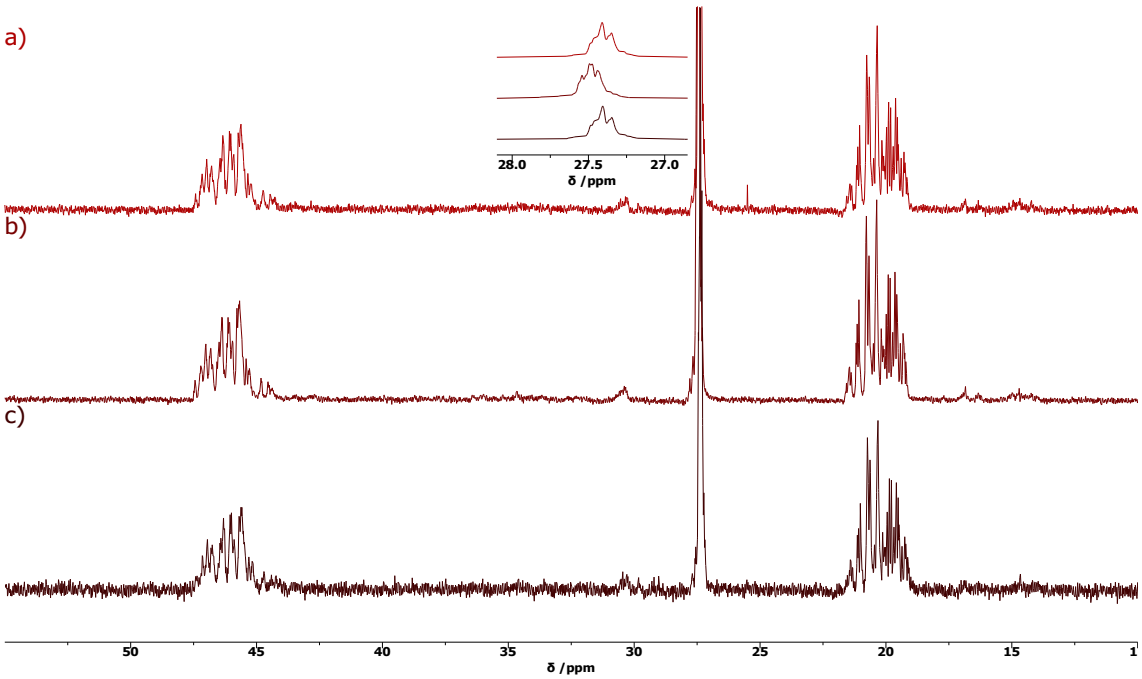

Figure A.168 $^{13}C\{^{1}H\}$ NMR spectra (151 MHz, chloroform-*d*, 298 K, $55 \leq \delta \leq 10$) of polypropylene synthesised by $\mathbf{2_{sMAO}}$ using a) 2500, b) 1000, and c) 250 equivalents of MAO. Polymerisation conditions: 10 mg catalyst, 2 bar propylene, 50 mL hexanes, $[Al_{MAO}]/[Ti] = 250–2500$, 30 °C, and 10 minutes.

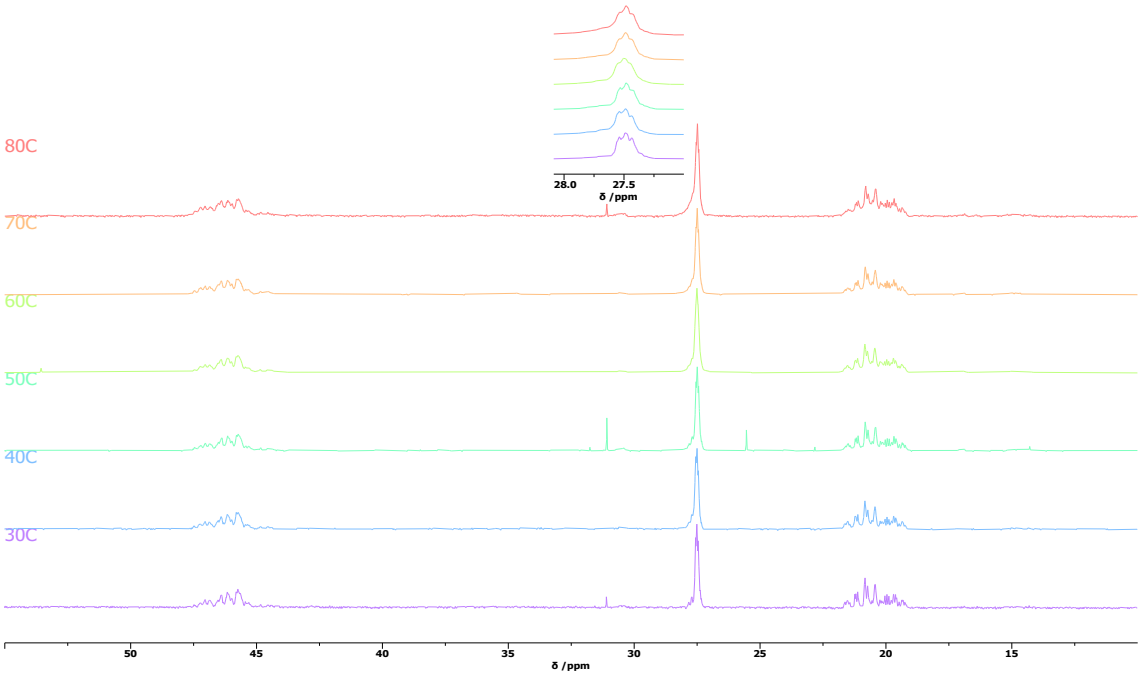

Figure A.169 $^{13}C\{^{1}H\}$ NMR spectra (126 MHz, chloroform-*d*, 298 K, $55 \leq \delta \leq 10$) of polypropylene synthesised by **12**$_{sMAO}$ at 30–80 °C. Polymerisation conditions: 10 mg catalyst, $[Al_{MAO}]/[Ti] = 1000$, 2 bar propylene, 50 mL hexanes, and 30 minutes.

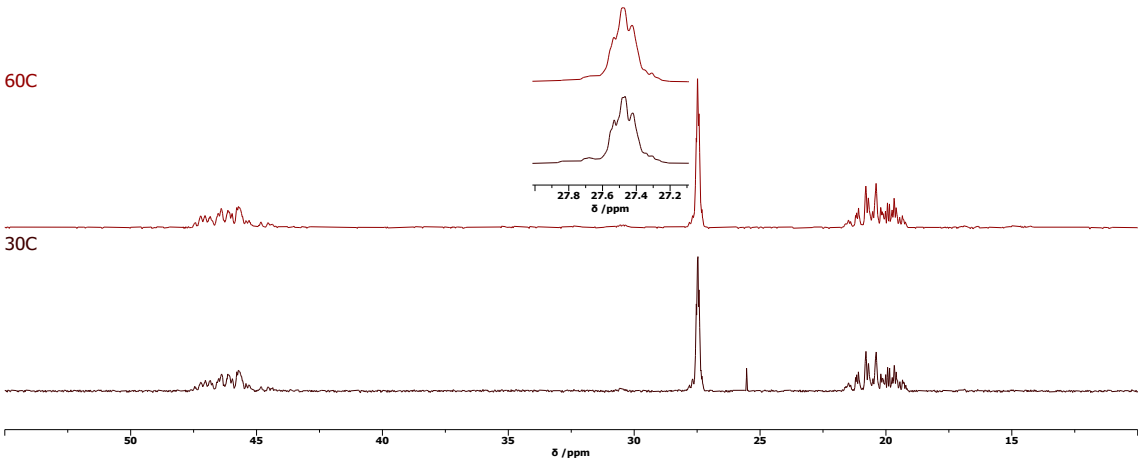

Figure A.170 $^{13}C\{^{1}H\}$ NMR spectra (126 MHz, chloroform-*d*, 298 K, $55 \leq \delta \leq 10$) of polypropylene synthesised by **13**$_{sMAO}$ at 30, and 60 °C. Polymerisation conditions: 10 mg catalyst, $[Al_{MAO}]/[Ti] = 1000$, 2 bar propylene, 50 mL hexanes, and 30 minutes.

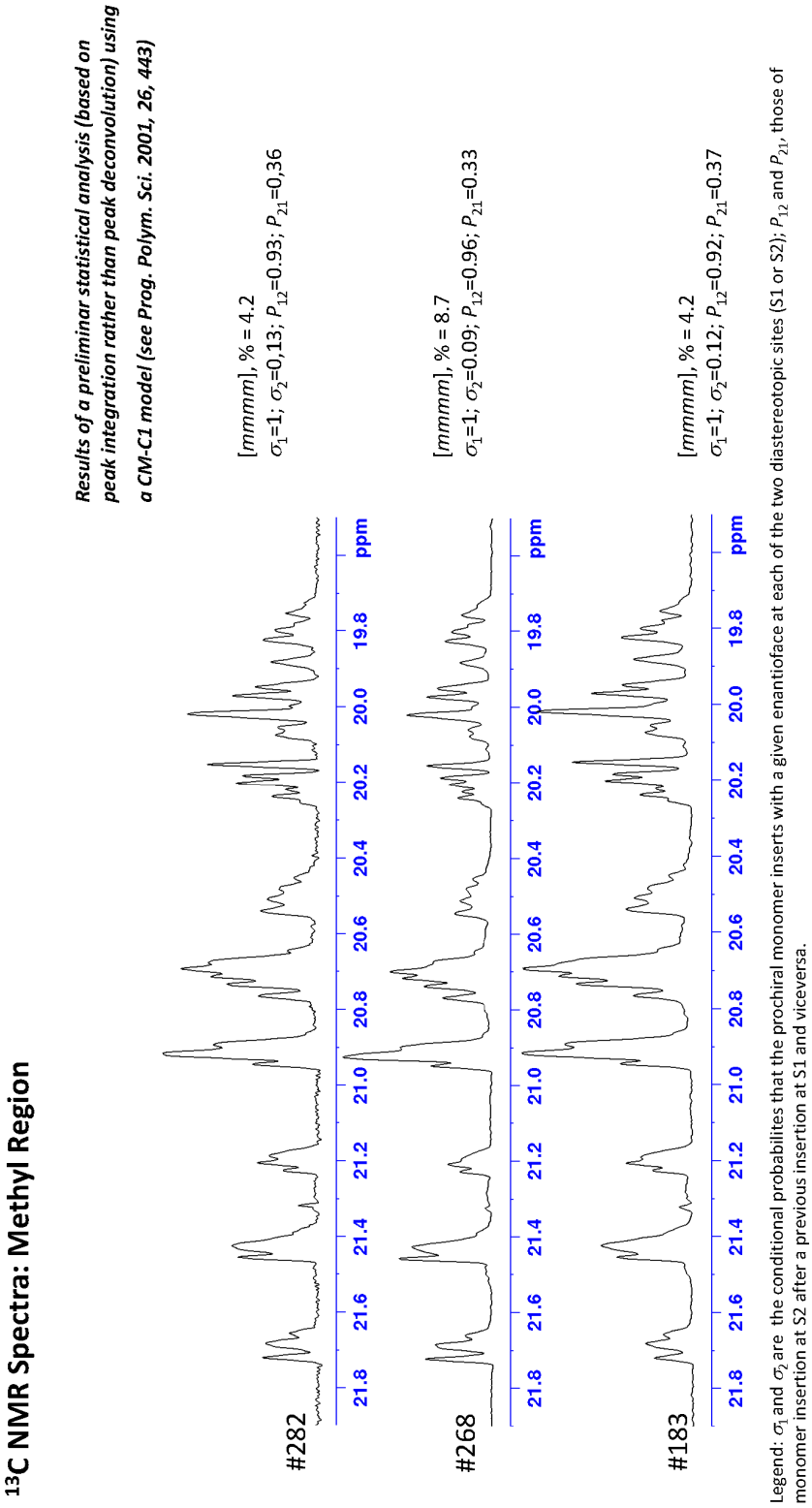

Figure A.171 NMR analysis from Prof. Roberta Cipullo (Università Federico II, Naples). N.B. #282 = **12**$_{sMAO}$, #268 = **13**$_{sMAO}$, #183 = **2**$_{sMAO}$.

A.3.6. Rheology

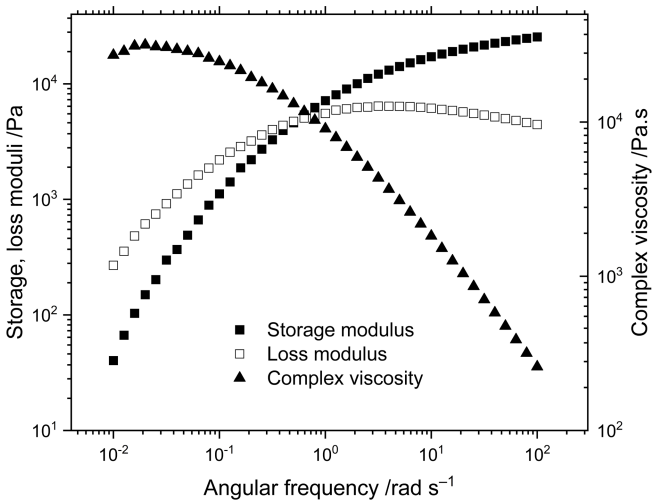

Figure A.172 Storage and loss moduli, and complex viscosity of UHMWaPP as a function of shear angular frequency.

A.3.7. Optical characterisation

Table A.10 Optical characterisation data for UHMWaPP samples at selected visible wavelengths. λ /nm, total transmittance (T_{tot}, %), diffuse transmittance (T_{diff}, %), and total reflectance (R_{tot}, %).

	a) Pressed at 160 °C Thickness 900 µm			b) Pressed at 80 °C Thickness 620 µm			c) Pressed at 180 °C Thickness 340 µm			d) Pressed at 160 °C Thickness 130 µm		
λ /nm	**T_{tot}**	**T_{diff}**	**R_{tot}**	**T_{tot}**	**T_{diff}**	**R_{tot}**	**T_{tot}**	**T_{diff}**	**R_{tot}**	**T_{tot}**	**T_{diff}**	**R_{tot}**
400	82.1	51.6	7.26	85.9	49.1	7.50	82.4	53.3	7.59	83.7	55.3	8.09
450	83.5	50.7	7.23	86.9	47.6	7.42	84.1	52.5	7.53	85.2	54.4	8.09
500	84.2	49.7	7.24	87.4	46.2	7.38	85.2	51.6	7.51	86.2	53.4	8.10
550	84.8	48.2	7.14	87.8	44.2	7.24	86.1	50.2	7.36	86.9	51.9	7.95
600	85.2	47.0	7.12	88.1	42.9	7.20	86.7	49.0	7.31	87.3	50.8	7.90
650	85.5	45.9	7.11	88.4	41.6	7.18	87.2	47.9	7.27	87.8	49.5	7.89
700	85.8	45.2	7.11	88.7	40.7	7.16	87.5	47.1	7.24	88.2	48.6	7.85
Average (380–750)	84.6	48.1	7.16	87.7	44.3	7.28	85.8	49.9	7.38	86.6	51.7	7.96

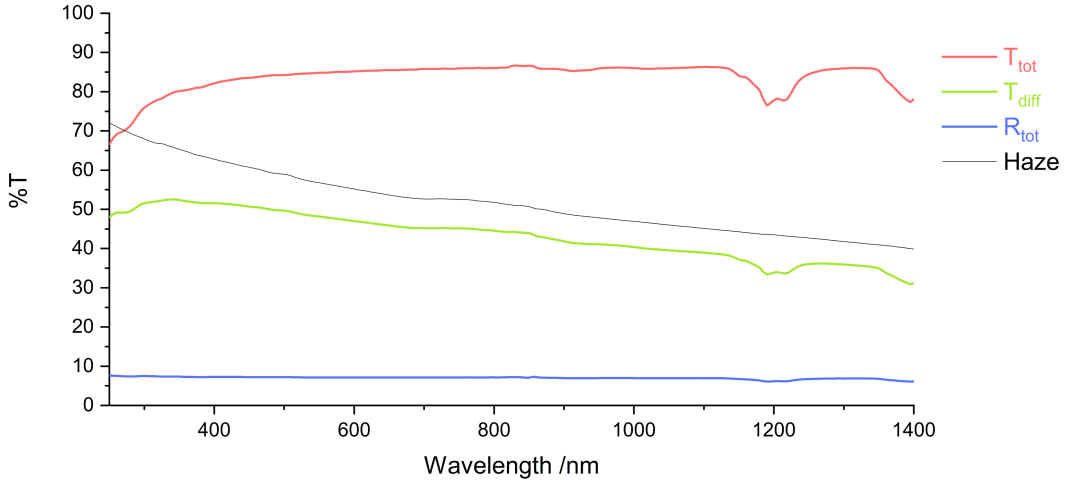

Figure A.173 Optical characteristics as a function of wavelength of sample a) (pressed at 160 °C, 900 µm) – total transmission (T_{tot}, %), diffuse transmission (T_{diff}, %), total reflectance (R_{tot}, %), and haze = T_{diff}/T_{tot}.

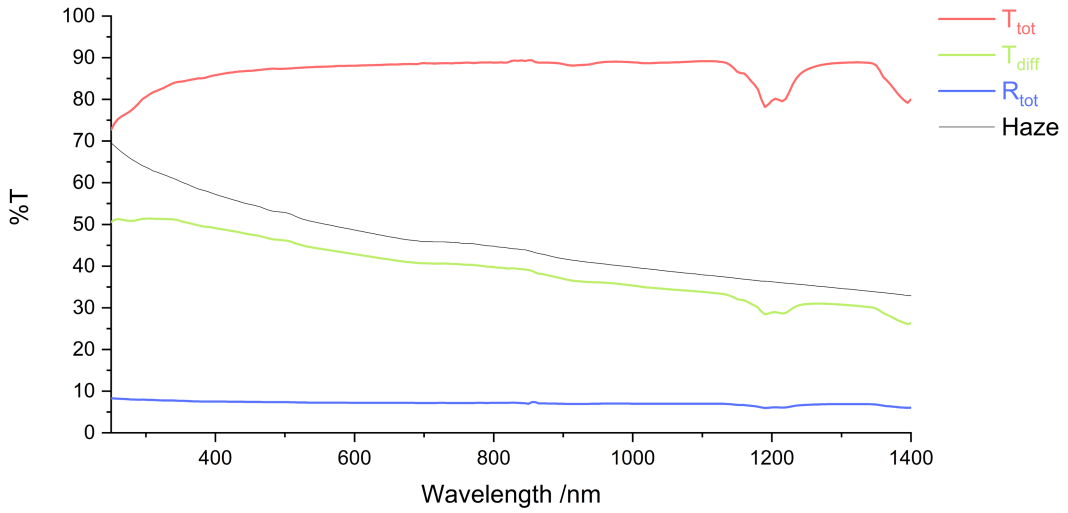

Figure A.174 Optical characteristics as a function of wavelength of sample b) (pressed at 80 °C, 620 µm) – total transmission (T_{tot}), diffuse transmission (T_{diff}), total reflectance (R_{tot}), and haze = T_{diff}/T_{tot}.

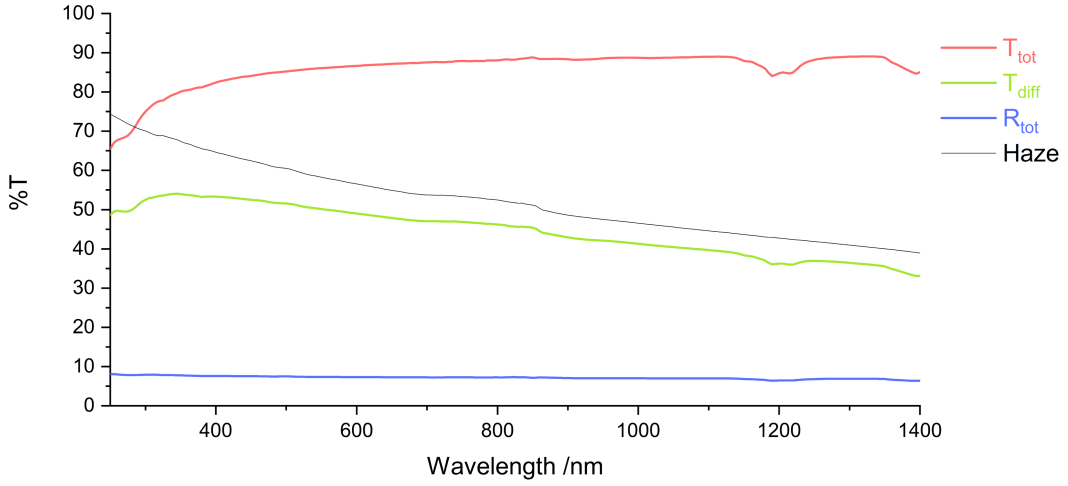

Figure A.175 Optical characteristics as a function of wavelength of sample c) (pressed at 180 °C, 340 µm) – total transmission (T_{tot}), diffuse transmission (T_{diff}), total reflectance (R_{tot}), and haze = T_{diff}/T_{tot}.

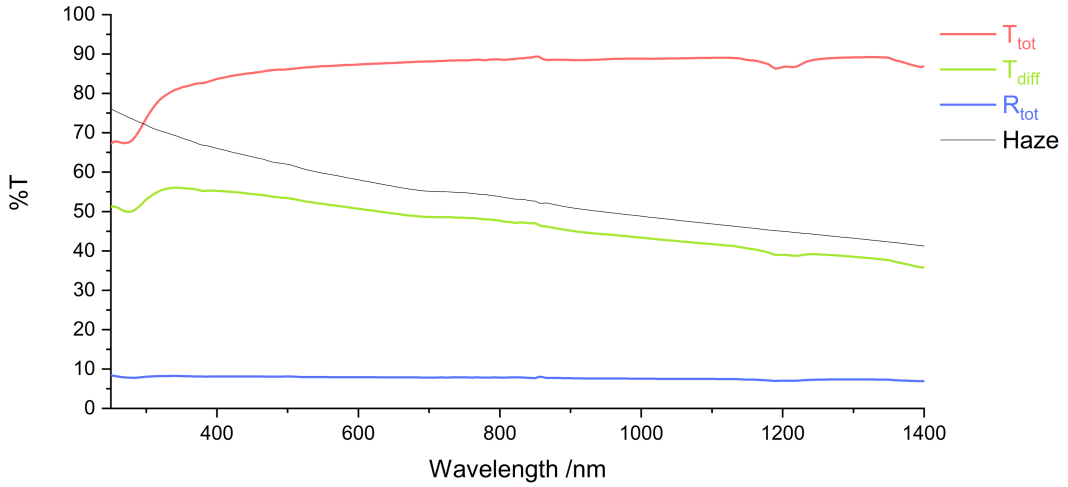

Figure A.176 Optical characteristics as a function of wavelength of sample d) (pressed at 160 °C, 130 µm) – total transmission (T_{tot}), diffuse transmission (T_{diff}), total reflectance (R_{tot}), and haze = T_{diff}/T_{tot}.

A.3.8. Mechanical characterisation (Norner AS)

Norner AS 06.12.21

Test report

TR no.	: R-211104-004	Tester	: TG		
Project no	: 221876	Pre-load	: 0,5	N	
Customer	: Oxford University	Speed, tensile modulus	: 1	mm/min	
Test standard	: ISO 527-2/5A	Test speed	: 50	mm/min	
Material	: CCR 299 UHMWPP	Load cell	: 5kN		
Temperature	: 22				

Test results:

	E_t	σ_Y	ε_Y	σ_M	ε_M	σ_B	ε_B	h	b	A_0
No.	MPa	MPa	%	MPa	%	MPa	%	mm	mm	mm²
1	-0,466	-	-	1,08	180,3	0,547	1934,5	0,87	4,3	3,74
2	1,28	-	-	1,05	182,2	0,596	1934,6	0,72	4,2	3,02
3	2,77	-	-	1,12	193,2	0,548	1918,6	0,82	4,2	3,44
4	-0,468	-	-	1,07	189,8	0,424	1849,9	0,63	4,1	2,58
5	-0,0258	0,549	20,1	1,06	172,7	0,491	1864,1	0,63	3,7	2,33

Statistics:

Series	E_t	σ_Y	ε_Y	σ_M	ε_M	σ_B	ε_B	h	b	A_0
n = 5	MPa	MPa	%	MPa	%	MPa	%	mm	mm	mm²
x̄	0,619	0,549	20,1	1,08	183,6	0,521	1900,3	0,734	4,1	3,02
s	1,40	-	-	0,0269	8,1	0,0661	40,4	0,1092	0,2345	0,58
ν	-	-	-	2,50	4,41	12,68	2,13	14,88	5,72	19,32

Series graph:

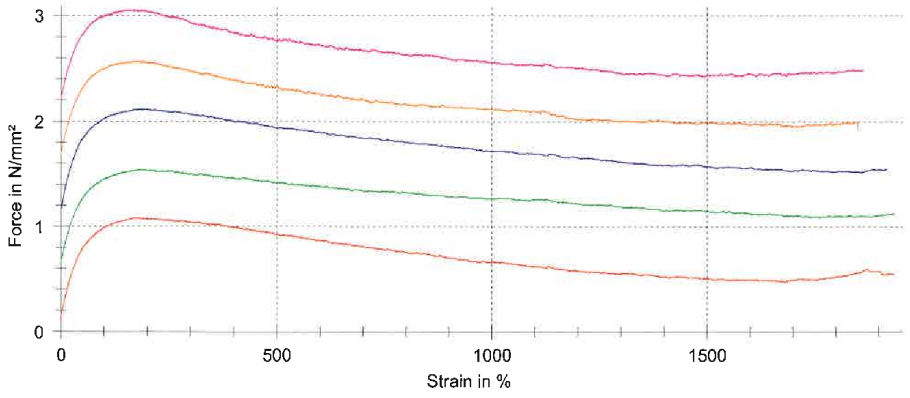

CCR 299 UHMWPP 180°C.ZP2 **Page 1/1**

Table A.11 Stress relaxation data from UHMWaPP.

No.	F_{max} /N	$dL(F_{max})$ /mm	$dL(F_{max})$ /%	a_0 /mm	b_0 /mm
1	3.084	59.77	119.5	0.90	3.92
2	3.411	59.78	119.6	0.90	4.09
3	3.010	59.91	119.8	0.82	4.16
4	3.031	59.93	119.9	0.85	4.16
Statistics, n = 4					
$\bar{x}$	3.134	59.85	119.7	0.868	4.08
s	0.188	0.085	0.1709	0.0395	0.113
ν [%]	5.985	0.143	0.1428	4.55	2.77

A.4. Supplementary data for Chapter Five

A.4.1. Ethylene-propylene copolymerisation data

Table A.12 Polymerisation data using $\mathbf{2_{sMAO}}$. Polymerisation conditions: 10 mg catalyst, [Al]/[Ti] = 1000, 30 minutes, 50 mL hexanes.

p(E) /bar	p(P) /bar	Temperature /°C	Cocatalyst	Activity /kg_{EPM} mol^{-1} h^{-1} bar^{-1}	M_w /kDa	PDI	x_P (wt%)
2	0	60	MAO	1684 ± 476	2631.3	5.5	0.0
1	1	60	MAO	547 ± 289	290.4	3.1	54.0
0	2	60	MAO	3156 ± 677	633.9	2.2	100.0
2	0	60	TIBA	3719 ± 106	2087.5	5.2	0.0
1.5	0.5	60	TIBA	3107 ± 214	158.7	2.6	20.0
1	1	60	TIBA	3313 ± 64	149.7	2.3	42.5
0.5	1.5	60	TIBA	2803 ± 109	162.5	2.4	70.2
0	2	60	TIBA	279 ± 2	256.5	2.4	100.0
1	1	30	TIBA	2885 ± 229	275.2	2.6	41.0
1	1	40	TIBA	2674 ± 46	234.4	2.3	41.2
1	1	50	TIBA	3726 ± 168	168.8	2.4	40.1
1	1	60	TIBA	3313 ± 64	149.7	2.3	42.5
1	1	70	TIBA	3464 ± 97	147.1	2.6	43.2
1	1	80	TIBA	2157 ± 501	127.1	2.4	47.1
1	1	90	TIBA	1623 ± 476	97.6	2.6	47.3

A.4.2. Ethylene-propylene-diene terpolymerisation data

Table A.13 Polymerisation data using $\mathbf{2}_{\mathbf{sMAO}}$. Polymerisation conditions: 10 mg catalyst, 150 mg TIBA, 30 minutes, 50 mL hexanes, 60 °C.

p(E) /bar	*p*(P) /bar	ENB /µL	[ENB] /mM	Activity /kg_{EPM} mol^{-1} h^{-1} bar^{-1}	M_w /kDa	PDI	x_E (mol%)	x_P (mol%)	x_{ENB} (mol%)
1	1	0	0.0	3313 ± 64	149.7	2.3	43.6	56.4	0.0
0.6	0.6	78	11.6	5155 ± 254	165.4	2.4	55.9	42.2	1.8
1	1	156	23.2	2903 ± 155	199.9	2.5	56.1	39.8	4.1
1	1	312	46.4	1622 ± 281	185.1	2.7	58.3	37.0	4.7
0.6	0.6	625	92.9	1065 ± 38	203.9	3.2	51.0	35.6	13.4

A.4.3. Propylene-hexene copolymerisation data

Table A.14 Polymerisation data using $\mathbf{2}_{\mathbf{sMAO}}$. Polymerisation conditions: 10 mg catalyst, [MAO]/[Ti] = 1000, 30 minutes, 50 mL hexanes.

C6 /µL	[C6] /mM	Temperature /°C	Activity /kg_{EPM} mol^{-1} h^{-1} bar^{-1}	M_w /kDa	PDI	x_{C6} (mol%)
0	0.0	60	3213 ± 595	633.9	2.2	0.0 ± 0.0
156	24.9	60	1812 ± 42	477.3	2.3	1.8 ± 0.6
312	49.9	60	1426 ± 136	493.3	2.4	2.7 ± 0.5
625	100.0	60	1875 ± 446	434.9	2.3	6.6 ± 0.3
937	149.9	60	1645 ± 107	448.1	2.3	5.7 ± 1.1
1250	199.9	60	860 ± 280	466.6	2.3	8.4 ± 0.2

A.4.4. Ethylene-linear-α-olefin copolymerisation data

Table A.15 Polymerisation data using $\mathbf{2}_{\mathbf{sMAO}}$. Polymerisation conditions: 10 mg catalyst, 150 mg TIBA, 30 minutes, 50 mL hexanes.

n	LAO /μL	[LAO] /mM	T_p /°C	Activity /kg_{EPM} mol^{-1} h^{-1} bar^{-1}	M_w /kDa	PDI	x_{LAO}, GPC-IR (wt%)	x_{LAO}, ^{13}C NMR (wt%)	T_m /°C	α (%)
6	156	24.9	30	2285 ± 693	2021.4	3.2	0.0		122.3	47
6	312	49.9	30	2196 ± 865	1501.4	3.8	3.1		117.7	44
6	625	100.0	30	3824 ± 1756	856.8	3.3	11.1		104.5	41
6	156	24.9	40	2430 ± 230	1987.4	3.3	0.0		121.5	48
6	312	49.9	40	2245 ± 55	1527.4	4.0	4.9		114.5	42
6	625	100.0	40	4002 ± 903	669.7	4.2	9.1		113.2	17
6	156	24.9	50	3507 ± 244	1699.0	3.9	0.7		118.7	48
6	312	49.9	50	3871 ± 18	1290.9	4.8	5.3		114.4	39
6	625	100.0	50	3227 ± 230	292.9	3.3	14.7		95.3	17
6	156	24.9	60	3388 ± 15	1516.3	4.2	1.9	4.2	115.6	33
6	312	49.9	60	4218 ± 219	1070.5	4.9	5.0	6.7	112.9	20
6	625	100.0	60	2540 ± 50	181.7	3.0	15.3	19.7	82.3	22
6	937	149.9	60	2417 ± 270	191.6	3.6	23.5	31.1	61.8	24
6	1250	199.9	60	1942 ± 645	194.5	2.9	29.4	37.4	55.4	13
6	2500	399.8	60	3044 ± 55	162.2	2.7	46.5	61.6	-	Amorphous
6	5000	799.7	60	2590 ± 696	169.1	2.5	66.6	86.0	-	Amorphous
6	156	24.9	70	3494 ± 139	1057.5	4.7	2.9		116.4	42
6	312	49.9	70	4013 ± 316	807.1	5.6	4.9		115.1	39
6	625	100.0	70	2602 ± 12	182.2	3.5	17.4		82.2	33
6	156	24.9	80	3533 ± 440	875.7	4.7	4.9		115.8	45

6	312	49.9	80	2254 ± 185	185.9	3.5	5.8		114.6	42
6	625	100.0	80	3477 ± 133	146.0	3.2	3.4		98.1	20
6	156	24.9	90	1607 ± 593	332.9	7.7	5.3		110.2	39
6	312	49.9	90	1669 ± 284	154.3	4.0	11.0		108.5	36
6	625	100.0	90	1919 ± 162	125.7	3.2	18.6		74.6	22
8	156	19.9	30	1991 ± 229	2473.8	4.2	0.0		126.3	56
8	312	39.8	30	2057 ± 150	2334.8	4.7	1.8		124.6	50
8	625	79.6	30	3057 ± 141	1262.4	4.3	10.1		115.3	34
8	156	19.9	40	2239 ± 58	2389.5	3.9	0.0		124.4	54
8	312	39.8	40	2467 ± 454	2018.6	3.8	1.0		121.0	45
8	625	79.6	40	4486 ± 167	933.0	3.9	10.2		111.1	34
8	156	19.9	50	2624 ± 327	1739.4	4.6	0.8		119.7	49
8	312	39.8	50	2999 ± 16	1583.3	4.1	1.3		115.8	45
8	625	79.6	50	3800 ± 88	884.8	4.5	7.0		108.2	32
8	156	19.9	60	2729 ± 87	1619.1	4.2	2.1	1.8	123.2	63
8	312	39.8	60	2952 ± 29	1231.4	4.7	3.3	4.5	115.5	45
8	625	79.6	60	4184 ± 135	631.9	4.2	7.3	8.6	114.5	40
8	937	119.4	60	2823 ± 191	206.2	3.0	17.1	17.3	101.0	27
8	1250	159.3	60	2253 ± 633	183.3	3.1	26.7	24.3	90.6	10
8	2500	318.5	60	2964 ± 1223	166.2	2.5	51.3	65.8	-	Amorphous
8	5000	637.0	60	5875 ± 315	152.4	2.5	70.1	95.7	-	Amorphous
8	156	19.9	70	2515 ± 262	1163.4	4.1	2.6		124.1	54
8	312	39.8	70	2945 ± 890	916.3	4.5	4.3		120.1	52
8	625	79.6	70	2442 ± 44	208.6	4.2	14.3		114.7	46
8	156	19.9	80	2623 ± 198	997.6	4.8	4.2		118.5	45

8	312	39.8	80	3033 ± 89	537.0	5.2	8.2		114.7	37
8	625	79.6	80	2420 ± 2	167.4	3.4	24.3		85.2	22
8	156	19.9	90	2111 ± 119	288.5	6.6	6.7		118.2	40
8	312	39.8	90	1807 ± 124	138.7	3.3	12.3		103.3	37
8	625	79.6	90	2013 ± 65	132.7	3.2	23.5		53.9	18
12	156	14.1	30	2501 ± 67	3284.9	3.4	0.0		131.3	63
12	312	28.1	30	2481 ± 189	3248.7	2.9	0.0		130.0	58
12	625	56.3	30	3486 ± 632	2389.4	4.8	1.3		123.7	49
12	156	14.1	40	2890 ± 70	3200.3	3.1	0.0		130.3	61
12	312	28.1	40	3269 ± 452	2838.9	3.3	0.2		126.7	54
12	625	56.3	40	3507 ± 36	2586.5	3.9	0.0		125.3	55
12	156	14.1	50	3335 ± 244	2205.7	2.7	0.0		128.7	59
12	312	28.1	50	3510 ± 164	2153.1	3.0	0.0		127.6	56
12	625	56.3	50	4253 ± 52	1498.5	4.0	2.0		118.4	42
12	156	14.1	60	3465 ± 80	1925.0	3.6	0.0	1.7	127.7	59
12	312	28.1	60	3876 ± 318	1646.7	3.9	0.0	3.7	124.1	48
12	625	56.3	60	5998 ± 280	979.7	5.1	3.2	9.6	117.4	36
12	937	84.4	60	4291 ± 869	198.0	3.5	17.6	30.5	105.5	7
12	1250	112.6	60	3180 ± 28	206.0	3.1	22.5	43.4	-	Amorphous
12	2500	225.3	60	5066 ± 237	191.8	2.7	37.1	55.7	-	Amorphous
12	5000	450.6	60	7928 ± 366	177.0	2.5	49.3	88.5	-	Amorphous
12	156	14.1	70	3675 ± 275	1597.9	4.0	0.0		125.7	55
12	312	28.1	70	3867 ± 230	969.7	5.1	1.5		118.1	45
12	625	56.3	70	3318 ± 309	229.7	4.1	13.1		115.7	29
12	156	14.1	80	2808 ± 163	989.7	5.2	0.0		122.0	61

12	312	28.1	80	3086 ± 100	697.4	4.4	0.1	116.7	53
12	625	56.3	80	2238 ± 318	200.3	4.4	13.7	104.7	27
12	156	14.1	90	2159 ± 97	776.6	5.6	0.0	120.7	55
12	312	28.1	90	1571 ± 293	147.8	3.7	10.4	107.8	34
12	625	56.3	90	1880 ± 96	128.4	3.5	16.7	94.5	20

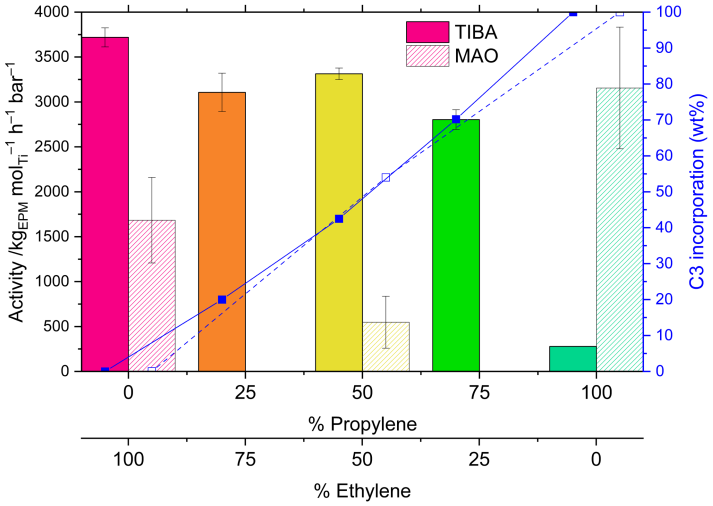

Figure A.177 Mean polymerisation activity and propylene incorporation as a function of monomer feed composition for **2**$_{sMAO}$/TIBA and **2**$_{sMAO}$/MAO. Polymerisation conditions: 10 mg **2**$_{sMAO}$, 2 bar total pressure, 50 mL hexanes, either 150 mg TIBA or MAO ([Al$_{MAO}$]/[Ti] = 1000), 60 °C, and 30 minutes. Incorporation determined by GPC–IR. Error bars shown at one standard deviation.

Linear regression:

TIBA: x_{C3} = (1.008 ± 0.04868) (%P) + (1.504 ± 2.78569); R^2 = 0.9906
MAO: x_{C3} = (1.00 ± 0.0462) (%P) + (–3.667 ± 3.164); R^2 = 0.9957

A.4.5. Gel-permeation chromatography

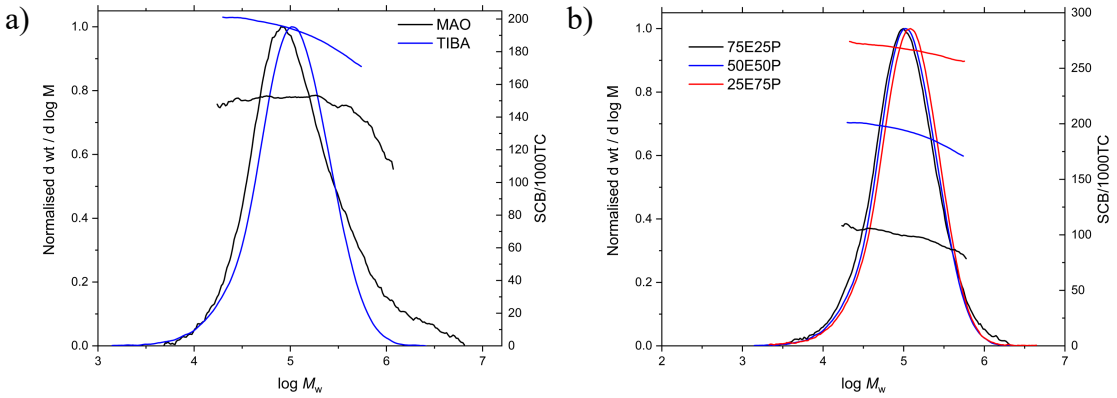

Figure A.178 Gel permeation chromatograms of EPM synthesised by $\mathbf{2}_{\mathbf{sMAO}}$ as a function of a) cocatalyst, or b) monomer feed composition. Polymerisation conditions: 10 mg catalyst, [Al]/[Ti] = 1000, 2 bar ethylene/propylene, 50 mL hexanes, and 30 minutes.

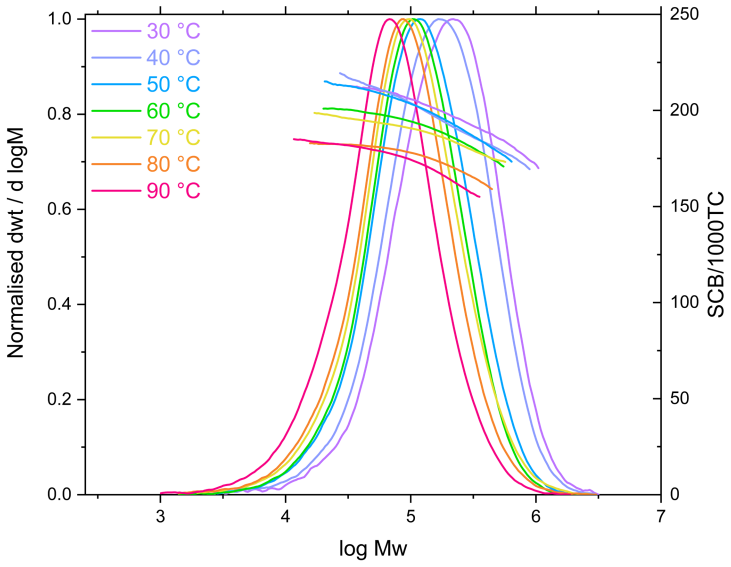

Figure A.179 Gel permeation chromatogram of EPM synthesised by $\mathbf{2}_{\mathbf{sMAO}}$ as a function of polymerisation temperature. Polymerisation conditions: 10 mg catalyst, 150 mg TIBA, 2 bar ethylene/propylene (50:50), 50 mL hexanes, and 30 minutes.

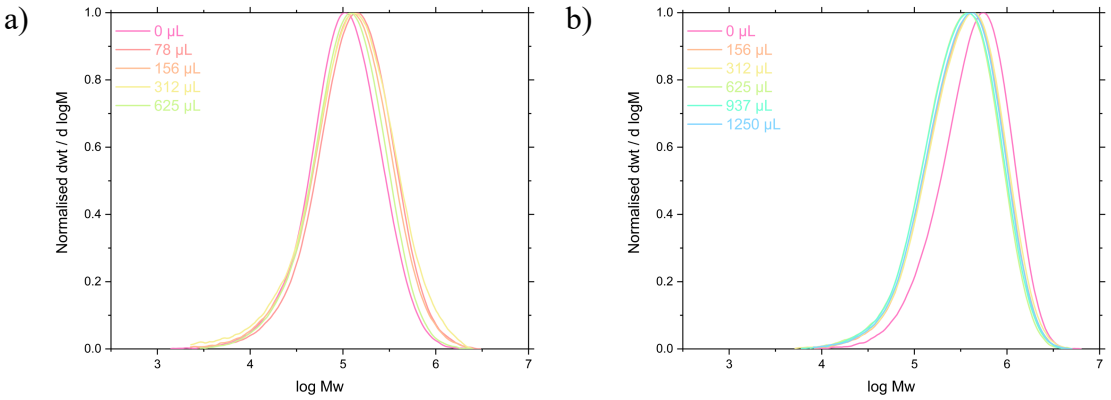

Figure A.180 Gel permeation chromatograms of a) EPDM or b) PH synthesised by **2**$_{sMAO}$ as a function of comonomer loading. Polymerisation conditions: a) 10 mg catalyst, 150 mg TIBA, 2 bar ethylene/propylene (50:50), 50 mL hexanes, and 30 minutes; b) 10 mg catalyst, [Al_{MAO}]/[Ti] = 1000, 2 bar propylene, 50 mL hexanes, and 30 minutes.

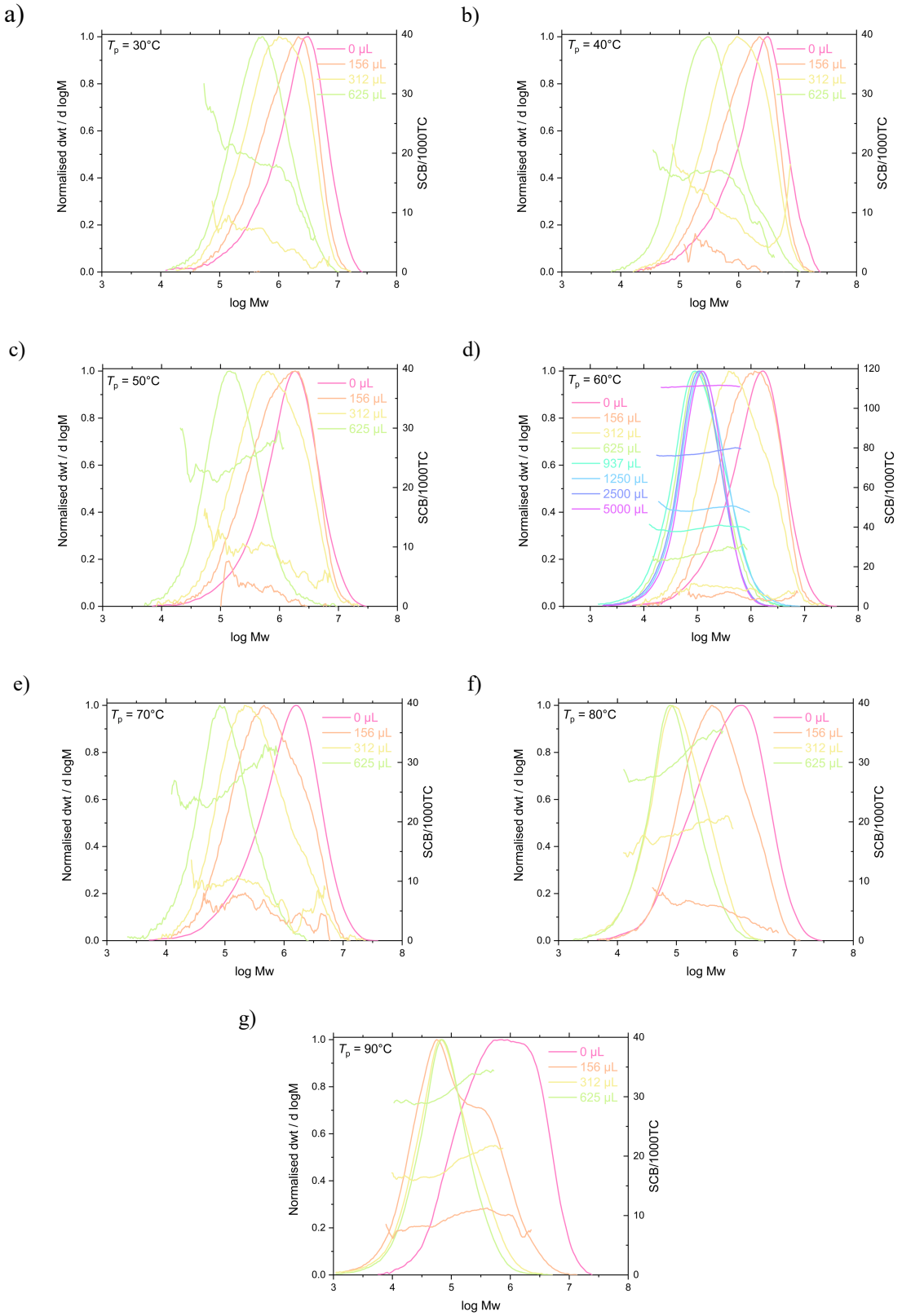

Figure A.181 Gel permeation chromatograms of LLDPE-C6 synthesised by $\mathbf{2}_{\mathbf{sMAO}}$ as a function of comonomer loading. Polymerisation conditions: 10 mg catalyst, 150 mg TIBA, 2 bar ethylene, 0–5 mL 1-hexene, 50 mL hexanes, 30 minutes, and 30–90 °C.

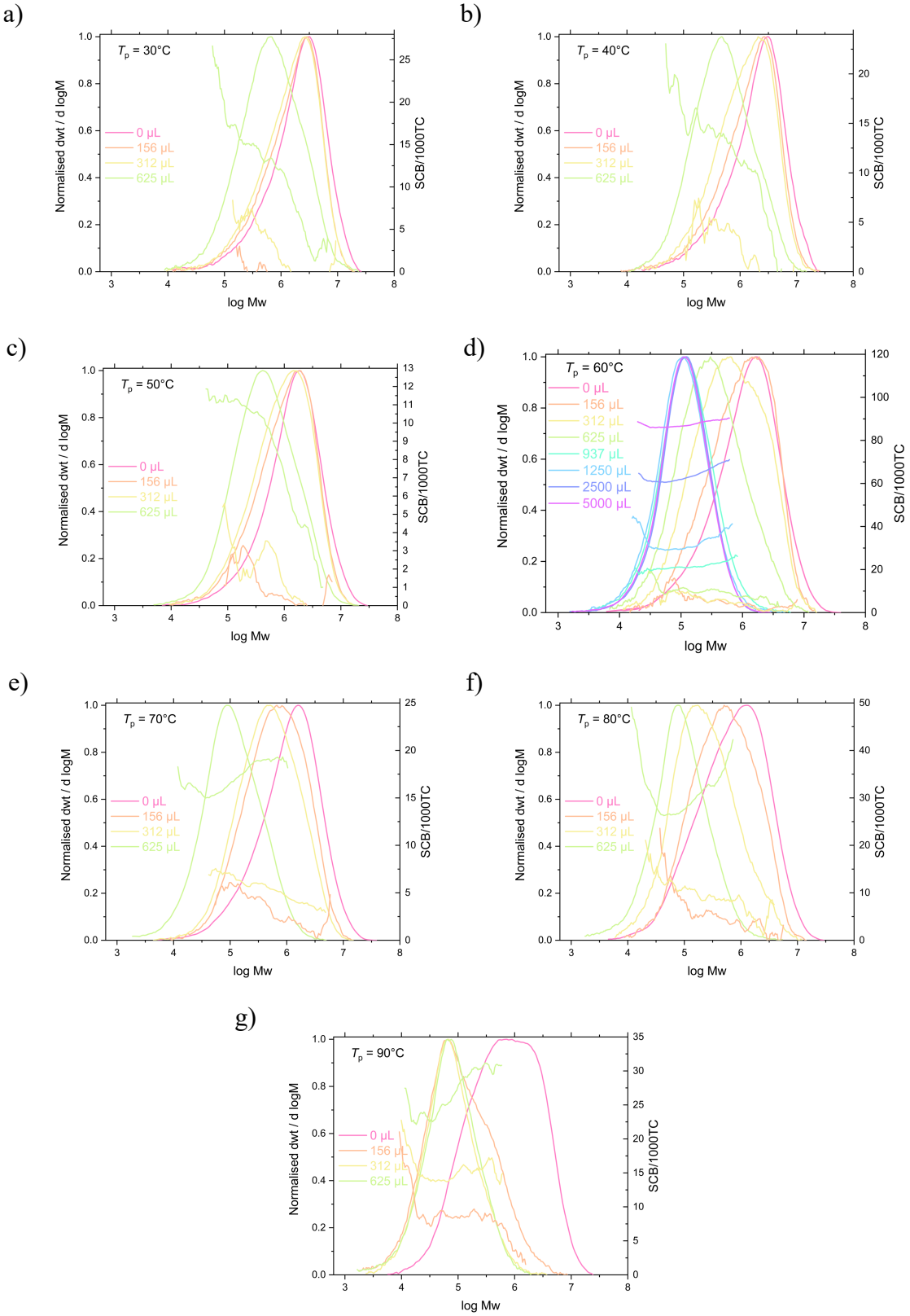

Figure A.182 Gel permeation chromatograms of LLDPE-C8 synthesised by $\mathbf{2}_{\mathbf{sMAO}}$ as a function of comonomer loading. Polymerisation conditions: 10 mg catalyst, 150 mg TIBA, 2 bar ethylene, 0–5 mL 1-octene, 50 mL hexanes, 30 minutes, and 30–90 °C.

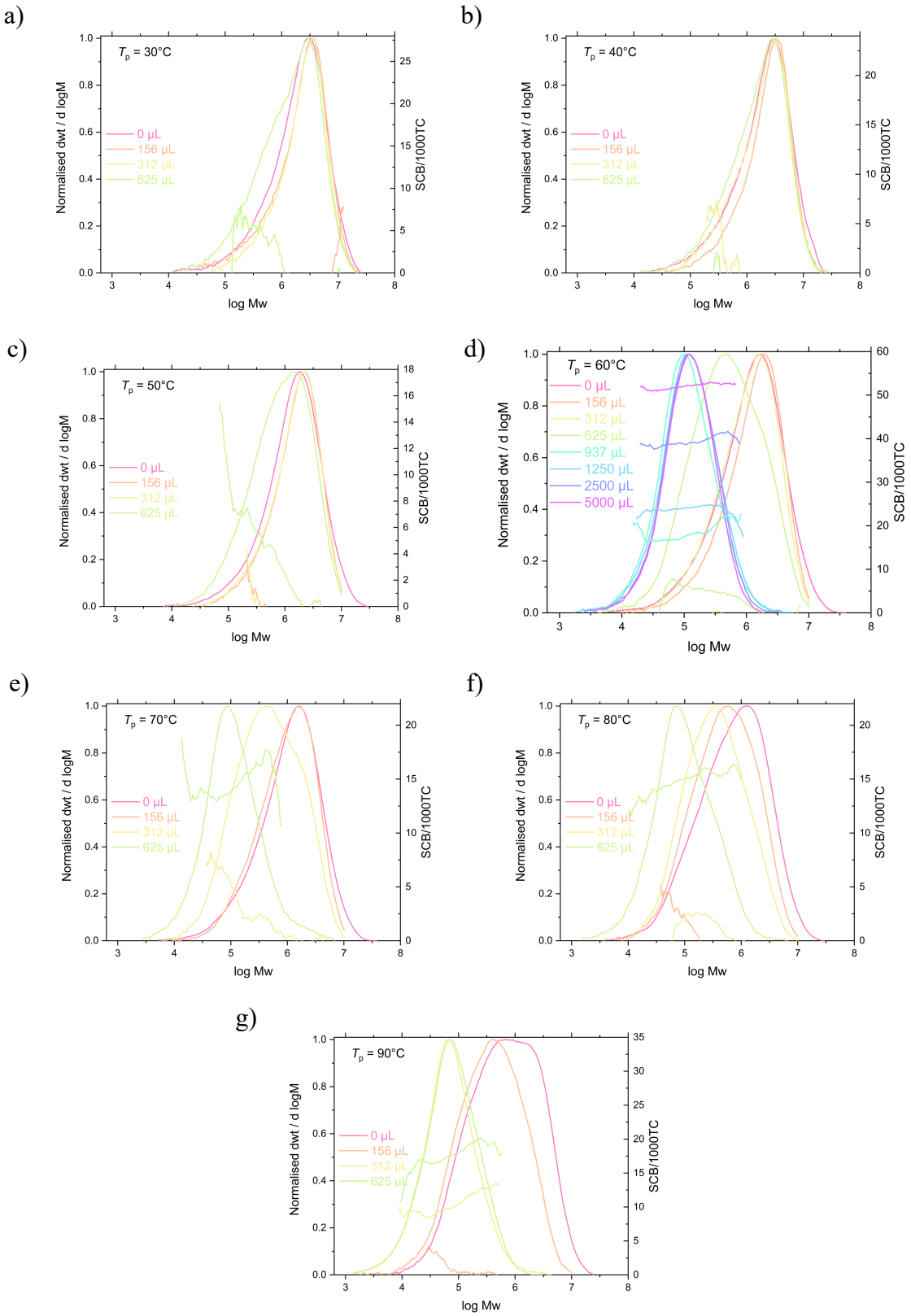

Figure A.183 Gel permeation chromatograms of LLDPE-C12 synthesised by $\mathbf{2}_{\mathbf{sMAO}}$ as a function of comonomer loading. Polymerisation conditions: 10 mg catalyst, 150 mg TIBA, 2 bar ethylene, 0–5 mL 1-dodecene, 50 mL hexanes, 30 minutes, and 30–90 °C.

A.4.6. Differential scanning calorimetry

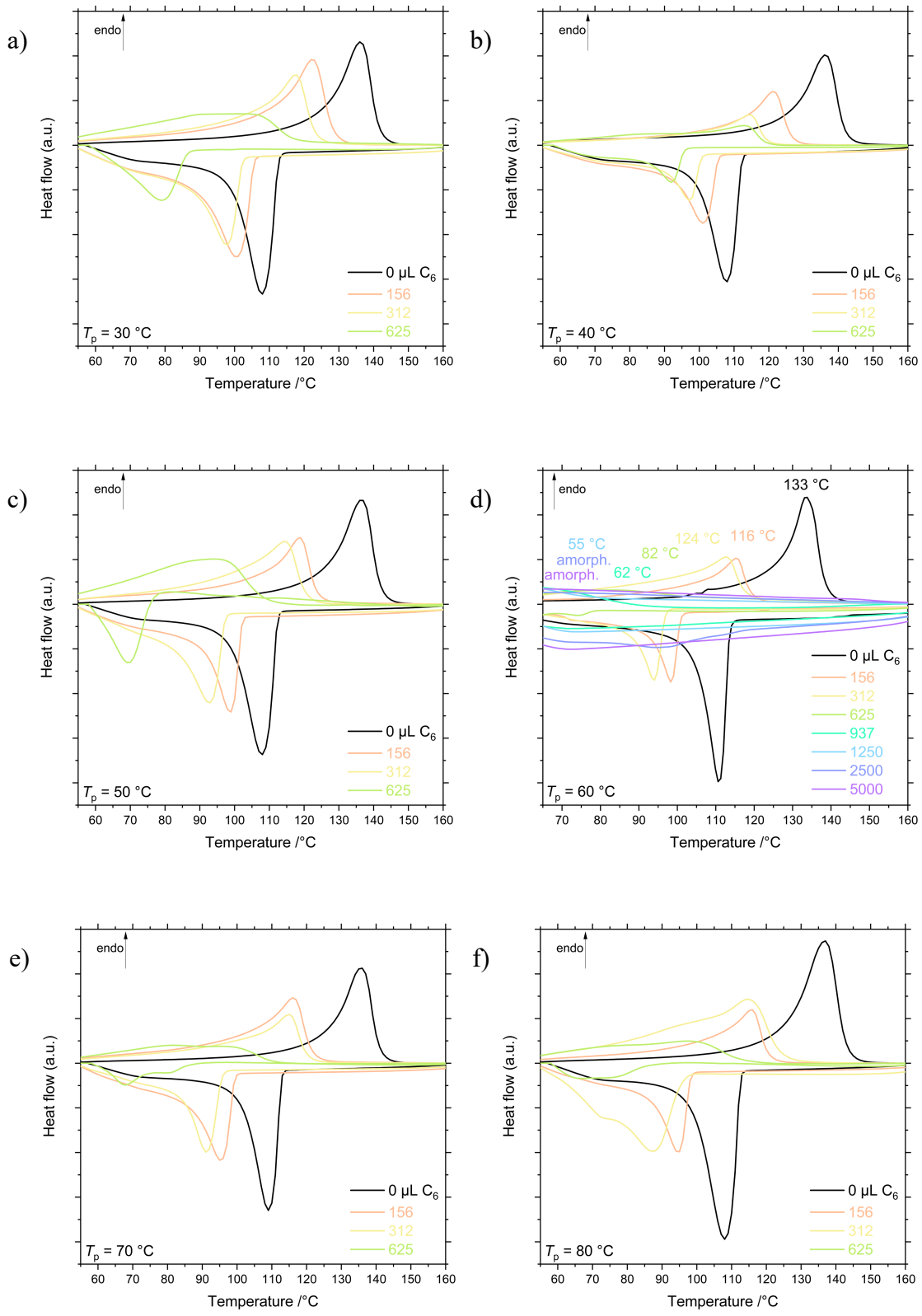

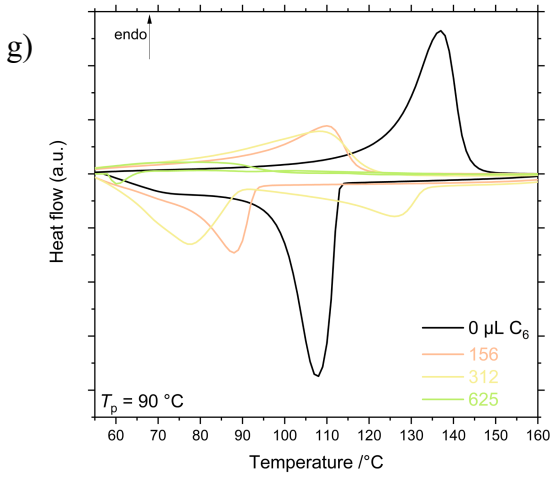

Figure A.184 Differential scanning calorimetry (20 K min^{-1}, second cycle plotted) of LLDPE-C6 synthesised by $\mathbf{2}_{\mathbf{sMAO}}$ as a function of comonomer loading. Polymerisation conditions: 10 mg catalyst, 150 mg TIBA, 2 bar ethylene, 0–5 mL 1-hexene, 50 mL hexanes, 30 minutes, and 30–90 °C.

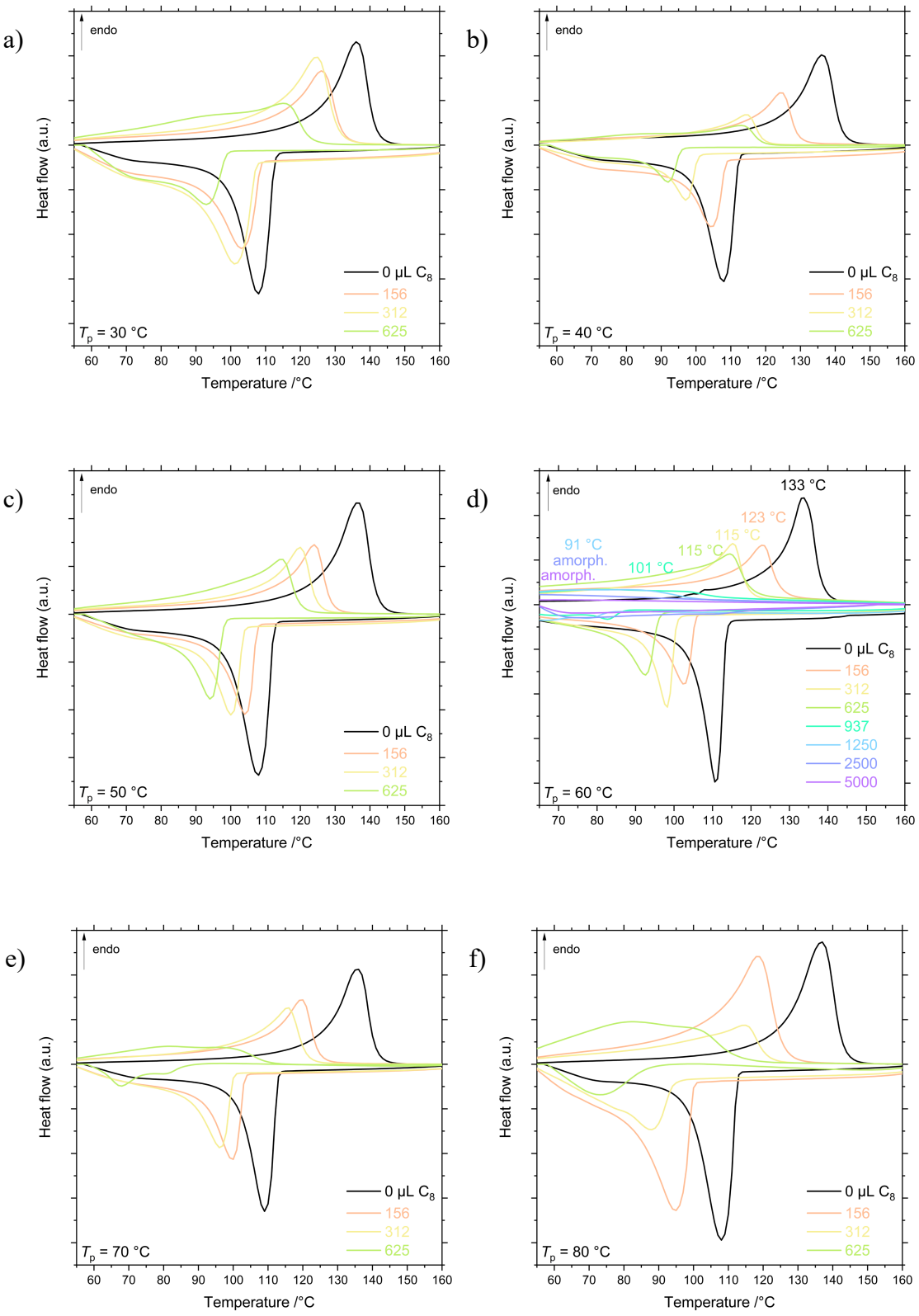
a)
endo
Heat flow (a.u.)
0 µL C8
156
312
625
Tp = 30 °C
Temperature /°C
b)
endo
Heat flow (a.u.)
0 µL C8
156
312
625
Tp = 40 °C
Temperature /°C
c)
endo
Heat flow (a.u.)
0 µL C8
156
312
625
Tp = 50 °C
Temperature /°C
d)
endo
133 °C
123 °C
115 °C
115 °C
91 °C
amorph.
101 °C
amorph.
Heat flow (a.u.)
0 µL C8
156
312
625
937
1250
2500
5000
Tp = 60 °C
Temperature /°C
e)
endo
Heat flow (a.u.)
0 µL C8
156
312
625
Tp = 70 °C
Temperature /°C
f)
endo
Heat flow (a.u.)
0 µL C8
156
312
625
Tp = 80 °C
Temperature /°C

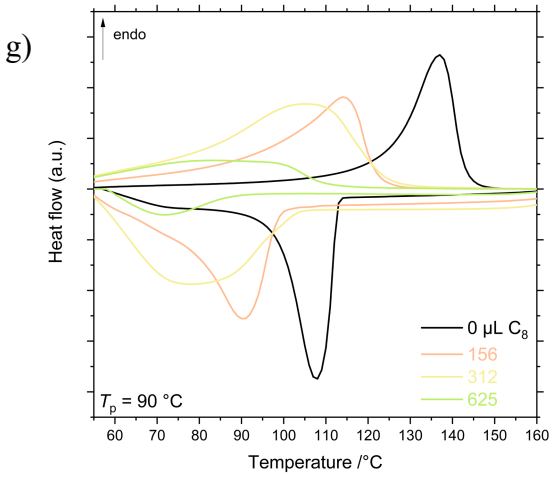

Figure A.185 Differential scanning calorimetry (20 K min^{-1}, second cycle plotted) of LLDPE-C8 synthesised by $\mathbf{2}_{\mathbf{sMAO}}$ as a function of comonomer loading. Polymerisation conditions: 10 mg catalyst, 150 mg TIBA, 2 bar ethylene, 0–5 mL 1-octene, 50 mL hexanes, 30 minutes, and 30–90 °C.

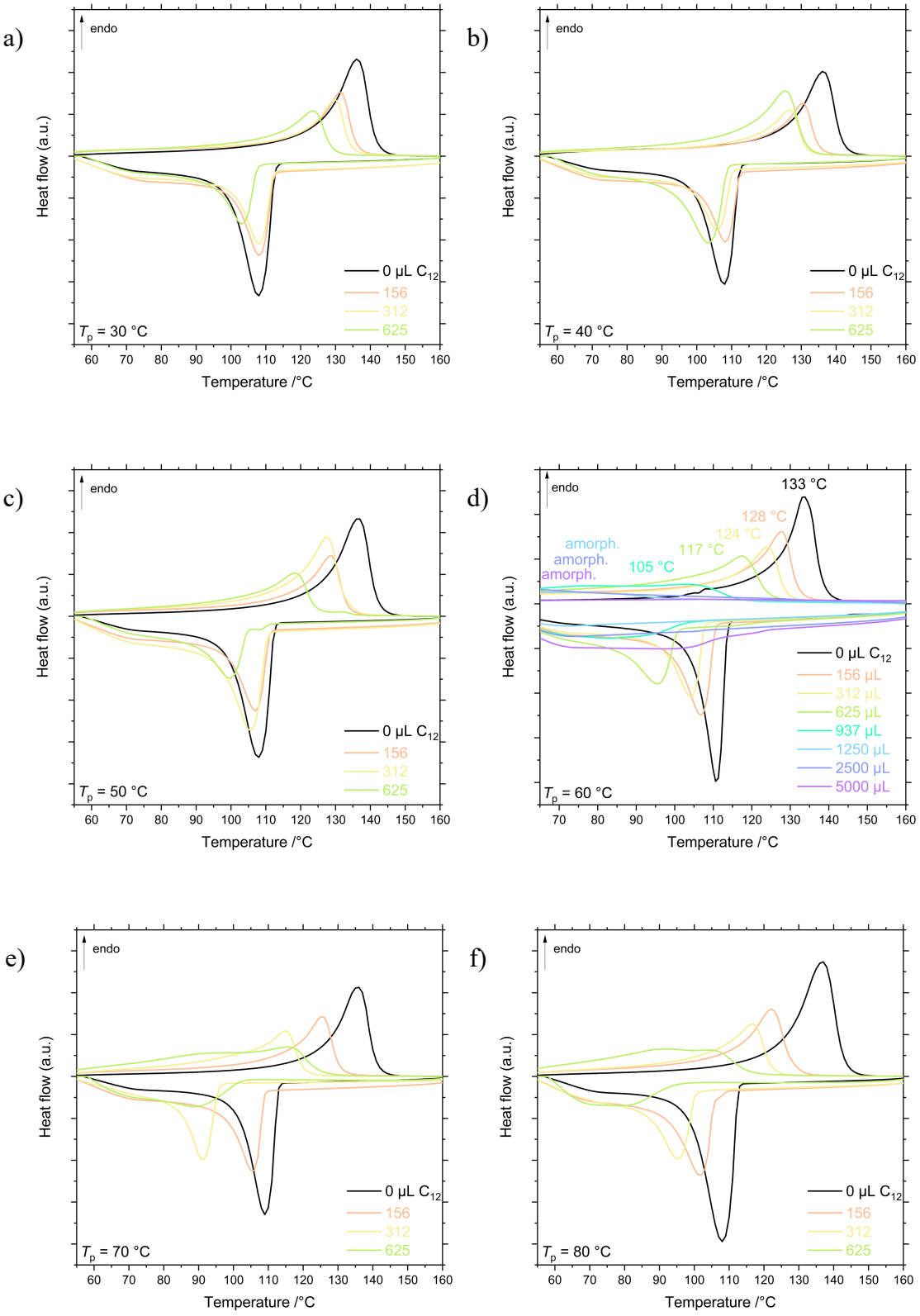
a)
endo
Heat flow (a.u.)
0 µL C12
156
312
625
Tp = 30 °C
60 70 80 90 100 110 120 130 140 150 160
Temperature /°C
b)
endo
Heat flow (a.u.)
0 µL C12
156
312
625
Tp = 40 °C
60 70 80 90 100 110 120 130 140 150 160
Temperature /°C
c)
endo
Heat flow (a.u.)
0 µL C12
156
312
625
Tp = 50 °C
60 70 80 90 100 110 120 130 140 150 160
Temperature /°C
d)
endo
133 °C
128 °C
124 °C
117 °C
105 °C
amorph.
amorph.
amorph.
Heat flow (a.u.)
0 µL C12
156 µL
312 µL
625 µL
937 µL
1250 µL
2500 µL
5000 µL
Tp = 60 °C
70 80 90 100 110 120 130 140 150 160
Temperature /°C
e)
endo
Heat flow (a.u.)
0 µL C12
156
312
625
Tp = 70 °C
60 70 80 90 100 110 120 130 140 150 160
Temperature /°C
f)
endo
Heat flow (a.u.)
0 µL C12
156
312
625
Tp = 80 °C
60 70 80 90 100 110 120 130 140 150 160
Temperature /°C

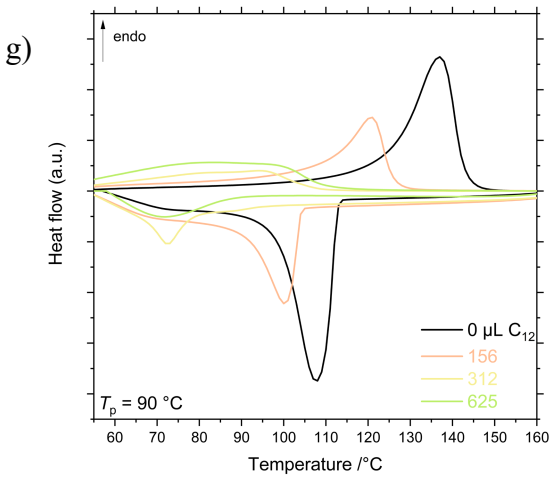

Figure A.186 Differential scanning calorimetry (20 K min^{-1}, second cycle plotted) of LLDPE-C12 synthesised by $\mathbf{2}_{\mathbf{sMAO}}$ as a function of comonomer loading. Polymerisation conditions: 10 mg catalyst, 150 mg TIBA, 2 bar ethylene, 0–5 mL 1-dodecene, 50 mL hexanes, 30 minutes, and 30–90 °C.

A.4.7. NMR spectroscopy

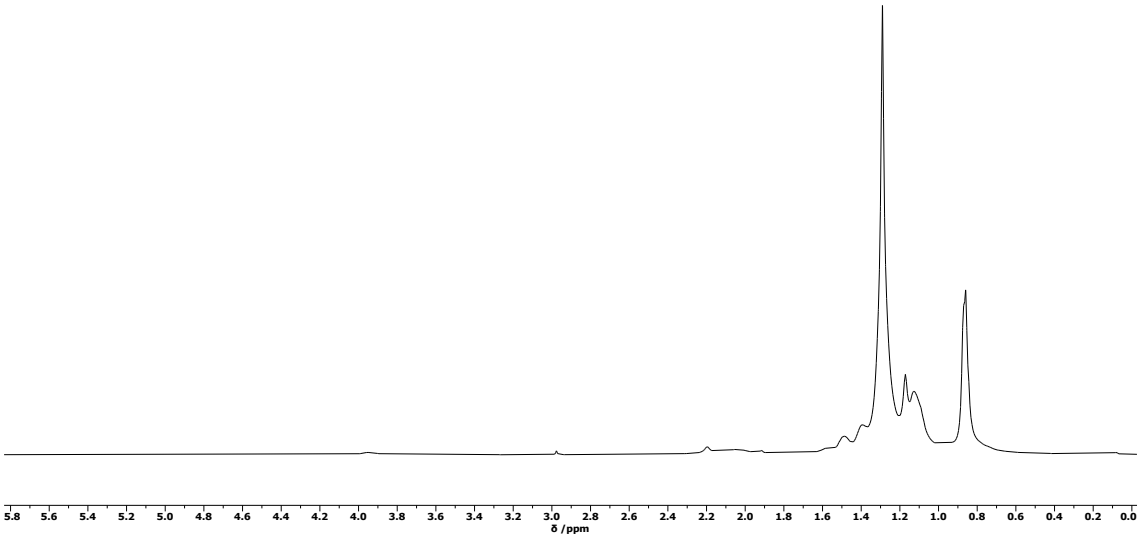

Figure A.187 ^{1}H NMR spectrum (500 MHz, 1,1,2,2-tetrachloroethane-d_2, Cr(acac)$_3$, 403 K) of EPM. Polymerisation conditions: 10 mg $\mathbf{2}_{\mathbf{sMAO}}$, 2 bar ethylene/propylene (50:50), [MAO]/[Ti] = 1000, 50 mL hexanes, 60 °C, and 30 minutes.

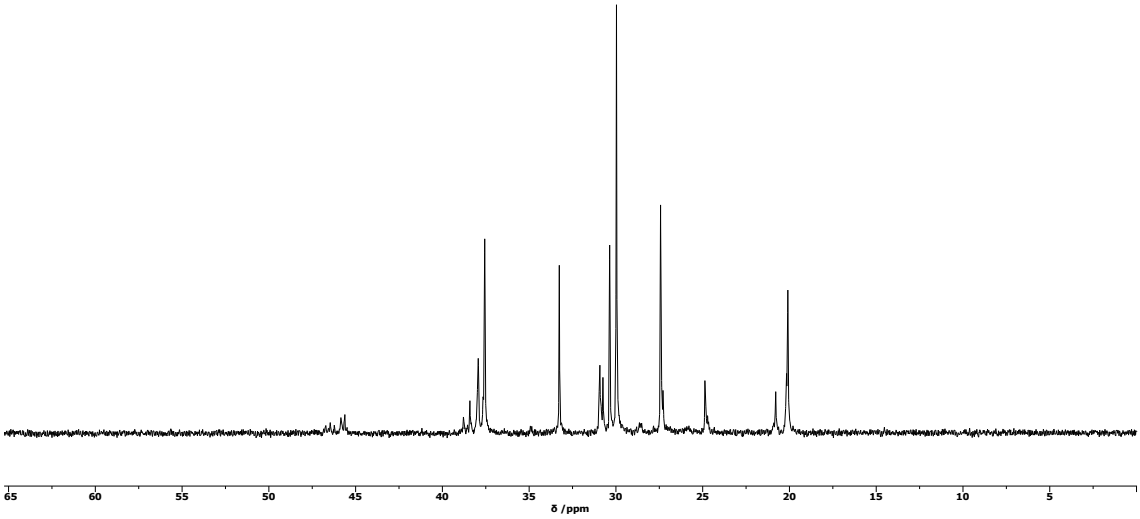

Figure A.188 Quantitative $^{13}C\{^{1}H\}$ NMR spectrum (126 MHz, 1,1,2,2-tetrachloroethane-d_2, $Cr(acac)_3$, 403 K) of EPM. Polymerisation conditions: 10 mg **2**$_{sMAO}$, 2 bar ethylene/propylene (50:50), [MAO]/[Ti] = 1000, 50 mL hexanes, 60 °C, and 30 minutes.

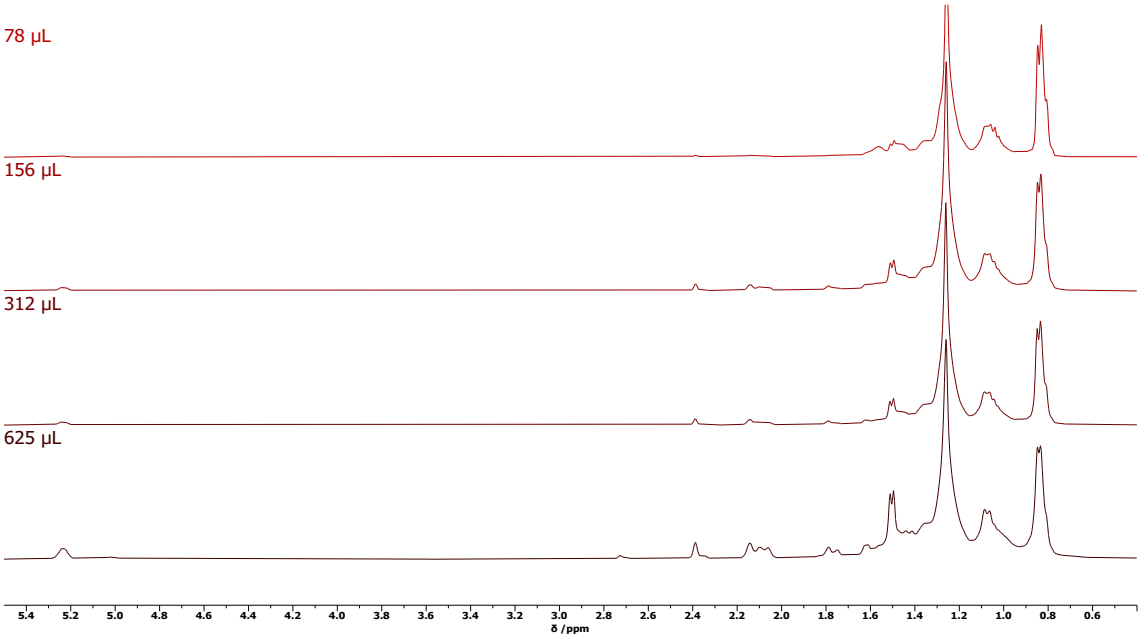

Figure A.189 ^{1}H NMR spectra (400 MHz, chloroform-d_1, 297 K) of EPDM as a function of ENB loading. Polymerisation conditions: 10 mg **2**$_{sMAO}$, 2 bar ethylene/propylene (50:50), 150 mg TIBA, 78–625 µL ENB, 50 mL hexanes, 60 °C, and 30 minutes.

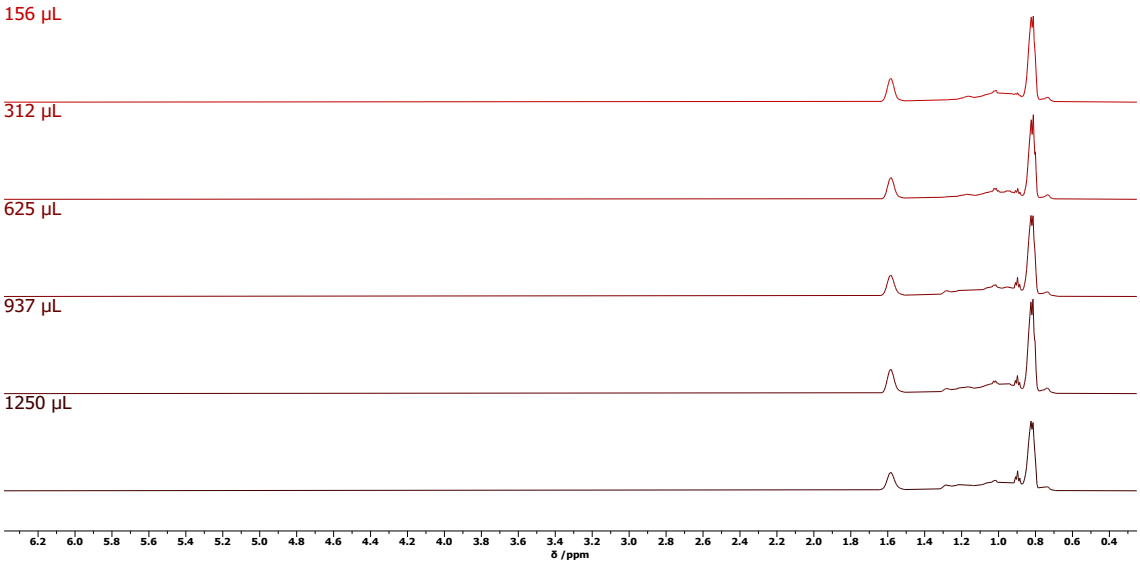

Figure A.190 ^{1}H NMR spectra (600 MHz, chloroform-d_1, 298 K) of PH as a function of C6 loading. Polymerisation conditions: 10 mg **2**$_{sMAO}$, 2 bar propylene, 150 mg TIBA, 156–1250 µL 1-hexene, 50 mL hexanes, 60 °C, and 30 minutes.

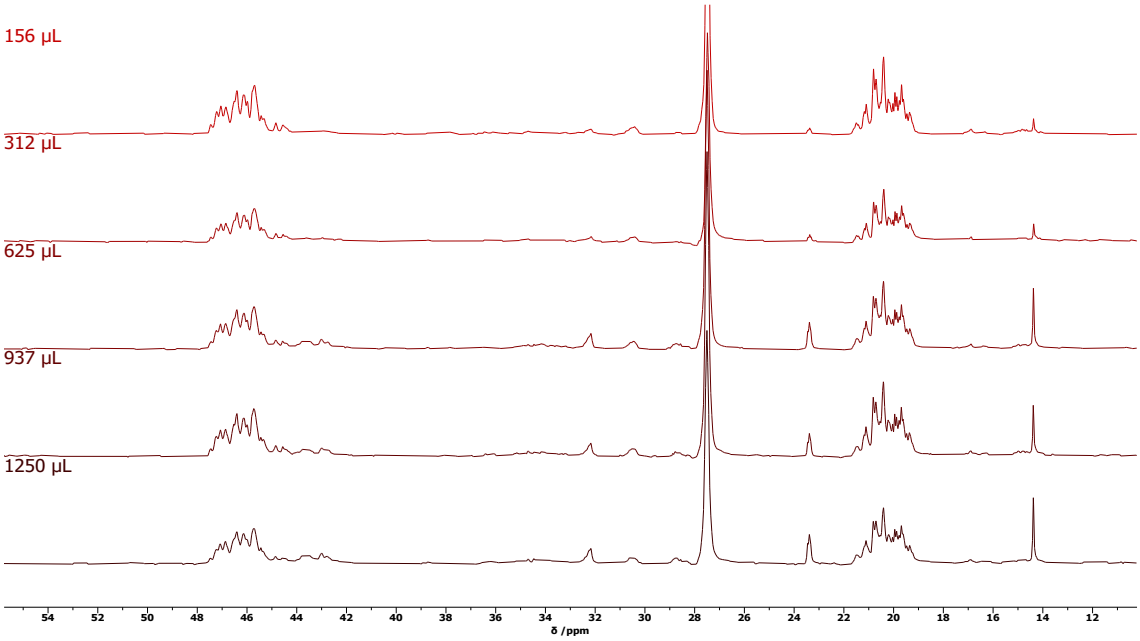

Figure A.191 Quantitative ^{13}C{^{1}H} NMR specta (151 MHz, chloroform-*d*, 298 K) of PH as a function of C6 loading. Polymerisation conditions: 10 mg **2**$_{sMAO}$, 2 bar propylene, 150 mg TIBA, 156–1250 µL 1-hexene, 50 mL hexanes, 60 °C, and 30 minutes.

A.4.8. Designer LLDPE

Table A.16 Target, predicted, and measured parameters for the polymerisations P1–3. M1 shown with a ± 95% confidence interval, experimental data shown as mean ± standard deviation

		Activity /kg_{LLDPE} mol^{-1} h^{-1} bar^{-1}	T_m /°C	α (%)	M_w /kDa	PDI	*x* (wt%)	Conditions	
	Target	*Maximise*	*110*	*Maximise*	*1000*	*Minimise*	-	T_p /°C	61
P1	M1	3424 ± 293	112 ± 4	39 ± 4	846 ± 101	4.1 ± 0.4	7.8 ± 1.7	LAO (C*n*)	8
	Experimental	*3175 ± 271*	*112 ± 3*	*39 ± 7*	*606 ± 281*	*4.1 ± 0.4*	*37.8 ± 4.7*	[LAO] /mM	59
	Target	*Maximise*	*100*	*45*	*500*	*5*	-	T_p /°C	80
P2	M1	2941 ± 322	107 ± 4	35 ± 4	493 ± 112	4.7 ± 0.4	7.1 ± 1.9	LAO (C*n*)	6
	Experimental	*2552 ± 112*	*117 ± 1*	*44 ± 9*	*153 ± 7*	*3.9 ± 0.1*	*7.3 ± 0.8*	[LAO] /mM	47
	Target	*Maximise*	*80*	*25*	*200*	*6.5*	-	T_p /°C	32
P3	M1	3188 ± 1074	95 ± 14	25 ± 13	146 ± 372	5.2 ± 1.3	18.3 ± 6.3	LAO (C*n*)	6
	Experimental	*2286 ± 99*	*58 ± 2*	*23 ± 2*	*355 ± 35*	*3.0 ± 0.1*	*27.5 ± 3.3*	[LAO] /mM	168

Table A.17 Points specifying desirability functions for the optimisation of model M1 towards the properties of P1–3.

	Activity /kg_{LLDPE} mol^{-1} h^{-1} bar^{-1}		T_m /°C		α (%)		M_w /kDa		PDI	
	Value	Weight	Value	Weight	Value	Weight	Value	Weight	Value	Weight
P1	5000	0.9	120	0.1	75	0.98	1500	0.01	8	0.1
	2000	0.3	110	1	50	0.5	800	1	5.5	0.2
	500	0.05	100	0.1	30	0.05	650	0.01	2.5	0.9
P2	5000	0.9	110	0.1	60	0.1	600	0.1	6	0.1
	2000	0.3	100	1	45	1	500	1	5	1
	500	0.05	90	0.1	30	0.1	400	0.1	4	0.1
P3	5000	0.9	90	0.1	35	0.1	250	0.1	7.5	0.1
	2000	0.3	80	1	25	1	200	1	6.5	1
	500	0.05	70	0.1	15	0.1	150	0.1	5.5	0.1

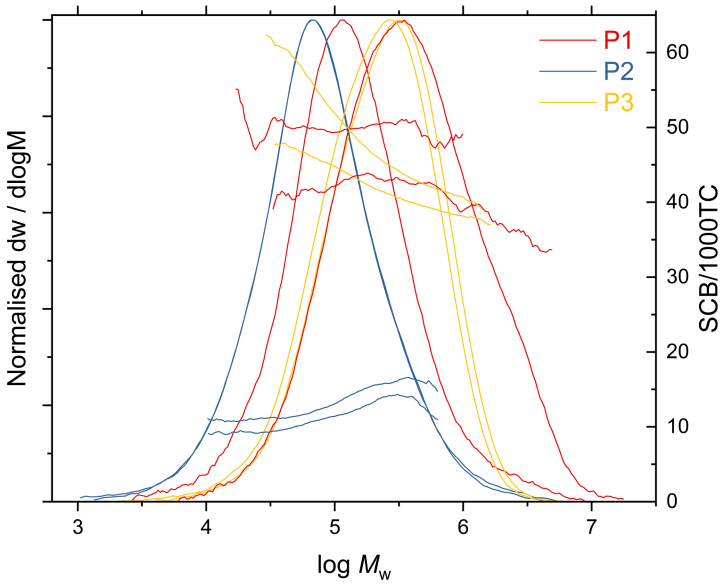

Figure A.192 Gel permeation chromatograms of LLDPE samples P1–3 synthesised by **2**$_{sMAO}$. Polymerisation conditions: 10 mg catalyst, 150 mg TIBA, 2 bar ethylene, 50 mL hexanes, and 30 minutes; P1: 61 °C, 463 µL 1-octene; P2: 80 °C, 294 µL 1-hexene; P3: 32 °C, 1050 µL 1-hexene.

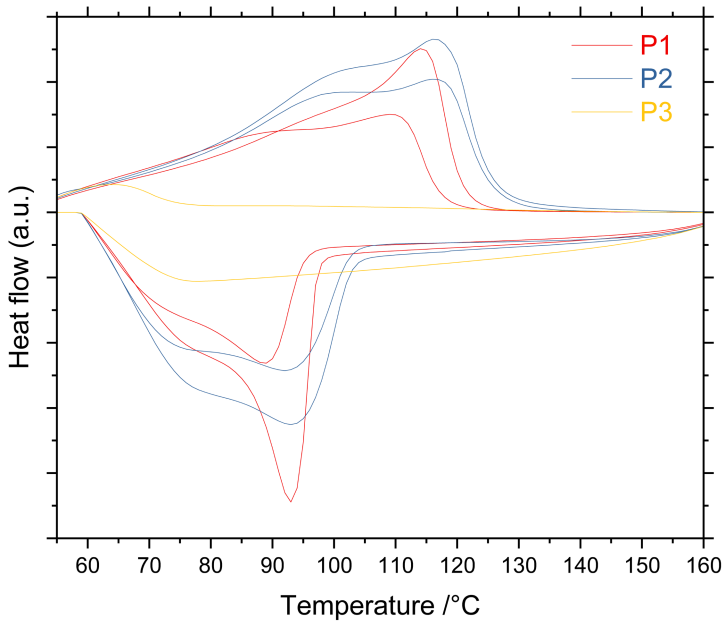

Figure A.193 Differential scanning calorimetry of LLDPE samples P1–3 synthesised by **2**$_{sMAO}$. Polymerisation conditions: 10 mg catalyst, 150 mg TIBA, 2 bar ethylene, 50 mL hexanes, and 30 minutes; P1: 61 °C, 463 µL 1-octene; P2: 80 °C, 294 µL 1-hexene; P3: 32 °C, 1050 µL 1-hexene.

See Appendix B for M1 analysis of variance (ANOVA).

A.5. Mechanical testing report (Norner AS)

Test Report

Report ID.	Norner project no	Date	Classification
NO21750	2218766	07.12.2021	Confidential

Customer / Contact / Reference	Customer Responsible
University of Oxford / Clement Collins Rice	Jørgen Nyhus

Title

Ultra-high Molecular samples for testing

Author(s)	Approved by
Thea Høibjerg Glittum	Heidi Nornes Bryntesen

Background

Two samples have arrived for testing

- **CCR298** – Ultra-high Molecular Weight Polyethylene (UHMWPE), ca. 25g
- **CCR299** – Ultra-high Molecular Weight amorphous Polypropylene (UHMWaPP), ca. 30g

The following test have been done

- Density (according to ISO 1183)
- Tensile (according to ISO 527 using 5A test specimens)

Conclusions/Proposals

Results from testing is given in table 1 and 2

Proposal for further work (optional)

Attachments (optional)

Legal notice[1]

Norner AS
Asdalstrand 291
NO-3962 Stathelle
Norway

Tel: +47 35 57 80 00
Web: www.norner.no
Mail: post@norner.no

Org.nr: NO898736 032MVA

1 Introduction

Two samples have arrived for testing:

- **CCR298** – Ultra-high Molecular Weight Polyethylene (UHMWPE), ca. 25g
  - For routine tensile stress-strain testing, according to international standard test methods. Sample preparation by press+milling as suggested.
  - If there is enough material to measure impact strength, that would be very desirable too.
- **CCR299** – Ultra-high Molecular Weight amorphous Polypropylene (UHMWaPP), ca. 30g
  - This is a reasonably novel material, so we're looking to characterise it as fully as possible. As it is rubbery, looking at elastic stress-strain hysteresis (see attachment) as well as more standard ultimate tensile strength would be brilliant.

The PP sample was cut and milled to powder like material before further handling. Both samples were added a thermal stabilizer (BHT) before pressed into pates (size 80x60x1mm). From the plates test specimens were stamped out.

The following test have been done

- Density (according to ISO 1183)
- Tensile (according to ISO 527 using 5A test specimens)

2 Experiment/methods

Sample preparation:

The PP sample needed to be milled and homogenized before plate pressing. The PP felt jelly-like and was first cut up by a scissor and then milled using a cooling unit (liquid nitrogen)

Both samples were added BHT before pressed to plates, this to prevent degradation during heating.

The samples were pressed using first 200° and then 180 °C for the PP and 180°C for the PE sample.

Figure below shows the plates pressed, sample stamped out from the plate and tensile dogbones after end testing.



Figure 1 CCR298 (UHMWPE) CCR299 (UHMWaPP)

2.1.1 Density/ Specific weight/ ISO 1183-1 2012

Method	Method to determine the density of solid plastics. According to ISO 1183-1 2012 Method A, Immersion method
Definitions	Density (ρ) is the relationship between the mass (m) and the volume (V) of a specific amount of material, results are given in kg/m³ or g/cm³.
Instrument	Analytical weight, Mettler Toledo XS204, with 4 decimals, density kit and density program.
Specimen type	Specimens shall be in a suitable void-free form, and minimum 1g.
Test conditions	Testing at room temperature Parallels: 3

2.1.2 Tensile test / ISO527-1/-2

Method	Determination of tensile properties – Based on ISO 527-1/2 Part1: General principles Part 2: Test conditions for moulding and extrusion plastics
Instrument	Zwick Z010 at room temperature
Definitions	Modulus, MPa – slope of the stress/strain curve in the strain interval between 0.05 % and 0.25 %. Strain at strength, % - strain at which the strength is reached Stress at break, MPa – stress at which the specimen breaks Strain at break, % - when the break occurs before yielding
Specimen type	5A: Punched from a plate
Test conditions	Testing speed: 50 mm/min Tensile modulus: 1 mm /min Test temperature: 23 °C Gauge length Type: 5A:L0= 20 mm Gripping Distance L: 50 mm Parallels: 5

3 Results

3.1.1 Density/ Specific weight/ ISO 1183-1

Table 1 – results from density

	Results in kg/m³
CCR298	930
CCR299*	876

* CCR299 sample pressed at 180 °C and 200°C gave the same result

3.1.2 Tensile test / ISO527-1/-2

The CCR299 gave no reasonable results when measuring the modulus. The elongation for this was higher than we were able to test so the sample was stopped at 1900%

Table 2 – Tensile results (standard deviation)

	Tensile modulus MPa	Tensile strength MPa	Tensile strain at strength (%)	Tensile stress at break (MPa	Tensile strain at break
CCR298	627 (66.5)	50.9 (3.2)	198 (18.3	50.2 (3.6)	200% (18.3)
CCR299*	NR	1.08 (0)	184 (8.1)	NR (stopped)	>1900%

* CCR299 sample pressed at 180 °C and 200°C gave the same result

[i] ***Legal notice***

Norner has sought to make this document reasonably accurate and reliable within the resource and time frame. The information contained in this document is given in good faith. Norner cannot assume any liability expressed or implied in the presentation of this data, nor should information contained herein be construed as granting license to practice any methods or compositions of matter covered by patents.

Appendix B - ANOVA

Least Squares Fit
Effect Summary

Source	LogWorth	PValue
Temperature of polymerisation (°C)	32.969	0.00000
[Comonomer] /mM	24.894	0.00000
Temperature of polymerisation (°C)*Temperature of polymerisation (°C)	9.023	0.00000
Temperature of polymerisation (°C)*Carbons in LAO	8.031	0.00000
[Comonomer] /mM*[Comonomer] /mM	5.559	0.00000
Temperature of polymerisation (°C)*[Comonomer] /mM	5.129	0.00001
Carbons in LAO*[Comonomer] /mM	3.469	0.00034
Carbons in LAO	3.217	0.00061 ^
Carbons in LAO*Carbons in LAO	1.870	0.01350

Response Activity /kg/mol/h/bar
Whole Model
Actual by Predicted Plot

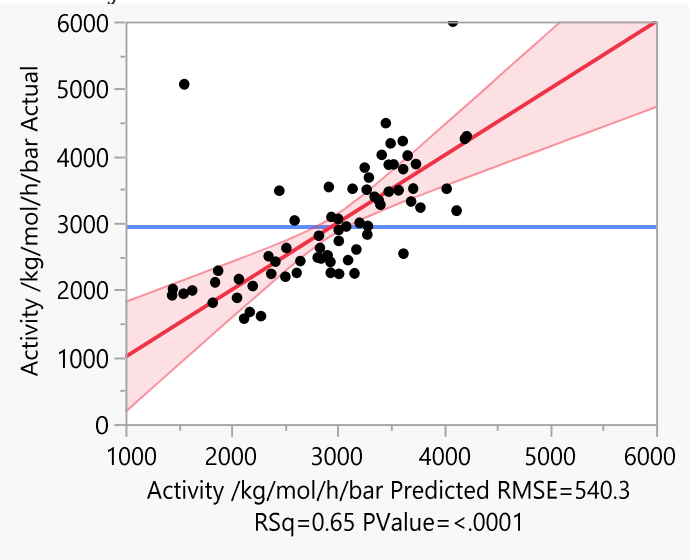

Residual by Predicted Plot

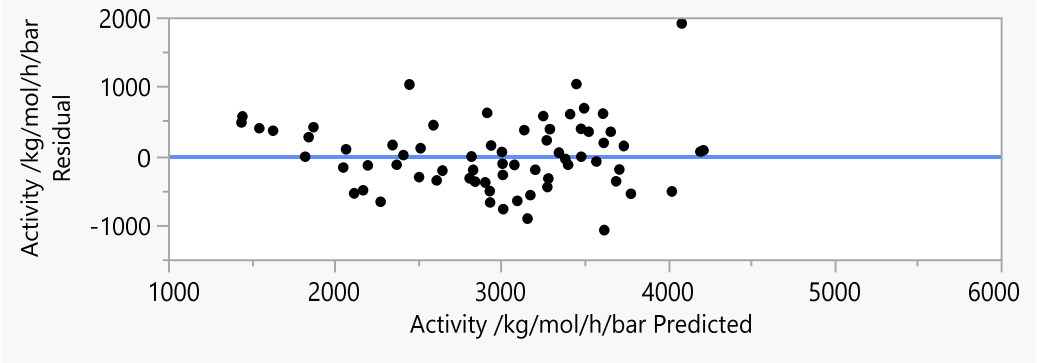

Studentized Residuals

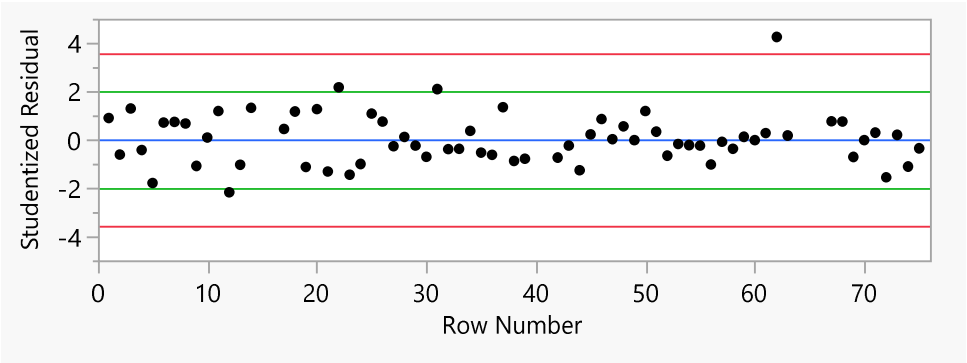

Externally studentized residuals with 95% simultaneous limits (Bonferroni) in red, individual limits in green.

Summary of Fit

RSquare	0.64713
RSquare Adj	0.592374
Root Mean Square Error	540.3003
Mean of Response	2951.417
Observations (or Sum Wgts)	68

Analysis of Variance

Source	DF	Sum of Squares	Mean Square	F Ratio
Model	9	31050924	3450103	11.8185
Error	58	16931618	291924	**Prob > F**
C. Total	67	47982542		<.0001*

Parameter Estimates

Term	Estimate	Std Error	t Ratio	Prob>|t|	LSV0.05	LSN0.05	AdjPower0.05
Intercept	3560.143	407.3258	8.74	<.0001*	815.3512	12.4	1.0000
Temperature of polymerisation (°C)	-14.38824	3.529178	-4.08	0.0001*	7.064418	20.2	0.9681
Carbons in LAO	35.49275	34.6939	1.02	0.3105	69.44738	252.1	0.0512
[Comonomer] /mM	7.6262428	2.607642	2.92	0.0049*	5.219763	33.9	0.7547
(Temperature of polymerisation (°C)-60)*(Carbons in LAO-8.61765)	-2.796495	1.475937	-1.89	0.0631	2.954409	75.5	0.3391
(Temperature of polymerisation (°C)-60)*([Comonomer] /mM-52.9853)	-0.492235	0.135047	-3.64	0.0006*	0.270326	23.7	0.9224
(Carbons in LAO-8.61765)*([Comonomer] /mM-52.9853)	0.5175746	1.200147	0.43	0.6679	2.402355	1407.0	0.0500
(Temperature of polymerisation (°C)-60)*(Temperature of polymerisation (°C)-60)	-1.413549	0.193864	-7.29	<.0001*	0.38806	13.0	1.0000
(Carbons in LAO-8.61765)*(Carbons in LAO-8.61765)	46.442738	18.51938	2.51	0.0150*	37.07056	44.6	0.6006
([Comonomer] /mM-52.9853)*([Comonomer] /mM-52.9853)	-0.139085	0.036646	-3.80	0.0004*	0.073355	22.3	0.9421

Effect Tests

Source	Nparm	DF	Sum of Squares	F Ratio	Prob > F
Temperature of polymerisation (°C)	1	1	4852200	16.6214	0.0001*
Carbons in LAO	1	1	305523	1.0466	0.3105
[Comonomer] /mM	1	1	2496869	8.5531	0.0049*
Temperature of polymerisation (°C)*Carbons in LAO	1	1	1048004	3.5900	0.0631
Temperature of polymerisation (°C)*[Comonomer] /mM	1	1	3878334	13.2854	0.0006*
Carbons in LAO*[Comonomer] /mM	1	1	54293	0.1860	0.6679
Temperature of polymerisation (°C)*Temperature of polymerisation (°C)	1	1	15520293	53.1654	<.0001*
Carbons in LAO*Carbons in LAO	1	1	1835918	6.2890	0.0150*
[Comonomer] /mM*[Comonomer] /mM	1	1	4205058	14.4046	0.0004*

Residual Normal Quantile Plot

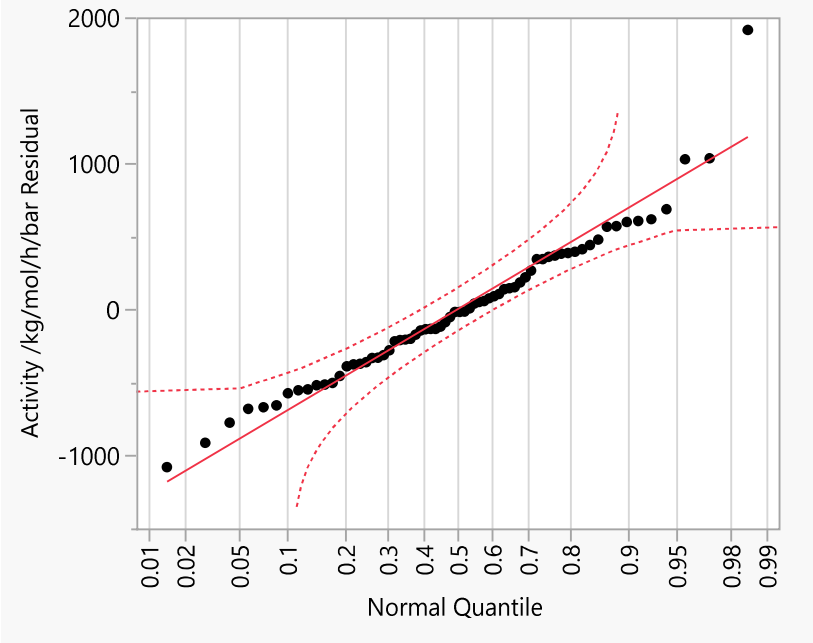

Temperature of polymerisation (°C)
Leverage Plot

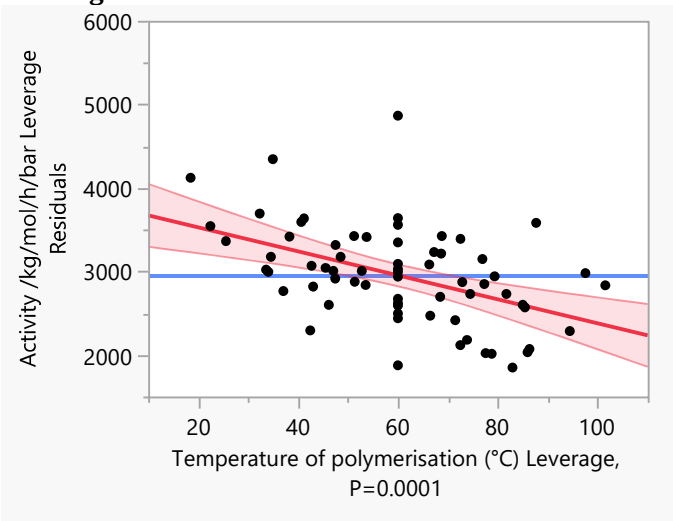

Carbons in LAO
Leverage Plot

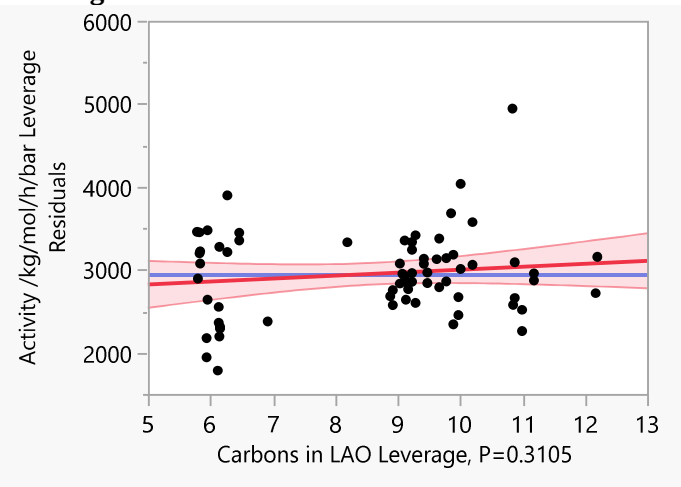

[Comonomer] /mM
Leverage Plot

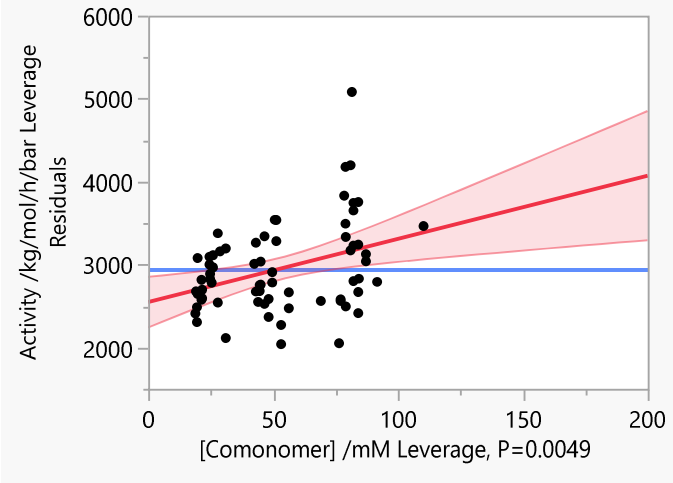

Temperature of polymerisation (°C)*[Comonomer] /mM
Leverage Plot

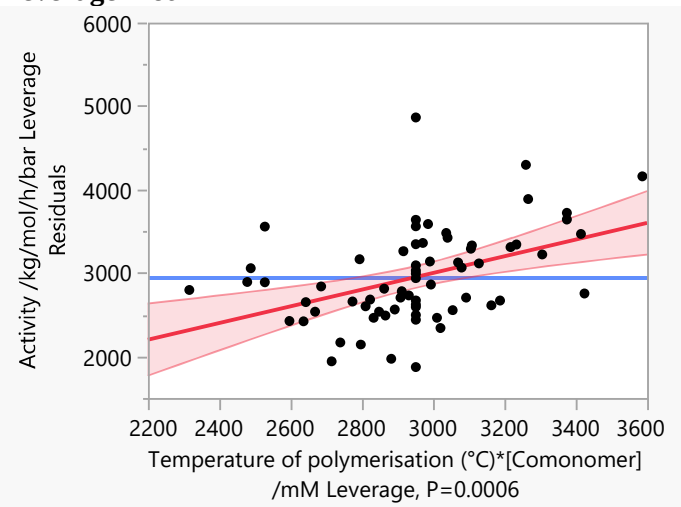

Temperature of polymerisation (°C)*Carbons in LAO
Leverage Plot

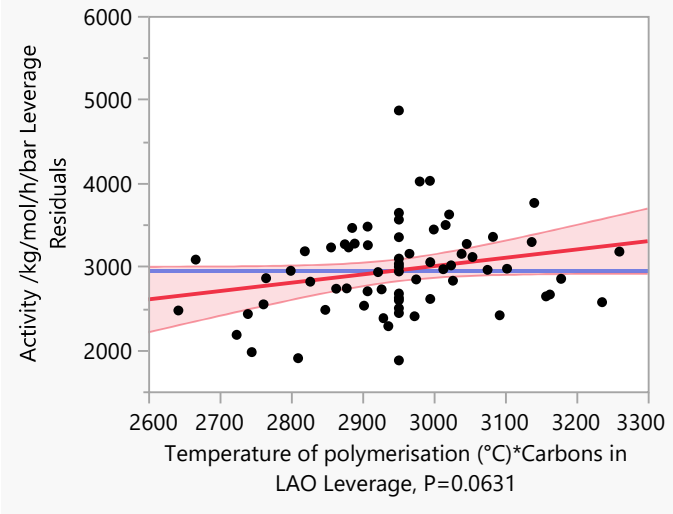

Carbons in LAO*[Comonomer] /mM
Leverage Plot

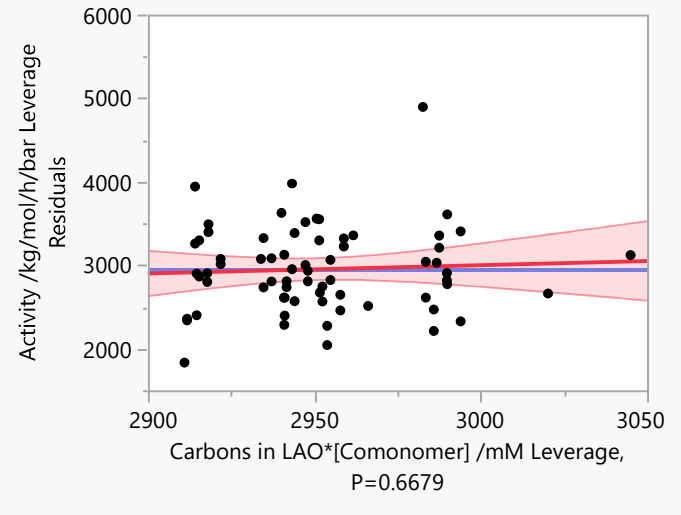

Temperature of polymerisation (°C)*Temperature of polymerisation (°C) Leverage Plot

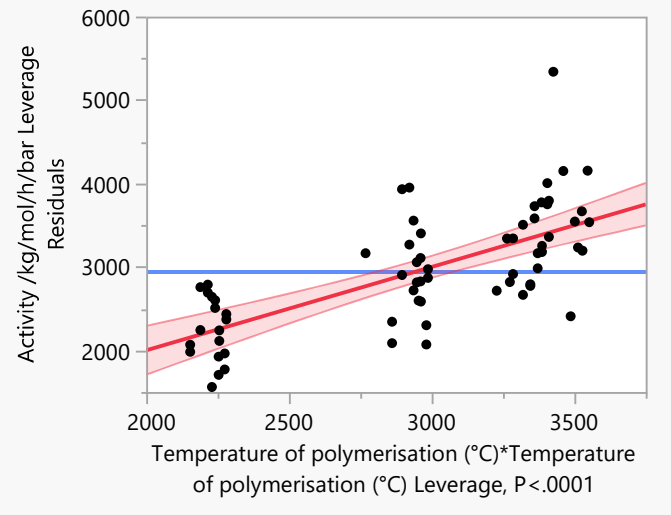

Carbons in LAO*Carbons in LAO Leverage Plot

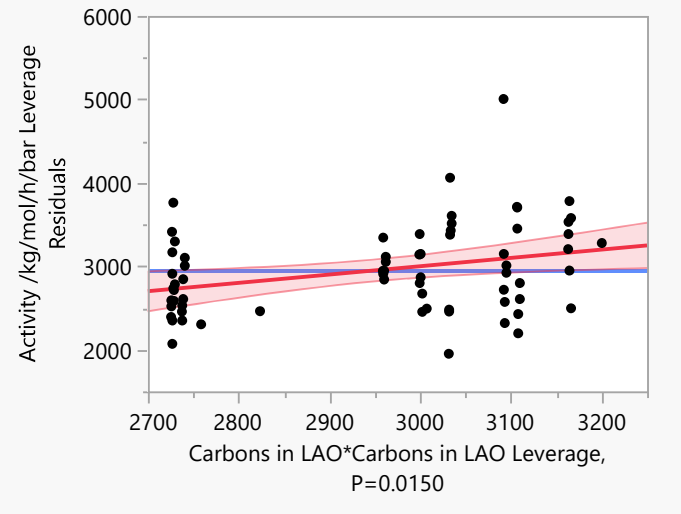

[Comonomer] /mM*[Comonomer] /mM Leverage Plot

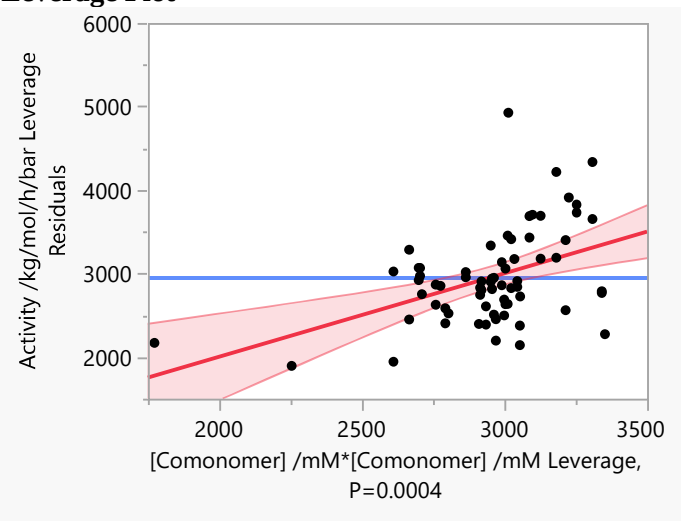

Joint Factor Tests

Term	DF	Sum of Squares	F Ratio	Prob > F
Temperature of polymerisation (°C)	4	22552869	19.3140	<.0001*
Carbons in LAO	4	5143993	4.4052	0.0035*
[Comonomer] /mM	4	10795156	9.2448	<.0001*

Response Tm (°C)
Whole Model
Actual by Predicted Plot

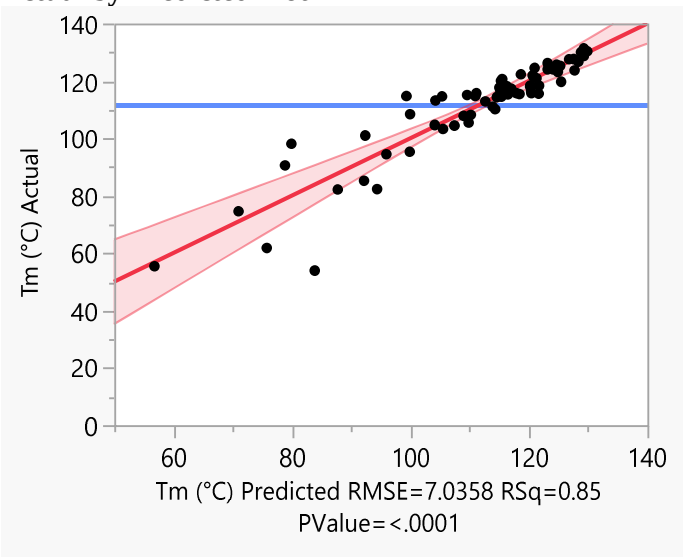

Residual by Predicted Plot

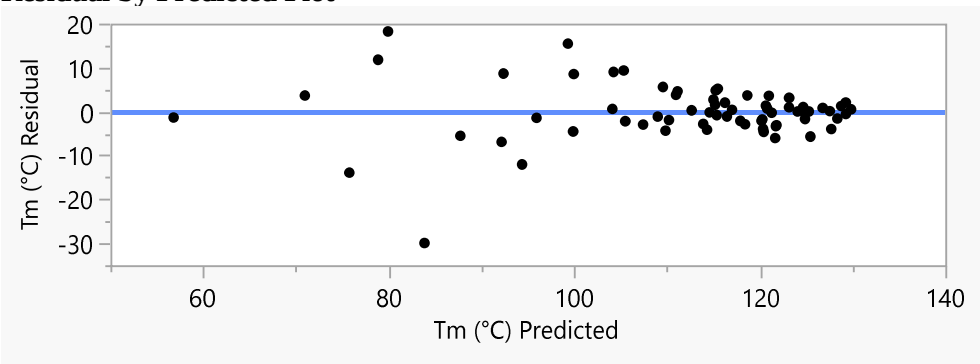

Studentized Residuals

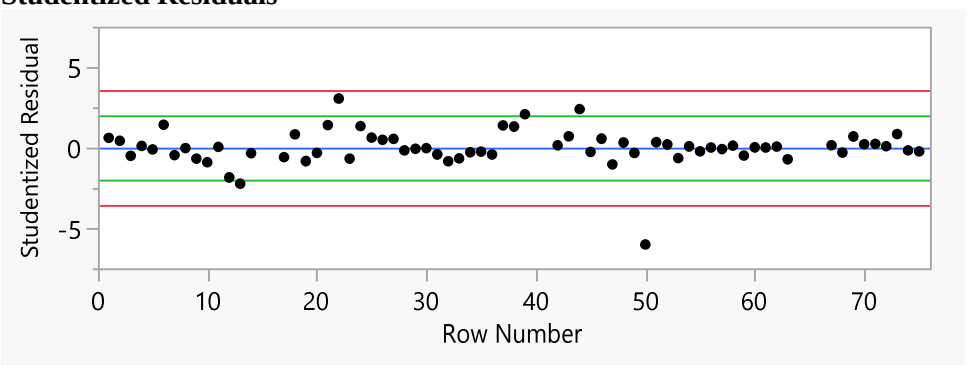

Externally studentized residuals with 95% simultaneous limits (Bonferroni) in red, individual limits in green.

Summary of Fit

RSquare	0.849384
RSquare Adj	0.826012
Root Mean Square Error	7.035801
Mean of Response	111.6446
Observations (or Sum Wgts)	68

Analysis of Variance

Source	DF	Sum of Squares	Mean Square	F Ratio
Model	9	16191.485	1799.05	36.3427
Error	58	2871.145	49.50	**Prob > F**
C. Total	67	19062.629		<.0001*

Parameter Estimates

Term	Estimate	Std Error	t Ratio	Prob>|t|
Intercept	144.73515	5.304205	27.29	<.0001*
Temperature of polymerisation (°C)	-0.37504	0.045957	-8.16	<.0001*
Carbons in LAO	1.0877474	0.451785	2.41	0.0193*
[Comonomer] /mM	-0.314953	0.033957	-9.28	<.0001*
(Temperature of polymerisation (°C)-60)*(Carbons in LAO-8.61765)	-0.03932	0.01922	-2.05	0.0453*
(Temperature of polymerisation (°C)-60)*([Comonomer] /mM-52.9853)	-0.007137	0.001759	-4.06	0.0001*
(Carbons in LAO-8.61765)*([Comonomer] /mM-52.9853)	0.0181297	0.015628	1.16	0.2508
(Temperature of polymerisation (°C)-60)*(Temperature of polymerisation (°C)-60)	-0.005752	0.002524	-2.28	0.0264*
(Carbons in LAO-8.61765)*(Carbons in LAO-8.61765)	-0.070285	0.24116	-0.29	0.7717
([Comonomer] /mM-52.9853)*([Comonomer] /mM-52.9853)	-6.846e-5	0.000477	-0.14	0.8864

Effect Tests

Source	Nparm	DF	Sum of Squares	F Ratio	Prob > F
Temperature of polymerisation (°C)	1	1	3296.6969	66.5966	<.0001*
Carbons in LAO	1	1	286.9594	5.7969	0.0193*
[Comonomer] /mM	1	1	4258.5847	86.0277	<.0001*
Temperature of polymerisation (°C)*Carbons in LAO	1	1	207.1885	4.1854	0.0453*
Temperature of polymerisation (°C)*[Comonomer] /mM	1	1	815.4314	16.4725	0.0001*
Carbons in LAO*[Comonomer] /mM	1	1	66.6168	1.3457	0.2508
Temperature of polymerisation (°C)*Temperature of polymerisation (°C)	1	1	257.0326	5.1923	0.0264*
Carbons in LAO*Carbons in LAO	1	1	4.2048	0.0849	0.7717
[Comonomer] /mM*[Comonomer] /mM	1	1	1.0188	0.0206	0.8864

Residual Normal Quantile Plot

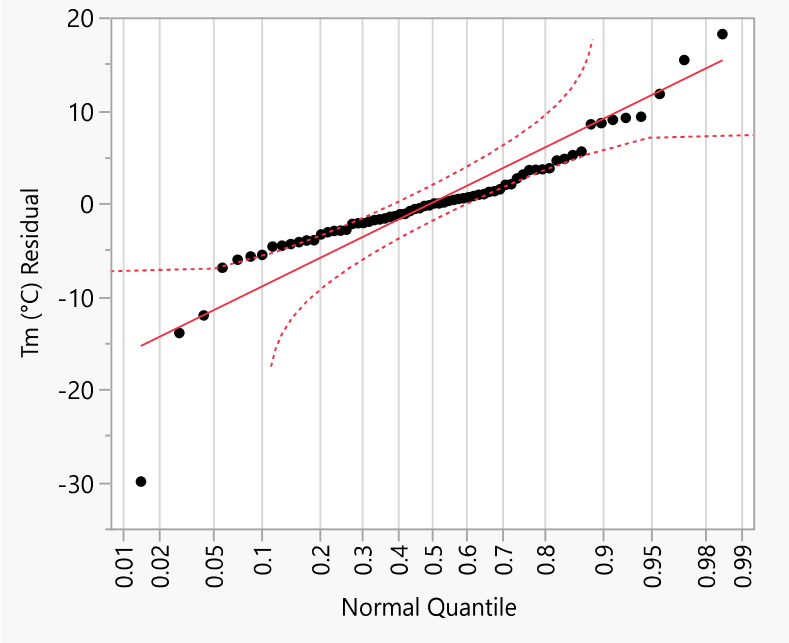

Temperature of polymerisation (°C)
Leverage Plot

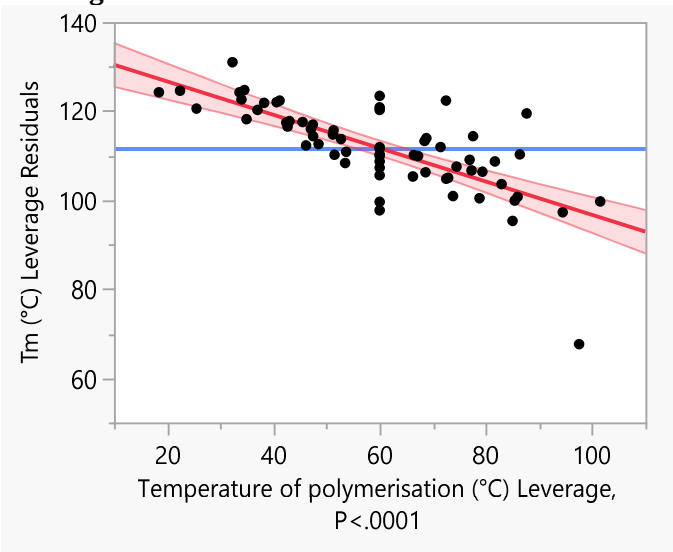

Carbons in LAO
Leverage Plot

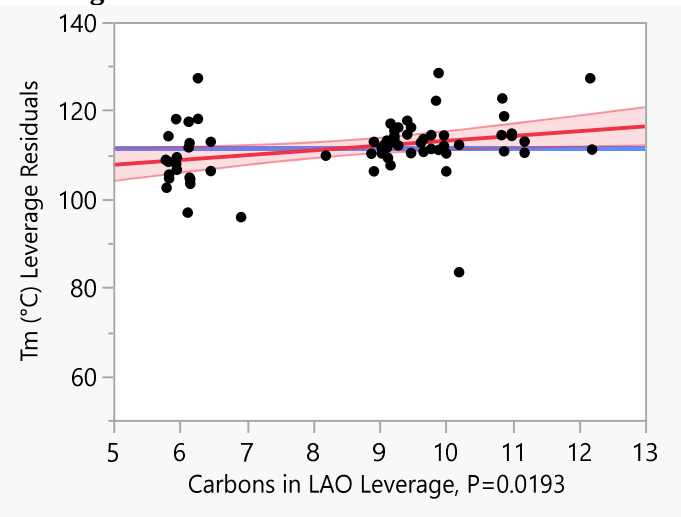

[Comonomer] /mM
Leverage Plot

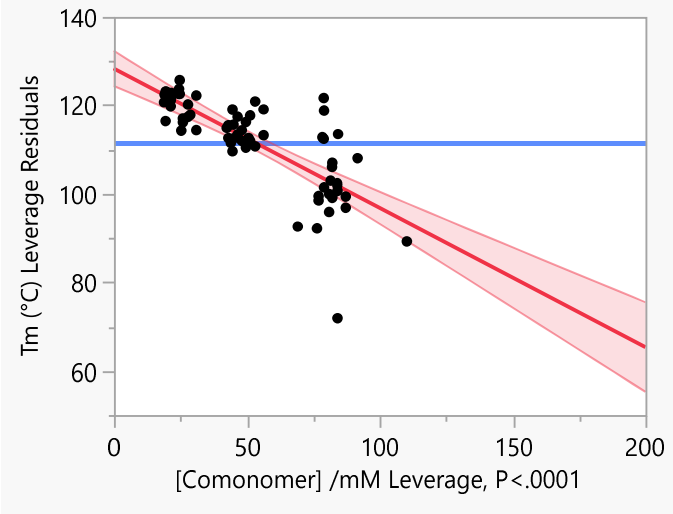

Temperature of polymerisation (°C)*[Comonomer] /mM
Leverage Plot

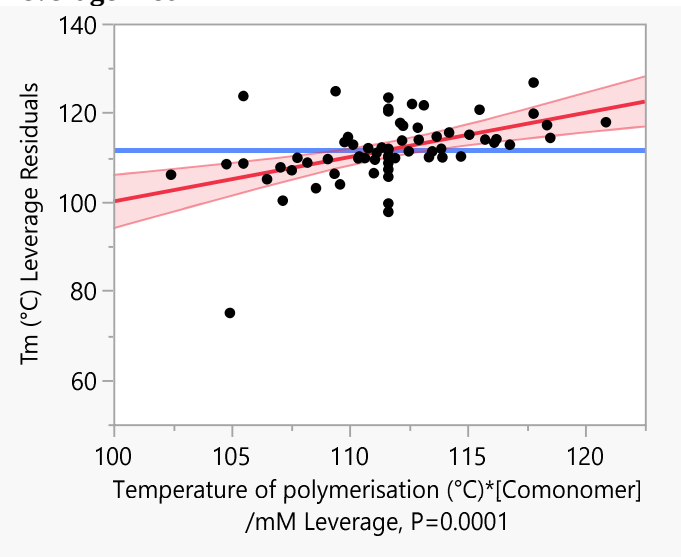

Temperature of polymerisation (°C)*Carbons in LAO
Leverage Plot

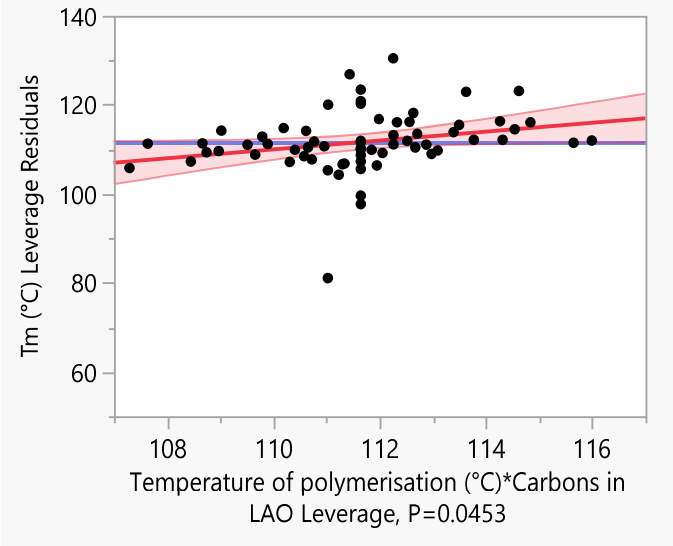

Carbons in LAO*[Comonomer] /mM
Leverage Plot

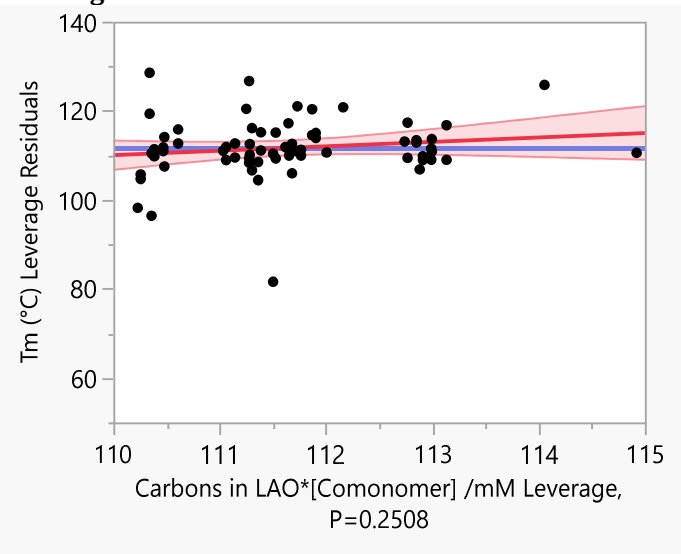

Temperature of polymerisation (°C)*Temperature of polymerisation (°C) Leverage Plot

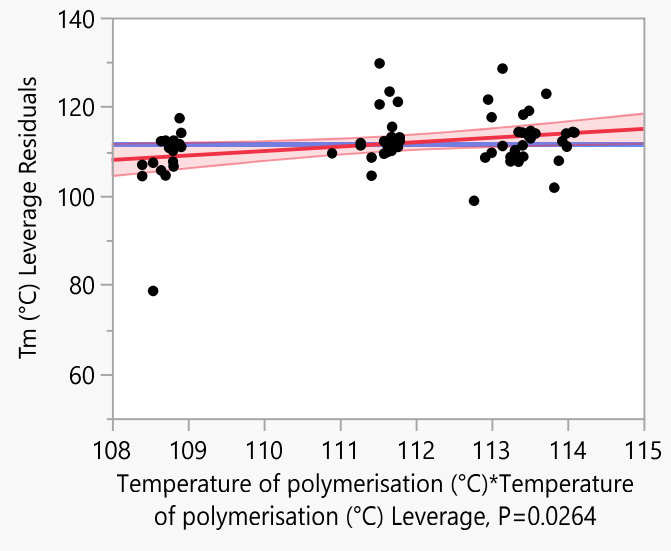

Carbons in LAO*Carbons in LAO Leverage Plot

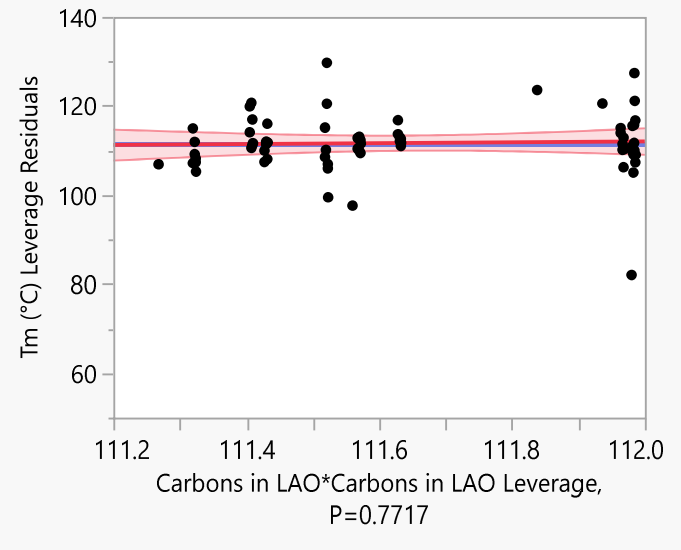

[Comonomer] /mM*[Comonomer] /mM Leverage Plot

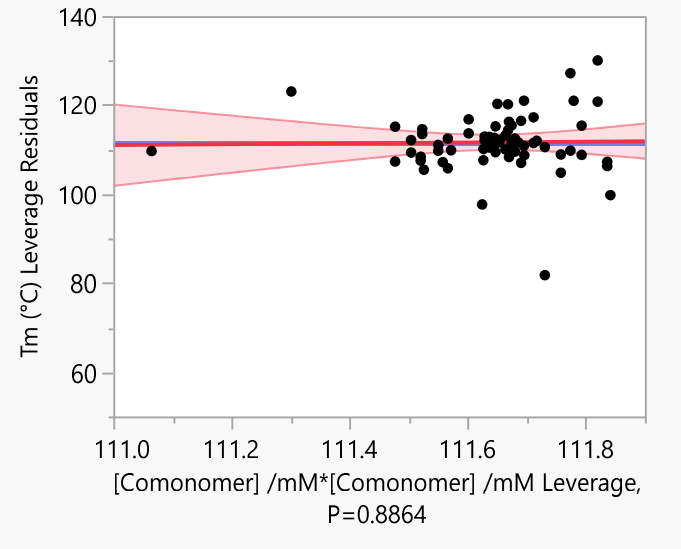

Response Crystallinity (%)
Whole Model
Actual by Predicted Plot

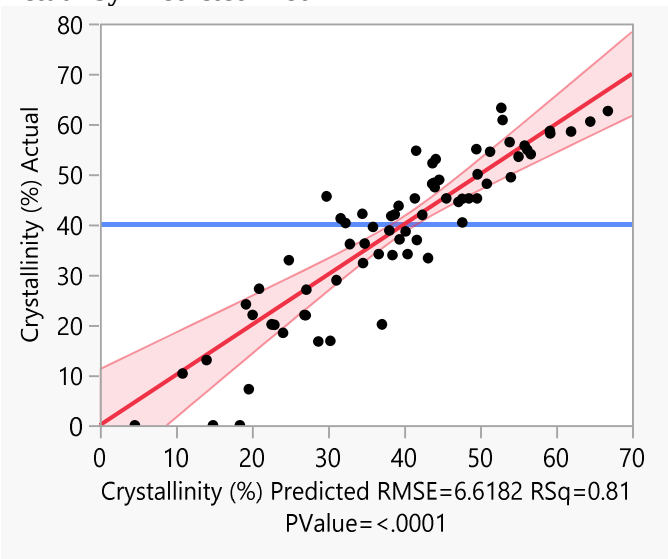

Residual by Predicted Plot

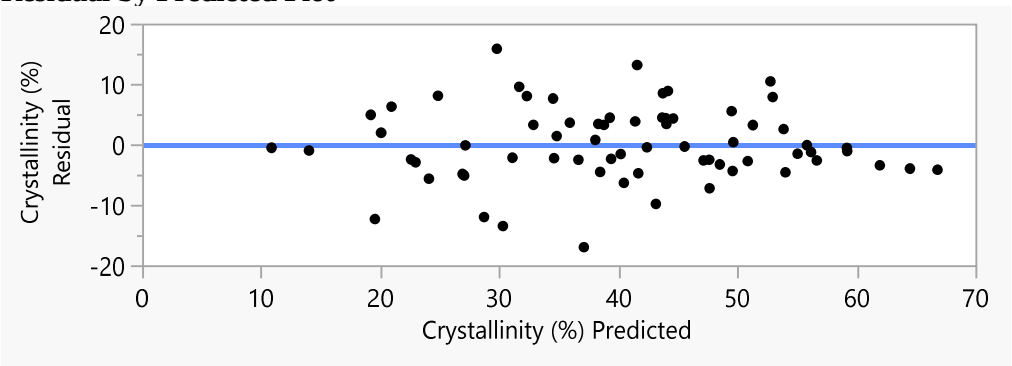

Studentized Residuals

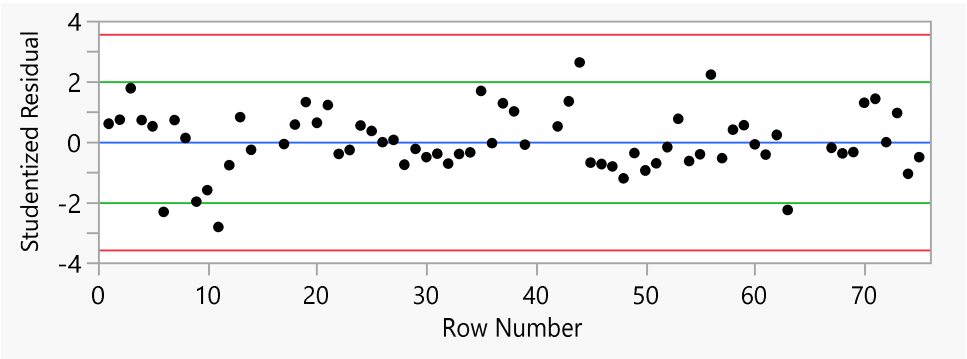

Externally studentized residuals with 95% simultaneous limits (Bonferroni) in red, individual limits in green.

Summary of Fit

RSquare	0.806991
RSquare Adj	0.777041
Root Mean Square Error	6.618191
Mean of Response	40.22206
Observations (or Sum Wgts)	68

Analysis of Variance

Source	DF	Sum of Squares	Mean Square	F Ratio
Model	9	10621.770	1180.20	26.9448
Error	58	2540.427	43.80	**Prob > F**
C. Total	67	13162.197		<.0001*

Parameter Estimates

Term	Estimate	Std Error	t Ratio	Prob>|t|
Intercept	70.514524	4.989374	14.13	<.0001*
Temperature of polymerisation (°C)	-0.218333	0.043229	-5.05	<.0001*
Carbons in LAO	0.4560566	0.424969	1.07	0.2876
[Comonomer] /mM	-0.372819	0.031941	-11.67	<.0001*
(Temperature of polymerisation (°C)-60)*(Carbons in LAO-8.61765)	-0.040559	0.018079	-2.24	0.0287*
(Temperature of polymerisation (°C)-60)*([Comonomer] /mM-52.9853)	-0.001723	0.001654	-1.04	0.3020
(Carbons in LAO-8.61765)*([Comonomer] /mM-52.9853)	-0.055993	0.014701	-3.81	0.0003*
(Temperature of polymerisation (°C)-60)*(Temperature of polymerisation (°C)-60)	-0.001149	0.002375	-0.48	0.6304
(Carbons in LAO-8.61765)*(Carbons in LAO-8.61765)	-0.578051	0.226846	-2.55	0.0135*
([Comonomer] /mM-52.9853)*([Comonomer] /mM-52.9853)	0.0005023	0.000449	1.12	0.2677

Effect Tests

Source	Nparm	DF	Sum of Squares	F Ratio	Prob > F
Temperature of polymerisation (°C)	1	1	1117.2807	25.5084	<.0001*
Carbons in LAO	1	1	50.4431	1.1517	0.2876
[Comonomer] /mM	1	1	5967.2015	136.2361	<.0001*
Temperature of polymerisation (°C)*Carbons in LAO	1	1	220.4455	5.0330	0.0287*
Temperature of polymerisation (°C)*[Comonomer] /mM	1	1	47.5109	1.0847	0.3020
Carbons in LAO*[Comonomer] /mM	1	1	635.4212	14.5072	0.0003*
Temperature of polymerisation (°C)*Temperature of polymerisation (°C)	1	1	10.2518	0.2341	0.6304
Carbons in LAO*Carbons in LAO	1	1	284.4137	6.4934	0.0135*
[Comonomer] /mM*[Comonomer] /mM	1	1	54.8484	1.2522	0.2677

Residual Normal Quantile Plot

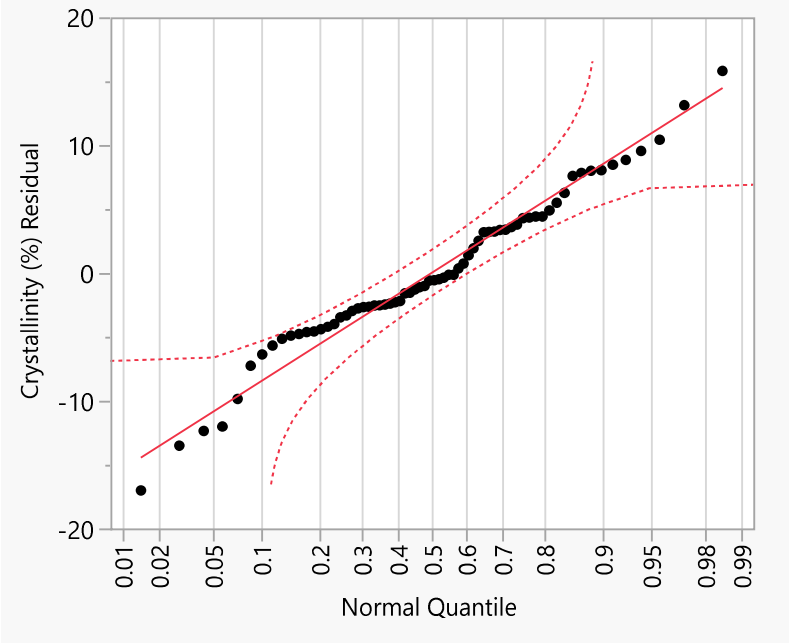

Temperature of polymerisation (°C)
Leverage Plot

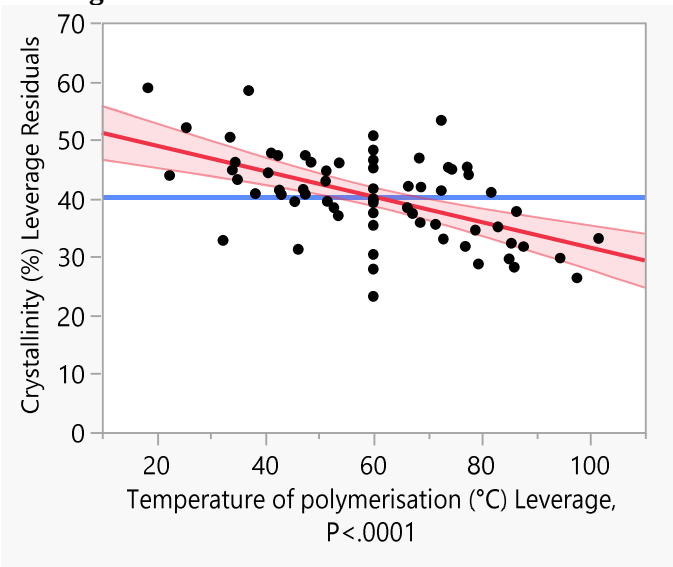

Carbons in LAO
Leverage Plot

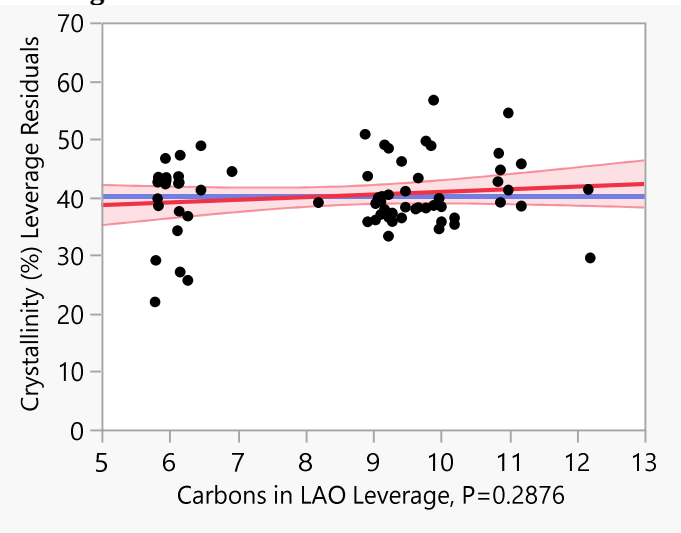

[Comonomer] /mM
Leverage Plot

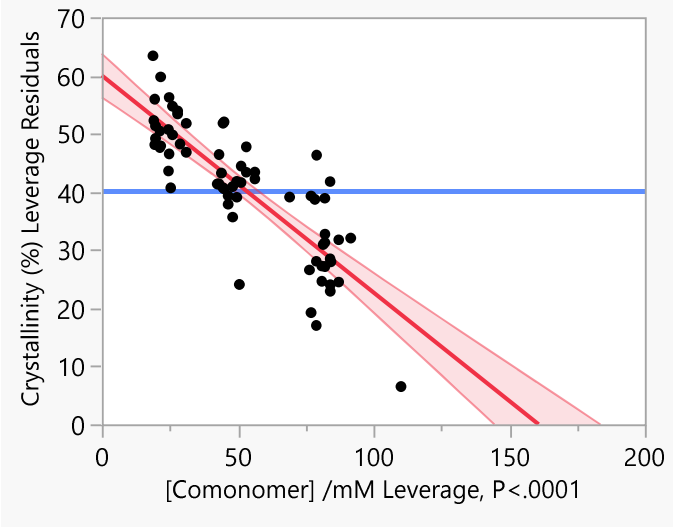

Temperature of polymerisation (°C)*[Comonomer] /mM
Leverage Plot

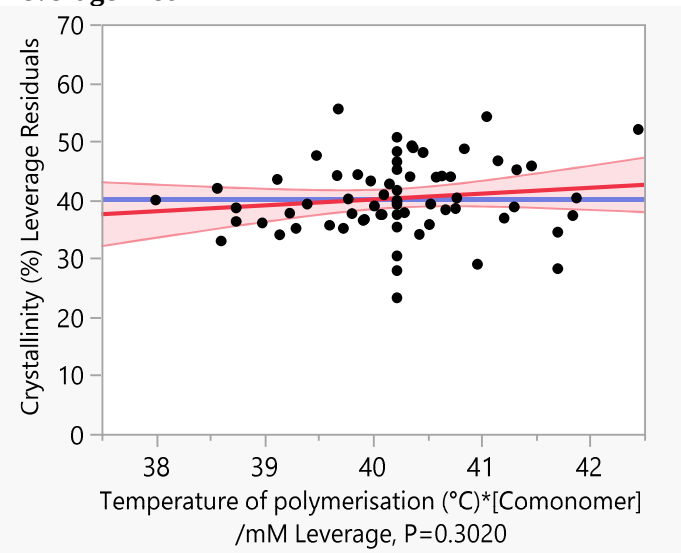

Temperature of polymerisation (°C)*Carbons in LAO
Leverage Plot

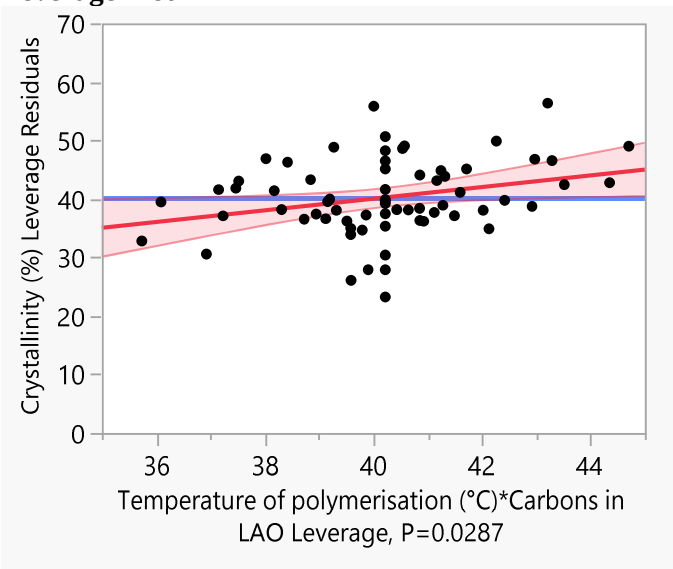

Carbons in LAO*[Comonomer] /mM
Leverage Plot

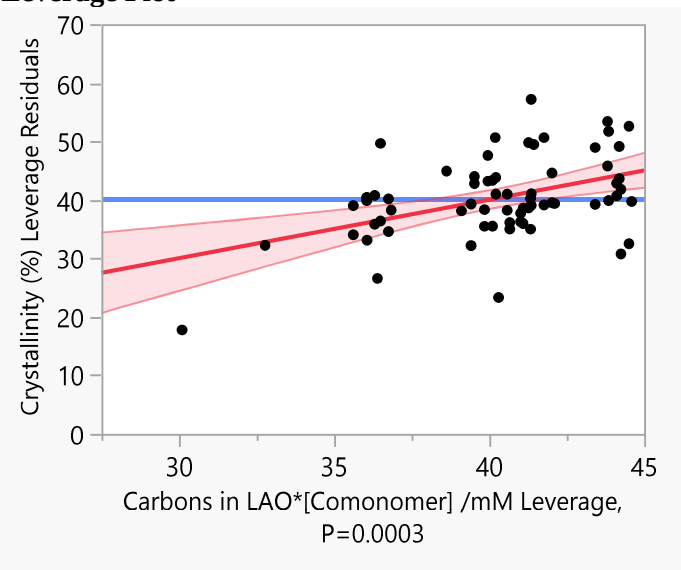

Temperature of polymerisation (°C)*Temperature of polymerisation (°C) Leverage Plot

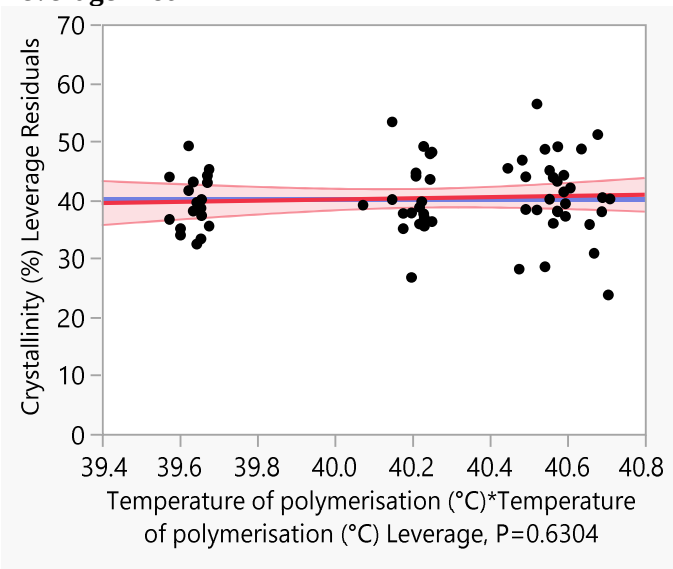

Carbons in LAO*Carbons in LAO Leverage Plot

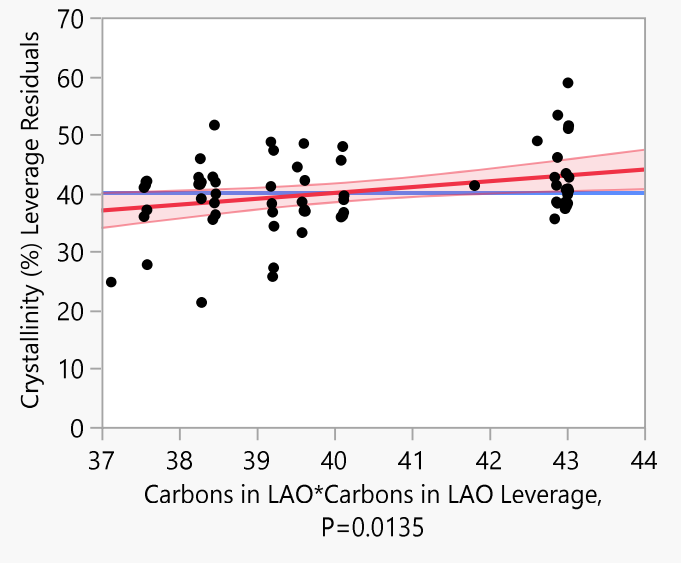

[Comonomer] /mM*[Comonomer] /mM Leverage Plot

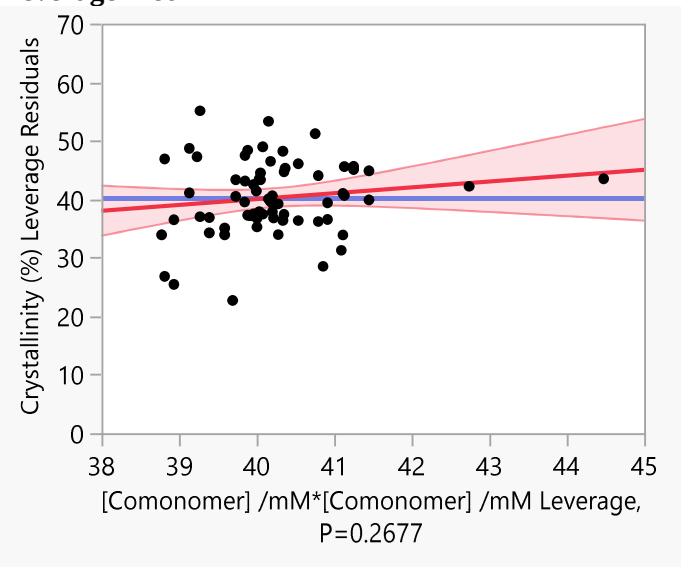

Response Mw (kDa)
Whole Model
Actual by Predicted Plot

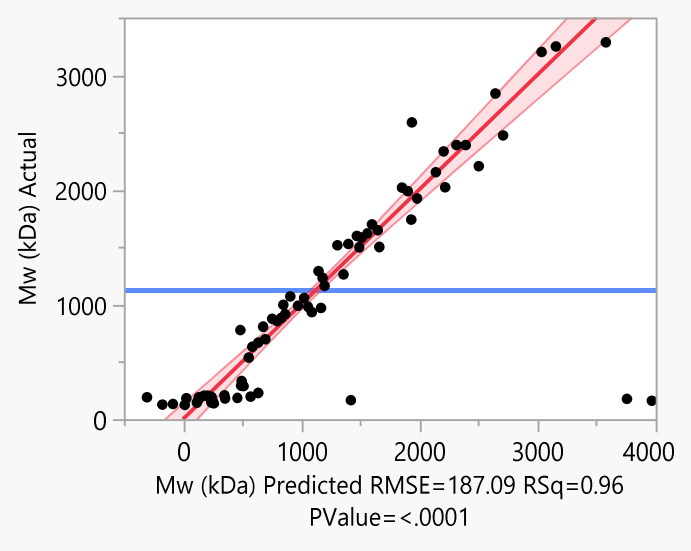

Residual by Predicted Plot

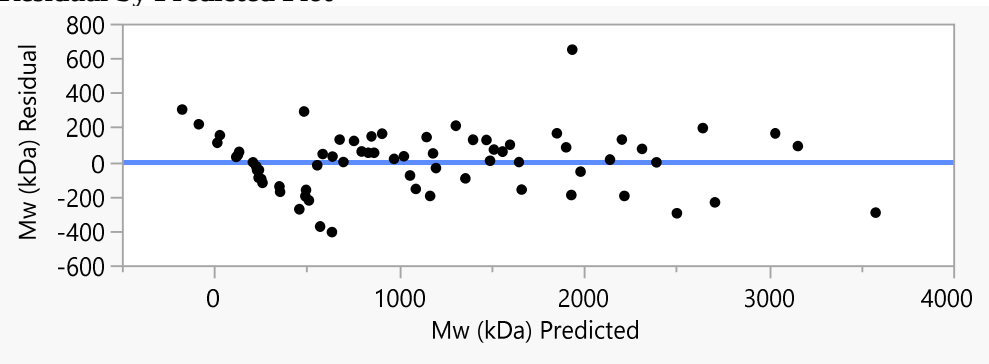

Studentized Residuals

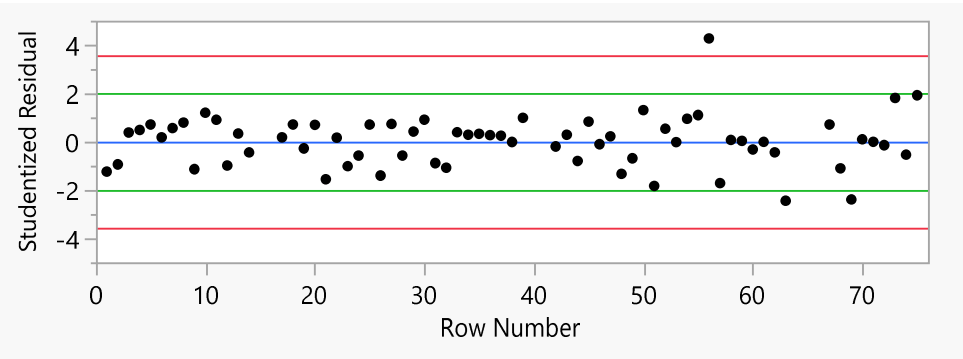

Externally studentized residuals with 95% simultaneous limits (Bonferroni) in red, individual limits in green.

Summary of Fit

RSquare	0.961941
RSquare Adj	0.956036
Root Mean Square Error	187.0931
Mean of Response	1129.462
Observations (or Sum Wgts)	68

Analysis of Variance

Source	DF	Sum of Squares	Mean Square	F Ratio
Model	9	51314384	5701598	162.8849
Error	58	2030223	35004	**Prob > F**
C. Total	67	53344607		<.0001*

Parameter Estimates

Term	Estimate	Std Error	t Ratio	Prob>|t|
Intercept	3398.7491	141.0472	24.10	<.0001*
Temperature of polymerisation (°C)	-31.82694	1.22207	-26.04	<.0001*
Carbons in LAO	43.572195	12.01367	3.63	0.0006*
[Comonomer] /mM	-16.41031	0.902964	-18.17	<.0001*
(Temperature of polymerisation (°C)-60)*(Carbons in LAO-8.61765)	-3.424549	0.511082	-6.70	<.0001*
(Temperature of polymerisation (°C)-60)*([Comonomer] /mM-52.9853)	0.2091869	0.046764	4.47	<.0001*
(Carbons in LAO-8.61765)*([Comonomer] /mM-52.9853)	-0.945084	0.415582	-2.27	0.0267*
(Temperature of polymerisation (°C)-60)*(Temperature of polymerisation (°C)-60)	0.0558349	0.06713	0.83	0.4090
(Carbons in LAO-8.61765)*(Carbons in LAO-8.61765)	-2.089985	6.412819	-0.33	0.7457
([Comonomer] /mM-52.9853)*([Comonomer] /mM-52.9853)	0.0659239	0.01269	5.20	<.0001*

Effect Tests

Source	Nparm	DF	Sum of Squares	F Ratio	Prob > F
Temperature of polymerisation (°C)	1	1	23741767	678.2618	<.0001*
Carbons in LAO	1	1	460451	13.1543	0.0006*
[Comonomer] /mM	1	1	11561336	330.2876	<.0001*
Temperature of polymerisation (°C)*Carbons in LAO	1	1	1571599	44.8979	<.0001*
Temperature of polymerisation (°C)*[Comonomer] /mM	1	1	700438	20.0103	<.0001*
Carbons in LAO*[Comonomer] /mM	1	1	181027	5.1716	0.0267*
Temperature of polymerisation (°C)*Temperature of polymerisation (°C)	1	1	24215	0.6918	0.4090
Carbons in LAO*Carbons in LAO	1	1	3718	0.1062	0.7457
[Comonomer] /mM*[Comonomer] /mM	1	1	944713	26.9888	<.0001*

Residual Normal Quantile Plot

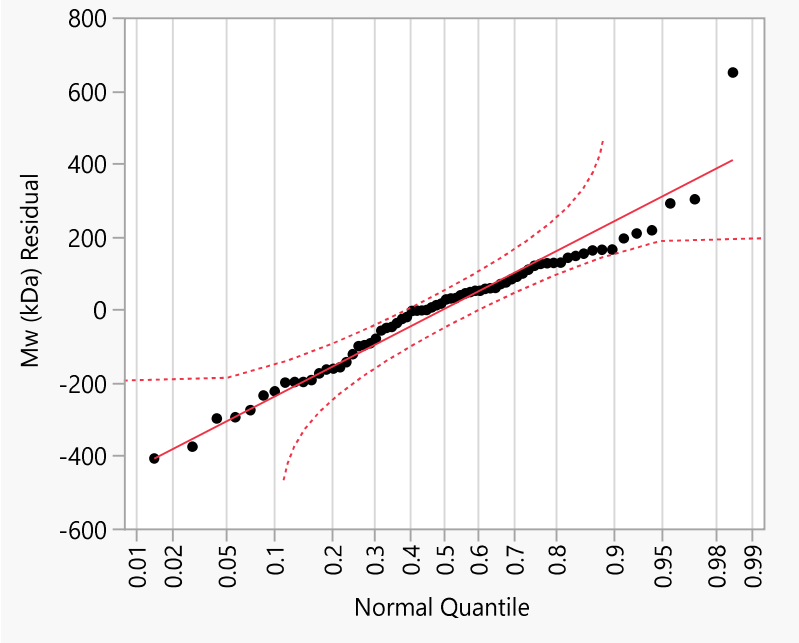

Temperature of polymerisation (°C)
Leverage Plot

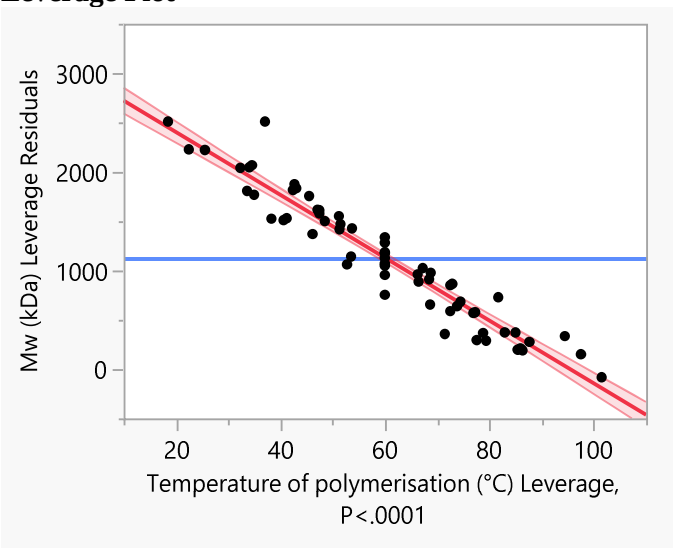

Carbons in LAO
Leverage Plot

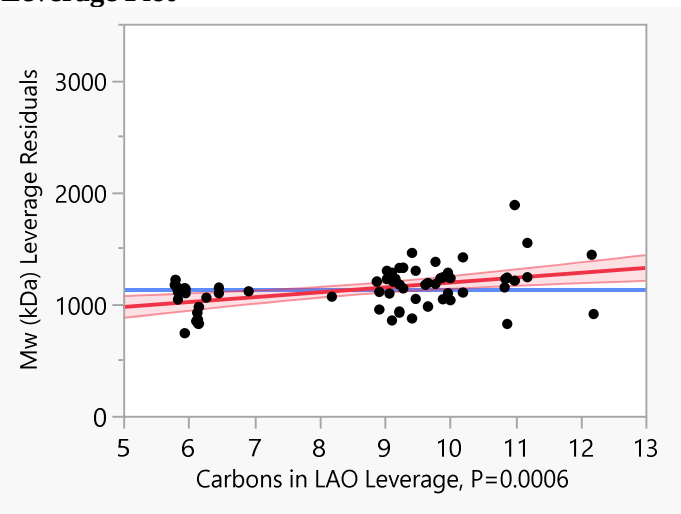

[Comonomer] /mM
Leverage Plot

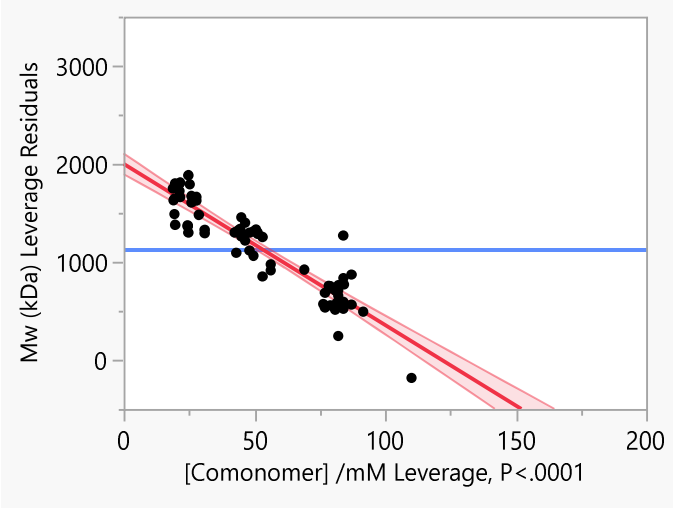

Temperature of polymerisation (°C)*Carbons in LAO
Leverage Plot

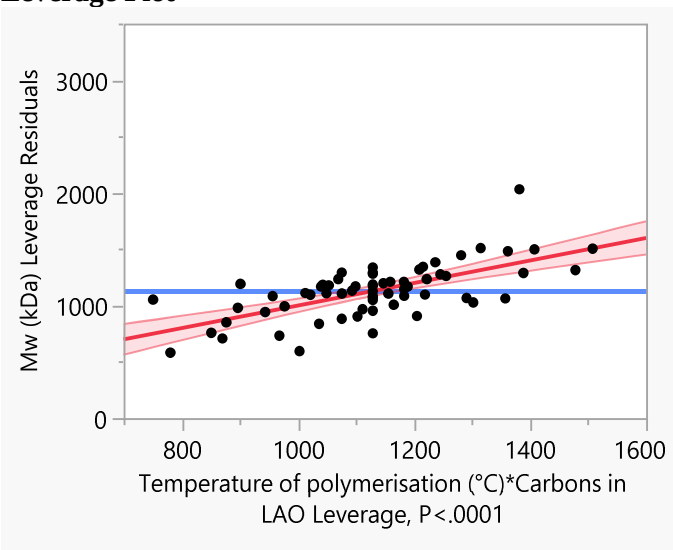

Temperature of polymerisation (°C)*[Comonomer] /mM
Leverage Plot

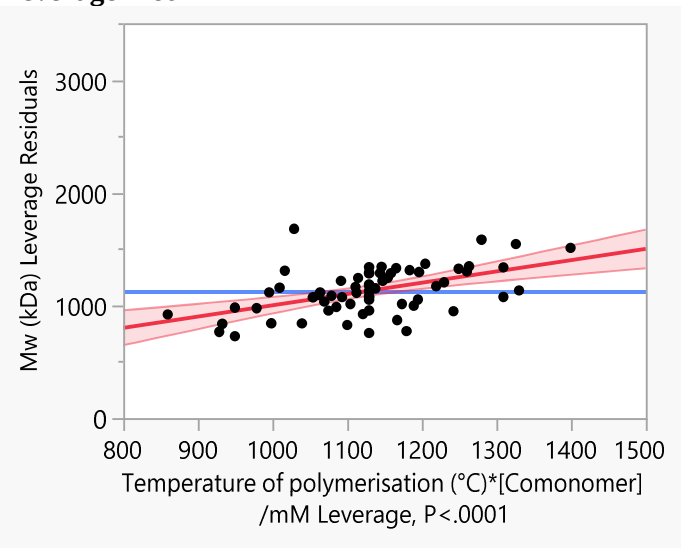

Carbons in LAO*[Comonomer] /mM
Leverage Plot

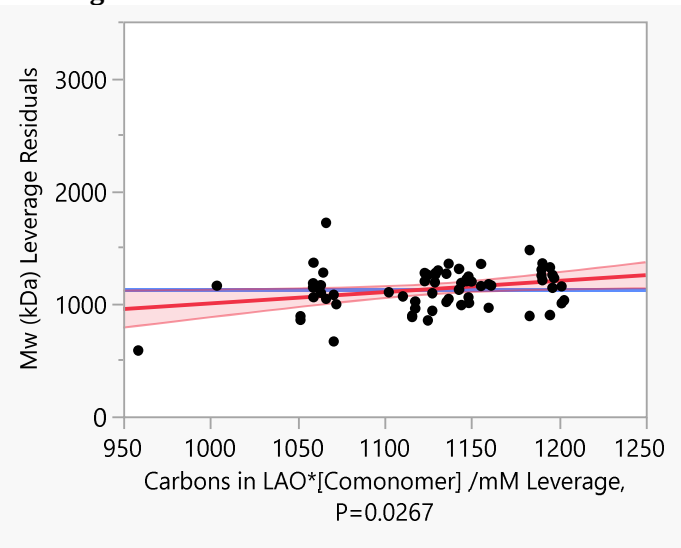

Temperature of polymerisation (°C)*Temperature of polymerisation (°C) Leverage Plot

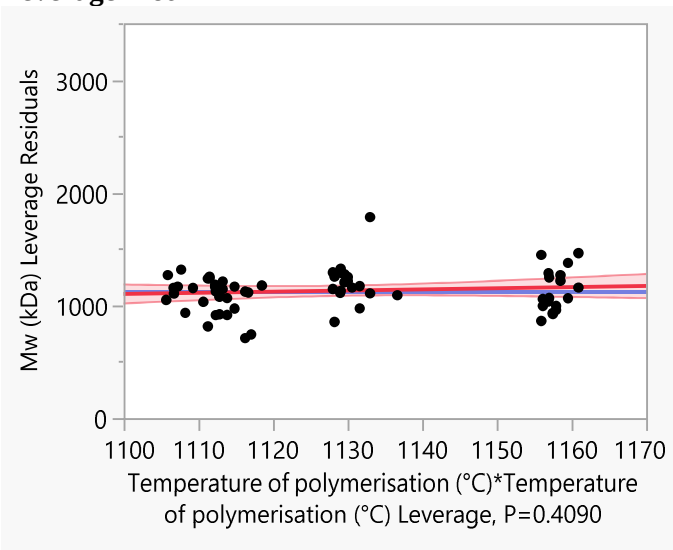

Carbons in LAO*Carbons in LAO Leverage Plot

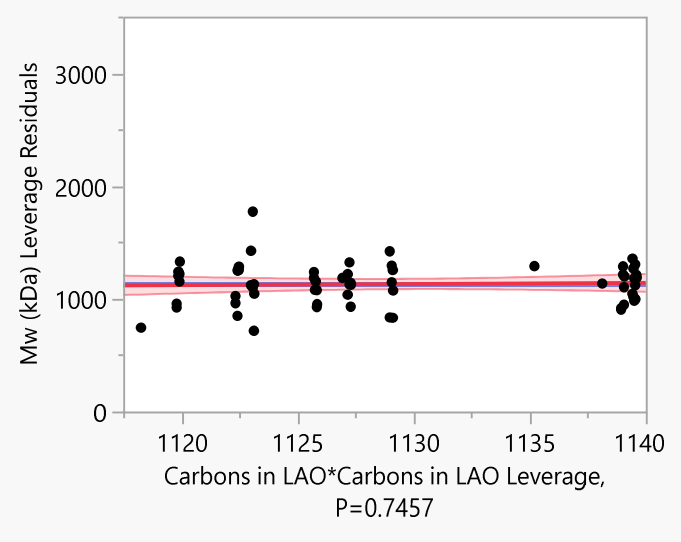

[Comonomer] /mM*[Comonomer] /mM Leverage Plot

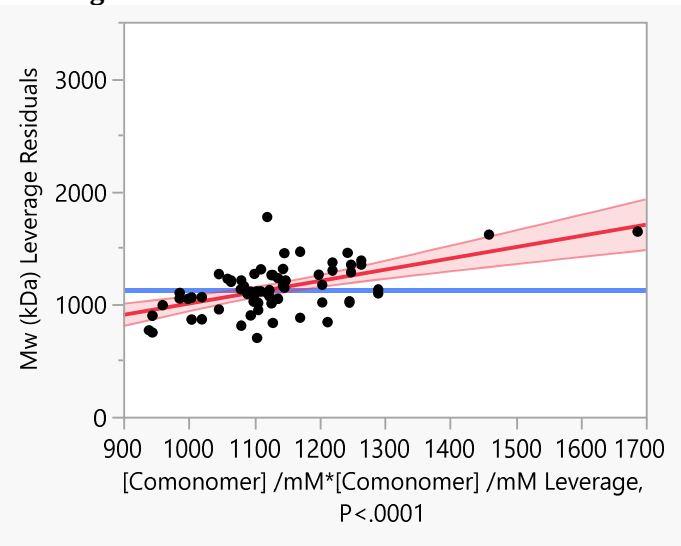

Response PDI
Whole Model
Actual by Predicted Plot

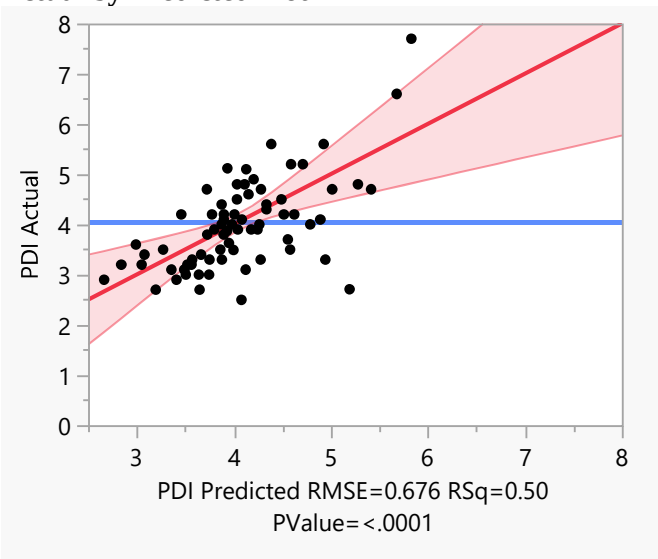

Residual by Predicted Plot

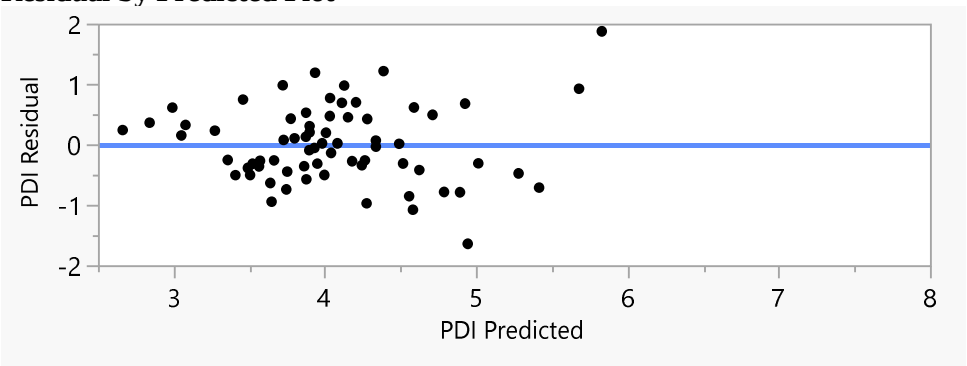

Studentized Residuals

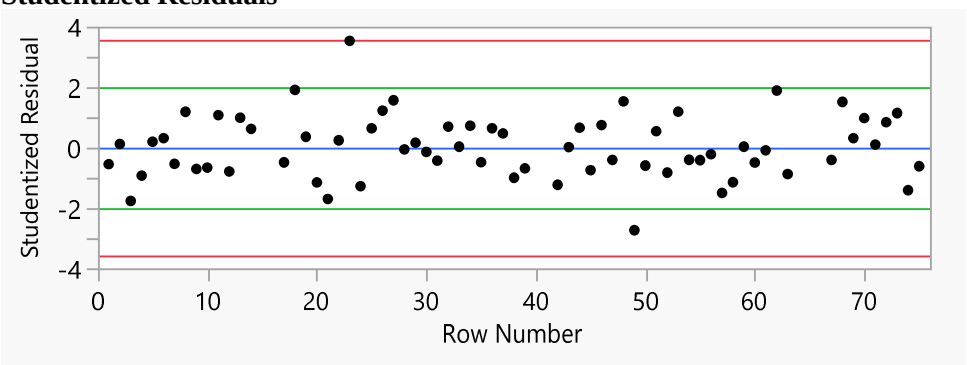

Externally studentized residuals with 95% simultaneous limits (Bonferroni) in red, individual limits in green.

Summary of Fit

RSquare	0.498783
RSquare Adj	0.421008
Root Mean Square Error	0.675981
Mean of Response	4.061912
Observations (or Sum Wgts)	68

Analysis of Variance

Source	DF	Sum of Squares	Mean Square	F Ratio
Model	9	26.374497	2.93050	6.4132
Error	58	26.503154	0.45695	**Prob > F**
C. Total	67	52.877651		<.0001*

Parameter Estimates

Term	Estimate	Std Error	t Ratio	Prob>|t|
Intercept	4.3749622	0.509614	8.58	<.0001*
Temperature of polymerisation (°C)	0.0078468	0.004415	1.78	0.0808
Carbons in LAO	-0.03187	0.043406	-0.73	0.4658
[Comonomer] /mM	-0.008374	0.003262	-2.57	0.0129*
(Temperature of polymerisation (°C)-60)*(Carbons in LAO-8.61765)	-0.002806	0.001847	-1.52	0.1340
(Temperature of polymerisation (°C)-60)*([Comonomer] /mM-52.9853)	-0.000832	0.000169	-4.92	<.0001*
(Carbons in LAO-8.61765)*([Comonomer] /mM-52.9853)	0.0027619	0.001502	1.84	0.0710
(Temperature of polymerisation (°C)-60)*(Temperature of polymerisation (°C)-60)	5.8238e-5	0.000243	0.24	0.8111
(Carbons in LAO-8.61765)*(Carbons in LAO-8.61765)	-0.007633	0.02317	-0.33	0.7430
([Comonomer] /mM-52.9853)*([Comonomer] /mM-52.9853)	3.6984e-5	4.585e-5	0.81	0.4232

Effect Tests

Source	Nparm	DF	Sum of Squares	F Ratio	Prob > F
Temperature of polymerisation (°C)	1	1	1.443131	3.1582	0.0808
Carbons in LAO	1	1	0.246333	0.5391	0.4658
[Comonomer] /mM	1	1	3.010736	6.5888	0.0129*
Temperature of polymerisation (°C)*Carbons in LAO	1	1	1.055363	2.3096	0.1340
Temperature of polymerisation (°C)*[Comonomer] /mM	1	1	11.071526	24.2291	<.0001*
Carbons in LAO*[Comonomer] /mM	1	1	1.545981	3.3833	0.0710
Temperature of polymerisation (°C)*Temperature of polymerisation (°C)	1	1	0.026345	0.0577	0.8111
Carbons in LAO*Carbons in LAO	1	1	0.049588	0.1085	0.7430
[Comonomer] /mM*[Comonomer] /mM	1	1	0.297336	0.6507	0.4232

Residual Normal Quantile Plot

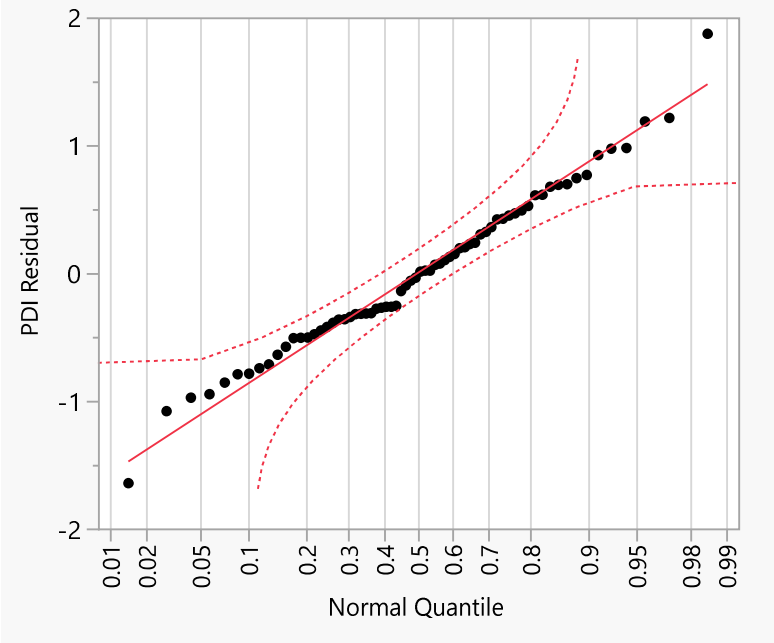

Temperature of polymerisation (°C)
Leverage Plot

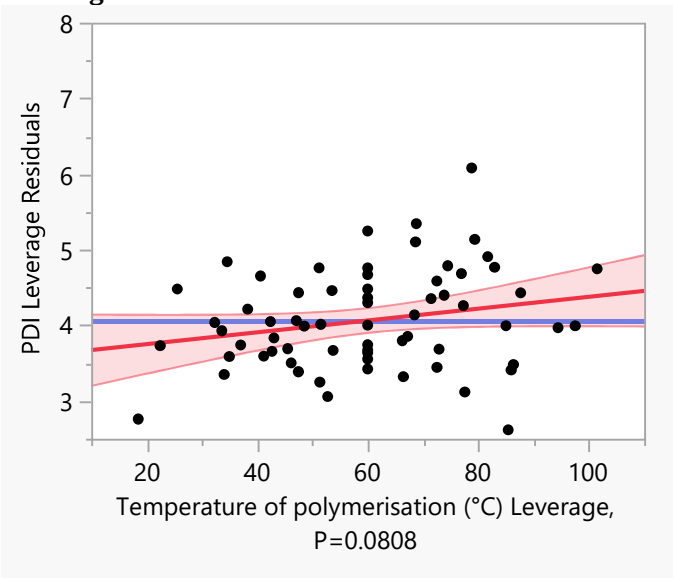

Carbons in LAO
Leverage Plot

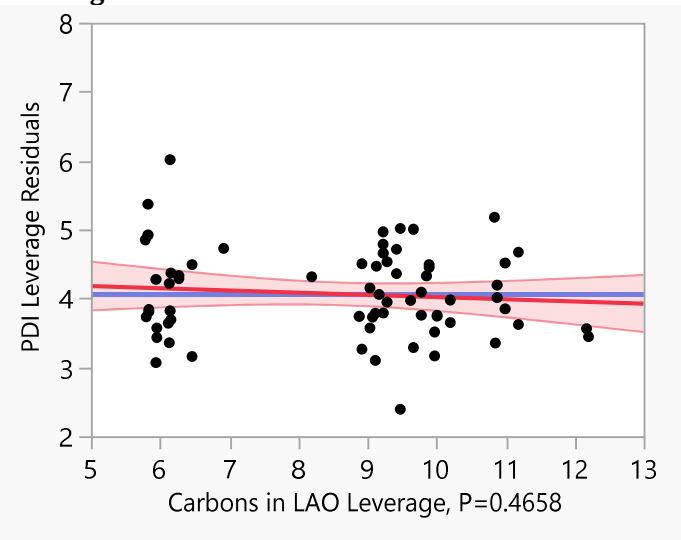

[Comonomer] /mM
Leverage Plot

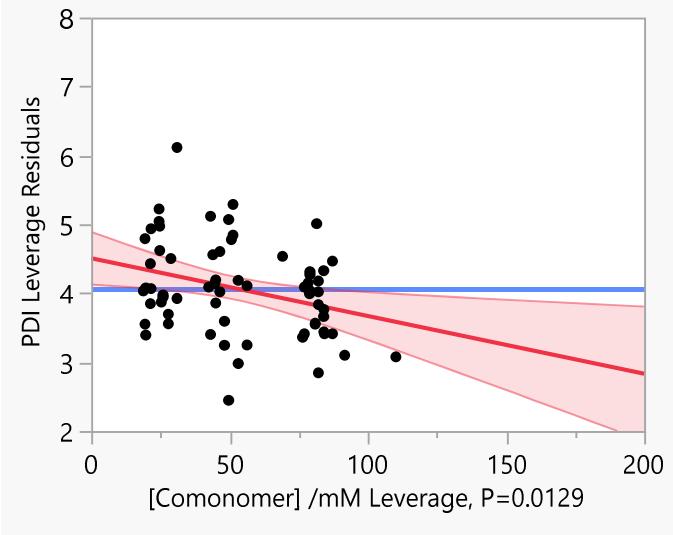

Temperature of polymerisation (°C)*[Comonomer] /mM
Leverage Plot

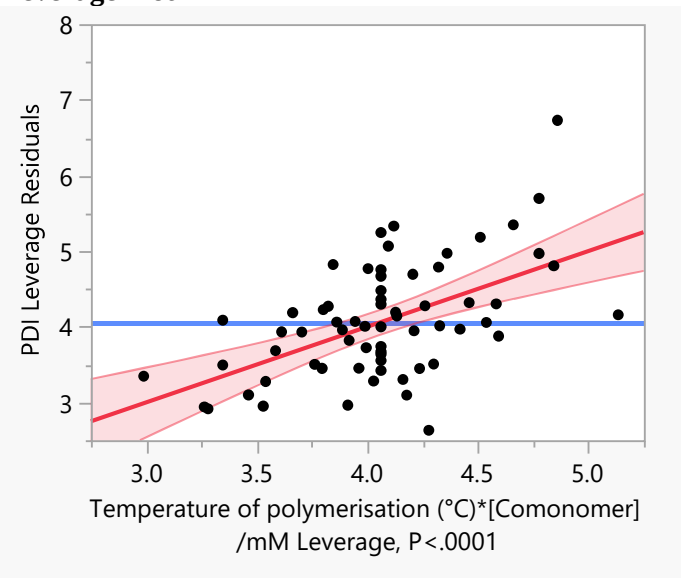

Temperature of polymerisation (°C)*Carbons in LAO
Leverage Plot

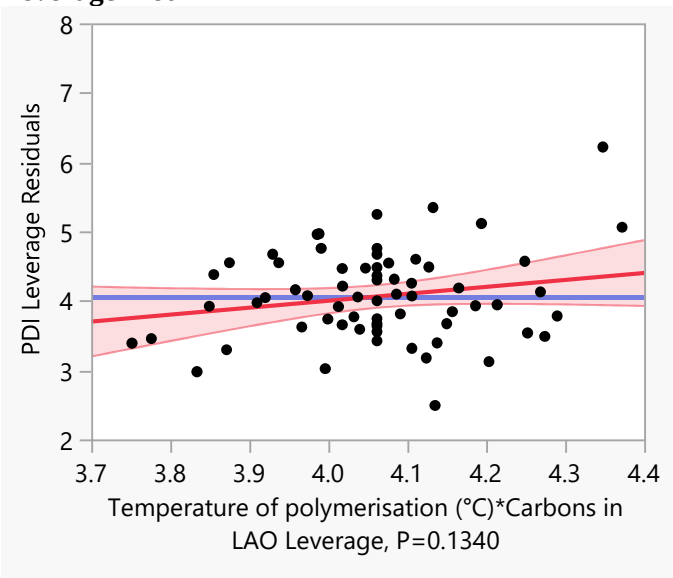

Carbons in LAO*[Comonomer] /mM
Leverage Plot

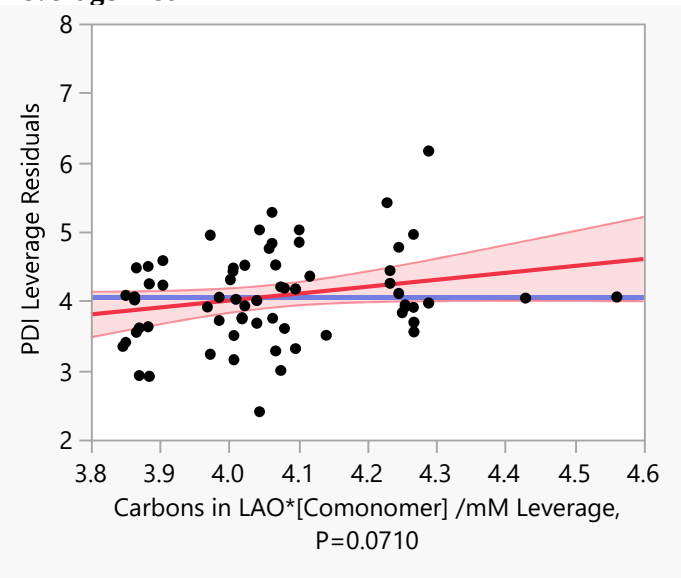

Temperature of polymerisation (°C)*Temperature of polymerisation (°C) Leverage Plot

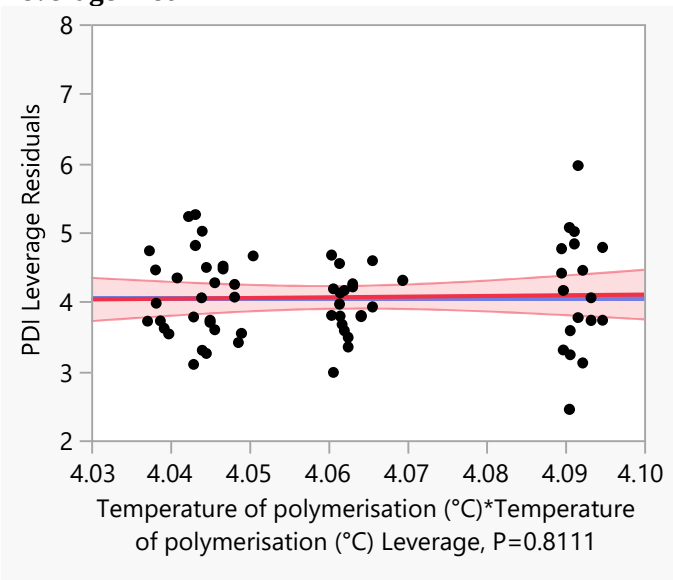

[Comonomer] /mM*[Comonomer] /mM Leverage Plot

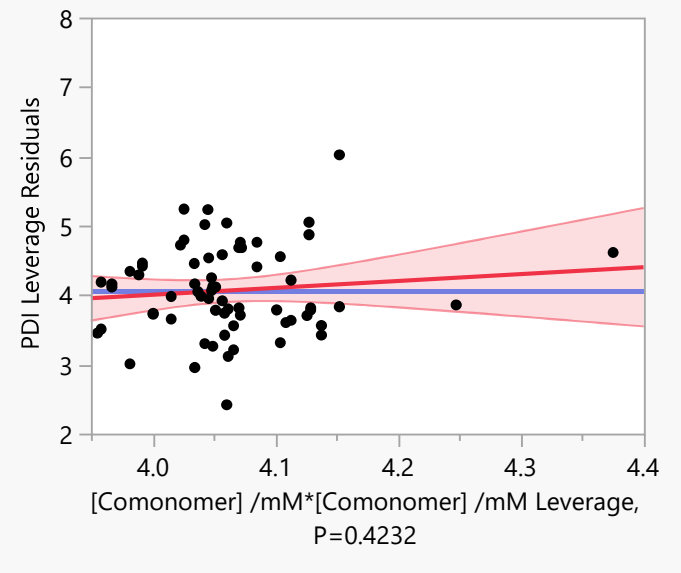

Carbons in LAO*Carbons in LAO Leverage Plot

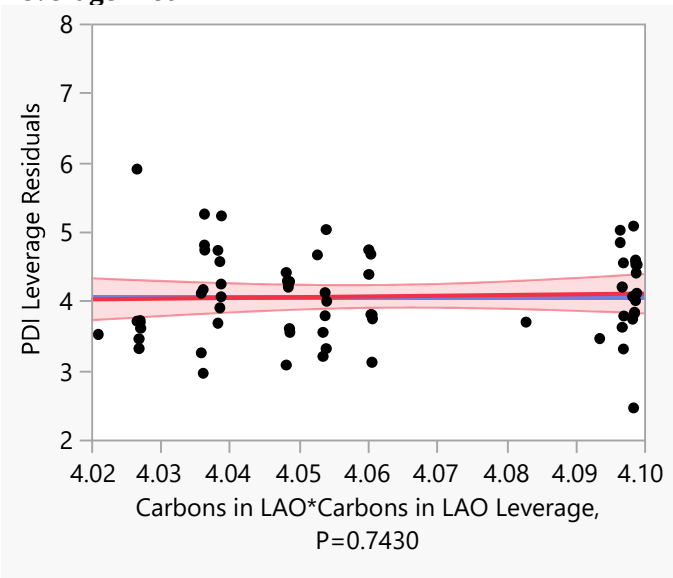

Response Incorporation (wt%)
Whole Model
Actual by Predicted Plot

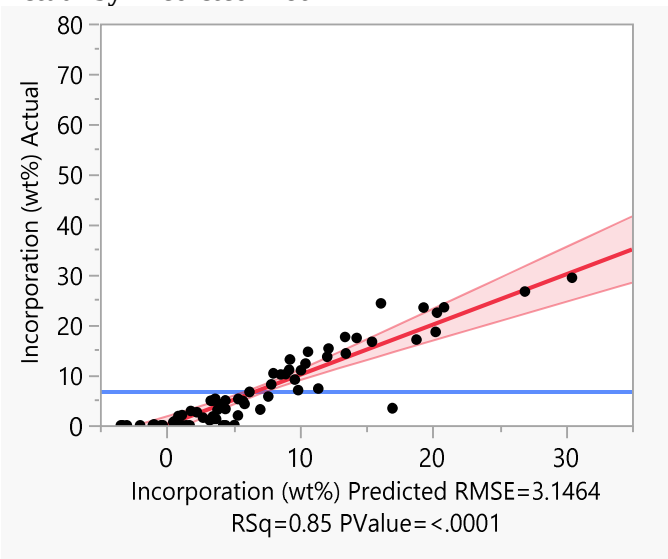

Residual by Predicted Plot

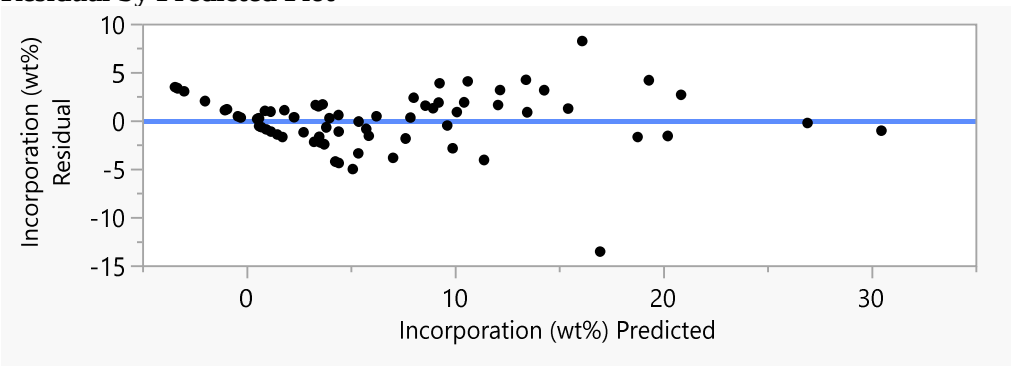

Studentized Residuals

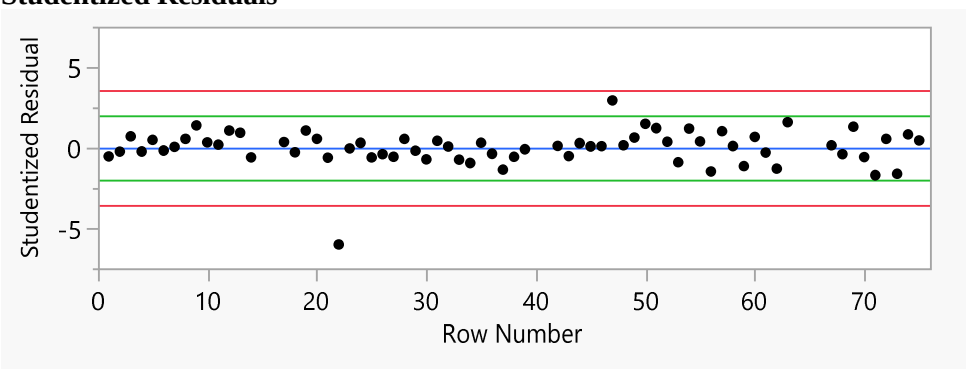

Externally studentized residuals with 95% simultaneous limits (Bonferroni) in red, individual limits in green.

Summary of Fit

RSquare	0.853353
RSquare Adj	0.830598
Root Mean Square Error	3.146371
Mean of Response	6.85
Observations (or Sum Wgts)	68

Analysis of Variance

Source	DF	Sum of Squares	Mean Square	F Ratio
Model	9	3341.2151	371.246	37.5009
Error	58	574.1799	9.900	**Prob > F**
C. Total	67	3915.3950		<.0001*

Parameter Estimates

Term	Estimate	Std Error	t Ratio	Prob>|t|
Intercept	-14.47983	2.372011	-6.10	<.0001*
Temperature of polymerisation (°C)	0.1446293	0.020552	7.04	<.0001*
Carbons in LAO	0.3735332	0.202036	1.85	0.0696
[Comonomer] /mM	0.179492	0.015185	11.82	<.0001*
(Temperature of polymerisation (°C)-60)*(Carbons in LAO-8.61765)	0.0135319	0.008595	1.57	0.1208
(Temperature of polymerisation (°C)-60)*([Comonomer] /mM-52.9853)	0.0015762	0.000786	2.00	0.0497*
(Carbons in LAO-8.61765)*([Comonomer] /mM-52.9853)	0.0124221	0.006989	1.78	0.0807
(Temperature of polymerisation (°C)-60)*(Temperature of polymerisation (°C)-60)	0.0028307	0.001129	2.51	0.0150*
(Carbons in LAO-8.61765)*(Carbons in LAO-8.61765)	-0.158362	0.107845	-1.47	0.1474
([Comonomer] /mM-52.9853)*([Comonomer] /mM-52.9853)	0.0001857	0.000213	0.87	0.3877

Effect Tests

Source	Nparm	DF	Sum of Squares	F Ratio	Prob > F
Temperature of polymerisation (°C)	1	1	490.2706	49.5240	<.0001*
Carbons in LAO	1	1	33.8394	3.4182	0.0696
[Comonomer] /mM	1	1	1383.1349	139.7155	<.0001*
Temperature of polymerisation (°C)*Carbons in LAO	1	1	24.5386	2.4787	0.1208
Temperature of polymerisation (°C)*[Comonomer] /mM	1	1	39.7680	4.0171	0.0497*
Carbons in LAO*[Comonomer] /mM	1	1	31.2744	3.1591	0.0807
Temperature of polymerisation (°C)*Temperature of polymerisation (°C)	1	1	62.2404	6.2871	0.0150*
Carbons in LAO*Carbons in LAO	1	1	21.3463	2.1563	0.1474
[Comonomer] /mM*[Comonomer] /mM	1	1	7.4996	0.7576	0.3877

Residual Normal Quantile Plot

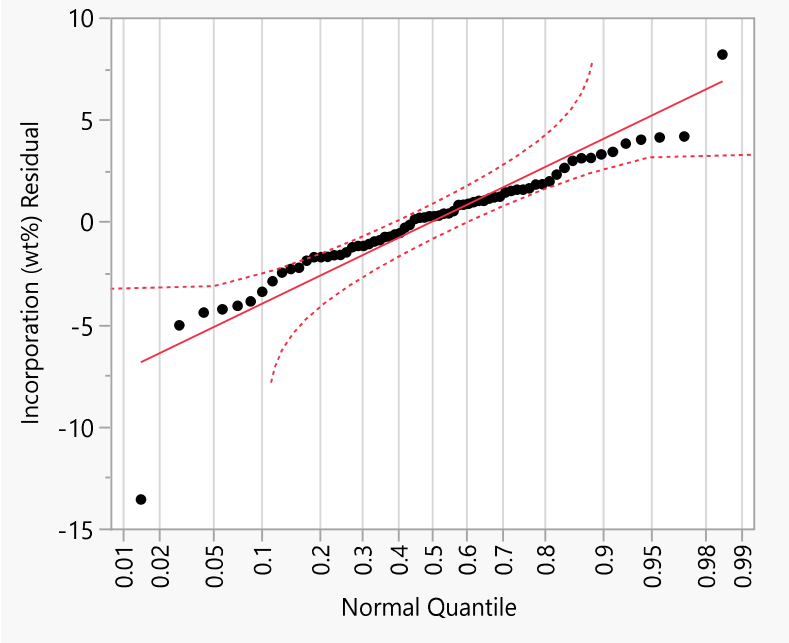

Temperature of polymerisation (°C)
Leverage Plot

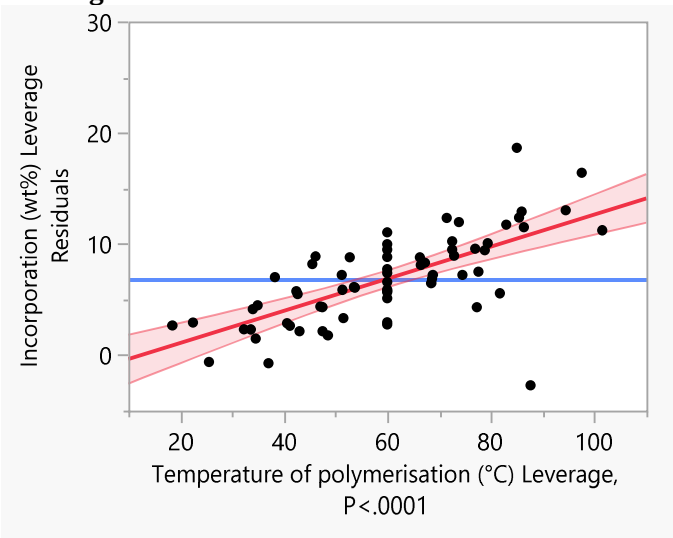

Carbons in LAO
Leverage Plot

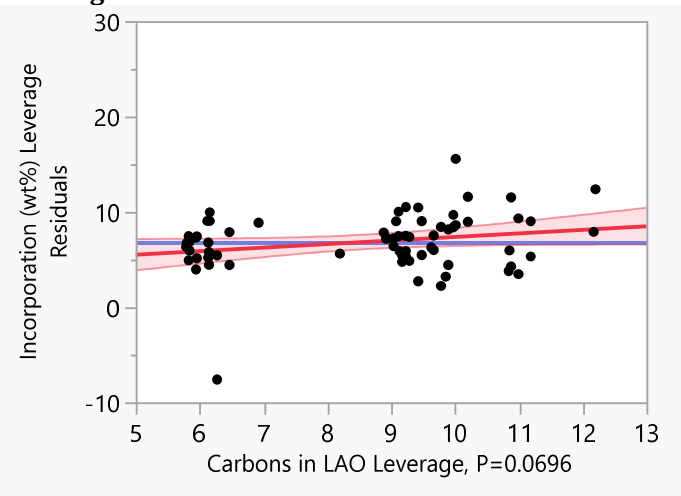

[Comonomer] /mM
Leverage Plot

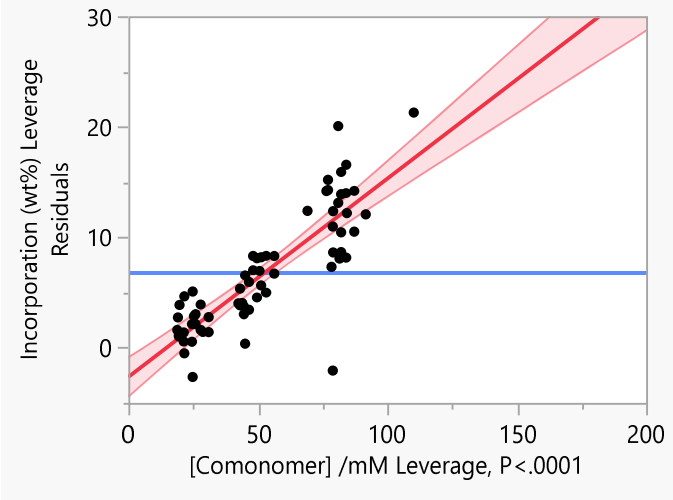

Temperature of polymerisation (°C)*Carbons in LAO
Leverage Plot

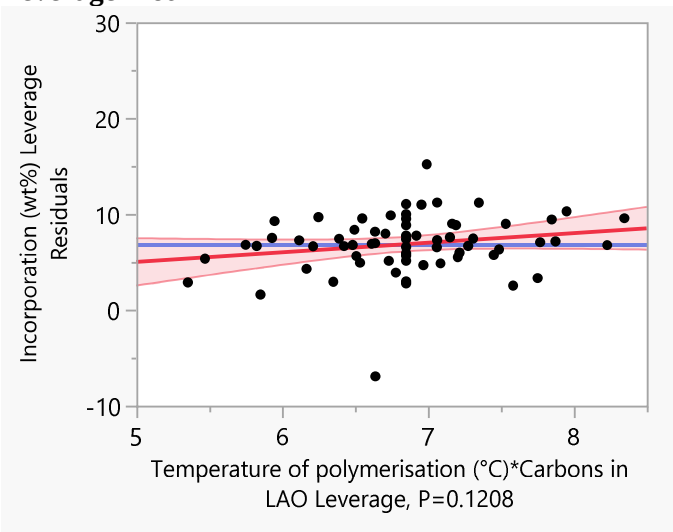

Temperature of polymerisation (°C)*[Comonomer] /mM
Leverage Plot

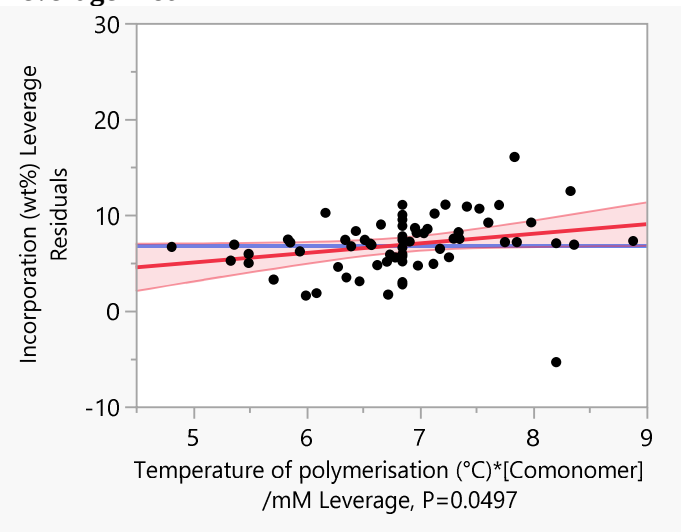

Carbons in LAO*[Comonomer] /mM
Leverage Plot

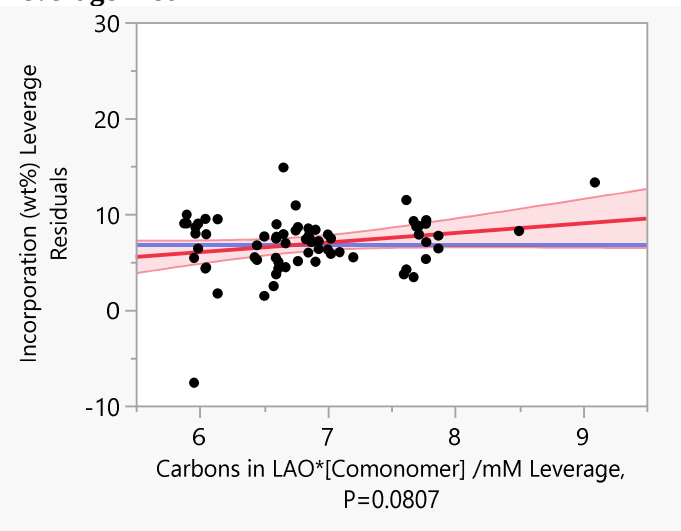

Temperature of polymerisation (°C)*Temperature of polymerisation (°C) Leverage Plot

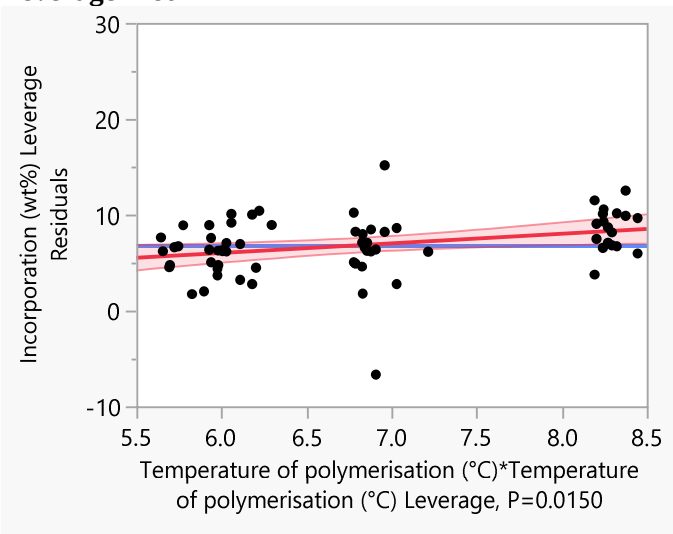

[Comonomer] /mM*[Comonomer] /mM Leverage Plot

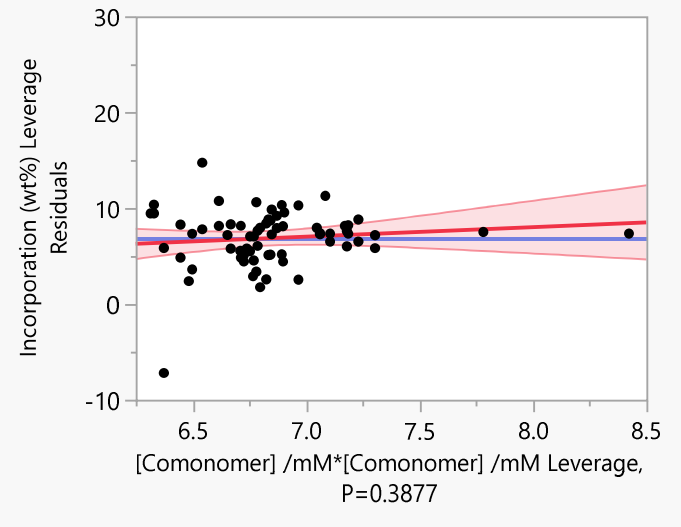

Carbons in LAO*Carbons in LAO Leverage Plot

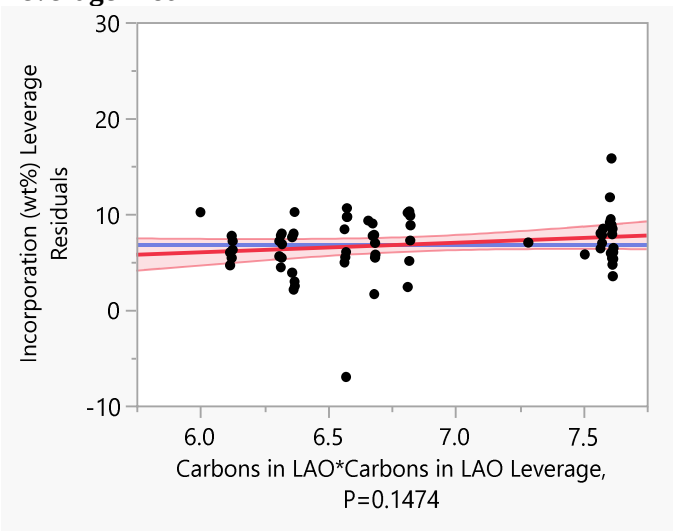

Appendix D

Those present 4th March 2023, "Dr Clem's Hand-In Party (Maybe)"

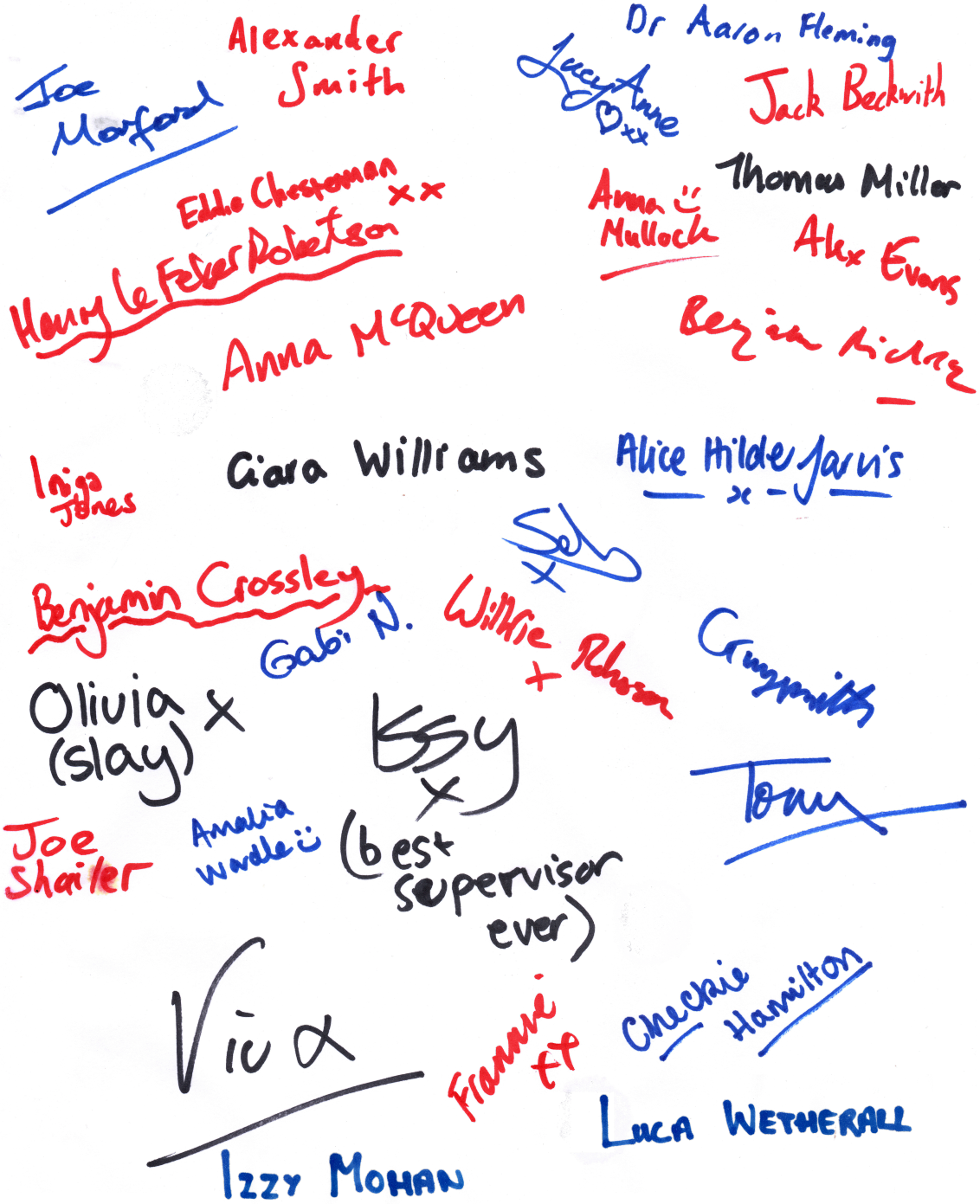

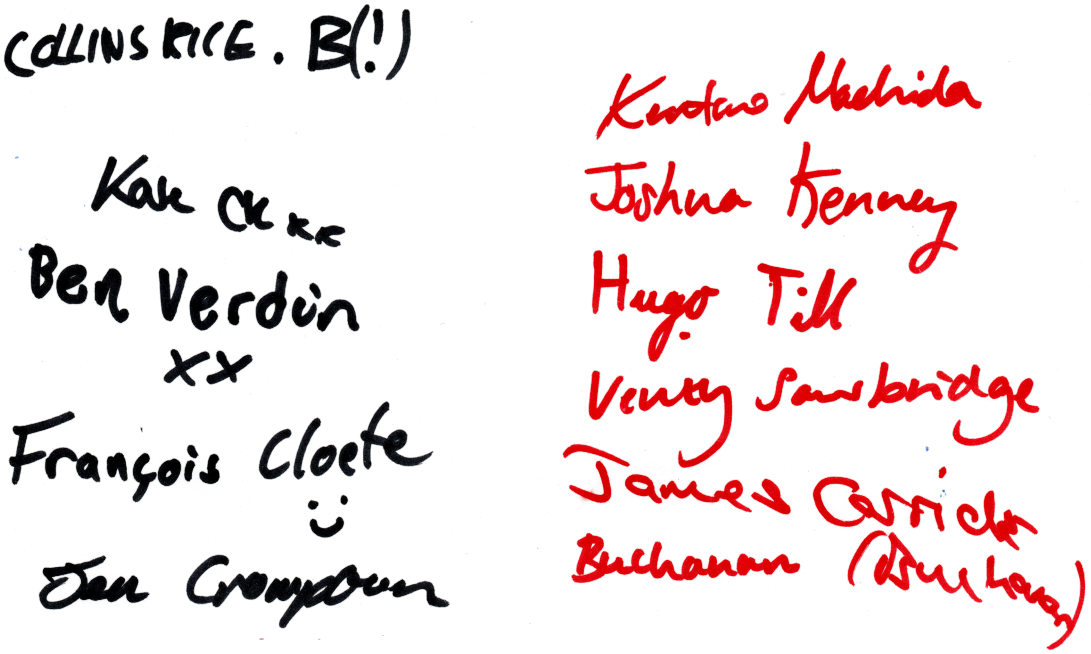
COLLINS RICE . B(!)
Kate Clarke
Ben Verdin
xx
François Cloete
Jan Crompton
Kentaro Machida
Joshua Kenney
Hugo Till
Venty Sandbridge
James Carrick
Buchanan (Buchanan)